Simulation of Critical Biomechanical Loads on the Lumbar Spine in Crash Situations for Automated Driving

Laura Kathrin Rieger

Munich 2024

Aus dem
Institut für Rechtsmedizin
Institut der Ludwig-Maximilians-Universität München

Simulation of Critical Biomechanical Loads on the Lumbar Spine in Crash Situations for Automated Driving

Dissertation
zum Erwerb des Doktorgrades der Humanbiologie
an der Medizinischen Fakultät der
Ludwig-Maximilians-Universität München

vorgelegt von
Laura Kathrin Rieger
aus Landshut

2024

Mit Genehmigung der Medizinischen Fakultät der
Ludwig-Maximilians-Universität München

Erstes Gutachten:	Prof. Dr. Steffen Peldschus
Zweites Gutachten:	Prof. Dr. Thomas Grupp
Drittes Gutachten:	Prof. Dr. Stefan Wirth
Dekan:	Prof. Dr. med. Thomas Gudermann
Tag der mündlichen Prüfung:	19.12.2024

Affidavit

LUDWIG-MAXIMILIANS-UNIVERSITÄT MÜNCHEN

Promotionsbüro Medizinische Fakultät

Eidesstattliche Versicherung

Rieger, Laura Kathrin

Ich erkläre hiermit an Eides statt, dass ich die vorliegende Dissertation mit dem Titel:

Simulation of Critical Biomechanical Loads on the Lumbar Spine in Crash Situations for Automated Driving

selbständig verfasst, mich außer der angegebenen keiner weiteren Hilfsmittel bedient und alle Erkenntnisse, die aus dem Schrifttum ganz oder annähernd übernommen sind, als solche kenntlich gemacht und nach ihrer Herkunft unter Bezeichnung der Fundstelle einzeln nachgewiesen habe.

Ich erkläre des Weiteren, dass die hier vorgelegte Dissertation nicht in gleicher oder in ähnlicher Form bei einer anderen Stelle zur Erlangung eines akademischen Grades eingereicht wurde.

Wolfsburg, der 4. Juli 2024

Laura Kathrin Rieger

Unterschrift

Disclaimer

„Ergebnisse, Meinungen und Schlüsse dieser Publikation sind nicht notwendigerweise die der Volkswagen Aktiengesellschaft.“

“The results, opinions and conclusions expressed in this publication are not necessarily those of Volkswagen Aktiengesellschaft.”

„Immer neugierig bleiben“
“Always stay curious”

Walter Maria Rieger

Contents

Declaration . . . V
Disclaimer . . . VII
Contents . . . XI
Acronyms . . . XIII
Publications . . . XVII
List of Figures . . . XIX
List of Tables . . . XXI

1 Zusammenfassung . . . 1

2 Abstract . . . 5

3 Own Contribution . . . 9
3.1 Contribution to Paper I . . . 9
3.2 Contribution to Paper II . . . 9

4 Introduction . . . 11
4.1 Lumbar Spine . . . 16
4.1.1 Lumbar Spine Anatomy & Physiology . . . 17
4.1.2 Lumbar Spine Injuries to Car Occupants . . . 21
4.1.3 Lumbar Spine Injury Tolerance . . . 26
4.1.4 Anthropometrical Variations of the Lumbar Spine . . . 28
4.2 Strategies to Investigate Lumbar Spine Biomechanical Tolerance . . . 30
4.3 Thesis Overall Aim and Objectives . . . 39

5 Reference Points Describing Spinal Posture . . . 41
5.1 Geometrical Construction of Vertebral Reference Points . . . 42
5.2 Solver-specific Modell Integration . . . 44

6 Paper I . . . 47

7 Paper II . . . 65

8 Application in Generic Environment . . . 81
8.1 Materials . . . 81
8.2 Methods . . . 84
8.2.1 Creation of FE-HBMs . . . 84
8.2.2 Generic Seat Setup . . . 86
8.2.3 Variabilities of the Spinal Alignment in Different Recline Positions 87
8.2.4 Investigation of the Global Behavior of the Positioned Spines Using the Generic Seat Test Setup . . . 88

8.3 Results . . . 89
8.3.1 Analysis of Occupant Kinematics . . . 89
8.3.2 Lumbar Kinematics . . . 90
8.4 Discussion . . . 92
8.4.1 Materials . . . 92
8.4.2 Methods . . . 93
8.4.3 Kinematic Comparison . . . 94
8.4.4 Fracture Detection . . . 95

9 Outlook & Conclusion . . . 97

Bibliography . . . 101

Appendix . . . 127
A.1 Preliminary Investigations - Intervertebral Discs . . . 127
A.1.1 Experimental Setup by Newell et al. (2019) . . . 127
A.1.2 Finite Element Simulation . . . 128
A.1.3 Validation Results . . . 129
A.2 Preliminary Investigations - Total Lumbar Spine . . . 130
A.2.1 Drop-Tower Experiment by Stemper et al. (2011b) . . . 130
A.2.2 Finite Element Simulation of the Drop-Tower Experiment . . . 131
A.2.3 Validation of the Total Lumbar Spine in a Subinjurious Load Case . . . 134
A.3 Subject-Specific Model Creation . . . 135
A.3.1 Geometry & Mesh Generation . . . 136
A.3.2 Model Positioning . . . 137
A.3.3 Model Assembly . . . 139
A.4 Drop-tower Simulation Setup Sensitivity . . . 142

Acknowledgements . . . 145

Acronyms

$\text{angle}_{\text{InterVB}}$	intervertebral angle
c_{BEP}	center point bottom endplate
c_{CR}	center of the spinal canal
c_{TEP}	center point top endplate
c_{VB}	center of the vertebral body
$+G\text{z}$	vertical impact acceleration
2D	two-dimensional
3D	three-dimensional
ABS	anti-lock braking system
ACC	adaptive cruise control
ADAC	Allgemeiner Deutscher Automobil-Club e.V.
AIS	Abbreviated Injury Scale
ALL	anterior longitudinal ligament
AO	Arbeitsgemeinschaft für Osteosynthesefragen
ASIS	anterior superior iliac spine
ASME	American Society of Mechanical Engineers
ATD	anthropometric test device
BMI	body mass index
CAD	computer aided design
CDF	cumulative distribution function
CL	capsular ligament
COG	center of gravity
CT	computer tomography
DoD	US Department of Defense
DOF	degrees of freedom
DRI	Dynamic Response Index
ESC	electronic stability control
FAA	US Federal Aviation Administration
FCI	Functional Capacity Index
FE	finite element
FEM	finite element method
FSU	functional spine unit

GIDAS	German In-Depth Accident Study
HAV	highly autonomous vehicle
HBM	human body model
ISL	interspinous ligament
ITL	intertransverse ligament
IVD	intervertebral disc
LF	ligamentum flavum
LL	lumbar lordosis
LMU	Ludwig-Maximilians-Universität Munich
LSU	lumbar spine unit
LVDT	Liner Variable Displacement Transducer
MAIS	Maximal Abbreviated Injury Scale
MCW	Medical College Wisconsin
MRI	magnetic resonance imaging
MTOCO	Multiple Node to one Node Constraint
NASS-CDS	US National Automotive Sampling System-Crashworthiness Data System
NBDL	US Naval Biodynamics Laboratory
NHP	nonhuman primate
NTSB	US National Transportation Safety Board
OEM	original equipment manufacturer
OTMCO	One Node to Multiple Nodes Constraint
PA	pelvic angle
PLL	posterior longitudinal ligament
PMHS	post mortem human surrogates
PMMA	polymethylmethacrylate
PSIS	posterior superior iliac spine
PTC	Performance Test Codes
SAE	Society of Automotive Engineers
SD	standard deviation
SECFO	Section Force
SSL	supraspinous ligament
THNOD	Nodal Time Histories
THOR	Test Device for Human Occupant Restraint

THUMS	Total HUman Model for Safety
TUC	THUMS User Community
UMTRI	University of Michigan Transportation Research Institute
VCP	Visual-Crash PAM

Publications

Publications in Journals[1]

Rieger, Laura K., Alok Shah, Sylvia Schick, Dustin B. Draper, Rachel Cutlan, Steffen Peldschus, and Brian D. Stemper (2024). Subject-specific geometry of FE lumbar spine models for the replication of fracture locations using dynamic drop tests. In: *Annals of Biomedical Engineering* 52, pp. 816-831. doi:10.1007/s10439-023-03402-y.

Rieger, Laura K., Mirko Junge, Rachel Cutlan, Steffen Peldschus, and Brian D. Stemper (2024). Simulative Investigation of the Required Level of Geometrical Individualization of the Lumbar Spines to Predict Fractures. In: *International Journal of Legal Medicine*, in press. doi:10.1007/s00414-024-03225-z.

Conference Proceedings

Rieger, Laura K., Julia Mühlbauer, and Steffen Peldschus (2022). "A 3D-analysis of the spine in different seatback recline angles and the effect on occupant kinematics in a frontal crash scenario using a THUMS human body model." Forum für Verkehrssicherheit, Munich, Germany.

Rieger, Laura K., Julia Mühlbauer, and Steffen Peldschus (2022). „Eine 3D-Analyse der Wirbelsäule in unterschiedlichen Rückenlehnenneigungen und Untersuchung des Effekts auf Insassenkinematik im Frontcrash unter Nutzung eines THUMS Menschmodells", 13. VDI Fahrzeugsicherheit, Berlin, Germany.

Rieger, Laura K., Dustin Draper, Alok Shah, Steffen Peldschus, and Brian D. Stemper (2022). "Subject-specific Lumbar Spine Finite Element Model Creation and Validation using Dynamic Compression." In: *Proceedings of the IRCOBI Conference*, pp. 886–887. IRC-22-104.

Rieger, Laura K., Fenna Neumann, Ryusuke Asahi, Tomohiro Izumiyama, Dustin Draper, Bengt Pipkorn, Michael Sprenger, and Steffen Peldschus (2023). "First Target Datasets for the Consideration of Postural Variety in FE HBM Analysis of the Lumbar Spine." In: *Proceedings of the IRCOBI Conference*, pp. 713–714. IRC-23-87.

1 These publications are part of the cumulative dissertation

List of Figures

4.1 Schematic representation of submarining. 14
4.2 Vertebral column 16
4.3 Vertebral body. 18
4.4 Schematic representation of an intervertebral disc. 19
4.5 Schematic representation of a functional spine unit. 20
4.6 Schematic representation of anatomical planes and different loading directions. 22
4.7 Injury types of the lumbar spine. 25
4.8 Comparison of ATDs and HBMs. 32
4.9 Sagittal cut in median plane of L3 to L5 THUMS v4.1. lumbar spine unit. 36

5.1 Schematic representation of the preparation of experimental data before construction of reference points. 42
5.2 Schematic representation of construction of vertebral reference points. 43
5.3 Visualization of the local coordinate system construction exemplified by a vertebral body. 44
5.4 Solver-specific model integration exemplarily for a THUMS v4.1 vertebra. 45

8.1 Schematic of MRI acquisition setup. 83
8.2 Spatial position of the 3D objects of three seating positions. 84
8.3 Alignment of the MRI data to THUMS v4.1 85
8.4 Process of using the MRI data for positioning of the THUMS v4.1 spine. 85
8.5 Model of the semi-rigid seat (front seat configuration). 87
8.6 Full-frontal, single 30-g (51 km/h ΔV) pulse. 87
8.7 Spinal alignment with 20 deg, 40 deg, and 60 deg seat back angles. . . 87
8.8 Intervertebral angles in the lumbar area, lumbar lordosis, and pelvic angle for three different seat recline angles. 88
8.9 Positioned and belted FE simulation models 88
8.10 Kinematic results of the upright (20 deg) and the two reclined positions (40 deg and 60 deg). 89
8.11 Angular kinematic results of the modified THUMS v4.1 lumbar spine. 90
8.12 Stress field maps of the maximum pressure of the lumbar vertebrae. . 91

9.1 Global kinematic results for the reclined position (45 deg). 99
9.2 Stress field maps of the maximum pressure of the lumbar vertebrae in whole body sled tests. 99

A.1 Schematic representation of the IVD validation setup. 129
A.2 A comparison of the force-displacement response of the experimental and numerical result. 129

A.3 Configuration of experimental setup drop-tower setup. 131
A.4 Schematic representation of experimental and simulative drop-tower setup. 132
A.5 Validation of the intervertebral evaluation concept. 134
A.6 A comparison of the force-time, moment-time, and angular displacement response of the experimental and numerical results. 134
A.7 Overview of the reconstruction of the subject-specific lumbar spine models. 135
A.8 Example of the resulting mesh of a segmented L3 vertebra. 137
A.9 Definition of midplanes. 138
A.10 Reorientation of the vertebrae. 139
A.11 Mesh morphing process. 140

List of Tables

4.1 Selected anthropometrical parameter variations. 29

8.1 Mechanical design and specifications of the semi-rigid seat as used in this study. 86

A.1 Shell and solid mesh quality parameters. 137
A.2 Drop-tower simulation setup sensitivity parameters. 142

1 Zusammenfassung

Verletzungen der lumbalen Wirbelsäule entstehen durch traumatische Ereignisse und reichen von Verletzungen der Bänder bis hin zu komplexen dislozierten Frakturen. Solche Verletzungen, wie zum Beispiel Wirbelfrakturen, können durch Destabilisierung der mechanischen Struktur der Wirbelsäule und insbesondere durch daraus resultierende Verlegung des Wirbelkanals erhebliche Behinderungen bei gesunden Menschen verursachen und hohe sozioökonomische Folgen haben. Primärursachen dieser Verletzungen sind multidirektionale, dynamische Belastungen, die bei Stürzen oder Unfällen mit Fahrzeugen auftreten können. Insbesondere die Entwicklung zu teil- und vollautonomen Fahrzeugen, die neue Sitzpositionen der Insassen erlauben (zum Beispiel Komfortpositionen (Reclined Seating)), stellt in der Fahrzeugentwicklung neue Herausforderungen dar, weil in diesen Positionen in Longitudinalrichtung höhere Kompressions- und Flexionskräfte gegenüber Standardpositionen auf die lumbale Wirbelsäule einwirken. Allerdings sind sowohl die Verletzungsmechanismen als auch der Einfluss anthropometrischer Unterschiede bei dynamischer Belastung noch nicht vollständig geklärt. Zielsetzung der vorliegenden Dissertation war es daher, eine Strategie für den Umgang mit anthropometrischen Unterschieden der lumbalen Wirbelsäule bei der Bewertung von Wirbelsäulenverletzungsrisiken im Rahmen der virtuellen Fahrzeugentwicklung mit menschlichen Körpermodellen, sogenannten Human Body Models (HBMs), zu entwickeln.

Um anthropometrische Unterschiede an der Wirbelsäule unabhängig von den zugrunde liegenden medizinischen Bildgebungsverfahren untersuchen und Auswertungsergebnisse auf modellbildende Wirbelsäulen-Abbildungen übertragen zu können, sind quantitative, eindeutige und nutzerunabhängige Auswertungsmethoden notwendig, die es ermöglichen, die genaue Position und Orientierung einzelner Wirbel zu bestimmen. Daher wird eine Methode zur Bestimmung der Position und Ausrichtung eines Wirbels über lokale Koordinatensysteme entwickelt, die sowohl für experimentelle Daten als auch für Finite-Elemente-Modelle (FE-Modelle) anwendbar ist. Darüber hinaus wird eine solverspezifische Methode zur Integration der lokalen Koordinatensysteme in ein HBM vorgestellt.

Diese Methoden fanden im ersten Teilprojekt Anwendung. Ziel dieses Teilprojektes war es zu bewerten, inwiefern subjektspezifische, explizite FE-Modelle der Lumbalwirbelsäule basierend auf klinischen Computertomographie-Aufnahmen (CT-Aufnahmen) kombiniert mit Materialdaten aus der Literatur experimentelle Reaktionen und Frakturstellen in einem dynamischen Fallturm-Testaufbau vorhersagen können. Weiterhin wurde untersucht, welche Auswertungsstrategie sich unter den vorgegebenen Randbedingungen als geeignet zeigt. Die CT-Aufnahmen sowie die experimentellen Ergebnisse des Fallturm-Testaufbaus wurden vom Medical College Wisconsin (MCW) zur Verfügung gestellt. Die Wirbelkörper wurden aus den CT-Scans segmentiert und zur

Erstellung von vier subjektspezifischen FE-Modellen der Lumbalwirbelsäule (T12-L5) genutzt. Weichteile des Total HUman Model for Safety (THUMS v4.1) wurden über Morphing-Verfahren integriert. Außerdem wurden für alle Modelle identische Materialeigenschaften des THUMS v4.1 verwendet. Zur Simulation der dynamischen Tests wurden entsprechende Belastungen und Randbedingungen aus den Experimenten genutzt.

Die Ergebnisse der Simulationen stimmten mit Kraft, Moment und kinematischen Reaktionen der experimentellen Daten überein. Über die Druckverteilung in den Modellen konnten jeweils Art und Position der Frakturen prädiziert werden. Im Vergleich zu Wirbelsäulenkomponenten, die keine Fraktur erlitten hatten, zeigten Wirbelsäulenhöhen, die im Experiment eine Wirbelkörperfraktur erlitten, höhere lokale Drücke in den anterioren Elementen auf. Gleichermaßen wiesen Wirbelsäulenhöhen, die im Experiment eine Fraktur der posterioren Strukturen erlitten hatten, einen höheren Druck in den posterioren Wirbelelementen im FE-Model auf. Es konnte gezeigt werden, dass eine subjektspezifische Modellierung der Wirbelsäulengeometrie und -ausrichtung zur Vorhersage von Art und Stelle der Frakturen unter dynamischer Belastung geeignet ist. Die simulative Auswertung des Drucks mit einer Filterung der Ergebnis-Skalen erwies sich zudem als geeigneter Auswertungsparameter.

Auf der Grundlage des ersten Teilprojekts wurde im zweiten Teilprojekt der erforderliche Grad der Individualisierung eines FE-Basismodells der Lumbalwirbelsäule untersucht, der notwendig ist, um experimentelle Reaktionen und Frakturen unter den Randbedingungen des dynamischen Fallturm-Testaufbaus zu replizieren. Ziel war es, die Wirbelsäulenparameter in der Sagittalebene zu identifizieren, die für das kinematische Verhalten in einer hochdynamischen Anwendung relevant sind, sowie eine Strategie vorzuschlagen, die es erlaubt, die Varianz systematisch in die Analyse einzubeziehen. Experimentelle Röntgenaufnahmen aus 26 Fallturmtests wurden verwendet, um drei Konfigurationen eines Lumbalenwirbelsäulenmodells zu erstellen: (1) Eine Basiskonfiguration mit der THUMS v4.1-Lendenwirbelsäule; (2) eine positionierte Konfiguration, bei der die THUMS v4.1-Lendenwirbelsäule so positioniert wurde, dass die Winkel zwischen den Wirbelkörpern denen aus den Röntgenbildern entsprachen; sowie (3) eine gemorphte und positionierte Konfiguration bei der die THUMS v4.1-Lendenwirbelsäule nicht nur positioniert, sondern auch die anterioren und posterioren Höhen der Wirbelkörper an die Röntgenbilder angepasst wurden. Jedes Modell wurde, wie im ersten Teilprojekt mit den entsprechenden Belastungen und Randbedingungen aus den Experimenten simuliert. Die Simulationsergebnisse von Kraft, Moment und kinematischer Reaktion wurden mit den experimentellen Daten verglichen und die Ähnlichkeit berechnet, um die Übereinstimmung der Simulationsergebnisse mit den experimentellen Daten zu bewerten. Die im ersten Teilprojekt entwickelte Auswertungsmethode fand zur Analyse des Auftretens und Lage von Frakturen Anwendung. Im Allgemeinen konnten die gemorphten und positionierten Modelle das Level der Wirbelsäule und das Frakturmuster besser nachbilden als die Modelle, die nur positioniert wurden. Da der Effekt jedoch relativ gering und der Aufwand für die Modellmodifikation im Vergleich dazu hoch war, wird für die Verwendung in Gesamtkörpermodellen zum

Zweck der Aufprallrekonstruktion oder Verletzungsvorhersage die reine Positionierung empfohlen.

Der Schwerpunkt des letzten Teilprojekts lag auf der Erprobung der vorgeschlagenen Anwendungsstrategie im Gesamtkörpermodell und einer dem Stand der Wissenschaft entsprechenden Abstrahierung eines Fahrzeugsitzes für das Labor mit dem Fokus auf die initiale Lumbalwirbelsäulenposition bei unterschiedlichen Neigungswinkeln der Rückenlehne. Dafür wurden Magnetresonanztomographiedaten (MRT-Daten) der Wirbelsäule eines Probanden in einer aufrechten Position und in zwei Positionen mit höherem Neigungswinkel der Rückenlehne angefertigt und zur Positionierung des THUMS v4.1 verwendet. Die drei positionierten und eingesessenen Modelle wurden jeweils in Schlittentests im 50 km/h Frontalcrash simuliert. Das Ergebnis war, dass die Neigungswinkel unterschiedliche Insassen- und Lumbalwirbelsäulenkinematiken hervorrufen, was zu unterschiedlichen Druckverteilungsmustern führt: Mit zunehmendem Neigungswinkel vergrößert sich die Fläche, in welcher der Druck auftritt und die Wahrscheinlichkeit einer Fraktur erhöht sich.

Die vorliegende Dissertation präsentiert eine detaillierte Analyse des Einflusses der Wirbelsäulenposition auf die Frakturwahrscheinlichkeit in dynamischen Anwendungen sowie einen Vorschlag zur Auswertung in Gesamtkörpermodellen. Die Arbeit stellt die Grundlage der Anwendung von Menschmodellen zur simulativen Belastungsbewertung der Lumbalwirbelsäule im Fahrzeugcrash dar. Welche individuelle lumbale Wirbelsäulenposition am gefährdetsten ist und wie sich lumbale Wirbelsäulenposition in Realfahrzeugsitzen und -umgebung verhält, kann in Folgestudien geprüft werden.

2 Abstract

Injuries to the lumbar spine are caused by traumatic events and range from ligament injuries to complex fracture dislocations. Such injuries like vertebral fractures can result in significant disability among healthy individuals and have significant socio-economic implications. This is due to the destabilization of the spine's mechanical structure and, specifically, the resulting displacement of the spinal canal. The primary causes of these injuries are multidirectional, dynamic loads that can occur during falls or vehicle crashes. In particular, the development of partially and fully autonomous vehicles, which allow new seating positions for occupants (e.g., comfort positions as reclined seating), pose new challenges in vehicle development because higher compression and flexion forces in the longitudinal act on the lumbar spine in these positions compared to standard positions. However, the injury mechanisms and the influence of anthropometric differences have not yet been fully understood under dynamic loading. The aim of this dissertation was therefore to develop a strategy for dealing with anthropometric differences in the lumbar spine when assessing spinal injury risks in the context of virtual vehicle development using human body models (HBMs).

To investigate anthropometric differences in the spine independently of the underlying medical imaging procedures and to be able to transfer evaluation results to modelling spine images, quantitative, unambiguous, and user-independent evaluation methods are required that make it possible to determine the exact position and orientation of individual vertebrae. Therefore, a method for determining the position and orientation of a vertebra via local coordinate systems is developed, which is applicable for both experimental data and finite element (FE) models. In addition, a solver-specific method for integrating the local coordinate systems into an HBM is presented.

This concept was applied in the first subproject. The objective of this subproject was to assess the extent to which subject-specific, explicit FE models of the lumbar spine based on clinical computed tomography (CT) images in conjunction with material data from the literature can predict experimental reactions and fracture sites in a dynamic drop-tower test setup. Furthermore, it was investigated which evaluation strategy is suitable under the given boundary conditions. The CT images and the experimental results of the drop-tower test setup were provided by the Medical College Wisconsin (MCW). The vertebral bodies were segmented from the CT scans and used to create four subject-specific FE models of the lumbar spine (T12-L5). Soft tissues from the Total HUman Model for Safety (THUMS v4.1) were integrated using morphing methods. In addition, identical material properties of THUMS v4.1 were used for all models. Corresponding loads and boundary conditions from the experiments were used to simulate the dynamic tests.

The results of the simulations were consistent with the experimental data in terms of force, moment, and kinematic reactions. The type and position of the fractures could be predicted via the pressure distribution in the models. Compared to spinal components that had not suffered a fracture, spinal levels that suffered a vertebral fracture in the experiment showed a higher-pressure distribution in the anterior elements. Similarly, spinal levels that had suffered a fracture of the posterior structures in the experiment showed a higher pressure in the posterior vertebral elements in the FE model. It was shown that subject-specific modelling of spinal geometry and alignment is suitable for predicting the type and location of fractures under dynamic loading. Simulative evaluation of the pressure with filtering of the result scales also proved to be a suitable evaluation parameter.

Based on the first subproject, the second subproject investigated the required degree of individualization of a FE base model of the lumbar spine necessary to replicate experimental responses and fractures under the boundary conditions of the dynamic drop-tower test setup. The aim was to identify the spinal parameters in the sagittal plane that are relevant for the kinematic behavior in a highly dynamic application and to propose a strategy that allows the spinal variance to be systematically included in the analysis. Three configurations of a lumbar spine model were created using experimental radiographs from 26 drop-tower tests: (1) a baseline configuration with the THUMS v4.1 lumbar spine; (2) a positioned configuration in which the THUMS v4.1 lumbar spine was positioned so that the angles between the vertebral bodies corresponded to the vertebral angles from the X-ray images; and (3) a morphed and positioned configuration in which the THUMS v4.1 lumbar spine was not only positioned but also the anterior and posterior heights of the vertebral bodies were adjusted to the X-ray images. As in the first sub-project, each model was simulated with the corresponding loads and boundary conditions from the experiments. The simulation results of force, moment, and kinematic response were compared with the experimental data and the similarity was calculated to assess the agreement of the simulation results with the experimental data. The evaluation method developed in the first subproject was used to analyze the occurrence and location of fractures. In general, the morphed and positioned models were able to replicate the level of the spine and the fracture pattern slightly better than the models that were only positioned. However, as the effect was relatively small and the cost of model modification was high in comparison, positioning only is recommended for use in whole-body models for the purpose of impact reconstruction or injury prediction.

The focus of the last subproject was on evaluating the proposed application strategy in the whole-body model and a state-of-the-art abstraction of a vehicle seat for the laboratory with focus on the initial lumbar spine position at different recline angles. For this purpose, magnetic resonance imaging (MRI) data of the spine of a volunteer in an upright position and in two positions with a higher backrest tilt angle were obtained and used to position the THUMS v4.1. The three positioned and seated models were each simulated in sled tests in a 50 km/h frontal crash. The result was that the tilt angles cause different occupant and lumbar spine kinematics, leading to different pressure distribution patterns: As the angle of inclination increases, the area on which the pressure acts increase, and the probability of a fracture increases.

This dissertation presents a detailed analysis of the influence of the spinal column position on fracture probability in dynamic applications and a proposal for evaluation in whole-body models. The work provides the basis for the application of human models for simulative load assessment of the lumbar spine in vehicle crashes. Which individual lumbar spine position is at risk most and how the lumbar spine position behaves in real vehicle seats and environments can be evaluated in follow-up studies.

3 Own Contribution

I, Laura Kathrin Rieger, was the first author of both publications in this cumulative dissertation. No shared authorships were applied. I was responsible for the study design, planning, literature search and literature review for both publications.

Furthermore, I acted as the first and main contact person for all involved co-authors as well as editors. Besides, I wrote both manuscripts, incorporated suggestions for changes from the co-authors and reviewers, and was subsequently responsible for handling the submission and review processes. Co-authors of both studies were engaged in the collection of experimental data, data interpretation and final editing of the publications.

3.1 Contribution to Paper I

With regard to the published results in Paper I, the contribution I made comprised the review of the experimental data regarding usability for simulation, the analysis and processing of the experimental data for the setup of the simulations, the development of a methodology for reconstruction of the subject-specific finite element (FE) models, the construction of the simulation models and the evaluation and interpretation of the results of the simulation models.

3.2 Contribution to Paper II

In Paper II, the contribution I made was the analysis of the experimental data, the development of a methodology to adapt the generic model in terms of size and position to the desired parameters, the automized setup of the simulations and the evaluation and interpretation of the simulation models.

4 Introduction

The implementation of vehicle safety regulations and consumer testing programs, in addition to improvements in road infrastructure, has led to a significant decline in the number of road traffic fatalities (Elvik et al., 2009; O'Neill, 2009; Glassbrenner, 2013; Kahane, 2015; van Ratingen et al., 2016). Despite the implementation of numerous safety measures, road traffic crashes continue to result in the deaths of approximately 1.3 million people worldwide each year and leave up to 50 million people with non-fatal injuries (WHO, 2020). In addition to the human suffering caused by road traffic injuries, they have a serious impact on national economies incurring estimated costs of 3 percent of their annual gross domestic product (WHO, 2018). Even though in high-income countries road injuries are no longer among the top ten causes of death, the number of traffic-related injuries and deaths in these countries are still in the hundreds or thousands per year (NHTSA, 2022).

Throughout the years, there has been a development of passive and active safety systems with the aim of enhancing the safety of vehicles. Among the earliest passive safety measures to be implemented the Volvo Car Corporation, Sweden introduced in 1959 the three-point seat belt to counteract vehicle traffic injuries (Bohlin, 1964). Seatbelts have been demonstrated to reduce the risk of fatal injury to front-seat passengers by 45 percent and the risk of moderate-to-critical injury by 50 percent (Elvik et al., 2009, pp. 600–609). The aforementioned effect is further enhanced by the appropriate deployment of front airbags. A reduction of approximately 15 percent in the incidence of fatal and serious injuries has been observed among belted drivers and passengers in airbag-equipped cars (Elvik et al., 2009, pp. 600–609). Starting in the 1970s the design of active safety systems such as anti-lock braking system (ABS), traction control, electronic stability control (ESC), brake assist, adaptive cruise control (ACC), blind spot detection, and lane departure detection, made a significant contribution to the improvement of road transport safety (Eskandarian, 2012, p. 4). It is anticipated that more recent technological developments, such as pedestrian detection systems and integrated safety concepts, in conjunction with forthcoming advances in vehicle communications, driver assistance, and autonomous driving in intelligent vehicles will result in the next phase of improvements in vehicle safety (Lubbe et al., 2018).

Highly Automated Vehicles

The development of highly autonomous vehicles (HAVs) is one of the largest endeavors in the modern automotive industry. According to a study by the Prognos research institute on autonomous driving for the Allgemeiner Deutscher Automobil-Club e.V. (ADAC), the share of new vehicles in which the driver can completely turn away from the driving task on all motorways will increase in the optimistic case from 2.4 percent to as much as 70 percent in 2050 (ADAC, 2023). These vehicles will be able to take over driving functions under certain conditions (SAE[1] Level 4) or under all conditions (SAE Level 5) allowing occupants to perform other tasks and opening up to greater range of seating positions while being transported from A to B (SAE, 2018). According to these future scenarios, reclining the seat back is one of the most requested features by customers associated with highly automated driving (Pettersson and Karlsson, 2015; Jorlöv et al., 2017; Östling et al., 2019) and many original equipment manufacturers (OEMs) have shown concept cars that include reclined seating (Motavelli, 2015).

Futurists posit that the advent of HAVs, equipped with sophisticated active safety features, will render passive safety systems obsolete (Buchholz, 2015). Some studies even predict crashes caused by passenger cars to be non-existent by 2070 at high levels of automation (Unselt et al., 2013). However, given that a mix of HAVs and those without high automation will be operating on public roads for the foreseeable future[2], entities still need to consider the possible scenario of other vehicles crashing into an HAV and how to best protect vehicle occupants[3] in these situations. That implies that besides active safety systems, passive safety systems will still be needed to contribute substantially to preventing fatalities and their further development and their deployment should not be abandoned (Lubbe et al., 2018). In addition, it is assumed that the frequency of occurrence of different crash scenarios will shift with mixed modal traffic (Unselt et al., 2013). In the event of a crash, passive safety systems should maintain their intended protection level and protect all occupants whether in HAVs or in non-HAVs as well as in any alternative seating or interior configuration (NHTSA, 2017).

Alternative Seating Positions

To provide occupants[2] with the best possible protection in the near future, the current passive safety systems must be examined for performance in new crash scenarios with alternative seating positions and, if necessary, new mitigation strategies must be developed (Boyle et al., 2019; Gepner et al., 2019). However, crash analyses for researching and understanding injury mechanisms are only partially suitable for the prediction of how things will develop with HAVs. Nevertheless, there is a requirement that past advances in safety systems shall be maintained in future crash scenarios. One possibility would be to identify aspects associated to HAVs in current accident scenarios. For instance, even today there are already occupants who self-report to recline their seat backs (Thorbole, 2016; Boyle et al., 2019; Goodworth and Canada, 2021). In an analysis of the German In-Depth Accident Study (GIDAS) from 2000 to 2019, 20 percent of occupant positions in traffic crashes were classified as either partially reclined or fully reclined (Schaefer et al., 2021), although most safety systems are

1 Society of Automotive Engineers (SAE)
2 as well as in the event of a malfunction
3 Occupants of the ego vehicle, as well as occupants of the opposing vehicle, occupants in HAVs and in non-HAVs

developed and approved by the manufacturer only for upright positions[4] (Volkswagen AG, 2021).

Studies of US National Automotive Sampling System-Crashworthiness Data System (NASS-CDS) frontal crashes (1995-2005) revealed that occupants seated in a fully reclined position had a 77 percent higher fatality rate than occupants in a partially reclined or upright position. However, only 0.3 percent of the occupants in this study were fully reclined (Dissanaike et al., 2008). A study of more recent crashes (2000-2015) by McMurry et al. (2018) showed similar results: belted and reclined occupants had a 21 percent higher risk of Maximal Abbreviated Injury Scale (MAIS) 2+ and a 69 percent higher risk of MAIS 3+ injuries, respectively. Again, the incidence of occupants in the reclined posture was only 0.1 percent. However, the low evidence for reclined occupants in studies of car crashes does not imply that only a small number of occupants is seating in a reclined position: In NASS-CDS, crash investigators determine the position of the occupants before an accident based on the vehicle inspection and interviews with the occupants - but the seating position is not consistently recorded as an analysis variable. For example, in the studies cited above, cases where the occupant posture was not recorded constituted 24 percent and 17.6 percent of the total, respectively. This might be due to the reason that, in the event of a crash with suspected spinal injury, one of the measures taken by the rescue personnel when rescuing vehicle occupants is to recline the seat back completely in order to slide a so-called *Spineboard* under the occupant, which can then be used to free him or her from the vehicle. The study of GIDAS crashes by Schaefer et al. (2021) mentioned in the previous section reports a higher number of belted reclined occupants (around 20 percent) with 107 percent, 209 percent and 266 percent greater risk for the injury severity levels MAIS 2+, MAIS 3+, and MAIS 4+, respectively. In this study the post-crash seatback position was included as a variable for the definition of the pre-crash seatback position.

There is a paucity of field data on frontal crashes involving occupants in a reclined seating position; nevertheless, the available evidence suggests that the interaction of a reclined seating position and the corresponding belt position may elevate the risk of injury and fatality (Dissanaike et al., 2008; McMurry et al., 2018). In 1988, a US National Transportation Safety Board (NTSB) study on the potential hazards of reclined seats concluded that the protection provided by a three-point seatbelt attached to a pillar is compromised when the seat is reclined and is therefore a “potentially dangerous combination in a moving vehicle” (NTSB, 1988). In particular, the risk of submarining can be increased by a reclined sitting position. Unfavorable occupant kinematics, such as submarining and the combined load on the lumbar spine caused by compression and flexion, due to the increased inclination angle of the backrest and the resulting altered load paths of the seatbelts, are also predicted by computer simulations (Richard et al., 2015; Thorbole, 2016) and laboratory assessments (Rawska et al., 2019; Richardson et al., 2020a). Both effects are briefly described hereafter.

4 The current regulations from legislators and consumer tests are also limited to upright positions. To date, there is no harmonized assessment standard for reclined positions.

Submarining

Submarining is defined as the sliding of the pelvic belt over the iliac crest (Adomeit and Heger, 1975; Figure 4.1). The forward displacement of the lower torso causes the forces of the lap belt to exert a direct load on the soft abdominal tissue (Schöneburg et al., 2003; Thorbole, 2016). In addition, submarining leads to hyperflexion and thus to a compressive load at injurious levels to the lumbar vertebral column (Richardson et al., 2020a). In particular, axial loading of the femur caused by knee-dashboard contact can also lead to lower extremity injuries (Rupp et al., 2008).

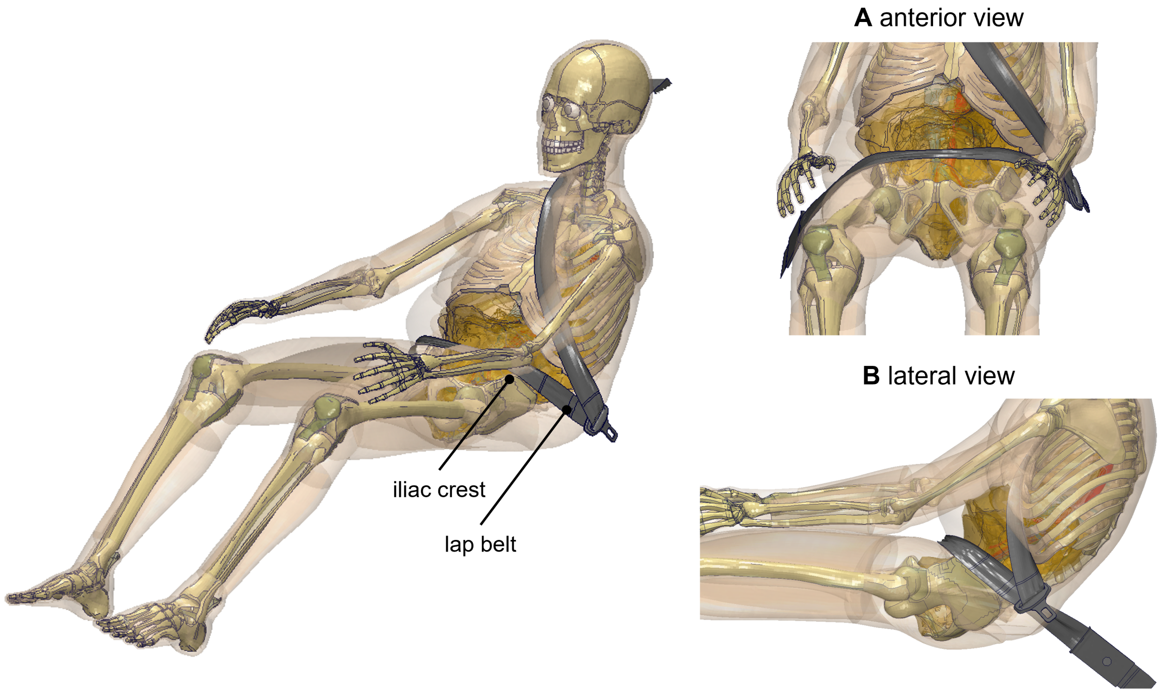

Figure 4.1: Schematic representation of submarining. **A** anterior view. **B** lateral view.

A number of vehicle design countermeasures have been investigated in an attempt to mitigate the risk of submarining. Among these are seat-pan angle and airbag (Shaw et al., 2018), knee bolster (Rawska et al., 2019) and a combination of pretensioners and force limiting retractors (Rouhana et al., 2003). In particular, "the abdominal injuries could be reduced by a better belt-pelvis interaction, easily achieved by a shift in lap belt anchor points and the introduction of lap belt pretensioners" (Reed et al., 2013). Furthermore, restraint systems with dual lap belt tensioners appear to successfully prevent submarining (Richard et al., 2015; Östling et al., 2017; Gepner et al., 2019).

Combined Lumbar Spine Loading

In comparison to an upright posture, a reclined posture during a frontal impact results in a greater horizontal crash vector, leading to a greater axial compression force within the lumbar spine. Additionally, a greater flexion moment is observed during torso pitch in this position (Tushak et al., 2022). There are indications, that the load transfer from the seat to the lumbar spine is even increased when submarining is prevented (Östling et al., 2017). It has been demonstrated that a reduction in both force and accelerations correlates with a lower incidence of injury (Östling et al., 2017). However, there is currently no officially accepted method for automotive applications to assess injury in the lumbar spine. Furthermore, there is no metric at which an acceptable safety level can be defined (Stemper et al., 2015b; Yoganandan et al., 2020).

In aviation, the lumbar load tolerance threshold during vertical accelerations is regulated in the US Federal Aviation Administration (FAA) regulations. The value was determined via a series of dynamic impact tests with aviation-specific pulses (Chandler, 1985) and a modified Hybrid II anthropometric test device (ATD) to capture lumbar loads (DeWeese et al., 2015). Measured lumbar loads were correlated to the Dynamic Response Index (DRI), a formerly derived injury risk criterion for ejection seat development. It describes the probability of injury in relation to the maximum spinal compression (Stech and Payne, 1969; DeStefano, 1972; Thyagarajan et al., 2014). Based on that a lumbar spine modification for the Hybrid III ATD was developed (van Gowdy et al., 1999).

Nevertheless, DRI does not account for the age and sex of occupants, which have been identified as potential factors affecting injury biomechanics (Pintar et al., 1998; Stemper et al., 2011a; 2015b), nor does it incorporate the effects of axial force or acceleration. In their 2018 study, Stemper et al. (2018) quantified the lumbar spine's tolerance for bony injury under vertical accelerative loading, as well as the factors that influence injury outcomes, including loading rate, peak force, age, and sex. Yoganandan et al. (2020) developed a criterion for assessing injury risk that considers axial and resultant force on the spine to be the primary contributors to injury. Recently, injury criteria considering both axial compression forces and flexion moments have been developed (Ortiz-Paparoni et al., 2021; Tushak et al., 2023).

4.1 Lumbar Spine

The spinal column, see Figure 4.2, is the articulated and mobile support of the torso and protects the spinal cord. The individual limbs of this column are called vertebrae. The presence of the vertebral column has given the name to the large group of vertebrates. In humans it consists of 33-34 vertebrae. The 24 most cranial vertebrae[5] remain mobile throughout life; they are also called true vertebrae. Caudally, they are followed by five sacral vertebrae, fused during embryogenesis to form a uniform bone, the os sacrum. The four to five most caudal vertebrae form the coccyx, os coccyges. The vertebrae fused to form the os sacrum and os coccyx are also referred to as false vertebrae. (Anderhuber et al., 2012)

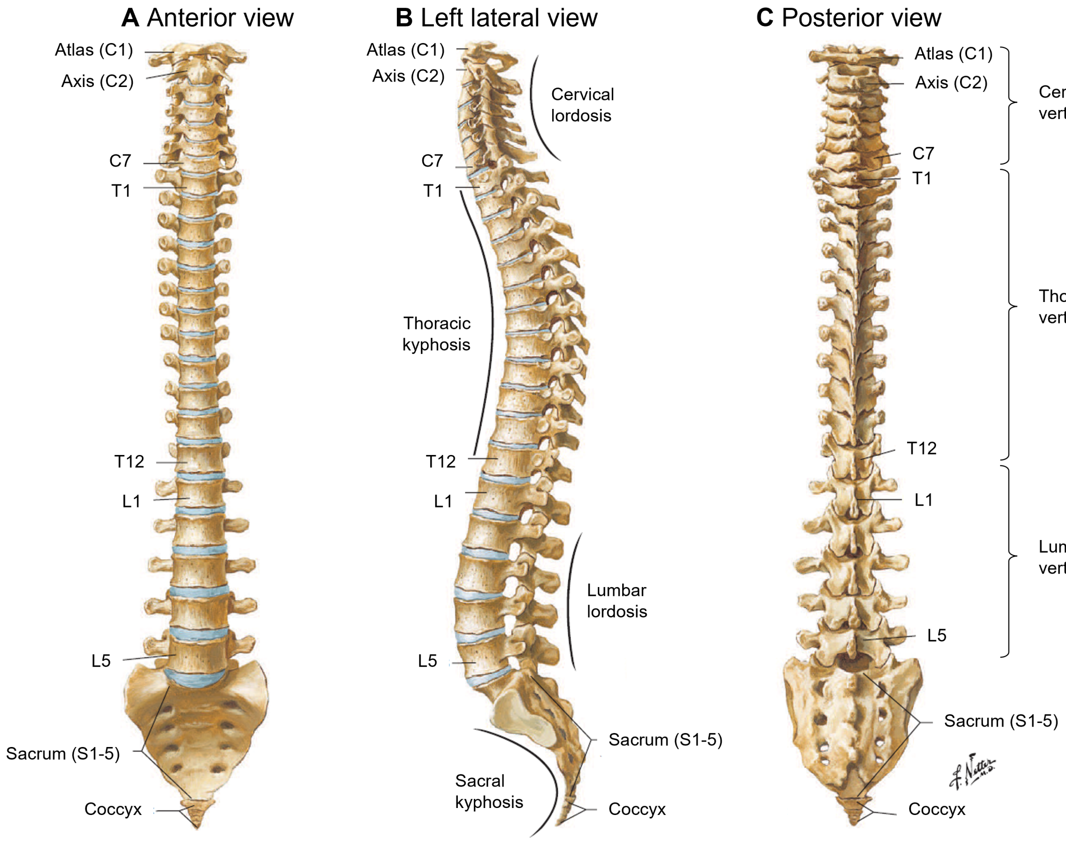

Figure 4.2: Vertebral column in **A** anterior view, **B** from left lateral and in **C** posterior view (modified after Netter (2017)).

The three basic biomechanical functions of the spine are: first, to transfer the weight and resulting bending moments of the head and trunk to the pelvis; second, to allow sufficient physiological movement between these body parts; and third, to protect the

5 Ordinarily, there are 7 cervical, 12 thoracic and 5 lumbar vertebrae. However, there are also deviations from the ordinary case (Rickenbacher et al., 2004).

spinal cord from potentially damaging forces and movements that can result from both physiological movements and trauma. (White and Panjabi, 1990)

The lumbar spine is located vertically between the thoracic spine and the sacrum and is made up of five bony vertebrae (L1-L5); its structural integrity is maintained by soft tissue including the intervertebral discs (IVDs), ligaments and, muscles, both under physiological and traumatic conditions (Putz, 1985). The anatomy of the lumbar spine and its physiology is described in the following. Afterwards, a classification of lumbar spine injuries, including their underlying mechanisms and clinical implications is outlined. Lumbar spine injury tolerance as well as anthropometrical variance are pointed out at the end of this section.

4.1.1 Lumbar Spine Anatomy & Physiology

The following is a brief description of the major components - vertebrae, intervertebral discs (IVDs) and ligaments - of the lumbar spine and their interaction.

Osteology of the Vertebrae

The vertebrae are the bony structures of the spine (Figure 4.3). “Within the different regions of the vertebral column, vertebrae vary in size and shape, but they all follow a similar structural pattern” (White and Panjabi, 1990). The lumbar vertebrae are significantly larger than the other vertebrae due to the load bearing characteristics of the spine (Putz, 1985). The nearly cylindrical vertebral body is the anterior part of each vertebra (White and Panjabi, 1990). Its cranial and caudal surfaces are kidney-shaped; its outer edges are concave. The vertebral bodies and the IVDs are connected to each other via the thin cartilaginous cranial and caudal endplates with thicker epiphyses (Putz, 1985).

The posterior part includes the pedicles, laminae, articular processes, transverse processes, and spinous processes. The pedicles are anchored to the posterior side of the vertebral body. The junction between the pedicles and the vertebral body is known as pars interarticularis. The laminae are quadrilateral in shape and extend posteriorly from the pedicles. There are a superior as well as an inferior articular process on each side of the vertebrae, one facing up and one facing down, forming facet joints between the adjacent vertebrae (Putz, 1985). Depending on the posture, these facet joints can bear up to 30 percent of the vertically applied F_z load (Adams and Hutton, 1985). A transverse process extends laterally on each side, originating between the pedicle and the lamina. It provides insertion points for posterior ligaments. The spinous process provides insertions points for spinal muscles; it is attached to the junction of the two posteriorly converging laminae and extends backwards (Putz, 1985).

The foramen vertebralis is the opening formed by the dorsal part of the vertebral body and the vertebral arch (medial side of the pedicles, laminae, and articular processes). It contains the spinal cord, which is protected by the bone forming the foramen. The terminal end of the spinal cord, conus medullaris, is located at the height of the first and second lumbar vertebrae. Thereafter, the structure of nerve fibers run distally (cauda equina). The spinal cord roots emerge from the spinal canal via a lateral arch between the pedicles of two adjacent vertebrae (intervertebral foramen, Figure 4.5). (Rickenbacher et al., 2004)

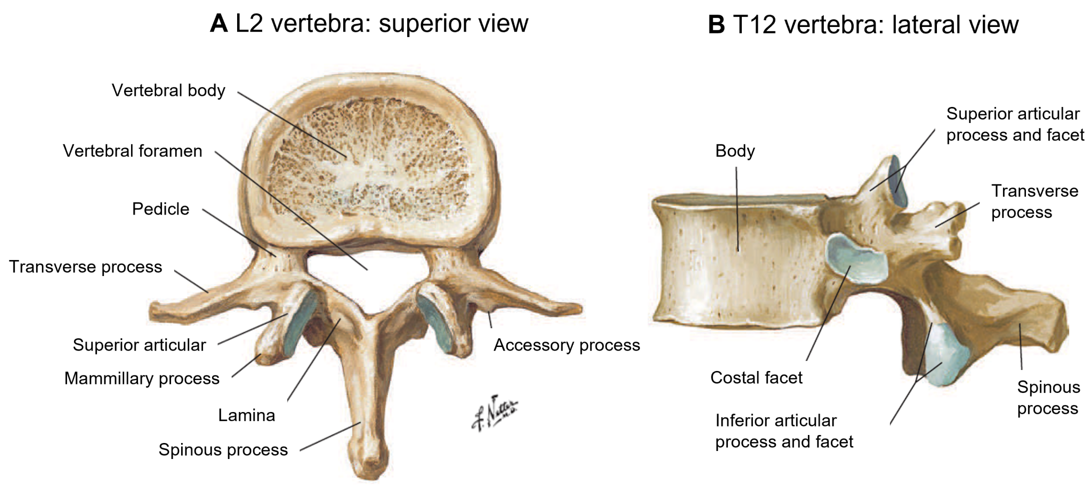

Figure 4.3: **A** Superior view of L2 vertebra and **B** lateral view of T12 vertebra (modified after Netter (2017)).

Each vertebral body consists of an inner core structure of cancellous (trabecular) bone. The trabecular bone contains the bone marrow. At the same time, it serves both to maintain the shape of the load-bearing outer shell of dense cortical bone and to transmit force to it (Prot et al., 2016). This composite structure provides bone with mechanical properties, advanced over its individual components, resulting in a light, strong, stiff, and tough material at the same time (Barthelat, 2015). Bone exhibits anisotropic material behavior and is viscoelastic, hardening under load and increasing its yield strength and fracture toughness with increasing strain rate (Wallace et al., 2013; Prot et al., 2016).

Intervertebral disc (IVD)

Two adjacent vertebral bodies are synchondrotically connected via the intervertebral discs (IVDs). The IVD is a soft tissue organ and the major load propagating structure between individual vertebrae and through the spine. The IVDs of the lumbar spine represent the most extensive avascular organs within the human body. Physiological loads in the lumbar spine in everyday activities such as walking can reach up to 2.5 times of the body weight (Cappozzo, 1984; McGill et al., 1995) or lifting up to 1300 N (Nachemson, 1970; Dreischarf et al., 2016). In dynamic loading conditions the response of the lumbar IVD is nonlinear and shows either pure softening or hardening dependent on preloading and the amplitude of the stimulus (Marini et al., 2016).

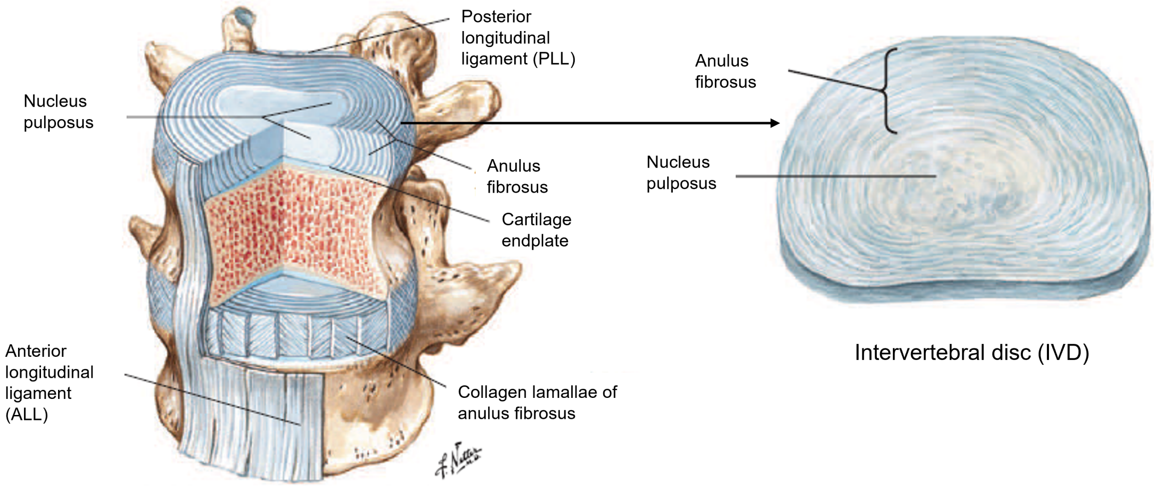

Figure 4.4: Schematic representation of an intervertebral disc (IVD). Concentric lamellae of collagen fibers surround the nucleus of collagen and hydrated proteoglycans (modified after Netter (2017)).

Composed of the annulus fibrosus and the nucleus pulposus, the IVD (Figure 4.4) functions as a load-bearing structure. The annulus fibrosus, a collagen-based matrix comprising multiple fibrocartilage layers, acts to translate compressive loads in collagen fiber tension. The nucleus pulposus, an incompressible mucoprotein gel, separates the vertebrae and serves to distribute the compressive forces exerted upon them. The gelatinous structure of the nucleus pulposus makes up 40–50 percent of the IVD volume of an adult (Pooni et al., 1986; Bayliss and Johnstone, 1992; Iatridis et al., 1996) and 25–50 percent of the transverse cross-sectional area (Perey, 1957; Nachemson, 1960; Newell et al., 2017b). The nucleus pulposus is under hydrostatic pressure due to its high water content. This pressure increases when compressive loading is applied (Keyes and Compere, 1932; McNally and Adams, 1992) and creates tension in the enclosing annulus fibrosus (Nachemson, 1963). The compressive stiffness of the compound lumbar IVDs is strain rate dependent (Kemper et al., 2007; Newell et al., 2019).

Functional spine unit (FSU)

An functional spine unit (FSU) is comprised by two adjacent vertebrae that are connected via the endplates by the IVD and at the pedicles by the facet joints. Each IVD or motion segment represents the smallest part of the spine that encompasses all of the above mentioned structures (Figure 4.5). Furthermore, the spinous processes, the transverse processes and the vertebral arches are connected to each other by a pronounced ligamentous apparatus. Ligaments provide stability, support, and mobility to the spine (Newell et al., 2017a).

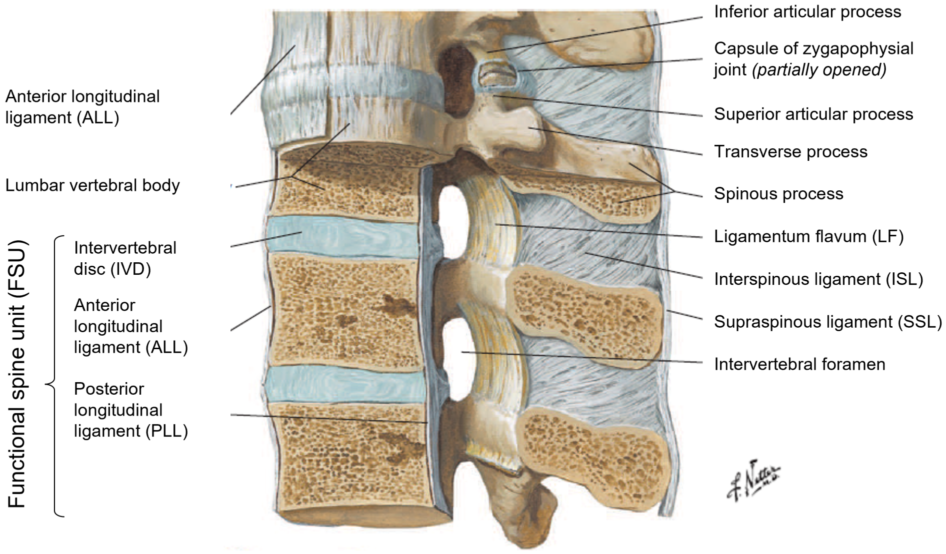

Figure 4.5: Schematic representation of a functional spine unit (FSU) and its ligamentous apparatus (modified after Netter (2017)).

Ligaments

Ligaments consist of elastin and collagen fibers and exhibit uniaxial structural properties (White and Panjabi, 1990). They react in tension and show strain rate dependent material behavior (Pintar et al., 1992b). Seven types of spinal ligaments can be distinguished in the lumbar spine: five extend over only two adjacent vertebrae, while two others cover several vertebrae.

The two last mentioned are the anterior longitudinal ligament (ALL) and posterior longitudinal ligament (PLL) and at the same time the spines' longest ligaments. They adhere anterior and posterior to the vertebral bodies. The former limits extension response of the spine, the later flexion response. The ligamentum flavum (LF) is notable for its high elastin content (80 percent), which contributes to its remarkable elasticity and is designed to maintain the functional spine unit (FSU). Therefore, it is always under pretension and effective in returning lamina to the neutral position following flexion. The primary aim of capsular ligaments (CLs) is to limit joint distraction by encapsulating the facet joints while simultaneously resisting hyperflexion. The interspinous ligament (ISL) interconnects the spinal processes; the tips of these processes along the spinal column are additionally connected via the supraspinous ligament (SSL). Both limit the flexion response of the spine. The intertransverse ligament (ITL) connects the transverse processes of two adjacent vertebrae and withstands rotation as well as lateral bending. (White and Panjabi, 1990)

Autochthonous Back Muscles

In addition to the ligaments, numerous back muscles support the stability and mobility of the spine (White and Panjabi, 1990). Part of these supporting and mobilising back muscles is a system of short and long muscle tractions, the autochthonous back muscles (Rickenbacher et al., 2004). The ligaments in conjunction with the internal pressure of the IVD ensure that the spinal column strives to regain a certain inherent shape after bending (elastic rod). The longitudinal ligaments in particular are involved in maintaining the spinal column. Meanwhile, the autochthonous musculature significantly influences the mobility of the spine. They are also significantly responsible for the shape of the spine. (Staubesand et al., 1985)

Physiological Lumbar Spine Range of Motion

Due to the almost vertical facet joint surfaces in the lumbar region, almost no rotation takes place here. Instead, it exhibits large ventral flexion (bending forward) and dorsal extension (stretching backward). Active in-vivo range of motion[6] of a lumbar FSU is 12 to 16 deg in flexion or extension, 6 deg in lateral bending, 2 deg in axial rotation and 0.1 to 1.9 mm in tension, compression, and shear. (White and Panjabi, 1990)

4.1.2 Lumbar Spine Injuries to Car Occupants

“Injury occurs when deformation exceed physiological limits of the tissue” (Stemper et al., 2015b). The deformation is the cumulative load exerted on the tissue. The profile of the tissue deformation is determined by the magnitude, speed, and direction or type of load. The term “pure load” refers to both linear forces and rotational bending moments. Linear forces can have any direction but are usually divided into the following components: (1) axial tension or compression perpendicular to the horizontal plane, (2) anterior-posterior shear perpendicular to the frontal plane, or (3) lateral shear perpendicular to the sagittal plane. Correspondingly, the components of the bending moment are categorized as follows: (1) flexion or extension in the sagittal plane, (2) lateral flexion in the coronal plane, and (3) axial torsion in the horizontal plane (Stemper et al., 2015b). Figure 4.6 shows exemplarily on a functional spine unit different loading directions.

6 Dvorak et al. (1988) showed that it is possible to achieve additional movement by applying external forces to the fully flexed or extended neck, which is considered passive in-vivo kinetics. The distinctions in active and passive in-vivo ranges of motion must be taken into account when interpreting laboratory and clinical normal range of motion studies (White and Panjabi, 1990).

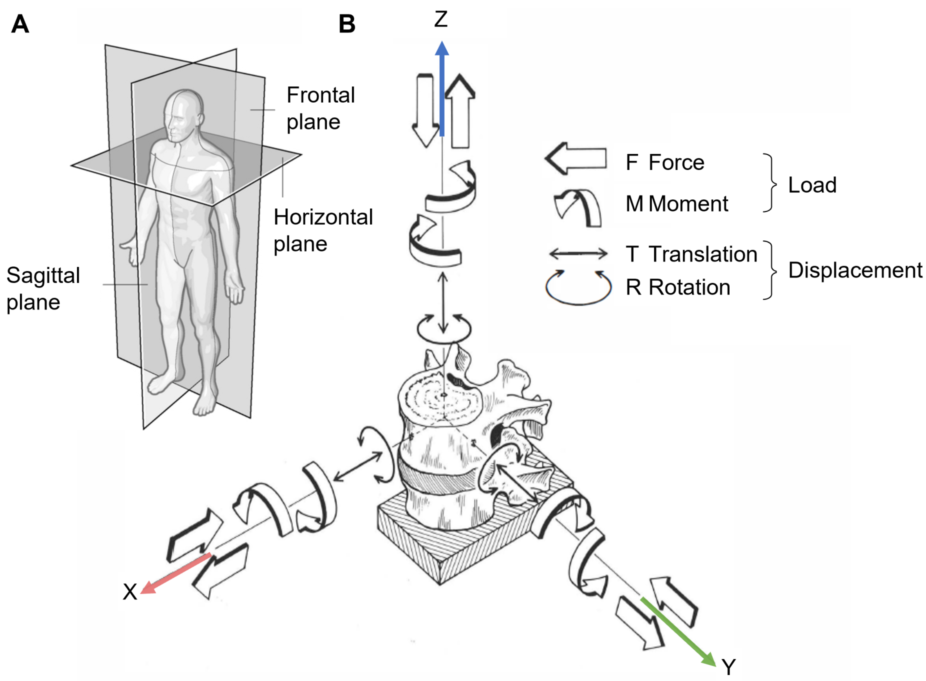

Figure 4.6: Schematic representation of **A** anatomical planes (modified after Anesthesia Key (2016)) and **B** different loading directions and resulting displacements (modified after White and Panjabi (1990)).

Loads can be applied to a system statically, quasi-statically, dynamically, or through explosive blast (speeds in excess of 35 m/s) depending on the loading rate. The speed range in automotive crashes is 5 to 30 m/s (King, 2018). Lumbar spine injuries result from the direct impact of force on the spinal column or certain vertebrae. Violence to the spine is usually caused by gross movement, acceleration of the body or torso, or blunt force trauma, in contrast to penetrating trauma.

Injury Classification

Injuries to the lumbar spine can be categorized in terms of stability (Nicoll, 1949), mechanism of injury (Holdsworth, 1963; Ferguson and Allen, 1984), morphology (Louis, 1977; Whitesides, 1977), prognostic aspects (Lob, 1954), or standardized clinical treatment with special focus on stabilization of spine injuries (Denis, 1983). A comprehensive classification scheme based on pathomorphological characteristics of the injuries was developed by Magerl et al. (1994). Based on Magerl's classification, the Arbeitsgemeinschaft für Osteosynthesefragen (AO) developed a system that both considers fracture morphology and factors relevant to clinical decision making (AO Spine, 2023). For the design of motor vehicles, injuries are described by injury severity via the anatomy based Abbreviated Injury Scale (AIS). In contrast, the AIS scoring scheme assesses the threat to life and not possible disabilities that may result from the consequences of injuries (King, 2018). King (2002) described the major modes of injuries to the spine in frontal and vertical decelerations and Stemper et al. (2015b) classified lumbar injuries due to loading mechanisms from the four external dynamic forces - tension, compression, shear or bending. The following is a summary of the injury types observed in dynamic axial acceleration events.

Burst Fractures

Burst fractures are the consequence of "pure compression transmitted directly along the z-axis of the vertebral bodies" (Stemper et al., 2015b, Figure 4.7 A). Due to the lumbar spine's inherent lordotic curvature, a pure state of compression can only be induced by preflexion (Holdsworth, 1963). This leads to a rather homogeneous compressive load in the vertebral body's axial plane, which in turn can lead to fracture of the anterior and posterior cortical bone. The burst pattern is the result of the fracture of one or both endplates caused by the axial force, which pushes the disc nucleus into the vertebral body (Holdsworth, 1963; Ferguson and Allen, 1984). In addition, neurological deficits can occur due to bone fragments being projected into the spinal canal (King, 2018). Fractures of the posterior element are also possible, although they are not a necessary condition for the classification in question. In the majority of cases, the ligaments remain intact, thereby maintaining the spine's mechanical stability. However, these injuries have been classified as both clinically stable (Ferguson and Allen, 1984) or unstable[7] due to progressive neurologic damage or progressive deformity after injury (Davies et al., 1980; Larson et al., 1999). Furthermore, Dai et al. (2004) and Wittenberg et al. (2002) found burst fractures commonly occurring in younger patients.

Anterior Wedge Fracture

Anterior wedge fractures are the result of axial compression coupled with flexion (White and Panjabi, 1990) or flexion only events (Holdsworth, 1963). The combined loading condition may be attributed to an axial load "applied anterior to the center of rotation of the vertebral segment or an axial load coupled with anterior bending of the torso" (Stemper et al., 2015b). On a tissue level, parts anterior to the center of rotation sustain compression while middle- and posterior-column parts are under tension. The wedge-shaped lateral profile characteristic of anterior wedge fractures is caused by a proportionally greater loss of height of the anterior vertebral body in relation to an often intact posterior vertebral body (Figure 4.7 B). If the posterior aspect of the vertebral body and the posterior ligamentous complex remain largely intact and the loss of anterior vertebral body height is less than 20 percent, the wedge fractures are defined as mild to moderate. These are considered stable (Westerborn and Olsson, 1951). Severe anterior wedge fractures are characterized by the protruding of the inferior facet joint over the superior articulating joint, irrespective of an impaired ISL, a fracture of the spinous process or a disc injury. These fractures described below are characterized as unstable and designated as fracture dislocations (Nicoll, 1949; Kifune et al., 1995; Yoganandan et al., 2014).

7 Clinical instability is "the loss of the ability of the spine under physiologic loads to maintain its pattern of displacement [mechanical instability] so that there is no initial or additional neurological deficit, no major deformity, and no incapacitating pain" (White and Panjabi, 1990).

Lateral Wedge Fracture

Two mechanisms are described in the literature by which lateral wedge fractures can occur - either flexion combined with rotation (Nicoll, 1949; White and Panjabi, 1990) or compression combined with lateral bending (Ferguson and Allen, 1984). Due to compression on the concave side and tension on the convex side, both mechanisms create unilateral wedging in which the opposite side remains intact. Compared to anterior wedge fractures, these injuries are manifest in the frontal plane and show a plane wedge-shaped profile. Lateral wedge fractures can also occur in combination with a fracture of the transverse process on the convex side and a fracture of the posterior intervertebral joint on the concave side (Nicoll, 1949). These injuries are typically regarded as clinically unstable, frequently accompanied by a prolonged unilateral neurological deficit.

Fracture Dislocation & Dislocations

In contrast to wedge fractures, fracture-dislocation fractures (Figure 4.7 C) are usually associated with a rupture of the posterior ISL and an associated dislocation (Nicoll, 1949). However, dislocations may occur even without any bony fracture (White and Panjabi, 1990). Facet dislocations may also be seen depending on the condition of the capsular ligaments. This can result in upward subluxation, protruding, forward dislocation with or without locking (Nicoll, 1949. The mechanism leading to dislocation injury is flexion in conjunction with axial rotation or lateral bending. Furthermore, “a large, coupled shear component can contribute to fracture dislocations” (White and Panjabi, 1990). From a clinically perspective, fracture dislocations are regarded unstable and prone to progressive deformity and acute neurological deterioration (Nicoll, 1949; Kaufer and Hayes, 1966; Ferguson and Allen, 1984).

Chance Fractures

The Chance fracture was first described in 1948 by George Chance (Chance, 1948). Injuries are caused by flexion combined with distraction. Characteristic of these fractures is the progression from the posterior region of the neural arch to the superior endplate (Figure 4.7 D). Frequently the splitting of the spinous process is involved. These injuries in car crashes were often attributed to the use of a lap seatbelt (Howland et al., 1965; Anderson et al., 1991). In particular, these mechanisms of injury appear to occur with improper use of lap belts or with immature pelvises to which restraint is to be provided (Howland et al., 1965; Anderson et al., 1991; Raney and Bennett, 1992). However, other authors have stated that these injuries are rarely seen in children (Gallagher and Heinrich, 1990).

The pelvic belt can slip over the iliac wings (see section *Submarining* for reference) and acts as a pivot point around which the spine rotates, can then lead to tension injuries in the posterior lumbar vertebrae (Steckler et al., 1969). By providing a shoulder belt, which is worn properly, to support the upper body with the introduction of the 3-point belt, the likelihood of these injuries can be minimized[8]. Clinically, these injuries are

8 Hence the introduction of the 3-point belt (Bohlin, 1964).

considered stable and the likely incidence of neurological deficit is low (Nicoll, 1949; Raney and Bennett, 1992).

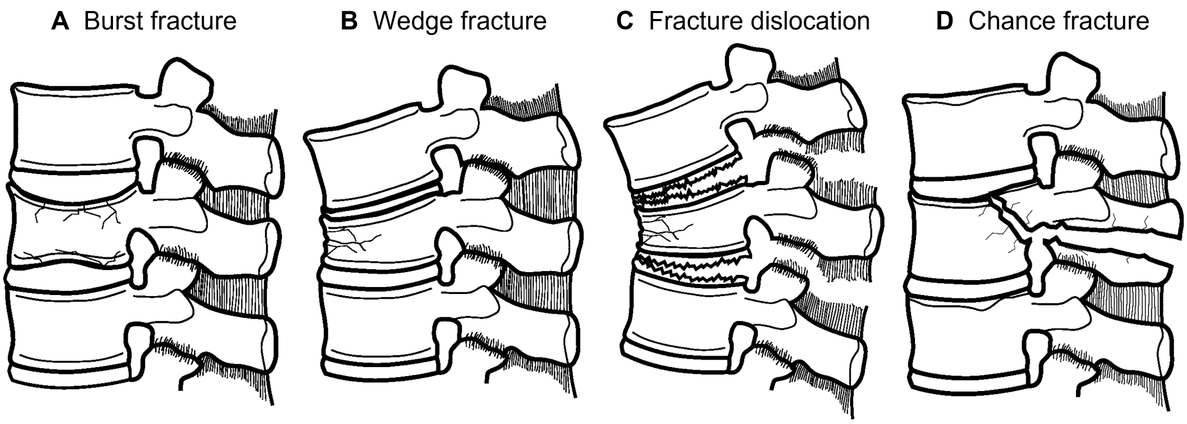

Figure 4.7: Injury types of the lumbar spine classified according to loading mechanism. **A** Burst fracture resulting from pure compression. **B** Anterior wedge fracture resulting from axial compression and/or flexion. **C** Fracture dislocation - body fracture and facet dislocation - as a result of flexion associated with axial rotation or lateral bending or shearing. **D** Chance fracture resulting from flexion (modified after Stemper et al. (2015b)).

Injury Frequency

As of now, lumbar spine injuries are relatively uncommon in automotive accidents (Müller et al., 2014; Kent et al., 2023). However, injuries of the lumbar spine are also of particular concern because their prevalence has remained mostly unchanged (Wang et al., 2009; Pintar et al., 2012), while the prevalence of other kinds of injuries has decreased (Isaksson-Hellman and Norin, 2005). In the historical context, frontal collisions have consistently resulted in a higher prevalence of lumbar spine injuries relative to other crash directions[9] (Pintar et al., 2012; Shaikh et al., 2020).

Compression and burst fractures occurred frequently at the transition between the thoracic and lumbar regions (T11-T12) and in the lower lumbar spine (L3-L5), most frequently at L1 (Pintar et al., 2012; Kaufman et al., 2013; Rao et al., 2014; Shaikh et al., 2020). The mechanism underlying these injuries has so far been characterized as compression loading or combined compression-flexion loading (Roaf, 1960; Holdsworth, 1963; Tran et al., 1995; Adams and Dolan, 2011).

As described in the beginning with the advent of HAVs and the associated higher prevalence of reclined seating positions, the lumbar spine loading mechanism might be amplified; studies have shown that reclined occupants are subjected to axial compression and flexion in the lumbar spine simultaneously and possibly out-of-phase (Ji et al., 2017; Katsuhara et al., 2017; Forman et al., 2019; Gepner et al., 2019; Rawska et al., 2019; Tang et al., 2020), with increasing recline angle increasing lumbar axial force

9 Frontal crashes are also significantly more prevalent than other crash types (Forman et al., 2019).

and flexion moment (Boyle et al., 2019; Rawska et al., 2019). In addition, compression and burst fractures were found in post mortem human surrogates (PMHS) subjected to frontal impact with occupants in upright postures (Begeman et al., 1973) and in reclined postures (Richardson et al., 2020a; Baudrit et al., 2022; Somasundaram et al., 2022; Richardson et al., 2023). The authors describe similar initial axial compression of the lumbar spine followed by forward rotation of the trunk, what resulted in a superposition of compression and flexion.

4.1.3 Lumbar Spine Injury Tolerance

To investigate the problem of injuries caused by acceleration in military environments, the US Department of Defense (DoD) conducted nonhuman primate (NHP) experiments at the US Naval Biodynamics Laboratory (NBDL) in the 1970's. The analysis focused in particular on the respective injuries and on the definition of injury risk curves based on vertical impact acceleration ($+G$z) experiments. In an effort to better understand the underlying mechanism of spinal injury, the kinematics and associated injuries of a subset of the data was re-evaluated. According to the analysis, the development of injuries during vertical acceleration seems to be caused by a flexion posture in conjunction with the torso load caused by the restraint. The injuries sustained by the NHP in this study are comparable to those that are evident in the automotive and military environments. However, appropriate scaling techniques, enabling comparison of the acceleration thresholds to human tolerances under $+G$z loading are difficult to define and were not defined. (Abraczinskas et al., 2018)

Since then, the lumbar spine has been the subject of numerous biomechanical studies. The spectrum of these investigations has ranged from isolated tissues and spinal segments such as lumbar columns to analyses of whole body cadavers. The reaction of the lumbar spine was examined under quasi-static and dynamic as well as physiological, degenerative, and traumatic conditions. The load was applied across all types (including bending, compression, and shear). In addition to focusing on understanding the biomechanics of the injury and the development of fracture patterns, these studies also compared surgical instrumentation techniques and measured the obstruction of the spinal canal. This research has yielded information regarding the effects of physiologic factors and injury tolerance. This thesis cannot provide a comprehensive overview of the complete state of biomechanical research in the area of the lumbar spine, although some of the relevant findings are discussed below.

To quantify the response of the structure and material of isolated components, tests were carried out on vertebral bodies, ligaments and annular tissue, among others. For instance, Pintar et al. (1992a) and Pintar et al. (1992a) characterized the quasi-static, dynamic, and viscoelastic behavior of isolated ligaments and annular tissue. Failure tolerance of isolated vertebral bodies has been quantified for compression (Hutton and Adams, 1982; Willén et al., 1984; Brinckmann et al., 1989; Ochia et al., 2003; Stemper et al., 2015a), flexion (Yoganandan et al., 1988b; Osvalder et al., 1990; Belwadi and Yang, 2008; Arregui-Dalmases et al., 2010), and combined anterior posterior shear and flexion (Osvalder et al., 1993; Belwadi and Yang, 2008). The investigation of the mechanics of vertebral body fractures has generally demonstrated an higher fracture tolerance at increased loading rates (Perey, 1957; Kazarian and Graves, 1977; Ochia et al., 2003; Stemper et al., 2012). As endplate strength is hypothesized to be decisive in the development of vertebral burst fractures (Holdsworth, 1963), studies on endplate tolerance were conducted too. These studies demonstrated that the tolerance of the endplate depends on both the test rate (Ochia et al., 2003) and the selected surface area (Hou and Yuan, 2012). Vertebral fracture displacement, force and stress were reported in the range of $2.3-6.5\,\mathrm{mm}$, $4.9-14.9\,\mathrm{kN}$ and $3.7-7.0\,\mathrm{N/mm^2}$, endplate fracture force and fracture stress were measured in the range of $55-170\,\mathrm{N}$ and $6.3-7.5\,\mathrm{N/mm^2}$.

Additionally, other studies on lumbar spine segments have published response data from axial compression (Yoganandan et al., 1988a; Kifune et al., 1995; Duma et al., 2006; Stemper et al., 2010; Yoganandan et al., 2013) or tension (Willén et al., 1984; Stemper et al., 2010) and from flexion (Yoganandan et al., 1994; Belwadi and Yang, 2008). An age-dependency was shown by Willén et al. (1984). Furthermore, these studies indicate, that burst fractures tend to occur generally under higher-rate loading scenarios (Perey, 1957; Willén et al., 1984; Kifune et al., 1995; Panjabi et al., 1995; 1998). Comparison of the reported fracture tolerance limits of spine segments tested in neutral and preflexed position indicate the importance of posture. They reveal that preflexion decreases fracture tolerance (Perey, 1957; Willén et al., 1984; Kifune et al., 1995; Panjabi et al., 1995; 1998; Langrana et al., 2002). There are also indications that the fracture tolerance increases with increasing axial load rates in a neutral specimen position (Ochia et al., 2003).

The above-mentioned experiments differed from earlier whole body PMHS and human body model (HBM) studies in terms of the boundary conditions. They were also quasi-static (Yoganandan et al., 1988b; Belwadi and Yang, 2008). Accordingly, the same conclusions cannot be drawn for car crashes with a high level of loading. Certain boundary conditions also resulted in kinematics and kinetics that are not comparable with flexion and torso inclination (Yoganandan et al., 1988b; Duma et al., 2006). A more recent study tried to overcome these issues and characterized failure tolerance of the lumbar spine in joint compression-flexion (Tushak et al., 2022). Fracture forces on lumbar spine segments were in the range of $2.8-13.2\,\mathrm{kN}$ depending on the tested lumbar spine level and the used testing apparatus.

To understand the lumbar spines' physiological reactions and injury tolerance, it is beneficial to perform tests on the entire lumbar spine, taking into account the lordotic curvature as well as all ligamentous structures. Two studies illustrate the dependency between fracture tolerance and loading rate. Looking at the two studies in parallel, despite different test protocols, it can be stated that fracture tolerance increases by 40 percent with dynamic loading. Yoganandan et al. (1990) examined complete lumbar spines in quasi-static tests ($2.5\,\mathrm{mm/s}$) in compression-flexion mode and observed fracture at an average load of $3.8 \pm 0.5\,\mathrm{kN}$ (mean±SD), whereas Duma et al. (2006) performed dynamic compression loading at a rate of $1.0\,\mathrm{m/s}$ and recorded a fracture tolerance as a combination of compression force and bending moment of between 5.4 ± 0.5 kN and 201.0 ± 51.0 Nm respectively.

A subsequent study from Stemper et al. (2011b) quantified the biomechanical tolerance to axial acceleration using compression rates between $0.5 - 1.3$ mm/s, rates of onset ranging from $228 - 2638$ g/s and peak accelerations of $20.7 - 65.0$ g. In general, the results (force-based tolerance: $5.2 - 7.8$ kN) of Stemper et al. (2017) are in accordance with previous experiments and shorter lumbar vertebral segments (3 - 5 vertebrae). However, in studies with single vertebral bodies, the authors described a higher tolerance and attributed this to a different mechanism of injury with structural failure of the cortices (Ochia et al., 2003; Stemper et al., 2015b).

In general, the findings of Stemper et al. (2017) indicated that force-based tolerance ($5.2 - 7.8$ kN) was consistent with previous shorter-segment lumbar spine testing (3 - 5 vertebrae). However, studies incorporating isolated vertebral bodies reported higher tolerance, which was attributed to a different injury mechanism involving structural failure of the cortical shell (Ochia et al., 2003; Stemper et al., 2015b). The conclusion of the study by Stemper et al. (2017) that more violent exposures lead to more injuries in the caudal lumbar spine is a new finding regarding the formation of injury patterns. According to the authors, two factors significantly promote caudal shift when high loading rates are applied: firstly, increased injury tolerance of the lower lumbar spine and secondly, faster mobilization of the inertial mass (Stemper et al., 2017).

4.1.4 Anthropometrical Variations of the Lumbar Spine

Each person's lumbar spine is individual and therefore has anthropometric variations. These are morphological (e.g., with regard to the height of the vertebral bodies) but also with regard to the alignment of the vertebral bodies and the spine. Inherently, this alignment is different for every person. In addition, there is the influence of different seating postures in different vehicles. This also changes the effect of the applied load and the injury tolerance, and therefore also the individual risk of injury (Stemper et al., 2015a; Izumiyama et al., 2018).

Posture is defined as "A position of a person's body or body parts" (American Heritage, 2023), whereas spinal position/orientation is physiologically determined. Whole spinal alignment has been studied in different postures in numerous studies. For further details regarding spinal alignment, reference is made to section 8.1. This subsection will focus on anthropometric variations underlying the variability of spinal alignments.

In the above-mentioned studies lumbar spine segments or columns were either tested in a preflexed, a neutral, or a preextended position. These positions correlate with the postures - preflexed, nominal and preextended - denoted and determined by Reed et al. (2013) through the University of Michigan Transportation Research Institute (UMTRI) study on seated soldiers. While the neutral (unloaded) position is inherently dependent only on the shape of the vertebrae and IVDs (Whitcome et al., 2007), the flexed and extended positions are additionally determined by the lumbar spines' range of motion (Reed et al., 2013).

Studies have analyzed vertebral body shape variation in the lumbar spine (Masharawi et al., 2008; Abu-Leil et al., 2016), lumbar facet orientation (Masharawi et al., 2004; 2005; 2007), neural arch shape variation (Masharawi, 2012) and of the lumbar IVDs (Abu-Leil et al., 2016). The variance of selected anthropometric parameters is listed in Table 4.1.

Table 4.1: Selected anthropometrical parameter variations of the lateral lumbar spine. Parameter variations include all genders, populations, heights, and weights. Age ranges from 20 to 80 years (Masharawi et al., 2008; Abu-Leil et al., 2016).

Lumbar level	**Ant. VB height** Mean±SD in mm	**Post. VB height** Mean±SD in mm	**Ant. IVD height** Mean±SD in mm	**Post. IVD height** Mean±SD in mm
L1 resp. L1-L2	24.9±2.5	27.5±2.3	5.3±1.6	2.3±1.2
L2 resp. L2-L3	25.8±2.5	27.5±3.3	6.0±1.8	2.7±1.6
L3 resp. L3-L4	26.1±2.2	27.0±2.8	7.0±1.9	3.3±1.8
L4 resp. L4-L5	25.8±2.5	25.4±2.8	8.8±1.9	3.2±1.5
L5 resp. L5-S1	26.8±2.7	23.2±2.9	10.1±3.5	1.9±1.8

4.2 Strategies to Investigate Lumbar Spine Biomechanical Tolerance

In assessing the effectiveness of passive safety systems to protect occupants in crash events, the use of anthropometric test devices (ATDs) in combination with ATD-related load limits is required by law in the design of vehicle safety systems (Pischinger and Seiffert, 2021). ATDs serve as human surrogates and are used since tests with the potential for injury cannot be performed on living subjects for ethical reasons (King, 2018). ATDs are equipped with sensors to be able to define protection criteria on the one hand and to be able to measure legal requirements in terms of limits on the other hand. The ATD related regulations are essentially based on injury criteria and load limits, which are determined by crash analyses and biomechanical experiments. In this context, crash analysis is used to determine types and mechanisms of injuries and biomechanical experiments to explore load limits. These biomechanical load limits and injury risk curves form the basis for load limits and injury risk curves related to test facilities (ATDs). They also depend on the type of ATD used, the load case and world-region-specific requirements. (Pischinger and Seiffert, 2021)

It can be reasonably deduced that reliable tolerance limits necessitate a substantial quantity of laboratory-based injury data, preferably from human subjects[10]. Insights can be drawn in biomechanics from volunteer trials, sports medicine, animal studies, or cadaveric studies. Voluntary tests and findings from sports medicine are limited to the extent that the testable load level must be far below irreversible injuries[11] and the measurement possibilities are limited. In addition to the questionable ethical justifiability of animal experiments, the transferability of the findings to humans is only possible to a limited extent. In cadaveric tests on human bodies, the loading characteristics are known, and the injury is ideally directly detectable/measurable. However, muscle tone, vascular pressures, possible protective postures (bracing) and support reactions are difficult (but not impossible) to reproduce in cadaveric tests (Hardy, 2002). In addition, due to the limited availability of PMHS, PMHS are mostly older subjects or subjects altered by disease.

ATDs are usually available in three standardized sizes: 5th percentile female (1.51 m; 46.8 kg), and 50th male (1.75 m; 78.2 kg) as well as 95th percentile male dummy (1.87 m; 102.7 kg)[12]. They are load case-dependent (Pischinger and Seiffert, 2021). In the 1940s ATDs were developed based on cadaveric tests of male and female PMHS and animal studies to be biofidelic[13]. That ATDs reflect the responses of the human body to

10 The deliberate infliction of injury upon a human being constitutes an unethical practice. Therefore, the human subjects employed in the conduct of tolerance testing are instrumented cadavers donated for scientific research purposes (King, 2018).

11 There are sports such as football, rugby and boxing that can cause irreversible injuries.

12 In the Hybrid-III family, 5th percentile female and 95th percentile male are scaled 50th percentile male dummies. For the 5th percentile female, the pelvis has been adapted with 5th percentile female radiology scans (Mertz et al., 1989).

13 Biofidelity is a measure of the representation quality of physical human characteristics (ISO/TR 9790, 1999).

external stimuli - their biofidelity - is tested using cadaveric or volunteer tests. The main difficulty for biofideltiy adjustment and determination of injury risk curves is the paucity of adequate biomechanical data. The majority of biomechanical experiments are carried out with a relatively small sample size (usually single-digit), which have very different failure thresholds (for example through age). Censored biomechanical data further impedes the estimation of injury thresholds of the population tested and the extrapolation of results to specific percentiles. That is, no tests are performed directly at the specimens' level of failure because the stimulus has an unknown deviation from the level of failure (Mertz, 2002). Nevertheless, ATDs have evolved since their initial introduction and now exist in a digital format as finite element (FE) models. Numerous issues arising in terms of physical crashes (e.g., calibration, sensor failures) that need to be managed when using hardware dummies can be circumvented by such FE models. In addition, simulation models can be used to repeat a large number of variants only limited by computational power. They also feature safety, cost efficiency and reproducibility.

At present, there is no consensus regarding the acceptable limits for lumbar loading in vehicle occupants. Further research is therefore needed to investigate and formulate injury criteria[14]. The challenge is the lack of crash research data available for the development of injury criteria. This lack of data motivates the use of human body models (HBMs). A validated[15] HBM can be used to analyze non-standard driving postures, such as in autonomous driving or reclined seating positions, and reduce the costs of conducting PMHS tests. Besides, HBMs offer the possibility to develop safety systems taking into consideration various human anthropometries. Figure 4.8 shows an exemplarily comparison of an FE Hybrid-III 50th Male ATD and a THUMS v4.1 HBM with particular regard to spinal depiction.

14 In an endeavor to enhance the biofidelity of the Test Device for Human Occupant Restraint (THOR), the lumbar spine region was revised and equipped with additional sensors (Ridella and Parent, 2011). Besides mechanical problems that occurred during positioning in reclined positions (Forman et al., 2021), biofidelity evaluations of Hybrid-III 50th Male and the THOR-50M in frontal impact sled tests in reclined position, revealed differences between the two ATDs in the spine force signals along the z-axis and spine moment about the y-axis. The differences, which can be attributed to differences in the location of compliant elements, should be resolved before an injury risk prediction metric is developed (Shin et al., 2022).

15 Validation is a prerequisite to use HBMs in vehicle safety systems design.

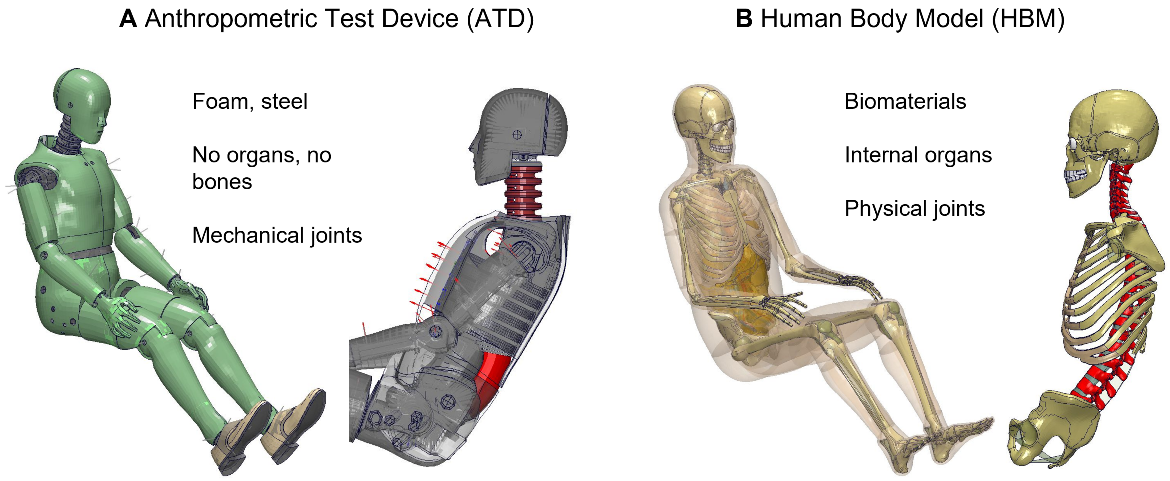

Figure 4.8: Comparison of **A** anthropometric test devices (ATDs) and **B** human body models (HBMs) exemplarily for a Hybrid-III 50th Male ATD and a THUMS v4.1 HBM with particular regard to spinal depiction. Injury risk is based on sensor measurements with ATDs, and the dummy type is dependent on the load case. HBMs enable the analysis of injury mechanisms and one model can be used to assess several load cases.

Basic Principles of Risk Evaluation using HBMs

The motivation to use virtual testing in regulatory and consumer testing has increased over the last decades (Automotive World, 2020). Besides replacing real testing based procedures by virtual testing and extending the scope of protection by adding combined real and virtual testing procedures, EuroNCAP has put virtual testing using HBMs on the Roadmap 2030 (Eggers and Peldschus, 2022). Other NCAPs are also considering the adoption of HBMs as part of virtual testing in the near future. Additionally, several projects like the EU-Project OSCCAR (OSCCAR, 2020) or VIRTUAL (VIRTUAL, 2023) were conducted in the past years. Addressing the limitations of ATDs, HBMs have been adopted by all major OEMs worldwide as tool of choice, e.g., for the evaluation of new seat configurations in the interior of the vehicle.

HBMs are an attempt to describe the human body in crash behavior numerically. Depending on the development of modeling techniques in injury biomechanics, the model can be categorized to either lumped-mass models (Hodgson et al., 1967), linkage models (McHenry, 1963), or FE models (Huang et al., 1994). However, the most common technique of HBM modeling which allows the most detailed geometrical representation of the human body and direct estimation of injuries is the finite element method (FEM) (Iwamoto et al., 2002; Yang et al., 2006). Logically, FEM is based on the numerical solution of a complex system of partial differential equations. Therefore, the computational domain (e.g., a solid) is divided into finitely many subdomains (e.g., subbodies or elements) of simple shape, e.g., into many small cuboids or tetrahedra. Due to their simple geometry, their physical behavior can be calculated with known shape functions. The physical behavior of the entire body is then simulated by how these elements react to forces, loads, and boundary conditions as well as how loads and reactions are propagated from one element to the next by specific problem-dependent continuity conditions that must be fulfilled by the shape functions.

To facilitate the rapid and precise simulation of highly dynamic events, explicit[16] solvers are used for equation solving (Sun et al., 2000). Two of the explicit FE analysis codes used for automotive crash simulation studies are the commercial crash simulation codes Virtual Performance Solution (VPS, ESI Group, Rungis Cedex, France) and LS-DYNA (LSTC, DYNAmore, Gesellschaft für FEM Ingenieurdienstleistungen mbH, Stuttgart, Germany) (Iwamoto et al., 2002). At Volkswagen, VPS is used for the virtual safety design of vehicle structures.

There are several commercially available and open-source HBMs on the market[17]. What most of them have in common is that they are developed in LS-DYNA. To be able to couple vehicle projects based on VPS with HBMs based on LS-DYNA, either a two-process approach is necessary or a translation from LS-DYNA-based HBMs to VPS. As coupling of methods can shorten the design cycles, HBMs were translated to VPS (Yang, 2018a). Translation and robustness check was performed by ESI Group (Rungis Cedex, France). The family of HBMs is constantly growing, two models that are available in VPS and are also most widely used are the Total HUman Model for Safety (THUMS, Toyota Motor Corporation, Toyota, Japan) and the Global Human Body Model Consortium (GHBMC, Elemance, LLC, Winston Salem, USA).

Toyota Motor Corporation & Toyota Central R&D Labs launched the first version of THUMS in 2000 in LS-DYNA. Since then, due in part to increases in computing power capabilities, newer numerical models became more detailed and anatomically refined with improved material properties (Yang et al., 2006). Due to its computing stability in the cluster the THUMS v4.1 AM50 occupant model in VPS was selected for this study. THUMS v4.1 is generated by integrating component models of the head, torso, and extremities. The model consists of approximately 1.8 million elements and 630,000 nodes. Its height is 178.6 cm and its weight is 74.3 kg, close to what is defined as a 50th percentile adult male in dummy technology (175 cm, 78.2 kg) (NHTSA, 2023). THUMS v4.1 is a passive human body model, meaning only passive musculature structures are modeled (Toyota Motor Corporation, 2011). Since the present study focuses on the comparison of the HBM with cadaver test data, this approach seems to be sufficient here (Kallieris et al., 1995).

16 "In nonlinear implicit analysis, the solution of each step requires a series of trial solutions (iterations) to establish an equilibrium within a certain tolerance. In explicit analysis, no iteration is required as the nodal accelerations are solved directly" (DYNAmore GmbH, 2023).

17 The existence of different HBMs in different solvers poses new challenges for the automotive industry. To be able to use the HBMs for vehicle safety systems design, there have been harmonization efforts since 2022. One aspect that must be critically appreciated is that different solvers partially provide different results (with the same setup) (Gepner et al., 2019) and that the application of HBMs can lead to large deviations in the response to the smallest changes.

Biofidelity and impact responses of numerical human models are verified[18] and partially validated[19] against available experimental data both on component level and on whole-body levels by the developer (Toyota Motor Corporation, 2011). Using this hierarchical approach allows the complexity of the human body system to be decomposed into smaller, more manageable problems, which can then be addressed (Oberkampf et al., 2004). Validation can be performed on two different levels. On the first level, a set of predictions generated by a deterministic model is compared with experimental data. In other words, FE models that are conceptualized for material property identification are to be validated against highly repeatable experimental data. In contrast, the second level entails the comparison of one single set of deterministic model predictions against the corridors or distribution functions derived from multiple experimental datasets. This level of validation is predicated on the assumption that the material properties, loading, and boundary conditions are known, yet the experimental data lacks sufficient reproducibility. (Yang et al., 2006).

However, much of the available data was not acquired for the purposes of model validation. As a consequence, the studies often do not provide sufficiently detailed boundary conditions of the experiment (Yang et al., 2006), lack information necessary for simulative modeling (Funk et al., 2004; Forman et al., 2012; G. Park et al., 2018), or even the experiments are inherently incompatible for simulative modeling. Another aspect that comes into effect here is that most biomechanical experiments examine physiological (for example Wilke et al., 1998) or quasi-static loading conditions (for example Tushak et al., 2022). In injury biomechanics, the often time-dependent, anisotropic and strain rate dependent human tissues must be further characterized under high-speed automotive conditions to cover all potential responses in automotive settings and to reflect the application/assessment load case as closely as possible (Eggers and Peldschus, 2022).

Materials that are characterized and validated according to the application load case are a necessary prerequisite for the deduction of injury mechanisms based on validated models and the investigation of impact reactions under conditions where experiments are difficult to perform (Yang et al., 2006). In addition, injury prediction on a tissue level, a key advantage of HBMs in contrast to ATDs, can only be exploited using validated models. Validation of HBMs is elementary to ensure biofidelity and to be able to use them for the design of vehicle safety systems. However, whether the biofidelity of HBMs is superior to current ATDs is questionable. While simulation models of ATDs[20] can be matched with their physical counterparts, HBMs are reliant on PMHS tests. However, to what extent PMHS tests are comparable with real-world data is unclear.

18 In the Performance Test Codes (PTC) 60/V&V 10 (ASME, 2020), the American Society of Mechanical Engineers (ASME) defines verification as “the process of determining that a computational model accurately represents the underlying mathematical model and its solution”.

19 In accordance with the ASME definition, validation is the process of quantifying the accuracy of predictions generated by a FE model in comparison to real experimental data.

20 The development of ATDs, however, is based on the same reference experiments due to their limited availability.

HBMs have ideally omni-directional usability, meaning they are load-case independent and can theoretically be placed in any seating position (Pipkorn et al., 2018), although they are usually delivered and validated by the supplier in only two positions: upright for pedestrian application and seated in a standard driver posture for occupant simulation. ATDs, in contrast, can only be used in specific load cases. A side crash dummy can only measure rib displacements in a side crash, for example. The positioning of an HBM is not only a challenge for its application in non-standard seating positions but also for their validation and for future virtual testing procedures. The developed positioning methods can be categorized into geometry-based (Jani et al., 2012; Chhabra et al., 2017) and simulation-based methods (Beillas and Berthet, 2017; Germanetti et al., 2020). Every positioning method for HBMs has its own issues and challenges (C. Klein et al., 2021).

Although HBMs could represent a diverse population (e.g. age, size, body mass index (BMI), gender), they are usually limited to a few sizes that resemble the dummies (e.g. 50th percentile male, 5th percentile female), and developing additional age/size models by conventional methods is costly (Jolivet et al., 2015). To simulate variance within population, the concept of parametric human FE modeling on the basis of mesh morphing is used (Shi et al., 2014). The basic concept behind parametric human FE modeling is to morph/scale[21] a baseline model into different geometries (Hu et al., 2012). In a significant number of studies non-rigid deformation techniques were used to morph FE models into distinct target geometries at the level of a single bone (Couteau et al., 2000; Grosland et al., 2009; Bryan et al., 2010; Grassi et al., 2011; Hazrati Marangalou et al., 2013; Bonaretti et al., 2014), an organ (Besnault et al., 1998; Salo et al., 2015), a body region (O'Reilly and Whyne, 2008; Bucki et al., 2010; Li et al., 2012; Shi et al., 2014; Shim et al., 2014; Teshima et al., 2015; Zhang et al., 2016; O'Cain et al., 2019), or to whole-body human models (Vavalle et al., 2014; Jolivet et al., 2015; K. F. Klein et al., 2015; Nérot et al., 2015; Schoell et al., 2015; Zhang et al., 2016; Zhu et al., 2016; Beillas and Berthet, 2017). What they all have in common is the dependency on the presence of anthropometric data on which the baseline FE models are to be morphed to adapt not only the geometry, but also to transform the respective risk assessment functions.

In the science of biomechanics, the level of detail or complexity of the simulation model depends on the desired application, the available computing power, time, cost, and the stability of the numerical model. In automotive injury biomechanics, the first area of interest is to ensure that the kinematics of the human model correctly depict the kinematics of the occupant in crash scenarios. After this has been established, the injury risk can be assessed. Therefore, in the virtual human body depiction, the complexity of the body parts is reduced to a meta-level between the organ level and the tissue level (Yang et al., 2006). On the one hand, this allows the representation of

21 Scaling refers to the targeted modification of an existing model and can be conducted out on almost all of the modelling parameters (including dimensional definition - geometry, mass and inertia, surface and sensor locations; restraints and constraints - joints and restraints, contact; muscle models and actuators as well as output) possible model parameters. Whereas morphing refers to a targeted change in geometry. (Yang et al., 2006)

elementary material properties, and, on the other hand, it reduces the computation time and increases the stability (Yang, 2018b). The reduction of complexity in a virtual depiction is described below based on the lumbar spine model in THUMS v4.1 used in this study.

A THUMS v4.1 sagittal cut in median plane of a L3 to L5 lumbar spine unit is shown exemplarily in Figure 4.9. The lumbar spine model in THUMS v4.1 (T12 to L5) includes all skeletal parts (vertebrae) and the major soft tissues (IVDs and ligaments). In the VPS model, the structure is comprised of solid, shell, and bar elements. It consists of 60,637 elements in total. Each vertebra is composed of shell elements for the cortical bones as well as solid elements for spongious bones. Solid elements are also used to model IVDs. *Tension-only bar elements* were used to model the fibers of the discs. Shell elements are used for the ligaments. All parts in the lumbar spine model are modelled as deformable. The bones are assumed to be elastic viscoplastic, while foam type materials are assumed for the IVDs. The IVDs are further classified into nucleus and annulus fibrosus, which have different material definitions (Figure 4.4). Within a vertebral bone, the cortical bone and spongiosa are rigidly conjoined. Inferior and superior articular process are connected via membrane elements forming the CL[22]. To describe the contact situation between two adjacent vertebral bones, an *automatic surface to surface contact* is defined over the entire spinal column. The ligaments' stiffness is characterized by two force versus strain curves for unloading and loading. Endplates and discs as well as ligaments and vertebral bones at the attachment point share the same nodes.

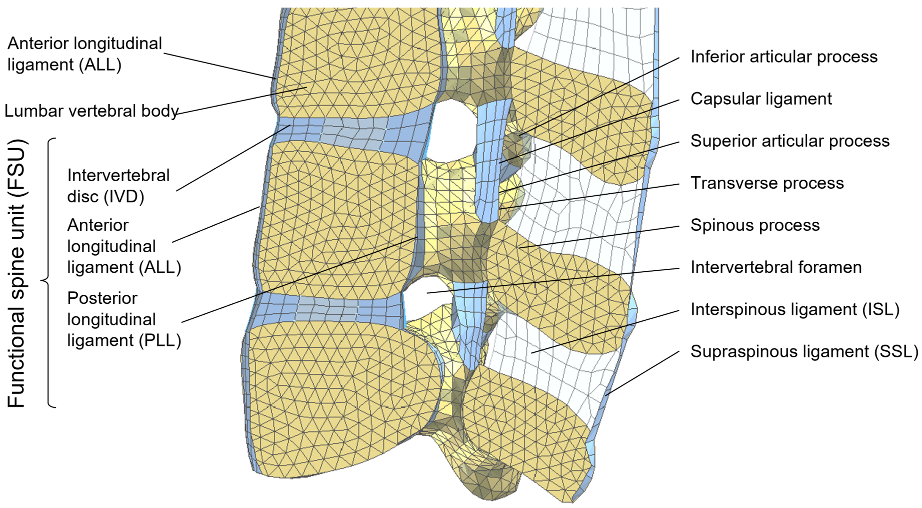

Figure 4.9: Sagittal cut in median plane of L3 to L5 lumbar spine unit of THUMS v4.1. The spinal cord was not included for the sake of clarity.

22 The facet joints are not modelled as joints.

Experimental techniques typically yield only limited measurements[23], such as the failure strain, maximum force, maximum deflection, and/or peak acceleration at specific locations. In contrast, a FE model enables the investigation of a much broader range of response variables, including stress that cannot be measured using experimental techniques and at any location within the model (Yang, 2018b).

The protection of automobile occupants against injuries requires a strategy to use the superior features of FE models. These methods may be grouped into two categories: deterministic and probabilistic. Deterministic models are designed to predict an exact occurrence (or number) of defined injuries based on a single set of model features, i.e., occupant features. They are limited in that they are intended to predict injury in a binary fashion (injured/not injured) on the basis of a specific set of occupant characteristics. As a result, the ability of deterministic methods is restricted to predict injury occurrence in a population with varying physical characteristics. In contrast, probabilistic methods attempt to predict the probability of injury in a given scenario, affected by variations in occupant or collision characteristics. Unlike the standard dummy technology, it is feasible because of the high level of modeling detail possible to incorporate probabilistic analyses into FE model injury prediction in a 'bottom-up'[24] approach. This is an improvement over empirical strategies because it allows injury prediction based on known variations in anthropometry, skeletal mechanics, tempora mutantur et cetera.

In general, a bottom-up approach starts with a prior power analysis in which the required sample size of a defined set of parameters is to be determined. This is followed by the sampling procedure, where the design matrix based on the distribution of the parameters is defined and the FE models are generated. In the third step, characterization of probability distributions of predefined response variables uncertainty and characterization of the relationship of input variables and model response sensitivity is analyzed. Two such studies by Forman et al. (2012, 2022), which developed an analysis strategy for the prediction of rib fracture risks, exploited this concept via incorporating known variations of rib cortical bone ultimate strain. Their analysis assumed that each fracture was an independent event, where a fracture at one site does not affect the probability of fracture at another site. According to the authors, there is evidence suggesting that a small to moderate number of rib fractures have negligible effect on the overall stiffness of the chest. Thus, they limited the prediction of incremental changes in the number of rib fractures in their study. Whether this assumption is also permissible for other areas of the body remains questionable. Studying distinct fracture occurrence after destabilization through initial fractures would require the

23 In experimental biomechanics there is a trade-off in how many sensors can be attached and how these sensors affect the material behavior or kinematic/dynamic response behavior under test. (Hardy, 2002). For example, sensors can lead to artificial stiffening, weakening of bones or crack limiting, affecting bone fracture behavior (Richardson et al., 2020c).

24 In the 'top-down' approach, the occurrence of injuries (often in a cadaver model) is related to dummy measurements under adjusted collision conditions. In the 'bottom-up' approach, on the other hand, subject variations or collision characteristics occurring at the component level can be included in the simulation strategy.

use of a frangible FE model implementing probabilistic methods in the simulation matrix design. However, a probabilistic approach requires an (experimentally) obtained cumulative distribution function (CDF) of anthropometrical parameters and a FE model, which can be adapted to the defined parameters.

4.3 Thesis Overall Aim and Objectives

For the case of the lumbar spine, many different injury patterns have been observed in traditional seating positions[25] (Begeman et al., 1973; Patrick and Levine, 1975; Kallieris et al., 1984; Rouhana et al., 2003; Uriot et al., 2015) and for the case of reclined seating positions there are still many unknowns, not only about injury type and injury prevalence but also concerning the spinal kinematics and how ergonomic and subject specific factors will influence both kinematic and injury outcomes. Therefore, the aim of this study is to establish a strategy for handling anthropometrical lumbar spine differences in assessing spinal injuries within virtual vehicle development with HBMs. This study focuses on the following objectives:

- ***To design a method to identify the position and orientation of a vertebra.***

To be able to investigate anthropometrical differences in the spine, quantitative unambiguous measurements enabling determination of the exact position and orientation of each vertebra regardless of the type of data is needed.
Thus, the first objective of this thesis is to develop a method for identification of position and orientation of a vertebra equally applicable to experimental data and FE models.

- ***To investigate if subject-specific whole lumbar spine models could match failure patterns and injury mechanisms.***

The initial lumbar spine position seems to claim a major role in kinematic responses in simulations of a dynamic load case (Draper, 2022). Other considerable variations in the kinematics might result from the deviation of simulative and experimental boundary conditions, age dependency of material properties and vertebral morphometry.
Therefore, the second objective of this thesis is to assess failure patterns and injury mechanisms matching capabilities of subject-specific lumbar spine models. The focus in this study lies in morphometrical differences of vertebral bodies and IVDs while neglecting differences in material properties.

- ***To propose a methodology on an approach to deal with different anthropometry in vehicle development.***

It has been shown that the influence of some morphometrical spinal features on the response of numerical models is negligible and they do not need to be modeled overly accurate (Niemeyer et al., 2012). The characteristics of the geometry of the lumbar spine that induce the most significant changes in responses need to be better understood. Specifically, the hypothesis was that lumbar spine simulation models are sensitive to changes in direction of force transmission either caused through changes in initial intervertebral angles (non-pathological spinal curvature variances) or vertebral wedging.

25 These studies were conducted using (semi-)rigid seats. This is only partially applicable to derive injury events in commercial vehicle seats, but nevertheless offers an advantage in the investigation of occupant or restraint systems compared to commercial vehicle seats due to clearly definable simple properties, repeatability of the tests and high comparability between studies (Richardson et al., 2020a).

Thus, the third objective is to formulate positioning specifications to define uncertainties in tissue-based load limits stemming from anthropometric differences.

5 Reference Points Describing Spinal Posture

Previous studies have analyzed whole spinal alignments in different positions through medical imaging data (Hardacker et al., 1997; Janssen et al., 2009; Ames et al., 2013; M. S. Park et al., 2013; Parenteau et al., 2014; Sato et al., 2021; Izumiyama et al., 2022). Usually spinal alignment is described using global angles of spinal segments on sagittal two-dimensional (2D) data - either X-rays (Andersson et al., 1979; Rocabado, 1983; Harrison et al., 2000; Berthonnaud et al., 2005; Roussouly et al., 2005; Armijo-Olivo et al., 2006; Mac-Thiong et al., 2007; de Carvalho and Callaghan, 2012; S.-M. Park et al., 2015; Izumiyama et al., 2018; 2022), midsagittal magnetic resonance imaging (MRI) (Sato et al., 2021) or computer tomography (CT) images. These global angles were originally derived from scoliosis studies and diagnoses (Cobb, 1948) and have also been the used in studies on automotive injuries with human body models (HBMs) to identify relevant global trends (Izumiyama et al., 2018; 2022). Besides, the geometrical center of the vertebral bodies in 2D data was also used to study spinal alignment patterns (Sato et al., 2021).

However, the use of midsagittal images can be disadvantageous as information in the other planes is neglected and in case of three-dimensional (3D) imaging data the choice of the midsagittal image is somehow subjective. Furthermore, the construction of the geometric center of the vertebral body can be ambiguous as there are several ways to calculate the geometrical center. Besides, the determination of the spinal segmental angles is dependent on the wedging of the vertebral bodies. Global spinal segmental angles can be useful, but they lack the detailed information required to correctly position a spinal model vertebra by vertebra (Draper, 2022). For the implementation and investigation of different spinal alignments via HBMs, information about the precise position of a vertebral body and its angle in relation to its adjacent vertebra would be necessary.

Therefore, a method non-ambiguously describing spinal alignment in the global coordinate system equally applicable to finite element (FE) models as well as human beings is needed. In addition, a method for determining the position that can be used for both experimental data and Fe models removes an uncertainty factor and also guarantees the consistency of the positions of both sources (Draper, 2022).

Reference points would allow not only the comparison of different HBMs but also of HBMs and real human beings. Besides, they would serve for the standardization of pre- and post-processing procedures, known as harmonization, in the use of HBMs, helping to build up a kinematic chain for positioning of HBMs and could serve as re-meshing constraint (Fuchs and Peldschus, 2016). A method for geometrical determination of reference points and integration of a local coordinate system was proposed by Draper et al. (2020). This approach is applicable to both experimental data (in this case X-rays and 3D CT scans or MRI scans) as well as for FE models to reproduce this data. Besides, this standardized framework is code agnostic and has the objective of facilitating more consistent comparisons across and within data sources.

However, the drawback of the method is that it relies on perfect axial symmetry of the vertebra in the sagittal plane. Most of the vertebra in FE models show perfect axial symmetry in the sagittal plane (Yang, 2018c), actual human vertebrae in contrast show normal asymmetry (Masharawi and Salame, 2011). Therefore, the method developed by Draper (2022) was extended by also taking in consideration the level of information in the third dimension. Additionally, an approach for the integration of local coordinate systems is presented in the subsequent. The method is implemented semi-automated via a Python script and is available for download via the THUMS User Community (TUC) repository.

5.1 Geometrical Construction of Vertebral Reference Points

Experimental vertebrae need to be segmented before application of the methodology. Figure 5.1 exemplarily shows the segmentation process on a CT data set. Segmentation can be done via a semi-automated threshold method (A), followed by filling, and smoothing of the 3D-reconstructed structure (B & C) and exporting the vertebra in the form of a nodal structure (D) (e.g., via the .stl file format).

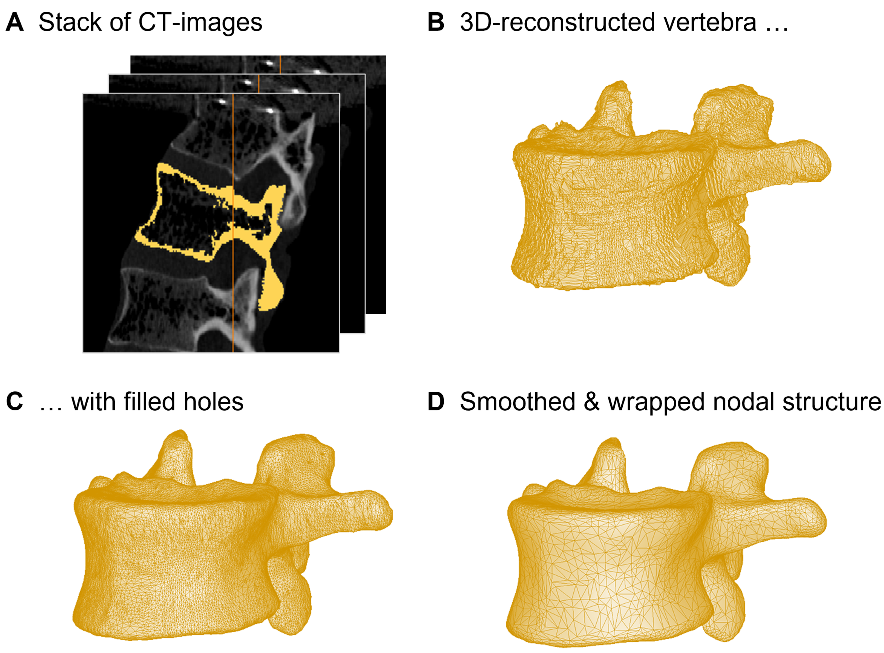

Figure 5.1: Schematic representation of the preparation of an experimental dataset before geometrical construction of vertebral reference points. **A** shows a stack of computer tomography (CT) images from lateral, **B** a 3D-reconstructed vertebra, **C** a 3D-reconstructed vertebra with filled holes and **D** an exportable nodal structure with a smoothed surface exemplarily for a second lumbar vertebra (L2).

The next steps are the same for both the experimental vertebral data and the finite element method (FEM) vertebral data (Figure 5.2). The procedure commences with the identification of both vertebral endplates and the subsequent assignment of a respective plane. This is achieved by identifying the best fitting plane for all nodes of each endplate. The area center of each of the endplates is the mean of the selected nodes for each of the endplates and is defined as the endplates' center points c_{TEP} and c_{BEP}.

To create the center plane, the best fitting planes assigned to the endplates are then averaged. The center of the vertebral body c_{VB} is specified by the intersection between the midplane and the line which connects the two midpoints of the upper and lower endplates. The normal of the midplane intersecting the center of the vertebral body c_{VB} describes the local z-axis of the vertebra.

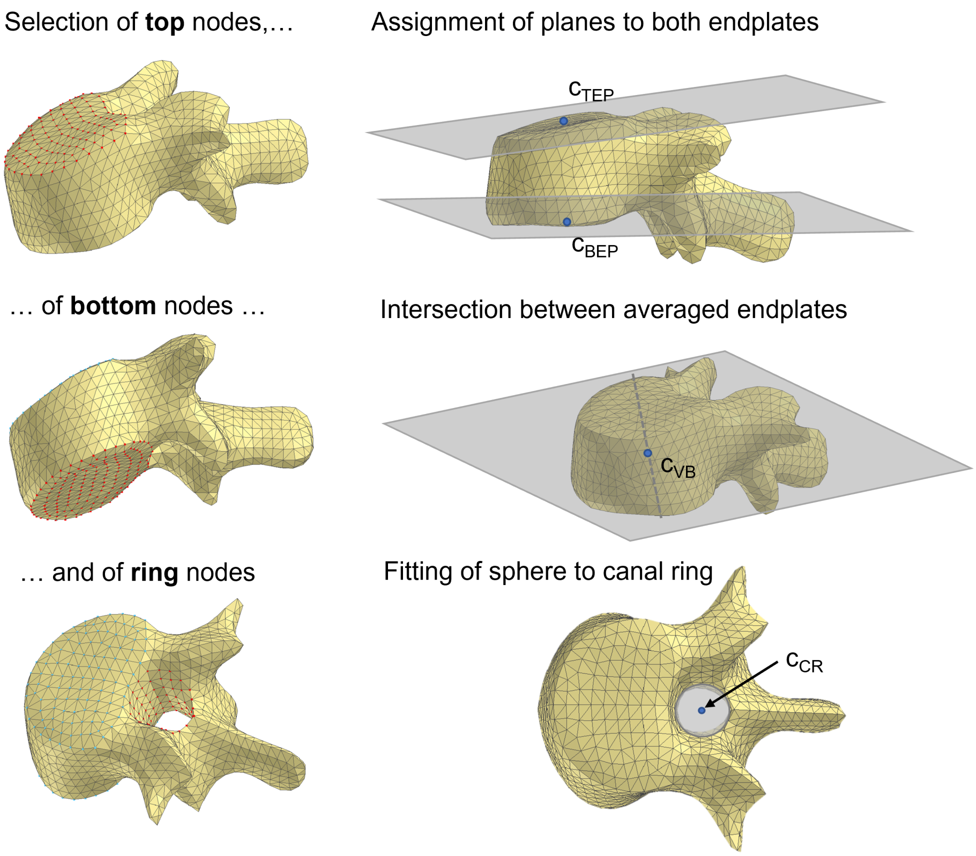

Figure 5.2: Schematic representation of construction of vertebral reference points exemplarily for L2 vertebra of a FE model.

On the basis of the selected nodes of the inner surface of the spinal canal ring, the interpolated centroid[1] is calculated to define the local x-axis.

1 Arithmetic mean or average position of all points on the surface of the object

The local x-axis is defined as the vector originating from the projected center point of the spinal canal on the new midplane c_{CR} to the center point of the vertebral body c_{VB}. The local y-axis is defined via the cross product of the local x-axes and z-axes. A schematic visualization of the local coordinate construction is shown in Figure 5.3.

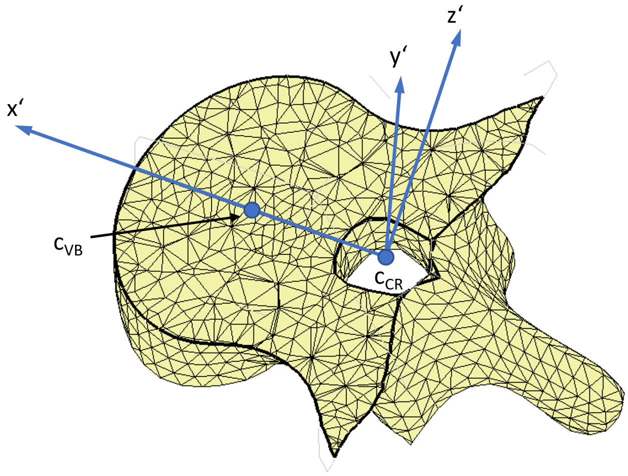

Figure 5.3: Visualization of the local coordinate system construction exemplified by a vertebral body. Local x-, y- and z-axis are shown as well as center of the vertebral body and center of the spinal canal.

Axis conventions follow the description of the Scoliosis Research Society (Stokes, 1994) with local x-axis anterior, local y-axis to the left and local z-axis cephalad.

5.2 Solver-specific Modell Integration

In this section, a method to integrate the calculated reference nodes in an HBM spine in Visual-Crash PAM (VCP) is presented (Figure 5.4). However, the integration of the reference nodes is in general possible in any solver. For visualization of the reference nodes for the center of the vertebral body, the local x- and z-axis were connected via *bar elements* and saved as new *Part*. The translational and rotational degrees of freedoms (DOFs) of these three nodes were then tied via *Multiple Nodes to one Node Constraints (MTOCOs)* to the corresponding DOF of the center of gravity (COG). Afterwards the motion of the *MTOCO* (dependent node) was constraint by the motions of the nodes of the upper and lower endplates (independent nodes) by *One Node to Multiple Nodes Constraints (OTMCOs)*.

For evaluation of intervertebral kinematics *Nodal Time Histories (THNODs)* were created for the center of vertebral body node and the node describing the local x-axis. Furthermore, self-rotating frames were defined for each vertebra via the node center of the vertebral body, the node for local x-axis and the node for local z-axis. To evaluate section forces in each vertebra *Section Forces (SECFOs)* have been defined along the midplane as a section with the new local coordinates systems as force and moment output.

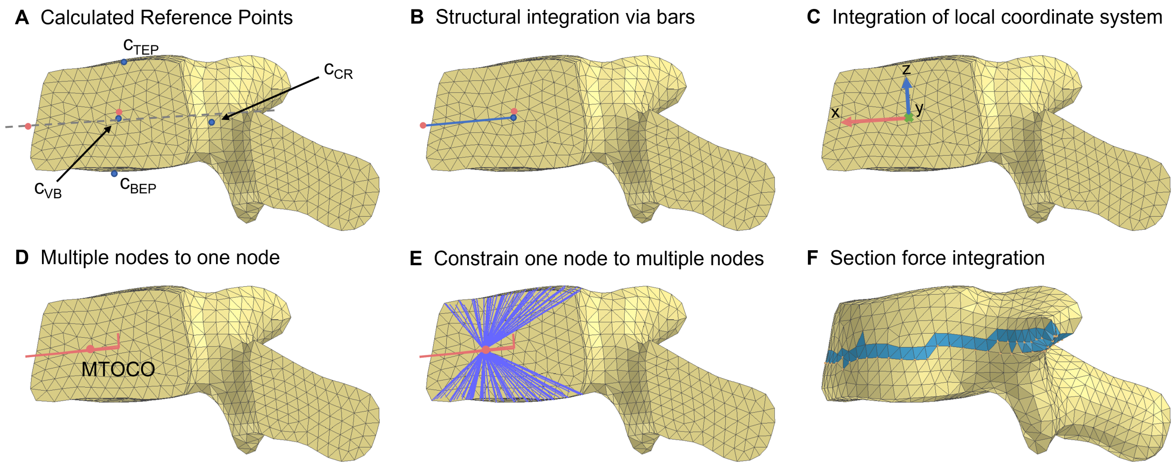

Figure 5.4: Solver-specific model integration exemplarily for a vertebra from THUMS v4.1. **A** Reference points and **B** visualization via *bar elements*. **C** Integration of a local coordinate system and **D** summary of reference points to one node (*Multiple Node to one Node Constraint (MTOCO)*). **E** Kinematic connection of the *MTOCO* to the vertebra (*One Node to Multiple Nodes Constraint (OTMCO)*). **F** Integration of a *Section Force (SECFO)*.

By integrating the local coordinate systems, the posture of the spine can be described quantifiably and unambiguously. Therefore, to validate the HBMs, the initial spinal posture of different HBMs can be compared with each other, with anthropometric data and also with experiments from the literature. Besides, it enables the harmonization of the measurement of kinetic and kinematic responses of HBMs. The above-mentioned methodologies were used in Paper I and Paper II as well as in chapter 8.

6 Paper I

Subject-specific geometry of FE lumbar spine models for the replication of fracture locations using dynamic drop tests.[1]

Rieger, Laura K., Alok Shah, Sylvia Schick, Dustin Draper B., Rachel Cutlan, Steffen Peldschus, and Brian D. Stemper

First published in *Annals of Biomedical Engineering* 52, pp. 816-831, 2024 by Springer Nature, DOI:10.1007/s10439-023-03402-y, reproduced with permission from Springer Nature.

Abstract

For traumatic lumbar spine injuries, the mechanisms and influence of anthropometrical variation are not yet fully understood under dynamic loading. Our objective was to evaluate whether geometrically subject-specific explicit finite element (FE) lumbar spine models based on state-of-the-art clinical computer tomography (CT) data combined with general material properties from the literature could replicate the experimental responses and the fracture locations via a dynamic drop tower-test setup. The experimental CT datasets from a dynamic drop tower-test setup were used to create anatomical details of four lumbar spine models (T12 to L5). The soft tissues from THUMS v4.1 were integrated by morphing. Each model was simulated with the corresponding loading and boundary conditions from the dynamic lumbar spine tests that produced differing injuries and injury locations. The simulations resulted in force, moment, and kinematic responses that effectively matched the experimental data. The pressure distribution within the models was used to compare the fracture occurrence and location. The spinal levels that sustained vertebral body fracture in the experiment showed higher simulation pressure values in the anterior elements than those in the levels that did not fracture in the reference experiments. Similarly, the spinal levels that sustained posterior element fracture in the experiments showed higher simulation pressure values in the vertebral posterior structures compared to those in the levels that did not sustain fracture. Our study showed that the incorporation of the spinal geometry and orientation could be used to replicate the fracture type and location under dynamic loading. Our results provided an understanding of the lumbar injury mechanisms and knowledge on the load thresholds that could be used for injury prediction with explicit FE lumbar spine models.

1 A closer description of the setups used to modify the annulus fibrosus stress-strain curve in tension and compression, a detailed description of the drop-tower test setup by Stemper et al. (2011b) and its corresponding simulation setup as well as a detailed description of the creation of the subject-specific models can be found in the Appendix.

Annals of Biomedical Engineering
https://doi.org/10.1007/s10439-023-03402-y

BMES BIOMEDICAL ENGINEERING SOCIETY

ORIGINAL ARTICLE

Subject-Specific Geometry of FE Lumbar Spine Models for the Replication of Fracture Locations Using Dynamic Drop Tests

Laura K. Rieger[1,2] · Alok Shah[3,4,5] · Sylvia Schick[1] · Dustin B. Draper[1] · Rachel Cutlan[4] · Steffen Peldschus[1] · Brian D. Stemper[3,4,5]

Received: 19 April 2023 / Accepted: 28 October 2023

Abstract

For traumatic lumbar spine injuries, the mechanisms and influence of anthropometrical variation are not yet fully understood under dynamic loading. Our objective was to evaluate whether geometrically subject-specific explicit finite element (FE) lumbar spine models based on state-of-the-art clinical CT data combined with general material properties from the literature could replicate the experimental responses and the fracture locations via a dynamic drop tower-test setup. The experimental CT datasets from a dynamic drop tower-test setup were used to create anatomical details of four lumbar spine models (T12 to L5). The soft tissues from THUMS v4.1 were integrated by morphing. Each model was simulated with the corresponding loading and boundary conditions from the dynamic lumbar spine tests that produced differing injuries and injury locations. The simulations resulted in force, moment, and kinematic responses that effectively matched the experimental data. The pressure distribution within the models was used to compare the fracture occurrence and location. The spinal levels that sustained vertebral body fracture in the experiment showed higher simulation pressure values in the anterior elements than those in the levels that did not fracture in the reference experiments. Similarly, the spinal levels that sustained posterior element fracture in the experiments showed higher simulation pressure values in the vertebral posterior structures compared to those in the levels that did not sustain fracture. Our study showed that the incorporation of the spinal geometry and orientation could be used to replicate the fracture type and location under dynamic loading. Our results provided an understanding of the lumbar injury mechanisms and knowledge on the load thresholds that could be used for injury prediction with explicit FE lumbar spine models.

Keywords Vertebral body fracture · Anthropometrical variations · Spinal geometry · FEM · Lumbar · Drop test

Introduction

Thoracic and lumbar injuries account for 79% of the total spinal injuries and usually result from high-energy trauma, particularly from high-energy falls (39%), traffic (26.5%), or sports accidents (5.2%) [1]. Lumbar spine injuries, such as vertebral fractures and ligament tears, are significant causes of disability for healthy individuals and can induce high socioeconomic consequences [2]. Approximately 50% of injuries ranging in severity from minor bony fractures to complex fracture dislocation may lead to disability [3]. Multidirectional dynamic loading mechanisms sustained during traumatic events, such as falls and motor vehicle crashes, are recognized as the primary causes of spinal injuries [1, 4, 5]. A better understanding of the link between injury mechanisms, injury morphology, and features of an

Associate Editor Sean S. Kohles oversaw the review of this article.

✉ Laura K. Rieger
laura.rieger@med.uni-munechen.de;
laura.rieger@volkswagen.de

1 Biomechanics and Accident Analysis, Ludwig-Maximilians-Universität (LMU), Munich, Germany

2 Occupant Protection System & Virtual Function Development, Volkswagen AG, Letter Box 011/1606, 38436 Wolfsburg, Germany

3 Department of Neurosurgery, Medical College of Wisconsin, Milwaukee, WI, USA

4 Department of Biomedical Engineering, Marquette University and Medical College of Wisconsin, Milwaukee, WI, USA

5 Neuroscience Research, Clement J. Zablocki Veterans Affairs Medical Center, Milwaukee, WI, USA

individual may be valuable to help injury prevention and clinical management.

In automotive applications, safety load limits have been successfully applied to protect passengers. For example, these load limits are dummy loading criteria with associated injury risk curves. However, there is currently no such criterion that is accepted for predicting lumbar spine injury in automotive crashes. Such a lumbar injury criterion would be helpful for evaluating the complex loading conditions and could result in the design of better safety systems. The first steps toward the development of this criterion involve a better characterization of the lumbar injury pathomechanisms, the corresponding final injury patterns, and the influencing factors.

Experimental and numerical studies have been used to identify spinal tolerance, which is the force or acceleration levels that the spine can sustain without major damage [6–8], and the spine pathomechanisms [9] under traumatic loading conditions. Most published studies have been focused on axial loading because of the prevalence of real-world injury events involving dynamic axial loads that include falls [10], motor vehicle collisions [11], and military scenarios, such as underbody blasts, aviator ejections, and helicopter crashes [12]. Currently, numerical human body models (HBMs) based on a finite element (FE) formulation are widely used for injury biomechanics research for automotive crashes and other high strain rate applications [13], as they can complement experimental work with additional biomechanical information. The models can be computationally efficient and provide reproducible and repeatable simulation results. In contrast to the FE simulations widely used in orthopedics, HBM-based crash simulations use FE models with solvers for explicit time integration, which usually have much coarser mesh densities for time-step limitations. Finite element modeling enables the comparison of the kinetic responses for the controlled loading rates, stress distribution, and failure propagation; these are difficult to obtain in experimental studies. These models can potentially be used to improve the understanding of spinal injury pathomechanisms.

HBMs, such as the Global Human Body Model Consortium (GHBMC) [14] and Total HUman Model for Safety (THUMS) [15], are among the most evaluated and widely used. These HBMs have been validated against experimental data at the component level and whole-body level and continue to be validated with the introduction of new experimental data for different body regions and loading scenarios as they become available.

In previous studies, the THUMSv5 and THUMSv4 lumbar spine (T12-L5) were compared against experiments with complex loading of the spine due to gross motion or acceleration of the upper body during impact [16, 17]. Based on vertebral kinematics, THUMSv5 and THUMSv4 were not able to replicate the vertebral kinematics measured in the physical experiments, and validation was not achieved [18, 19].

Based on previous studies, a subject-specific finite element model of lumbar spine segments could be used to predict the displacement field of human spine segments under physiological loading conditions [20–24]. Other researchers investigated whether single-level subject-specific finite element models could predict fracture outcomes in three-level spine segments under different loading rates [25] or evaluated the feasibility of modeling and performing finite element simulation of the whole lumbar spine from routinely acquired in vivo clinical data for biomechanical analysis. However, these models were mostly compared to data from the experimental and computational results in the literature. Spinal geometry appears to have a major influence on the response of numerical models of the lumbar spine [26–28]. Thus, the influence of anthropometrical parameters of the lumbar spine needs to be further investigated. The aim of this study was to evaluate whether the geometrical subject-specific finite element (FE) lumbar spine models based on a generic state-of-the-art FE model and the state-of-the-art clinical CT data combined with the generic material data from the literature could replicate the forces, moments, kinematic responses, and fracture locations in a dynamic drop tower-test setup as performed and reported by Stemper et al. [29].

Materials and Methods

Experiments

The physical basis for this study includes four experimental specimens that were tested as part of a larger effort focused on quantifying lumbar spine tolerance during dynamic axial compression as described in the studies by Stemper et al. [16, 29]. All lumbar spine specimens for this study were obtained from donors through the Wisconsin Donor Network. Consent for spine donation was obtained from the next of kin. The study protocol was approved by the Subcommittee on Human Studies at the Clement J. Zablocki Veterans Affairs Medical Center in Milwaukee, WI, USA. Stemper et al. experimentally quantified the whole lumbar spine (T12-L5) axial tolerance in combined compression and flexion through the use of a drop tower-testing setup (Fig. 1). Of the four specimens used for our analysis, one specimen was previously used for the analysis in Stemper et al. [16], and the other three specimens were not included in that study. To ensure compressive flexion loading, the drop tower consisted of two decoupled platforms attached to a monorail via low-friction bearings. Linear accelerometers were used at the lower and upper platforms to measure vertical accelerations.

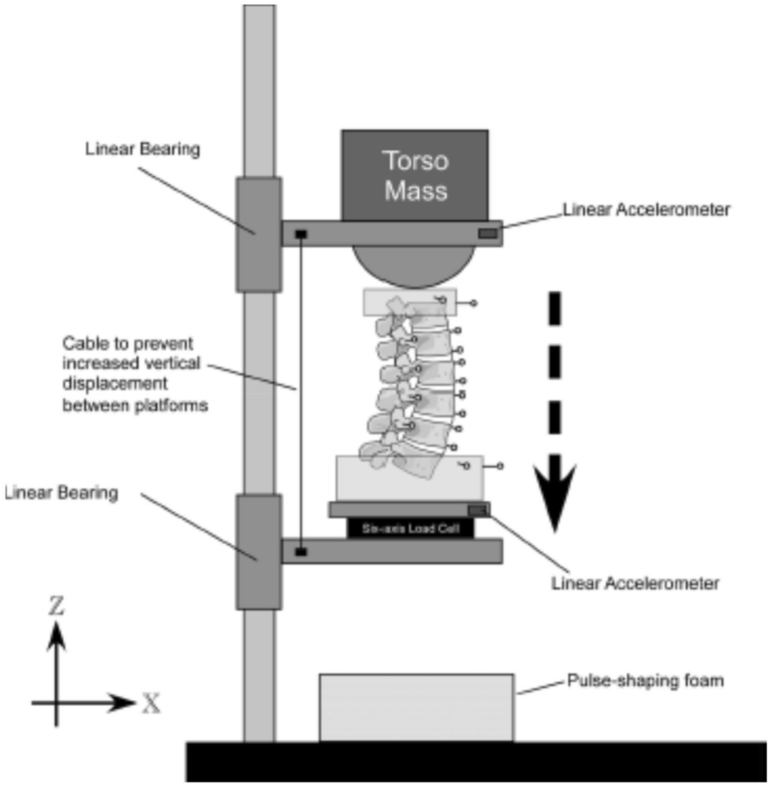

Fig. 1 Lumbar spine vertical acceleration model. Obtained permission from Stemper et al. J Biomech Eng 2011 [29]. The arrow on the right shows the direction of gravity

The measurements of the forces and moments were performed via a load cell that attached the caudal fixation of the specimen to the lower platform. Interaction between the upper platform and the superior specimen fixation was in the form of a laterally oriented cylinder. A piece of foam at the impact interface was used to form a realistic acceleration pulse. Specifically, foam was added to lengthen the acceleration versus time pulse to match the acceleration pulse measured at the seat during military aviator ejections [29]. A 32-kg mass was added to the upper platform to simulate the torso mass.

The CT scans prior to testing allowed for the evaluation of the intactness of each specimen. Cranial (T12) and caudal (L5) vertebrae were mounted in polymethylmethacrylate (PMMA) to facilitate attachment to the experimental apparatus. For consistency between the specimens, the L2–L3 intervertebral disk level was kept close to horizontal in the global coordinate system without changing the natural lordosis of each specimen. This was done during the PMMA potting procedure by holding the spine upright with the L2–L3 disk level in the horizontal position, allowing the spine to maintain its natural curvature, and the PMMA fixative was poured into a potting box to cover as much of the L5 vertebra without constraining the L4–L5 intervertebral disk and facet joints. The specimens were then preflexed with a 5 N-m moment in the sagittal plane while minimizing the off-center loads. 5 N-m was chosen because this value was within the physiologic range of the whole lumbar spine [30]. A cable was applied between the platforms to maintain the 5 N-m preload and to prevent specimen recoil before testing and major vertical displacement or impact during dynamic testing. Specifically, the cable allowed the upper platform to reduce the vertical distance from the lower platform during deceleration, inertially compressing the lumbar spine specimen; however, it would not allow the upper platform to move away from the superior aspect of the specimen. Each specimen was exposed to one or more dynamic tests from the specific drop heights until injury was detected. Bony injury was determined using post-test lateral and anterior-posterior X-rays, and the soft tissue injury was determined by comparing pre- to post-test segmental laxity as indicated by the specimen palpation. We also compared pre- to post-test sagittal flexibility of the spine as indicated by the T12-L5 motion during a static 5 N-m flexion moment. Testing was stopped if bony fracture was identified on post-test X-ray. Therefore, testing was stopped for Specimens I, II, and III when the fractures identified in Table 1 were identified. Specimen IV did not sustain bony injury, and segmental palpation identified laxity at more than one spinal level following the second dynamic test. Since segmental laxity was indicative of a possible soft tissue injury/subinjury, testing was stopped for Specimen IV following the second test; however, post-test examination of this specimen did not identify any specific soft tissue failure (e.g., ligamentous tear). Three-dimensional vertebral kinematics were recorded using a Vicon system (Vicon Corp., Oxford Metrics Group, Oxford England); this system tracked the three spherical targets on each vertebra, with one target placed in the anterior aspect of the body and one in each transverse process. Local Cartesian coordinate system origins were defined at mid-height and mid-width along the posterior wall of each vertebral body. Target motions were used to reconstruct vertebral kinematics. Sagittal segmental angulation was computed for each segment (T12-L1 through L4–L5) as the sagittal plane angle of one vertebra relative to the subjacent vertebra [16]. After each test, each specimen was checked for bony fracture, notable changes in the spinal alignment and their intervertebral disk heights using X-rays. The endplate or soft tissue injury was excluded through specimen palpation and flexion stiffness assessments. The type of fracture and affected spinal level were assessed using X-rays and post-test CT scans.

Simulation

Development of FE Models

To perform matched simulation from the Stemper [16, 29] experiments, subject-specific geometries were created. For the development of the subject-specific FE lumbar spine models, CT scans from the Stemper [16, 29] experiments were graded according to completeness and resolution (< 0.4355 × 0.4355, slice thickness 0.625 mm). Based on these criteria, four specimens were selected to be reanalyzed and converted into FE models. The CT scans of the four lumbar spine units (Table 1) were imported into Mimics (Version 22.0, Materialise, Plymouth, MI) for image segmentation, and then a semiautomated threshold method was used to segment the six lumbar vertebrae from each subject. Next, a smoothing process was performed to remove spikes and holes on the surface of the vertebral geometries.

Meshing was performed in ANSA preprocessor software (BETA CAE Systems SA, Epanomi, Thessaloniki). Quad meshing with a target element length of 2 mm of the outer surface of the segmented vertebral bodies was used to model cortical bone with a thickness of 1, 1.29, 1.29, 1.39, 1.72, and 1.98 mm as in the baseline THUMS v4.01 model from T12 to L5. In the corner areas, reconstruction, smoothing, and reshape options were used to check if triangular elements could be avoided to minimize stiffening effects. The remaining volume of each vertebra was considered as trabecular bone and modeled with tetrahedral elements. Table 2 lists the mesh quality parameters used to check the mesh quality of the shells and solids. After each vertebra was meshed using the quality parameters, the model was tested and passed the presurface meshing and prevolume meshing checks to ensure that there were no penetrations or close proximities.

As the CT scans were taken in the supine position, the poses of each lumbar vertebra were adjusted to match the test position. Therefore, in accordance with previous investigations on spinal segmental angles [31–38], the intervertebral angles illustrated in Fig. 2 were measured in midsagittal X-ray images using the image processing software ImageJ (http://rsb.info.nih.gov/ij/; US National Institutes of Health Bethesda, Maryland, USA). The intervertebral angles measured in this study were T12-L1, L1–L2, L2–L3, L3–L4, and L4–L5 in the 5 N-m preflexion condition that was used prior to each test. Here, each intervertebral angle was defined as the angle of the median plane between the superior and inferior surfaces of the vertebral body on the midsagittal plane. A positive angle indicated flexion or an upward angle from

Table 1 Age, sex, height, weight, and injury per specimen, which were used as the basis for the reconstruction of the subject-specific data

Specimen no.	Age/y	Sex	Ht/cm	Wt/kg	Injury	Impacts no.
Specimen I	16	F	168	59	L1 right pars interarticularis fracture L1 spinous fracture L1-L2 disk disruption L2 bilateral pedicle fracture L2 left pars interarticularis fracture	2
Specimen II	45	F	165	89	T12 spinous avulsion fracture* L1 wedge fracture	1
Specimen III	58	F	165	52	L5 bilateral pars fracture* L5 posterior superior body fracture*	1
Specimen IV	28	M	183	82	No obvious bony injury	2

*These fractures were regarded as potting fractures and were disregarded as potential artifacts

Table 2 Shell and solid mesh parameters

Shell mesh			Solid mesh		
Criteria	Calculation	Failed	Criteria	Calculation	Failed
Aspect ratio	PATRAN	10.	Aspect Ratio	PATRAN	10.
Skewness	PATRAN	62.	Skewness	PATRAN	65.
Warping	PATRAN	20.	Warping	PATRAN	20.
Jacobian	ANSA	0.3	Jacobian	ANSA	0.3
Min. angle quads	IDEAS	20.	Min. angle tetras	ABAQUS	20.
Max. angle quads	IDEAS	160.	Max. angle tetras	ABAQUS	150.
Min. angle trias	IDEAS	15.	Min. angle pentas	ABAQUS	13.
Max. angle trias	IDEAS	120.	Max. angle pentas	ABAQUS	160.
			Min. angle hexas	ABAQUS	20.
			Max. angle hexas	ABAQUS	160.
			Collapse		0.2

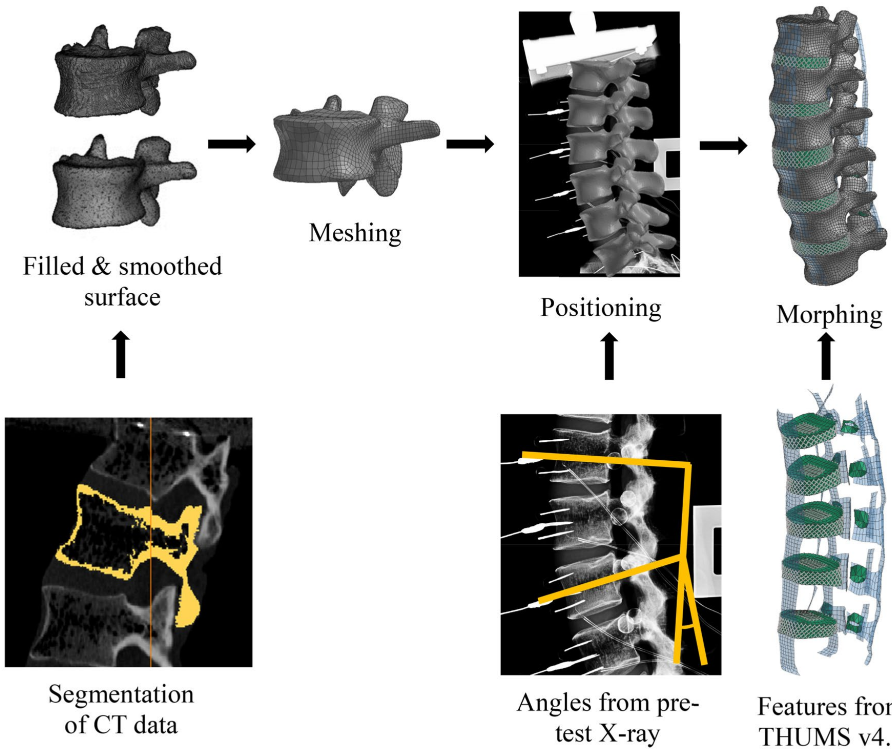

Fig. 2 Modeling approach for the detailed subject-specific lumbar spine units. The segmented vertebrae surfaces from the CT data are first smoothed. Then, the vertebrae are discretized using a meshing procedure and positioned to match the pretest position form measured in the X-rays. Afterward, disks and ligaments from THUMS v4.1 are integrated through a semiautomated morphing process

the horizontal plane, while a negative angle indicated extension or a downward angle from the horizontal plane (Fig. 3). The vertebral bodies were adjusted to match the measured angles from the X-rays via the definition of local coordinate systems for each body and rotation around the facet joints.

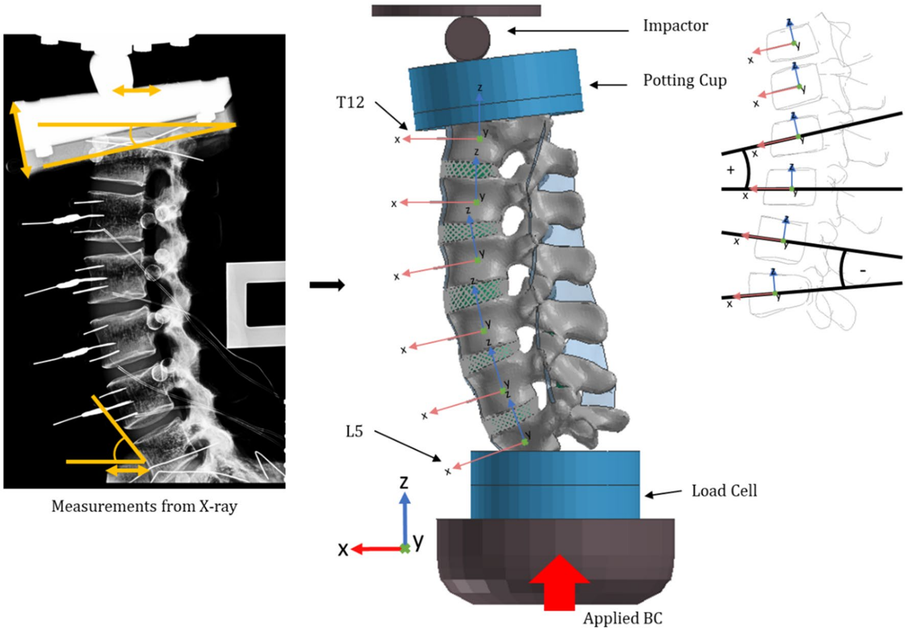

Fig. 3 Simulation setup with vertebral and global coordinate system, in which the lumbar spine unit was aligned in the setup according to pretest X-ray data (left). Picture on the right shows the definition of the sign convention used in this study. Positive angle is defined as flexion, negative angle is defined as extension. *BC* boundary condition

The geometry of the soft tissues, including disks, cartilage, and ligaments, was extracted from THUMS v4.1 and integrated into the positioned vertebrae by morphing in ANSA [39]. Material properties from THUMS v4.1 ESI008 (Table 3) were assigned to the structures. After the assembly of the model, reference points and section forces were integrated in each subject-specific model as described in the OSCCAR project [40] (Fig. 3).

Boundary and Loading Conditions

Finally, each subject-specific lumbar spine unit was rigidly attached via node constraints to upper and lower specimen pots to simulate PMMA embedding in Visual-Crash PAM (ESI Group, Rungis, France). To globally position the subject-specific lumbar spine units (LSUs) in the simulation setup, the distance of the lower potting to L5 in the x- and z-directions as well as the tilt angle of L5 to the global x-axis in the X-rays were measured. The height and tilt of the upper potting along with the position of the impactor for a nonstructural mass of 32 kg were individualized for each specimen according to pretest X-rays. Afterward, the upper potting was translated in the z-direction to the same position on the cranial end of the LSUs as shown in the X-rays. To model the relative movement between the upper potting and the impactor, a frictionless self-contact was implemented. On top of the impactor, a plate was added to the simulation setup, limiting the movement of the impactor in the z-direction in the rebound phase.

The outputs were analogously defined to the specimen experiments; forces and moments were measured in the global coordinate system via section forces in the upper and lower specimen pot. The accelerations measured in the experiment in the lower platform were applied as input to the lower specimen pot below the section force. This prevented the force and moment measurements from being influenced by the applied accelerations.

Boundary conditions for the cylinder and the lower platform allowed translation in the global z-direction and rotation around the global y-axis. In addition to the forces and moments, the vertebral kinematics were measured, as in the experiment. Gravity was applied to the entire setup as an acceleration field (Fig. 3).

Model Evaluation & Material Properties

The subject-specific models were evaluated against the specimen test data by comparing the kinetics (forces and

Table 3 Vertebral body, intervertebral disk, and ligament material definitions used in the lumbar models

Component		Material type and parameters in VCP			
Vertebral body		Elastic Plastic with Isotropic Damage for Shell Elements Stress–Strain Law Curves Formulation (MATTYP 16)			
	Cortical bone	Mass density	$\rho = 2.00E-06\frac{kg}{mm^3}$	Young's modulus	$E = 13.02GPa$
		Poisson's ration	$\upsilon = 0.3$	Yield point	$\varepsilon_P = 0.08$
		Elastic Plastic with Damage and Failure for Solid Elements Stress–Strain Law Curves Formulation (MATTYP 105)			
	Cancellous bone	Mass density	$\rho = 1.00E-06\frac{kg}{mm^3}$	Shear modulus	$G = 0.0166667GPa$
		Yield point	$\varepsilon_P = 0.0018$	Bulk modulus	$K = 0.022222GPa$
Intervertebral disk		Elastic-Plastic Solid with Isotropic and/or Kinematic Hardenings Bilinear Stress–Strain Law Formulation (MATTYP 1)			
	Nucleus pulposus	Mass density	$\rho = 1.00E-06\frac{kg}{mm^3}$	Shear modulus	$G = 4.33E-06GPa$
		Yield stress	$\sigma_y = 1.30E-05GPa$	Bulk modulus	$K = 0.0217GPa$
	Annulus fibrosus*	General Nonlinear Solid Foam (MATTYP 45)			
		Mass density	$\rho = 1.00E-06\frac{kg}{mm^3}$	Young's modulus	$E = 0.0021GPa$
		Non-Linear Tension-Only Bar Elements (MATTYP 205)			
		Mass density	$\rho = 5.33E-06\frac{kg}{mm^3}$	Stiffness	$k = 375kN$
		Null Material for Shell Elements (MATTYP 100)			
		Mass density	$\rho = 1.00E-06\frac{kg}{mm^3}$	Young's modulus	$E = 17.3GPa$
		Poisson's ration	$\upsilon = 0.3$		
Ligaments		Layered Material for Membrane Elements with Linear Fibers (MATTYP 150)			
	PLL/ALL	Mass density	$\rho = 1.00E-06\frac{kg}{mm^3}$	Shear modulus	$G = 0.0003325GPa$
		Poisson's ration	$\upsilon = 0.00$	Young's modulus	$E = 0.00325GPa$
	ITL/ISL/LF	Mass density	$\rho = 1.00E-06\frac{kg}{mm^3}$	Shear modulus	$G = 0.001545GPa$
		Poisson's ration	$\upsilon = 0.22$	Young's modulus	$E = 0.01508GPa$
	LN	Mass density	$\rho = 1.00E-06\frac{kg}{mm^3}$	Shear modulus	$G = 0.00309GPa$
		Poisson's ration	$\upsilon = 0.00$	Young's modulus	$E = 0.03016GPa$
		Elastic-Plastic for Shell Elements Single Stress–Strain Curve Points Formulation (MATTYP 103)			
	CL*	Mass density	$\rho = 1.16E-06\frac{kg}{mm^3}$	Young's Modulus	$E = 0.0037GPa$
		Yield stress	$\sigma_y = 0.0023GPa$	Poisson's ration	$\upsilon = 0.45$

Components marked with * have been modified from the baseline THUMS v4.1 ESI 008. The stress–strain curves for the annulus fibrosus ground matrix were fitted to the average stress–strain responses used in Newell et al. [42]

MATTYP = Material type in the VPS; E = Young's Modulus; ε_P = Yield Point; G = Shear Modulus; k = Stiffness; K = Bulk Modulus; υ = Poisson`s Ratio; ρ = Mass Density; σ_y = Yield Stress

moments measured at the caudal end) and vertebral kinematics. In the experiments, the target motions were used to reconstruct vertebral kinematics, and sagittal segmental angulation was computed for each segment (T12–L1 through L4–L5). A similar approach to analyze vertebral kinematics was performed in our study on the subject-specific data. Local coordinate systems defined in each vertebral body were used to calculate sagittal vertebral angles. For the calculation of the signs of the angles (negative—extension, positive—flexion), a plane was defined, which was spanned by two local x-vectors in the sagittal plane. The sign of the resulting vector product between the two local x-vectors defined the opening angle.

A stepwise reduction analysis was conducted to investigate the effect of the model's spinal structures on the kinetics and vertebral kinematics. The capsular ligament (CL) and annulus fibrosus were found to have the greatest influence on vertebral kinematics. Therefore, the material properties for the capsular ligament (CL) and the annulus fibrosus of THUMS v4.1 were modified to match the vertebral kinematics: Experimental results of the uniaxial tensile test available in the literature [41] were evaluated and directly input into the 103 material model for the CL in Visual-Crash PAM 17.5.2. The annulus fibrosus stress–strain curve in tension and compression from THUMS v4.1 was modified by implementing material properties from previous finite element studies available in Newell et al. [42] (Table 3).

Vertebrae Injury Predictors

To determine the mechanism of vertebral compression fracture and to identify threshold values, the pressure and first principal stress in the spongiosa as along with the first and third principal strains in the corticalis were investigated. This analysis was performed by determining the area of peak stress and strain in each vertebra at the time of experimental peak force. Fracture was defined as a gross structural failure predicted to occur when several adjacent elements exceeded a certain threshold [43], whereas a single element exceeding a threshold was more likely to be a simulation artifact. Therefore, the maximal and minimal values of the contour plots of the four models were set to the same overall maximal and minimal values identified from any of the four models. The contour plots were then filtered until only the elements defining a region of likely fracture were shown.

Results

Subject-specific geometrical models of 4 PMHS lumbar spines, including three female lumbar spines and one male lumbar spine, were created, and their responses were compared to the experimental data. Table 1 lists anthropometrical data from these four lumbar spines. One of the lumbar spines had no evidence of bony injury, while two specimens had sustained fractures near the fixation of the spine components. These fractures were excluded from the subsequent evaluation process, as they were fixation fractures that had occurred after the primary fracture, when the spine had become unstable. Therefore, only two different fracture types, a wedge fracture and a fracture in the posterior part of the vertebra, were considered.

Figure 4 shows the lumbar spine models that were created after segmentation of the vertebrae and meshing, positioning and integration of soft tissue with THUMS v4.1, through morphing in equal scaling. The degree of pretest lumbar lordosis was quantified as the Cobb angle; that is, the angle from the topmost endplate of T12 to the bottommost endplate of L5. This angle ranged from − 60.4 (major kyphosis) to − 14 deg (minor kyphosis).

FE Model Comparison

The responses of the simulation models were compared to the responses reported in the experiment. The kinetic responses for the z-force and y-moment can be found in Fig. 5. Figure 6 shows the kinematic responses measured within the functional spine unit in which the fracture occurred in the experiments, with the time of the peak force highlighted. For specimen I, an extension between L1 and L2 resulted in fractures in the posterior region.

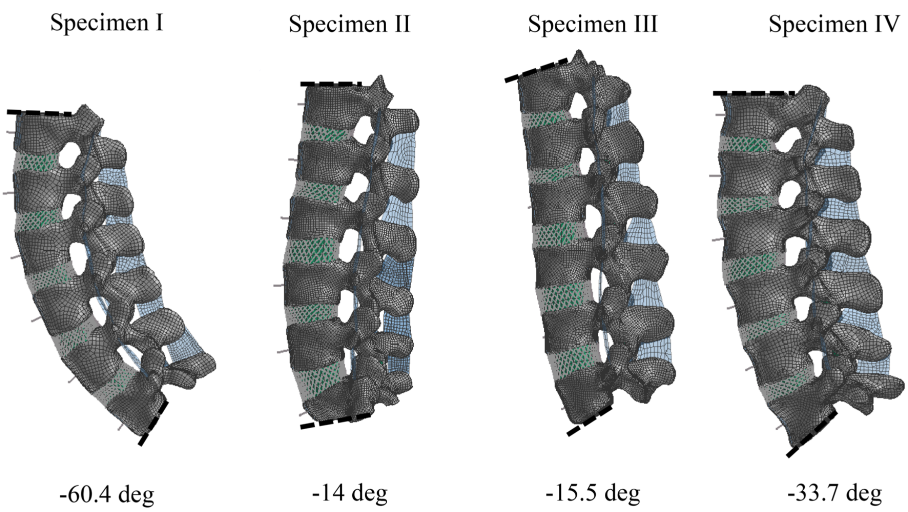

Fig. 4 Different postures from the four reconstructed lumbar spine (T12-L5) models after application of 5 N-m preload. The Cobb angles measured for each specimen from the top endplate of T12 to the bottom endplate of L5 is provided

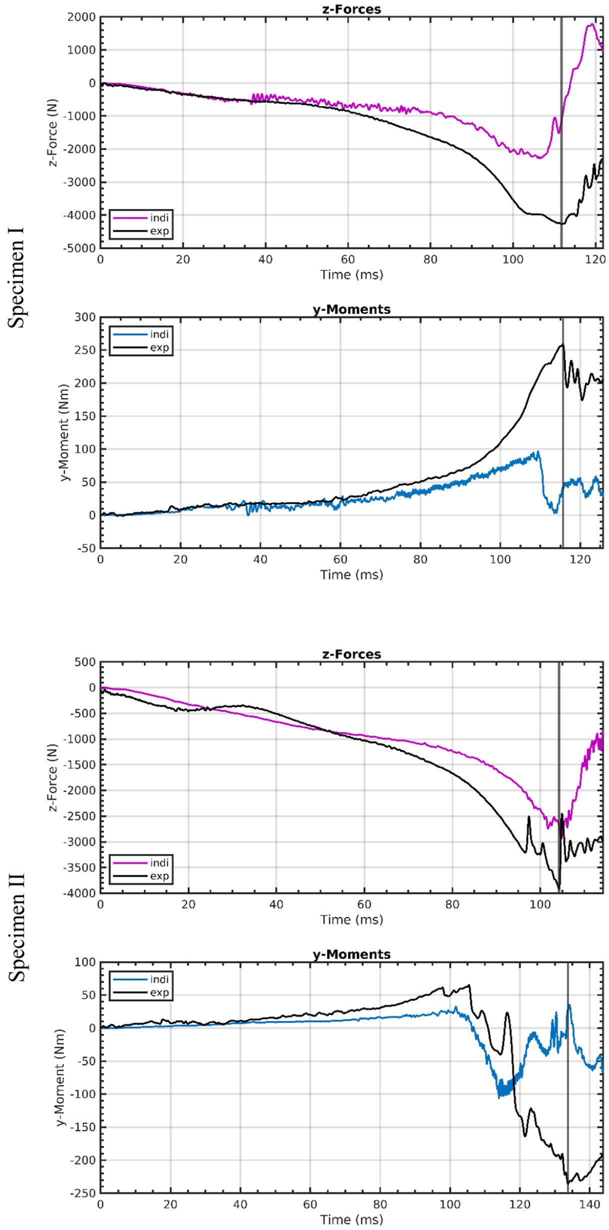

Fig. 5 Comparison of the z-forces and y-moments between the experimental (black lines) and simulation results from the subject-specific models (colored lines). Z-forces and y-moments have the highest amplitudes and are considered to have the highest potential for injury causation in this load case. Vertical black line marks the time of the experimental peak force

Fig. 5 (continued)

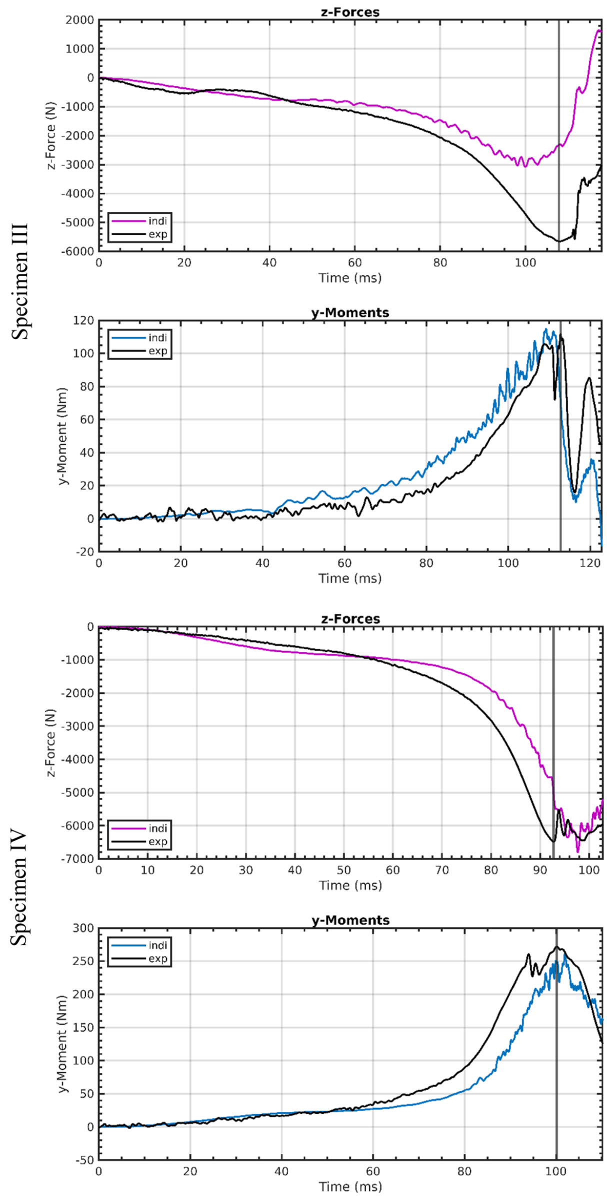

Specimen II experienced flexion between T12 and L1, which resulted in a wedge fracture at L1. No fracture was detected for specimens III and IV. Until the time of the experimental peak force, the simulation responses and experimental responses showed good agreement.

Analysis Regarding Fracture Prediction Capabilities

Generically, the fracture types observed in the experiment could be divided into vertebral body fractures (specimen II) and posterior element fractures (specimen I). In this

Fig. 6 Representative comparison of the angular displacement between the experimental (black line) and simulation results from the subject-specific models (colored lines) for an extension injury (**A**) and a flexion injury (**B**). Angular displacements for both models are zeroed by subtracting the respective initial angles

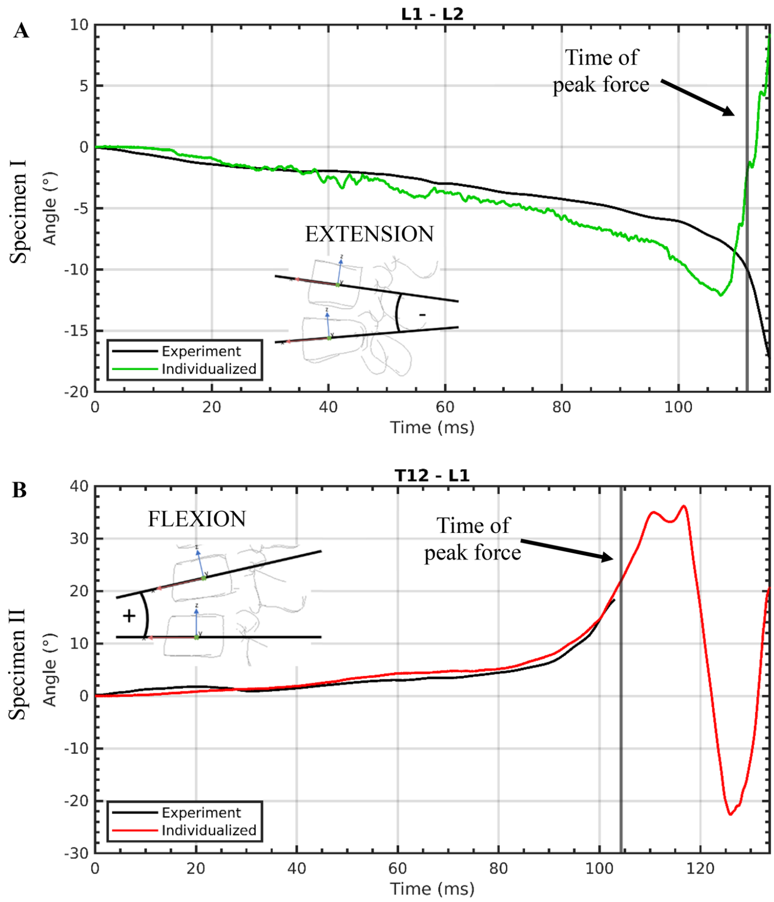

study, the pressure in the spongiosa was found to be the best indicator for fracture initiation. The time of the experimental peak force coincided with the time at which the highest pressures occurred in the specimens. In the simulation, the specimens (specimen II) with body fractures showed high pressure in the vertebral body. However, the specimens (specimen I) with posterior element fracture showed the highest pressure in the posterior elements of the vertebra.

In Fig. 7 shows the maximum pressure in the spongiosa of the vertebral bodies for each specimen model at time of peak force. The default color scheme was manually filtered until only the areas with high pressure were visible, resulting in a lower limit of 0.7 MPa. Specimens I and III had no areas with a pressure higher than 0.7 MPa, specimen IV showed an area with a pressure of 2.3 MPa at the anterior L4 bottom endplate, and specimen II had a distinct area with a pressure up to 3.5 MPa at the T12-L1 level (higher pressure at anterior T12 bottom endplate).

Fig. 8 shows the maximum pressure in the spongiosa for the complete vertebrae for each specimen model at the time of the peak force. The same visual filtering process as described in the section above was applied for this evaluation; a lower pressure value of 0.86 MPa and an upper limit of 6.5 MPa were obtained. Specimens I (L1–L2 level) and III (T12-L2 level) showed distinct areas with high pressure in the laminae and the transition to spinous processes. The areas of high pressure in specimen III showed no fracture in the experiment and included a lower number of elements compared to specimen I, which showed fractures in the posterior part. Specimen II showed high-pressure areas in the T12 bottom, L1 upper and bottom and L2 upper endplates, and specimen IV showed high-pressure areas spanning over both regions in the entire model (Fig. 8).

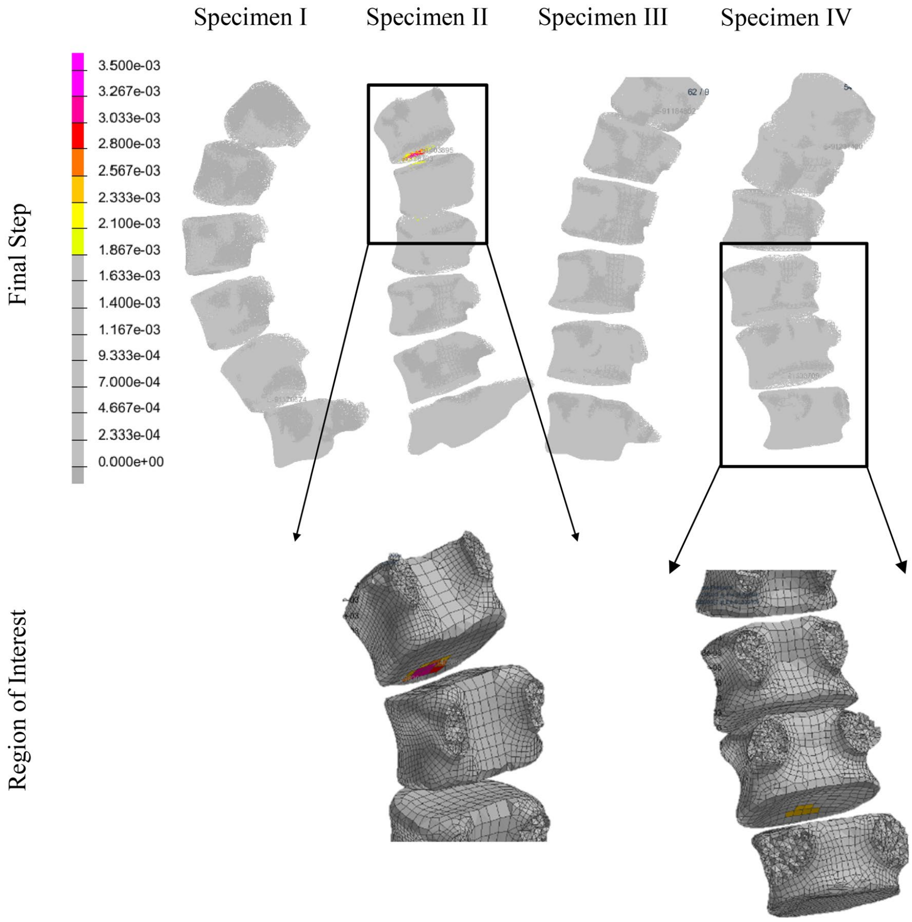

Fig. 7 Vertebral body fractures—Finite element model stress field maps of the maximum pressure in GPa of the spongiosa of the vertebrae bodies at the moment of peak force. The final step of the filtering is shown and shows how the distribution of pressure is allocated. In ROI, the area of highest pressure is shown. Posterior elements are removed, to concentrate evaluation to vertebral bodies

Discussion

The goal of this study was to investigate whether geometrically subject-specific FE lumbar spine models based on a generic FE model could replicate experimental responses and fracture locations in a dynamic drop tower-test setup. The study involved a direct comparison of four geometrically subject-specific FE models. Geometrically subject-specific models were generated from CAD vertebral data based on the experimental CT scans with the soft tissue parts of THUMS v4.1 integrated [44, 45]. Overall, we found that our models compared reasonably well to the experimental data and that our presented models could be used to predict results for a specific subject. Our method of geometric individualization used with constant material parameters reduced the necessary level individualization to a minimum, which could help to ease lumbar safety analysis in dynamic environments. Our results could serve as an orientation for the further development of the parameters of fracture prediction in the lumbar spine using crash simulation and human body models.

Representativeness of the Models for the Population

The angle measured from the top of T12 to the bottom of L5 ranged from minor kyphosis (– 14°) to major kyphosis

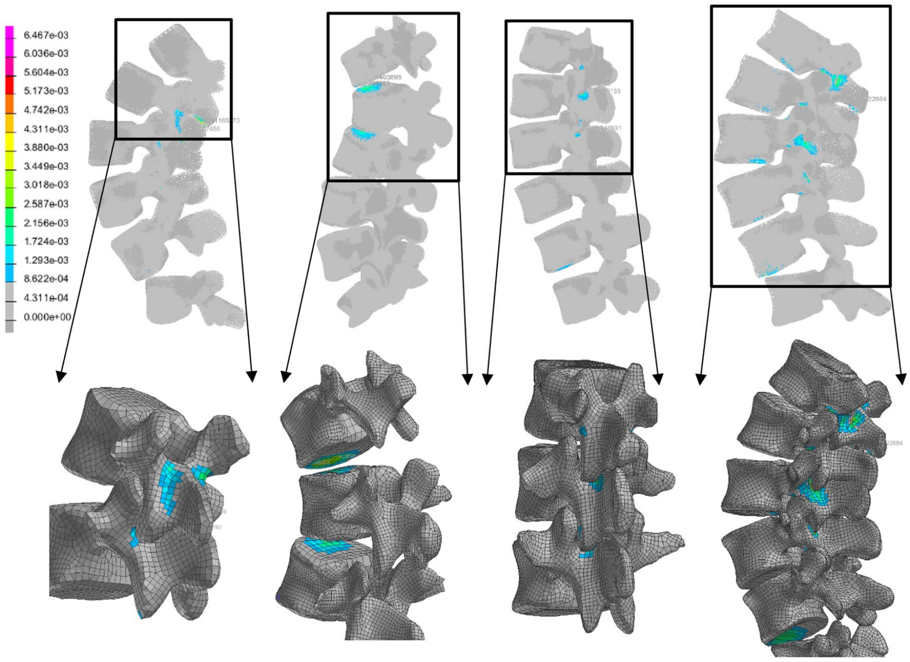

Fig. 8 Posterior element fractures: Finite element model stress field maps of the maximum pressure in GPa of the spongiosa of the vertebrae at the moment of peak force. The final step of the filtering is shown, and the distribution of pressure allocation is provided. In ROI, the area of highest pressure is shown

(−60.4°) in our models (Fig. 4). Izumiyama et al. analyzed the lumbar lordosis of males and females in the standing position [45] and in sitting with different seatback recline angles [44]. They found kyphotic lumbar lordosis for both asymptomatic males and females in the standing position (−9.2° to −45.6°) as well as for sitting with a reclined seatback angle (−2° to −25.3°). Our spines, which were preflexed to 5 N-m, had somewhat higher kyphotic curvatures at the time of testing. Based on this result, it appeared that the lumbar curvatures within our models were representative of the field of interest.

The choice of experimental model for this study was based on replicating lumbar spine biomechanics during high-rate vertical loading situations in military and civilian environments such as pilot ejections, helicopter crashes, and falls from height onto the pelvis [29]. In those situations, the pelvis is accelerated/decelerated and produces inertial compressive loads on the lumbar spine against the mass of the torso. This type of loading was replicated using decoupled platforms in the current experimental model [29], where the base of the lumbar spine was decelerated with the lower platform at the bottom of the drop tower, while the simulated torso mass attached to the upper platform produced a dynamic inertial compression load on the superior aspect of the lumbar spine. This novel experimental design is different from prior studies of lumbar spine compressive tolerance that produced dynamic compression to the superior aspect of the lumbar spine using an impact from a pendulum or falling mass [46, 47].

Model Generation

The specific aim of creating the FE models of the lumbar spine used in this study was to utilize existing models that were commonly applied in the design of automotive safety systems. Therefore, the disks, ligaments, and capsular ligaments were modeled as in THUMS v4.1. Furthermore, although the current modeling method used the bone surface of the facets to represent the anatomical shape of the facet cartilage surfaces and their respective gaps, the insertion of the capsular ligaments was generalized. Another limitation of the current method was that the intervertebral disks were not subject-specific disks based on medical image data but rather were transformed disks fit to the endplates of the subject. This aspect continues to be a focus in our ongoing studies.

In addition, the techniques used in this study utilized the sagittal alignment and positioning of the lumbar vertebral bodies from the pretest X-rays in 2D (the position in the frontal plane was maintained as in the CT scan). The CT-scanning objects in the pretest configuration could also generate information regarding the position in the frontal plane. Maintaining the scanned alignment ensured that the soft tissues were placed in a physically realistic location; however this did not account for any stress on the soft tissues at the time of the scan. This is a common problem in subject-specific modeling [48]. Incorporating a CT dataset with subjects in known, consistent and physiologically representative positions could potentially allow for more consistent modeling and alignment. Segmentation was performed via threshold definition and manual postprocessing as is state-of-the-art; however, threshold definition is dependent on the resolution of the CT data, and the necessary manual processing represents a source of uncertainty. In addition, a limited number of lumbar spine LSUs based on CT data resolution and completeness requirements on the CT data were used for model generation. A larger number of lumbar spine units were needed to generalize the findings in other specific spinal alignment patterns. Finally, the experimental setup was abstracted in the numerical implementation by applying the measured acceleration to the bottom potting based on the basic mechanical understanding and experience in the present study. This abstraction could introduce uncertainties into the system, which could weaken the reliability of the results. For future work, a more symbiotic development of experiments and simulations could enable the objectification of the modeling of injury mechanical experiments [49].

Comparison to the Experimental Data

The goal of our comparison was to evaluate a set of subject-specific model geometries using the same general material properties. In the true human population, material properties in the lumbar spine considerably vary and affect biomechanics [50]. Therefore, in line with a priori estimation, our models did not match the full range of results because we only included the geometric variation in our models and did not consider the material property variation. Our studies showed that our models could be used to reliably evaluate lumbar spine biomechanics, specifically within our intended research context of the replication of the vertebral kinematics, kinetics and fractures with a dynamic compression setup. In addition, the material properties were either modeled as in THUMS v4.01 or in the case of annulus fibrosus and CL taken from healthy, non-degenerated disks, and facet joints, respectively. However, degeneration can have a major influence on the kinematics and kinetics, and thus, affect the fracture behavior of lumbar vertebrae in physiological loading conditions [51]. Therefore, future studies should use the example Natarajan et al. [52–54] to investigate how degeneration affects highly dynamic loading conditions.

Fracture Prediction

In summary, the posterior elements of specimens I and III were fractured in the experiment. From our simulations, we found that the posterior parts had significantly higher pressure values compared to those from the anterior parts of these two specimens. Specimen II had a wedge fracture in L1 in the experiment, and excessive pressure was detected at the T12-L1 level and was particularly concentrated at the bottom endplate of T12. However, Specimen IV did not exhibit any bony injuries during the experiment, although an elevated pressure was observed.

Furthermore, our results indicated that a correlation between the initial orientation of the spine and the injury outcome was present. Apparently, the specimens with a larger Cobb angle tended toward fractures in the posterior region, whereas the specimens with a smaller Cobb angle tended to show fractures in the anterior part of the vertebral body. The model complexity required to accurately predict the subject-specific outputs, including the potential influence of unknown or not validated material properties, which needs to be further investigated in future studies. The fracture threshold differed between the vertebral bodies and the spinal processes with different maximum fracture predictor values. The size of the endplate area, which was significantly larger for males (size of endplate specimen IV, male 1430.6 mm^2; 1566.0–1925.1 mm^2) [55], could potentially influence the vertebral kinematics and therefore the injury outcomes [55, 56]. Large population-based probabilistic studies similar to the study design from Niemeyer et al. [27] is an appropriate way to analyze how the individual anatomical measures influence biomechanics. Future work should involve an investigation of the relevant geometrical anthropometrical spine parameters and the application of our findings in crash simulations with full bodies.

Acknowledgments This research was supported in part by the Office of Naval Research through Naval Air Warfare Center Aircraft Division Contract N00421-10-C-0049 and the Department of Veterans Affairs Medical Research.

Declarations

Conflict of interest The authors do not have any conflicts of interest to disclose.

References

1. Leucht, P., K. Fischer, G. Muhr, and E. J. Mueller. Epidemiology of traumatic spine fractures. *Injury*. 40(2):166–172, 2009. https://doi.org/10.1016/j.injury.2008.06.040.
2. Sundgren, P. C. M. P., M. M. D. Philipp, and P. V. M. P. Maly. Spinal Trauma. Amsterdam: Elsevier, 2007.

3. Rajasekaran, S., R. M. Kanna, and A. P. Shetty. Management of thoracolumbar spine trauma: an overview. *Indian J. Orthop.* 49(1):72–82, 2015. https://doi.org/10.4103/0019-5413.143914.
4. Groves, C. J., V. N. Cassar-Pullicino, and B. J. Tins. Chance-Type Flexion- Distraction Injuries in the Thoracolumbar Spine: MR Imaging Characteristics. Oak Brook: Radiological Society of North America, 2005.
5. Hsu, J. M., T. Joseph, and A. M. Ellis. Thoracolumbar fracture in blunt trauma patients: guidelines for diagnosis and imaging. *Injury*. 34(6):426–433, 2003. https://doi.org/10.1016/s0020-1383(02)00368-6.
6. Yoganandan, N., A. M. Nahum, and J. W. Melvin. Accidental Injury: Biomechanics and Prevention. New York: Springer, 2014.
7. Ortiz-Paparoni, M., J. Op't Eynde, J. Kait, B. Bigler, J. Shridharani, A. Schmidt, C. Cox, C. Morino, F. A. Pintar, N. Yoganandan, J. Moore, J. Y. Zhang, and C. R. Bass. The human lumbar spine during high-rate under seat loading: a combined metric injury criteria. *Ann. Biomed. Eng.* 49(11):3018–3030, 2021. https://doi.org/10.1007/s10439-021-02823-x.
8. Yoganandan, N., N. DeVogel, J. Moore, F. A. Pintar, A. Banerjee, and J. Y. Zhang. Human lumbar spine responses from vertical loading: ranking of forces via brier score metrics and injury risk curves. *Ann. Biomed. Eng.* 48(1):79–91, 2020. https://doi.org/10.1007/s10439-019-02363-5.
9. Sterba, M., C. -É. Aubin, E. Wagnac, L. Fradet, and P.-J. Arnoux. Effect of impact velocity and ligament mechanical properties on lumbar spine injuries in posterior-anterior impact loading conditions: a finite element study. *Med. Biol. Eng. Comput.* 57(6):1381–1392, 2019. https://doi.org/10.1007/s11517-019-01964-5.
10. Richter, D., M. P. Hahn, P. A. W. Ostermann, A. Ekkernkamp, and G. Muhr. Vertical deceleration injures: a comparative study of the injury patterns of 101 patients after accidential and intentional high falls. *Injury*. 27(9):655–659, 1996.
11. Pintar, F. A., N. Yoganandan, D. J. Maiman, M. Scarboro, R. W. Rudd, and W. Rodney. Thoracolumbar spine fractures in frontal impact crashes. *Ann. Adv. Automot. Med.* 56:277–283, 2012.
12. Stemper, B. D., N. Yoganandan, G. R. Paskoff, R. J. Fijalkowski, S. G. Storvik, J. L. Baisden, F. A. Pintar, and B. S. Shender. Thoracolumbar spine trauma in military environments. *Minerva Ortop. Traumatol.* 62:1–16, 2011.
13. Yang, K. H., J. Hu, and N. A. White. Development of numerical models for injury biomechanics research: a review of 50 years of publications in the Stapp Car Crash Conference. 2006.
14. Schwartz, D., B. Guleyupoglu, B. Koya, J. D. Stitzel, and F. S. Gayzik. Development of a computationally efficient full human body finite element model. *Traffic Inj. Prev.* 16(Suppl 1):49–56, 2015. https://doi.org/10.1080/15389588.2015.1021418.
15. Iwamoto, M., Y. Nakahira, and H. Kimpara. Development and validation of the Total HUman Model for Safety (THUMS) toward further understanding of occupant injury mechanisms in precrash and during crash. *Traffic Inj. Prev.* 16(Suppl 1):36–48, 2015. https://doi.org/10.1080/15389588.2015.1015000.
16. Stemper, B. D., S. Chirvi, N. Doan, J. L. Baisden, D. J. Maiman, W. H. Curry, N. Yoganandan, F. A. Pintar, G. R. Paskoff, and B. S. Shender. Biomechanical tolerance of whole lumbar spines in straightened posture subjected to axial acceleration. *J. Orthop. Res.* 36(6):1747–1756, 2018. https://doi.org/10.1002/jor.23826.
17. Schap, J. M., B. Koya, and F. S. Gayzik. Objective evaluation of whole body kinematics in a simulated, restrained frontal impact. *Ann. Biomed. Eng.* 47(2):512–523, 2019. https://doi.org/10.1007/s10439-018-02180-2.
18. Draper, D., A. S. Shah, S. Peldschus, and B. D. Stemper. Initial validation of a human body model lumbar spine using dynamic compression. In: Proceedings of the IRCOBI Conference, 2020, pp. 213–214.
19. Rieger, L. K., D. Draper, A. S. Shah, S. Peldschus, and B. D. Stemper. Subject-specific Lumbar Spine Finite Element Model Creation and Validation using Dynamic Compression. In: Proceedings of the IRCOBI Conference, 2022, pp. 886–887.
20. Garavelli, C., C. Curreli, M. Palanca, A. Aldieri, L. Cristofolini, and M. Viceconti. Experimental validation of a subject-specific finite element model of lumbar spine segment using digital image correlation. *PLoS One*. 17(9):e0272529, 2022. https://doi.org/10.1371/journal.pone.0272529.
21. Lee, C.-H., P. R. Landham, R. Eastell, M. A. Adams, P. Dolan, and L. Yang. Development and validation of a subject-specific finite element model of the functional spinal unit to predict vertebral strength. *Proc. Inst. Mech Eng. Part H*. 231(9):821–830, 2017. https://doi.org/10.1177/0954411917708806.
22. Skalli, W., S. Robin, F. Lavaste, and J. Dubousset. A biomechanical analysis of short segment spinal fixation using a three-dimensional geometric and mechanical model. *Spine*. 18(5):536–545, 1993. https://doi.org/10.1097/00007632-199304000-00004.
23. Xu, M., J. Yang, I. H. Lieberman, and R. Haddas. Lumbar spine finite element model for healthy subjects: development and validation. *Comput. Methods Biomech. Biomed. Eng.* 20(1):1–15, 2017. https://doi.org/10.1080/10255842.2016.1193596.
24. Campbell, J. Q., D. J. Coombs, M. Rao, P. J. Rullkoetter, and A. J. Petrella. Automated finite element meshing of the lumbar spine: verification and validation with 18 specimen-specific models. *J. Biomech.* 49(13):2669–2676, 2016. https://doi.org/10.1016/j.jbiomech.2016.05.025.
25. Rezaei, A., M. Tilton, Y. Li, M. J. Yaszemski, and L. Lu. Single-level subject-specific finite element model can predict fracture outcomes in three-level spine segments under different loading rates. *Comput. Biol. Med.* 137:104833, 2021. https://doi.org/10.1016/j.compbiomed.2021.104833.
26. Lee, C.-K., Y. E. Kim, C.-S. Lee, Y.-M. Hong, J.-M. Jung, and V. K. Goel. Impact response of the intervertebral disc in a finite-element model. *Spine*. 25(19):2431–2439, 2000.
27. Niemeyer, F., H.-J. Wilke, and H. Schmidt. Geometry strongly influences the response of numerical models of the lumbar spine—a probabilistic finite element analysis. *J. Biomech.* 45(8):1414–1423, 2012. https://doi.org/10.1016/j.jbiomech.2012.02.021.
28. Robin, S., W. Skalli, and F. Lavaste. Influence of geometrical factors on the behavior of lumbar spine segments: a finite element analysis. *Eur. Spine J.* 3(2):84–90, 1994. https://doi.org/10.1007/BF02221445.
29. Stemper, B. D., S. G. Storvik, N. Yoganandan, J. L. Baisden, R. J. Fijalkowski, F. A. Pintar, B. S. Shender, and G. R. Paskoff. A new PMHS model for lumbar spine injuries during vertical acceleration. *J. Biomech. Eng.* 133(8):081002, 2011. https://doi.org/10.1115/1.4004655.
30. Panjabi, M. M., T. R. Oxland, I. Yamamoto, and J. J. Crisco. Mechanical behavior of the human lumbar and lumbosacral spine as shown by three-dimensional load-displacement curves. *J. Bone Joint Surg. Am.* 76(3):413–424, 1994. https://doi.org/10.2106/00004623-199403000-00012.
31. Rocabado, M. Biomechanical relationship of the cranial, cervical, and hyoid regions. *J. Craniomandibular Pract.* 1(3):61–66, 1983. https://doi.org/10.1080/07345410.1983.11677834.
32. Park, S.-M., K.-S. Song, S.-H. Park, H. Kang, and K. Daniel-Riew. Does whole-spine lateral radiograph with clavicle positioning reflect the correct cervical sagittal alignment? *Eur. Spine J.* 24(1):57–62, 2015. https://doi.org/10.1007/s00586-014-3525-2.
33. Sato, F., Y. Miyazaki, S. Morikawa, A. FerreiroPerez, S. Schick, K. Brolin, M. Y. Svensson, and M. Svensson. The effect of seat back inclination on spinal alignment in automotive seating postures. *Front Bioeng. Biotechnol.* 9:684043, 2021. https://doi.org/10.3389/fbioe.2021.684043.

34. Roussouly, P., S. Gollogly, E. Berthonnaud, and J. Dimnet. Classification of the normal variation in the sagittal alignment of the human lumbar spine and pelvis in the standing position. *Spine*. 30(3):346–353, 2005.
35. Harrison, D. E., D. D. Harrison, R. Cailliet, S. J. Troyanovich, T. J. Janik, and B. Holland. Cobb method or Harrison posterior tangent method. *Spine*. 25(16):2072–2078, 2000.
36. Mac-Thiong, J.-M., H. Labelle, E. Berthonnaud, R. R. Betz, and P. Roussouly. Sagittal spinopelvic balance in normal children and adolescents. *Eur. Spine J.* 16(2):227–234, 2007. https://doi.org/10.1007/s00586-005-0013-8.
37. Armijo-Olivo, S., X. Jara, N. Castillo, L. Alfonso, A. Schilling, E. Valenzuela, R. Frugone, and D. Magee. A comparison of the head and cervical posture between the self-balanced position and the Frankfurt method. *J. Oral Rehabil.* 33(3):194–201, 2006. https://doi.org/10.1111/j.1365-2842.2005.01554.x.
38. Berthonnaud, E., J. Dimnet, P. Roussouly, and H. Labelle. Analysis of the sagittal balance of the spine and pelvis using shape and orientation parameters. *J. Spinal Disord. Tech.* 18(1):40–47, 2005. https://doi.org/10.1097/01.bsd.0000117542.88865.77.
39. Remus, R., A. Lipphaus, M. Neumann, and B. Bender. Calibration and validation of a novel hybrid model of the lumbosacral spine in ArtiSynth—the passive structures. *PLoS ONE*. 16(4):0250456, 2021. https://doi.org/10.1371/journal.pone.0250456.
40. Peldschus, S., A. Wagner, J. Muehlbauer, L. K. Rieger, J. Kerschreiter, J. Davidsson, C. Klug, S. Dussinger, and Schließler, Matthias, Eggers, Andre. Standardised validation procedure for qualifying the HBM to be used for assessing effectiveness of pilot protection principles, 2021.
41. Mattucci, S. F. E., J. A. Moulton, N. Chandrashekar, and D. S. Cronin. Strain rate dependent properties of younger human cervical spine ligaments. *J. Mech. Behav. Biomed. Mater.* 10:216–226, 2012. https://doi.org/10.1016/j.jmbbm.2013.04.005.
42. Newell, N., D. Carpanen, G. Grigoriadis, J. P. Little, and S. D. Masouros. Material properties of human lumbar intervertebral discs across strain rates. *Spine J.* 19(12):2013–2024, 2019. https://doi.org/10.1016/j.spinee.2019.07.012.
43. Forman, J. L., R. W. Kent, K. Mroz, B. Pipkorn, O. Bostrom, and M. Segui-Gomez. Predicting rib fracture risk with whole-body finite element models: development and preliminary evaluation of a probabilistic analytical framework. *Ann. Adv. Automot. Med.* 56:109–124, 2012.
44. Izumiyama, T., N. Nishida, H. Yamagata, R. Asahi, X. Chen, J. Ohgi, S. Sugimoto, and M. Fukushima. Analysis of individual variabilities for lumbar and pelvic alignment in highly reclined seating postures and occupant kinematics in a collision. In: Proceedings of the IRCOBI Conference, 2022, pp. 941–955.
45. Izumiyama, T., N. Nishida, H. Iwanaga, X. Chen, J. Ohgi, K. Mori, T. Hayashi, I. Sakuramoto, R. Asahi, S. Sugimoto, and M. Ueno. The analysis of an individual difference in human skeletal alignment in seated posture and occupant behavior using HBMs. In: Proceedings of the IRCOBI Conference, 2018, pp. 549–560.
46. Panjabi, M. M., H. Hoffman, Y. Kato, and J. Cholewicki. Superiority of incremental trauma approach in experimental burst fracture studies. *Clin. Biomech.* 15(2):73–78, 2000. https://doi.org/10.1016/s0268-0033(99)00048-0.
47. Willén, J., S. Lindahl, L. Irstam, B. Aldman, and A. Nordwall. The thoracolumbar crush fracture: an experimental study on instant axial dynamic loading: the resulting fracture type and its stability. *Spine*. 9(6):624–631, 1984. https://doi.org/10.1097/00007632-198409000-00014.
48. Campbell, J. Q., and A. J. Petrella. An automated method for landmark identification and finite-element modeling of the lumbar spine. *IEEE Trans. Biomed. Eng.* 62(11):2709–2716, 2015. https://doi.org/10.1109/TBME.2015.2444811.
49. Fuchs, T. Objektivierung der Modellbildung von verletzungsmechanischen Experimenten für die Validierung von Finite-Elemente Menschmodellen, 2018.
50. Lee, K. K., and E.-C. Teo. Material sensitivity study on lumbar motion segment (L2–L3) under sagittal plane loadings using probabilistic method. *Clin. Spine Surg.* 18(2):163–170, 2005. https://doi.org/10.1097/01.bsd.0000147658.60961.51.
51. Chosa, E., K. Goto, K. Totoribe, and N. Tajima. Analysis of the effect of lumbar spine fusion on the superior adjacent intervertebral disk in the presence of disk degeneration, using the three-dimensional finite element method. *J. Spinal Disord. Tech.* 17(2):134–139, 2004. https://doi.org/10.1097/00024720-200404000-00010.
52. Natarajan, R. N., J. R. Williams, and G. B. J. Andersson. Modeling changes in intervertebral disc mechanics with degeneration. *J. Bone Joint Surg. Am.* 88(Suppl 2):36–40, 2006. https://doi.org/10.2106/JBJS.F.00002.
53. Natarajan, R. N., J. R. Williams, and G. B. J. Andersson. Recent advances in analytical modeling of lumbar disc degeneration. *Spine*. 29(23):2733–2741, 2004. https://doi.org/10.1097/01.brs.0000146471.59052.e6.
54. Ruberté, L. M., R. N. Natarajan, and G. B. Andersson. Influence of single-level lumbar degenerative disc disease on the behavior of the adjacent segments—a finite element model study. *J. Biomech.* 42(3):341–348, 2009. https://doi.org/10.1016/j.jbiomech.2008.11.024.
55. Abu-Leil, S., Y. Floman, Y. Bronstein, and Y. M. Masharawi. A morphometric analysis of all lumbar intervertebral discs and vertebral bodies in degenerative spondylolisthesis. *Eur. Spine J.* 25(8):2535–2545, 2016. https://doi.org/10.1007/s00586-016-4673-3.
56. Masharawi, Y. M., N. Steinberg, and K. Salame. Lumbar facet orientation in spondylosis: a skeletal study. *Spine*. 32(6):176–180, 2007. https://doi.org/10.1097/01.brs.0000257565.41856.0f.

7 Paper II

Simulative investigation of the required level of geometrical individualization of the lumbar spines to predict fractures

Rieger, Laura K., Mirko Junge, Rachel Cutlan, Steffen Peldschus, and Brian D. Stemper

First published in *International Journal of Legal Medicine*, 138, pp. 1831-1844, 2024 by Springer Nature, DOI:10.1007/s00414-024-03225-z, reproduced with permission from Springer Nature.

Abstract

Injury mechanisms of the lumbar spine under dynamic loading are dependent on spine curvature and anatomical variation. Impact simulation with FE models can assist the reconstruction and prediction of injuries. The objective of this study was to determine which level of individualization of a baseline FE lumbar spine model is necessary to replicate experimental responses and fracture locations in a dynamic experiment. Experimental X-rays from 26 dynamic drop tower tests were used to create three configurations of a lumbar spine model (T12 to L5): baseline, with aligned vertebrae (positioned), and with aligned and morphed vertebrae (morphed). Each model was simulated with the corresponding loading and boundary conditions from dynamic lumbar spine experiments. Force, moment, and kinematic responses were compared to the experimental data. Cosine similarity was computed to assess how well simulation responses match the experimental data. The pressure distribution within the vertebrae was used to compare fracture risk and fracture location between the different models. The positioned models replicated the injured spinal level and the fracture patterns quite well, though the morphed models provided slightly more accuracy. However, for impact reconstruction or injury prediction, the authors recommend pure positioning for whole-body models, as the gain in accuracy was relatively small, while the morphing modifications of the model require considerably higher efforts. These results improve the understanding of the application of human body models (HBMs) to investigate lumbar injury mechanisms with FE models.

International Journal of Legal Medicine
https://doi.org/10.1007/s00414-024-03225-z

ORIGINAL ARTICLE

Simulative investigation of the required level of geometrical individualization of the lumbar spines to predict fractures

Laura Kathrin Rieger[1,2] · Mirko Junge[2] · Rachel Cutlan[4] · Steffen Peldschus[1] · Brian D. Stemper[3,4,5]

Received: 27 November 2023 / Accepted: 22 March 2024

Abstract

Injury mechanisms of the lumbar spine under dynamic loading are dependent on spine curvature and anatomical variation. Impact simulation with finite element (FE) models can assist the reconstruction and prediction of injuries. The objective of this study was to determine which level of individualization of a baseline FE lumbar spine model is necessary to replicate experimental responses and fracture locations in a dynamic experiment.

Experimental X-rays from 26 dynamic drop tower tests were used to create three configurations of a lumbar spine model (T12 to L5): baseline, with aligned vertebrae (positioned), and with aligned and morphed vertebrae (morphed). Each model was simulated with the corresponding loading and boundary conditions from dynamic lumbar spine experiments. Force, moment, and kinematic responses were compared to the experimental data. Cosine similarity was computed to assess how well simulation responses match the experimental data. The pressure distribution within the vertebrae was used to compare fracture risk and fracture location between the different models.

The positioned models replicated the injured spinal level and the fracture patterns quite well, though the morphed models provided slightly more accuracy. However, for impact reconstruction or injury prediction, the authors recommend pure positioning for whole-body models, as the gain in accuracy was relatively small, while the morphing modifications of the model require considerably higher efforts. These results improve the understanding of the application of human body models to investigate lumbar injury mechanisms with FE models.

Keywords Vertebral body fracture · Individualization · Spinal geometry · FEM · Lumbar spine · Drop test

Introduction

Thoracic spine and lumbar spine injuries account for 79% of all spinal injuries and are usually caused by high-energy trauma, mainly falls (39%), traffic crashes (26.5%), and sports accidents (5.2%) [1]. Analysis of injury and crash databases showed that the incidence of thoracolumbar fractures in motor vehicle crashes (MVCs) increased from 1986 to 2008 as a function of vehicle model (National Automotive Sampling System Crashworthiness Data System (NASS-CDS) [2]), from 1994 to 2002 (Crash Outcome Data Evaluation System data [3]), and from 1996 to 2011 with age and seat belt use (Crash Injury Research and Engineering Network (CIREN) [4]).

There are indications that the number of thoracolumbar fractures will increase due to the increase of non-traditional seating postures with the introduction of highly automated vehicles. A reclined seating position, in particular, is predicted to become more prevalent [5, 6] as the forward

✉ Laura Kathrin Rieger
laura.rieger@med.uni-munechen.de;
laura.rieger@volkswagen.de

1 Biomechanics and Accident Analysis, Ludwig-Maximilians-Universität (LMU), Occupant Protection System & Virtual Function Development, Volkswagen AG, Letter Box 011/1606 Wolfsburg, Munich 38436, Germany

2 Volkswagen AG, Wolfsburg, Germany

3 Department of Neurosurgery, Medical College of Wisconsin, Milwaukee, WI, USA

4 Department of Biomedical Engineering, Marquette University and Medical College of Wisconsin, Milwaukee, WI, USA

5 Neuroscience Research, Clement J. Zablocki Veterans Affairs Medical Center, Milwaukee, WI, USA

Published online: 02 May 2024

rotation of the upper torso occurs later in the reclined position compared to the upright posture, thus increasing the compression in the lumbar spine. Furthermore, a higher degree of thoracolumbar flexion is also associated with causing fractures [7].

Types of fractures vary from major (burst) compression type, with uniform compression of the vertebral body from posterior to anterior, wedge type where the anterior was more compressed than the posterior, and other types that did not fit either category [2, 4, 8]. Such observation can be expected, as the human spine is unique and complex in structure, characterized by complicated anatomy, inhomogeneous material composition, and non-linear material behavior, exposed to complex loading conditions [9]. These anatomical and material variations, combined with differences in load vector, drive varying injury outcomes in motor vehicle crashes.

Some studies investigated significant uncertainties in material properties, geometric configuration, and loading in biological systems [10]. For example, Putzer et al. [11] studied the influence of defined geometrical variations on physiological lumbar spine loading. They reported vertebral body height, disc height, and curvature of the lumbar spine as important. Meijer et al. [12] investigated the physiological range of geometrical dimensions on the stiffness of a motion segment. In their study, disk height had the most considerable influence.

Many studies on spinal alignment in different postures, inherently dependent on other spinal parameters (e.g., disc height, vertebral wedging), have been reported in medical literature the automotive field. For example, Izumiyama et al. [13] investigated skeletal alignment in an automotive seat and tried to clarify the differentiation by age, gender, and body type. Later, studies investigated the effect of the postural change between standard seating postures and a reclined posture in vehicles [14] and the effect of the seat back inclination on spinal alignments comparing spinal alignments of automotive seating postures in the 20° and 25° seat back angle and standing and supine postures [15].

The depiction of injury mechanisms for injury reconstruction or prediction requires a description of the relevant anatomical details. Therefore, the ultimate aim would be to consider all anatomical and pathological variants of the spine. Human body models (HBMs) are suitable as an evaluation methodology, especially for evaluating different anthropometries. HBMs are computationally efficient, reproducible, and repeatable, though their main advantage lies in individualization. They have been individualized on the full-scale level [16, 17] but also the component level [18, 19].

Individualization of full-scale HBMs can offer realistic occupant populations. Their generation and preparation for application would require a fully automated method to produce many whole-body FE human models representing sexes and a wide range of stature and body shapes, like the mesh morphing method presented by Zhang et al. [16]. They generated 100 human models with a wide range of variation. The main limitation of the study is its focus on statistical models of the ribcage, pelvis, femur, and tibia. At the same time, the other skeletal components were morphed using geometric relationships among the adjacent structures, but without reference to specific skeletal data. Nevertheless, even if it was possible to integrate all feasible spinal characteristics, actual parameters are usually unknown, and variability is inherent in living organisms. Finally, setting up individual-specific models for each spinal curvature is inefficient and not economical. Knowledge about the loss of precision with different simplifications in the individualization approach would be helpful.

Therefore, the objective of this study was to (1) identify the spine parameters in the sagittal plane responsible for kinematic behavior in a dynamic application and (2) propose an application strategy that allows systematic inclusion of variance in the analysis. To the author's knowledge, there are no investigations on the influence of geometrical parameters on the whole lumbar spine in dynamic lumbar spine compression. Hence, a component load case of the complete lumbar spine (T12-L5) by Stemper et al. [20] was used as an experimental validation load case, and the Total Human Model for Safety v4.1 (THUMS v4.1) lumbar spine was used to apply three different individualization levels: The first individualization level was the original (unchanged, baseline) THUMS v4.1 lumbar spine, the second level was created via positioning of the vertebrae according to sagittal imaging data from the experiment, and the third level, the highest level of individualization, included adaption of the height of the vertebral bodies via morphing and positioning of the vertebrae. All different models were assessed in the same load cases concerning global kinetics, vertebrae kinematics, and fracture prediction potential.

Materials and methods

Experiments

The basis for this study is an analytical study with Level of Evidence II by [20] Stemper et al. (2017), in which axial tolerance of 26 lumbar spines (T12-L5) in combined compression and flexion was experimentally quantified using a drop tower test (see Table S1). CT scans and lateral X-rays were obtained of each specimen to confirm spinal integrity (via CT scan) and positioning (via X-ray) before testing. Cranial (T12) and caudal (L5) vertebrae were embedded in polymethylmethacrylate to facilitate attachment to the experimental apparatus. The L2-L3 disc level was kept approximately horizontal in the global coordinate system without altering the natural specimen-specific lordosis to ensure consistency of pre-load between specimens.

Compressive flexion loading was applied to whole lumbar spine specimens using a drop tower with two decoupled platforms attached to a monorail via low-friction bearings. Each specimen was attached through a load cell to the lower platform, and a laterally oriented cylinder enabled interaction between the decoupled upper platform and the superior specimen fixation. A 5 Nm pre-flexion torque was applied at the superior specimen fixation while minimizing anterior-posterior and lateral shear forces. The specimen was held in that position with the laterally oriented cylinder. The relative position of the two platforms was fixed using a cable that allowed the upper platform to apply inertial compressive loads to the specimen by reducing the vertical distance to the lower platform during deceleration while also preventing specimen recoil before testing and significant vertical displacement or impact during dynamic testing. A 32 kg mass was added to the upper platform to simulate static torso mass of a 50th-percentile male.

At the bottom of the drop tower test setup, a piece of foam was used to form a realistic acceleration pulse. Linear accelerometers were used at the lower and upper platforms to measure vertical accelerations. Forces and moments were measured via a load cell, which was attached at the caudal fixation of the specimen to the lower platform.

Each specimen was exposed to one or more dynamic tests from specific drop heights until an injury was detected. An incremental paradigm was used, wherein drop heights were increased after non-injury tests. A Vicon system (Vicon Corp., Oxford Metrics Group, Oxford, England) with three spherical targets (one target placed in the anterior aspect of the body and one in each transverse process) was used to record three-dimensional vertebral kinematics. Local cartesian coordinate system origins were defined at mid-height and mid-width along the posterior wall of each vertebral body. Vertebral kinematics were reconstructed by using target motions. Sagittal segmental angulation was computed for each segment (T12-L1 through L4-L5) as the sagittal plane angle of one vertebra relative to the subjacent vertebra [20].

After each test, specimens were examined for fractures and abnormal changes in spinal alignment or disc heights using X-rays. Specimen palpation and flexion stiffness assessments excluded endplate or soft tissue injury. Testing of a specimen was immediately stopped when an injury was detected. Fracture classification and the affected spinal level were assessed using X-rays and post-test CT scans.

Simulation

Development of FE models

The THUMS (v4.1) lumbar spine for T12 to L5 with ligaments and intervertebral discs was selected for simulations. The material properties of the annulus fibrosus and the capsular ligament have been adapted according to data from the literature [21–23]. Local coordinate systems (LCS) have been defined for each vertebral body according to a previously published method [24].

The LCS were tied to and moved in conjunction with their respective vertebrae for the duration of each test, allowing for comparison with the PHMS experiment. All simulations were conducted in Visual-Crash PAM (ESI Group, Rungis, France).

The 26 different samples were simulated in three different configurations, i.e., in the *original* or *baseline* THUMS position, in a *positioned*, and a *morphed* version, resulting in a total of 78 simulations. For the morphed configuration, pretest midsagittal X-ray images were used to determine the anterior and posterior heights of the vertebral bodies and the anterior and posterior heights of the intervertebral discs. Following previous investigations on spinal segmental kinematics, angles [25–30, 15] were measured using the image processing software ImageJ for the positioned and the morphed configuration (http://rsb.info.nih.gov/ij/; US National Institutes of Health Bethesda, Maryland, USA).

No geometrical adaptations on the THUMS lumbar spine unit were made for the baseline configuration. The changes to the segmental angles were applied to place the model for the positioned configuration. For the morphed configuration, the lateral heights of the vertebral bodies were individualized using DFM morphing in ANSA (BETA CAE Systems SA, Epanomi, Thessaloniki). After adaption of the heights, the articulation tool for human body model positioning available in ANSA was used to position the models according to the intervertebral angles measured in the X-rays (see Fig. 1).

Boundary and loading conditions

A simplified setup of the drop tower apparatus was implemented while maintaining the boundary conditions to compare the simulations to previous PHMS experiments. The THUMS lumbar spine unit was rotated for the baseline configuration to keep the L2-L3 disc level approximately horizontal in the global coordinate system.

To globally position the positioned and the morphed configuration, the distance of the lower potting to L5 in x- and z-direction and the tilt angle of L5 to the global x-axis in the X-rays were measured. The height and the tilt of the

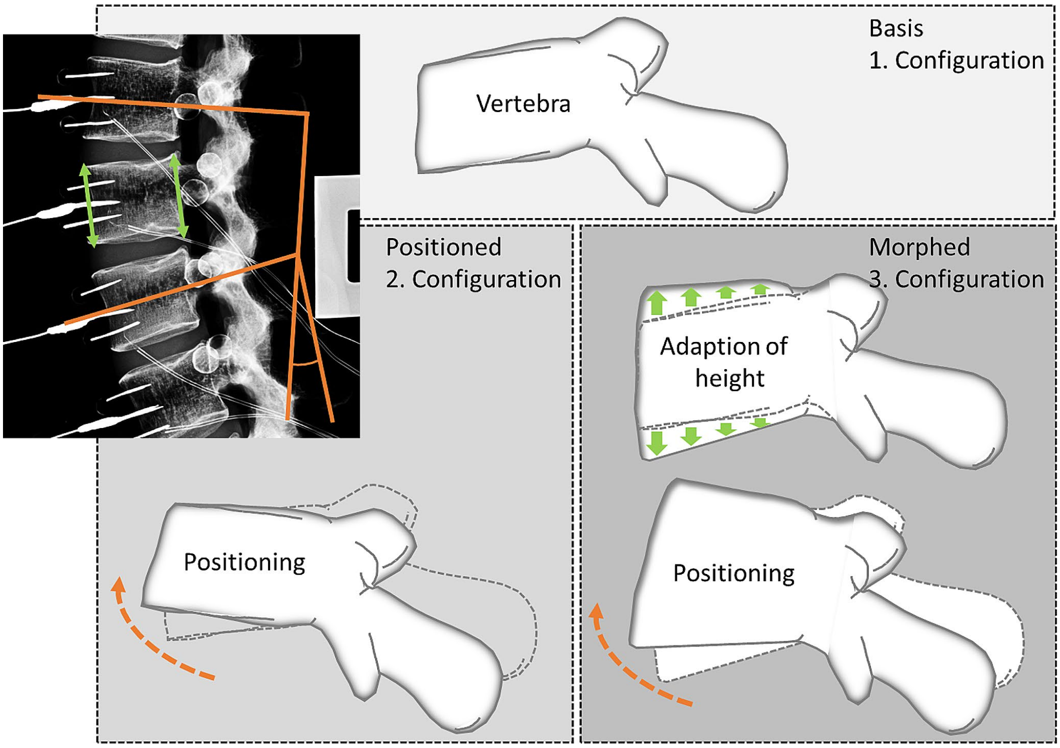

Fig. 1 Modelling approach for the three different lumbar spine configurations – morphed (3. Configuration), positioned (2. Configuration) and baseline (1. Configuration) – exemplarily shown on one vertebra

upper potting, as well as the position of the impactor with a non-structural mass of 32 kg, were individualized for each specimen according to the pretest X-rays. Then, the superior (T12) and inferior (L5) vertebrae were positioned in finite element models of aluminum potting cups, bone cement-like potting resin, and aluminum load cells used in the experiments.

The vertebrae's superior and inferior cortical shells were rigidly fixed to the deformable potting resin, and the potting resin was constrained to the rigid potting cups. Afterward, the upper potting was translated in z-direction to the same position on the cranial end of the LSUs as shown in the X-rays.

A frictionless self-contact was implemented to allow relative movement between the upper potting and the impactor. To limit the movement of the impactor in z-direction in the rebound phase, as was ensured by the cable in the experiments, a plate was added on top. To mimic the drop tower setup's release of boundary conditions, the cylinder and the lower platform allow translation in global z-direction and around global y-axis. Simulation responses were compared to PHMS kinetic and kinematic responses: section forces in the upper and lower specimen pot enable measuring of section forces in the global coordinate system.

The accelerations measured in the experiment in the lower platform are applied as input to the lower specimen pot below the section force to allow for accurate measurement. In addition to the forces and moments as measured in the specimen experiments, intervertebral kinematics were also measured in the simulation. Gravity was applied to the whole setup as an acceleration field. (see Fig. S1)

Model evaluation

The modified THUMS models were evaluated relative to the specimen test data by comparing the kinetics (forces and moments measured at the caudal end) and vertebral kinematics. In the experiments, target motions were used to reconstruct vertebral kinematics, and sagittal segmental angulation was computed for each segment (T12-L1 through L4-L5).

A similar approach to analyzing vertebral kinematics was performed in this study on the simulation data. Local coordinate systems defined in each vertebral body were used to calculate sagittal vertebral angles. For calculating the sign of the angles (negative - extension, positive - flexion) a plane was defined that spans each two local x-vectors in the sagittal plane. The sign of the resulting vector product between the two local x-vectors then determines the opening of the angle.

The similarity of the outputs of the simulation and the experimental results were analyzed until time of peak force was reached; it was assessed using the *cosine similarity* function in MATLAB (R2020a, The MathWorks, Inc., Natick, MA, USA). The closer the cosine similarity value is to 1, the smaller the cosine angle and the greater the match between vectors. Cosine similarity can be used as measure for numeric data that ignores zero-matches [31]. Here, the cosine similarity analysis was applied for each scalar (force or moment component) in the time diagram. The cosine value was also used to rate the simulation configurations for each specimen.

Vertebrae injury predictors

To identify the mechanism of vertebral compression fracture, the pressure (precisely, negative one third of the first invariant or trace of the stress tensor) of the spongiosa was analyzed. This analysis was performed by finding the peak pressure in each vertebra before the time of peak force is reached. Therefore, the maximal and minimal values of the scale of the contour plots of the models were set to the same overall maximal and minimal values. The contour plots were then filtered until only the elements exceeding a threshold were shown, which would then also define a potential fracture region.

Results

The experimental data of 26 PHMS from which lumbar spine data was obtained were used for simulation. Eleven of the 26 PHMS lumbar spines were from female donors, thirteen were from male donors, and for two, sex, mean age, height, and weight were unknown. The mean age, height, and weight of the female PHMS were 48 ± 12 yrs., 161 ± 11 cm, and 68 ± 19 kg, for the male PHMS 44 ± 12 yrs., 177 ± 6 cm, and 80 ± 11 kg, respectively. Experimental data of each specimen was used for the simulative setup of the baseline, positioned, or morphed configurations.

FE model validation

Global kinetic evaluation

Figure 2 shows the kinetic response of one specimen in all different configurations, i.e., baseline, positioned, and morphed. Compared to all other responses axes, the amplitude of z-force and y-moment is significantly higher; the primary focus is evaluating these responses.

For the *baseline* configuration, the kinetic model responses for z-force und y-moment were opposite to the experimental responses in half of the cases; for the other half, one of the responses was off in the opposite direction. For fourteen cases, the cosine value for the z-force responses of the baseline THUMS configuration is greater than 0.8, eight cases are between 0.5 and 0.8, and all other cases are less than 0.5. At the same time, for the y-moment, it is less than 0.8 for twenty-four cases and between 0.5 and 0.8 for five cases (see Fig. 3).

For the *positioned* configuration, in seven cases (27%), one model response was opposite to the experimental curves; for one case, none aligned with the experimental responses. The response aligned with the experimental responses for all other cases (77%). The cosine value for the z-force is in twenty-three cases greater than 0.5 and twenty-four cases greater than 0.8. For the y-moment in twelve cases, the z-force is greater than 0.5, and one specimen's response has a cosine value greater than 0.8. All other remaining responses are less than 0.5 (see Fig. 3).

Regarding the configuration with the *morphed* sagittal vertebral body heights, intervertebral discs, and positioned vertebrae, fifteen cases (58%) of all specimen's responses followed the same trend as the experimental responses - at least one of the responses aligned with the trend for twenty-one cases. The cosine value for the z-force was greater than 0.8 for nineteen cases and was between 0.5 and 0.8 for three cases. For the y-moment, eleven cases showed a cosine value greater than 0.8, and two, cosine values were between 0.5 and 0.8. The cosine values for the responses of the thirteen remaining specimens were lower than 0.5 (see Fig. 3).

Kinematic evaluation at vertebra level

Figure 4 shows the intervertebral kinematics per vertebra segment over time for one specimen across all configurations. The time history of these plots was used to calculate the cosine value for each curve. The results are listed in Fig. 5. For the *baseline* configuration, more than 10 to 22 specimen cases show a similarity value of less than 0.5, and 15 to 23 cases show at least a similarity value less than 0.8. The *positioned* configurations show similarity values less than 0.5 in 7 to 17 cases and less than 0.8 in 12 to 22 cases.

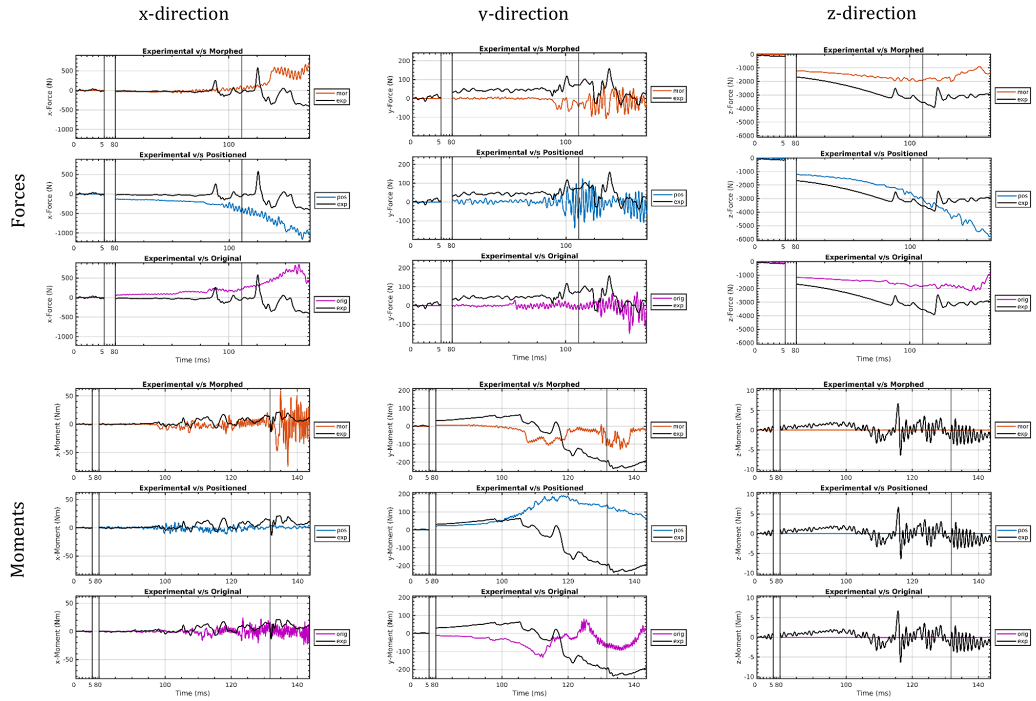

Fig. 2 THUMS simulation **kinetic** response (top – force, bottom - moment) in three different configurations compared to PMHS exemplarily for one specimen. THUMS curves are plotted starting at 80ms and for the duration of the simulation. Plots of other specimens can be found in the Supplementary Material

Specimens	x-Force			y-Force			z-Force			x-Moment			y-Moment			z-Moment		
	morphed	positioned	original	morphed	positioned	original	morphed	positioned	original	morphed	positioned	original	morphed	positioned	original	morphed	positioned	original
1	0.93146	0.91409	-0.79021	-0.37436	-0.053258	-0.011885	0.92083	0.9689	0.9395	0.15502	-0.049352	-0.11147	0.98904	0.99498	-0.96353	-0.7318	-0.7443	0.73952
2	0.16251	0.42267	-0.38891	-0.41253	0.035478	-0.057397	0.9724	0.97979	0.96945	-0.072318	-0.24875	0.045068	0.47576	-0.51523	0.053467	0.17657	-0.034114	0.23523
3	0.97329	0.96136	-0.92298	-0.049344	-0.18473	-0.071753	0.89501	0.96592	0.90088	-0.0003034	0.29831	-0.000474	0.95671	0.98759	-0.96888	0.065731	0.10537	0.068747
4	0.9584	0.99262	-0.92518	-0.74751	-0.011102	-0.23389	0.88884	0.95556	0.91828	-0.61925	-0.51106	-0.12641	0.84363	0.9795	-0.43832		-0.91229	0.089188
5	0.83238	0.82422	-0.70552	-0.0069264	0.11618	0.26686	0.99043	0.99527	0.98009	0.17577	0.46854	0.34734	0.51403	0.46812	-0.31808	-0.009023	0.077959	-0.43821
6	0.92998	0.90629	-0.83341	-0.089038	-0.49748	-0.64359	0.95998	0.98554	0.98151	0.057359	0.27089	0.4005	0.95541	0.92257	-0.60076	0.49018	0.44212	0.19912
7	-0.44825	-0.44488	0.58089	-0.094221	0.14368	-0.16356	0.36768	0.26581	0.38084	0.13683	0.0039214	-0.057551	0.33078	0.41163	-0.31164	0.11829	0.043977	-0.045798
8	-0.51095	-0.6122	-0.61882	-0.22358	0.13141	0.14532	0.49479	0.50942	0.43768	0.37363	-0.16814	-0.28175	0.35093	0.34184	0.64011	-0.0075177	-0.0010056	
9	0.96163	0.96301	-0.40419	-0.084708	0.23362	0.12797	0.97234	0.98918	0.60039	0.0049076	-0.32775	-0.2912	-0.78169	-0.75198	0.43384	-0.092008	0.0074712	
10	-0.18258	-0.56886	-0.68512	0.042082	0.043689	0.29491	0.75575	0.91585	0.63116	0.060419	-0.29836	0.12841	-0.41656	-0.76626	-0.85412	-0.016033	0.28091	0.24417
11	-0.17058	-0.024788	-0.35332	-0.047316	-0.096427	-0.11478	0.6565	0.44934	0.78818	0.1331	0.26724	0.34547	0.21862	-0.3449	0.43633	0.096826	-0.032086	0.020734
12	0.736	0.79497	0.32653	0.33397	0.037712	0.18115	0.94552	0.97449	0.91985	-0.47806	0.19013	-0.57951	0.81534	0.92375	0.28327	0.29029	-0.28132	0.1835
13	-0.64159	-0.79221	-0.93635	-0.0037063	-0.03961	0.17306	0.91441	0.91901	0.81736	-0.22502	0.080594	0.6088	0.53783	0.73616	0.96629	-0.26313	0.36133	0.36239
14	0.98995	0.98457	-0.19874	-0.35577	-0.79056	-0.20263	0.88728	0.92753	0.43371	0.63615	0.61233	0.33008	0.91194	0.89092	-0.49216	0.5855	0.67086	-0.14333
15	0.9727	0.97452	-0.76256	0.020963	0.13971	0.11804	0.9083	0.98407	0.51774	-0.55757	-0.62917	-0.16715	0.9648	0.98362	-0.18742	-0.51856	-0.89938	-0.41665
16	0.97883	0.98783	-0.97244	-0.13606	0.095016	0.099267	0.8556	0.93079	0.96527	0.39295	0.62651	0.23346	-0.76616	-0.785	0.22173	-0.0065322	0.44824	-0.49662
17	0.9783	0.99172	-0.9728	0.040047	0.062999	0.32934	0.93723	0.9693	0.91718	-0.2082	-0.51384	-0.57596	0.99403	0.99476	-0.90997	0.13125	-0.092261	0.29031
18	0.98557	0.9896	-0.88125	-0.067905	0.15163	-0.51993	0.96912	0.98307	0.95556	0.030097	-0.16174	0.44556	0.98179	0.97211	-0.9582	0.77243	0.8716	-0.53277
19	0.92607	0.95731	-0.081898	0.032302	-0.029239	-0.12089	0.98615	0.99102	0.56847	-0.10544	0.041524	0.24226	0.96466	0.96334	-0.3751	0.77611	0.75787	-0.16133
20	0.98856	0.97531	-0.89796	-0.051431	-0.069999	-0.10235	0.93565	0.97576	0.95256	0.44516	0.47423	0.32551	0.98119	0.9788	-0.90823	0.45107	0.82088	-0.33125
21	-0.50673	0.50477	-0.95376	-0.12216	-0.23932	-0.22426	0.9124	0.96671	0.91598	0.16916	0.27005	0.58674	-0.18681	-0.065637	-0.72112	-0.35568	-0.14447	0.059071
22	0.94851	0.98187	-0.73196	0.011769	0.23491	-0.029811	0.95596	0.99501	0.59283	0.039636	0.069435	0.03329	-0.53053	-0.748	0.61333	-0.029725	0.25548	-0.087507
23	-0.88642	-0.50499	-0.8202	0.50616	0.35518	0.65403	0.95376	0.96709	0.93485	-0.34903	-0.2393	-0.5731	0.34437	0.34798	-0.13988	-0.033333	-0.046764	0.21732
24	0.94904	0.96804	-0.82406	-0.64733	-0.56227	-0.1599	0.78337	0.84968	0.47008	0.28642	0.32731	0.25265	-0.77927	-0.79794	0.65802	-0.26006	-0.092467	
25	-0.96334	-0.95117	-0.90719	-0.17723	-0.17215	-0.10005	0.94818	0.96505	0.76587	-0.033473	-0.11365	0.1061	0.4562	0.52513	0.8042	-0.15194	0.088459	-0.78146
26	-0.69801	-0.8889	-0.78221	-0.13165	-0.28489	-0.10655	0.46	0.84909	0.5321	-0.059718	-0.081379	0.012967	0.28901	0.074014	0.49476	0.0020605	0.0067807	
	Cosine value																	

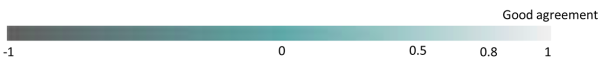

Fig. 3 Cosine value for all studied **kinetic** simulation specimen responses in continuous hot/cold spectrum. Darker colors represent smaller cosine values, lighter colors cosine values closer to 1

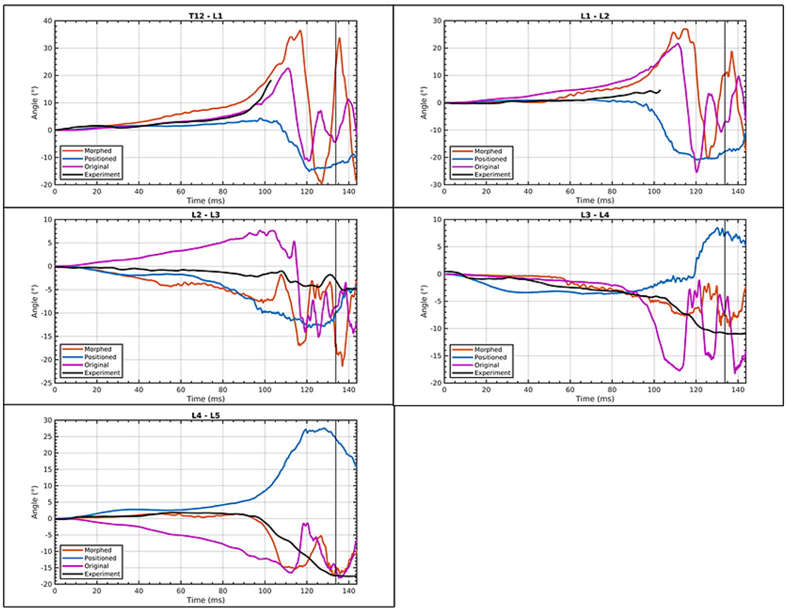

Fig. 4 THUMS simulation **kinematic** response in four different configurations (morphed, positioned, baseline) compared to PHMS exemplarily for one specimen. THUMS curves are plotted for the duration of the simulation. Plots of other specimens can be found in the Supplementary Material

Specimens	T12-L1			L1-L2			L2-L3			L3-L4			L4-L5		
1	morphed	positioned	original	morphed	positioned	original	morphed	positioned	original	morphed	positioned	original	morphed	positioned	original
2	0.97134	0.95462	-0.95917	0.92613	0.95289	-0.98465	0.98366	0.85996	-0.93785	0.55086	0.47422	-0.72999	0.94723	0.92486	-0.96513
3	0.7551	0.50381	0.71748	0.016023	-0.80415	-0.22746	0.91411	0.95296	0.11971	0.91547	-0.072935	0.81458	0.87906	-0.89323	0.5149
4	0.95489	0.96182	-0.9542	0.94588	0.94971	-0.97093	-0.66598	0.8659	-0.56923	-0.99136	-0.51415	0.96114	0.98799	0.97568	-0.97981
5	0.68773	0.82956	-0.62525	0.55809	0.8689	-0.18713	-0.40452	0.59918	0.10033	0.66385	0.60373	-0.62526	0.93137	0.91213	-0.89762
6	0.14665	-0.25025	0.020125	0.27774	0.084612	-0.43316	0.41237	0.27569	-0.49889	0.19346	-0.92728	-0.38316	0.43152	0.48127	-0.81936
7	0.96465	0.77723	-0.57506	0.92921	0.81468	-0.30313	-0.49512	-0.019917	0.42022	-0.23082	0.42186	0.34602	0.95508	0.92158	-0.76683
8	0.23812	0.29044	-0.21983	0.50446	0.50446	-0.31615	-0.52366	-0.52366	0.58021	-0.54323	-0.86625	0.63739	-0.43202	-0.68828	0.61249
9	0.37533	0.25173	0.29666	0.94409	0.91462	0.45136	0.97812	0.99495	0.91673	-0.63842	-0.36687	0.96821	0.91696	0.94251	-0.92585
10	0.96296	0.88861	0.12136	-0.88275	-0.84012	-0.28865	0.7087	0.75437	0.64629	-0.94084	0.31494	0.87338	-0.30663	-0.13004	-0.090626
11	0.79682	0.96846	0.59	-0.47711	-0.78706	0.12212	0.91851	0.3253	-0.68786	0.83512	0.83093	0.89224	-0.66213	-0.95747	-0.97368
12	0.85605	0.95291	-0.019208	0.87569	0.87703	-0.33269	-0.86392	-0.19541	0.83368	0.34226	0.29237	0.10838	0.85247	0.083157	0.79932
13	0.95757	0.97023	0.96279	0.95815	0.95393	0.97199	0.67394	-0.072259	0.88749	0.93682	0.92974	0.93926	0.69007	-0.7829	0.98623
14	0.97237	0.99334	0.978	0.97624	0.9566	0.98214	0.71727	0.93981	0.97506	-0.95646	-0.87219	-0.81559	0.85294	0.90353	0.99287
15	0.46199	0.68044	0.24621	0.93405	0.9417	0.49967	-0.76685	0.95033	0.5976	0.009637	0.49668	0.045277	0.98113	0.9852	-0.88101
16	0.98292	0.61059	-0.31824	0.98154	0.66827	-0.064563	0.99074	0.98102	0.31219	-0.95877	0.79439	0.95874	0.98431	0.97016	-0.87507
17	0.34276	0.479	0.062354	-0.2501	-0.30984	-0.38435	0.9412	0.21981	-0.70152	-0.92232	-0.94049	0.63419	-0.86241	-0.90376	0.46384
18	0.98753	0.96755	-0.80619	0.97906	0.94653	-0.71008	0.90029	0.99077	-0.42563	-0.95475	-0.72981	0.93106	0.98774	0.9902	-0.97081
19	0.98782	0.98958	-0.9623	0.92804	0.6272	-0.9389	-0.26096	0.98689	-0.92077	0.52214	0.76065	-0.61618	0.99039	0.99655	-0.98578
20	0.0060849	0.4155	0.74647	-0.24404	0.50209	0.46509	0.52707	0.72888	0.47778	0.57443	0.62398	0.87187	0.9813	0.98169	-0.79583
21	0.99152	0.88811	-0.7571	0.99288	0.64557	-0.6378	0.24501	0.080579	0.24269	-0.54917	0.92597	0.57585	0.98844	0.98506	-0.94514
22	0.79349	0.71082	0.33494	0.90203	0.77532	0.40933	-0.52425	-0.4243	0.13186	0.77152	0.92202	0.69035	0.90694	0.86751	0.80019
23							0.82805	-0.11334	-0.90198	-0.52375	-0.78498	0.34162	-0.40095	-0.72884	0.54804
24	0.63513	0.83753	0.33095	0.54046	0.76697	-0.12093	0.72174	0.88202	0.25067	-0.14933	-0.063871	-0.1624	0.94477	0.94266	0.90711
25	-0.86539	-0.89495	-0.51479	-0.87218	-0.82954	-0.71658	-0.038876	-0.59414	-0.33312	-0.82055	-0.45769	0.90464	-0.35932	-0.43575	-0.088087
26	0.16715	0.1487	-0.21275	-0.091364	0.02582	0.47613	0.89974	0.82057	0.47297	0.51913	0.42275	0.57581	0.57159	0.52942	0.69173
27	-0.21848	-0.061897	-0.44085	0.44483	0.26068	0.62716	0.66992	0.60119	0.51842	0.62508	0.66727	0.85524	0.6407	0.68144	0.86402
	Cosine value														

Good agreement

-1 0 0.5 0.8 1

Fig. 5 Cosine value for all studied **kinematic** simulation specimen responses in continuous hot/cold spectrum. Darker colors represent smaller cosine values, lighter colors cosine values closer to 1

4 to 14 cases showed a similarity value greater than 0.8, with the intervertebral kinematics between L3-L4 showing the least similarity. For the *morphed* configurations, 6 to 16 cases have a cosine value less than 0.5, 10 to 23 cases have a value less than 0.8, and 3 to 16 cases a similarity value greater than 0.8. Also, the intervertebral kinematics between L3 and L4 showed the least concordance for this configuration.

The trend and similarity assessment as a meta-analysis were used for filtering regarding consideration in terms of injury predictors. Based on that, only the positioned and the morphed configuration were evaluated.

Analysis regarding fracture prediction capabilities

Figure 6 shows exemplarily the stress field map of one specimen in the morphed configuration. Following our recently published analysis approach [23] the area of peak stress in each vertebra at the time of experimental peak force was determined. Therefore, the upper scale limit has been set to 3.5 MPa, the lower bound to 0 MPa for all specimen models in every configuration. The contour plot values were then further filtered until only the elements defining a region of likely fracture were shown. For the specimen that sustained a wedge fracture at L1 classified as a flexion-compression fracture, a stress pressure pattern between T12 and L1 in a triangular shape with highest stresses in the anterior region of L1 becomes visible. The contour plots for all other specimens can be found in the supplementary material; besides flexion-associated fractures, which resulted in wedge or burst fractures, fractures which can be attributed to extension primarily affecting the spinous processes were observed in the experiments.

The contour plots have been rated and classified according to the following criteria: identification of extension or flexion fractures and identification of the fracture region reported in the experiments. Table 1 combines the meta-analysis results for the kinetic data in three categories (good, fair, bad) and the results of the contour plots, i.e., whether the correct fracture mechanism at the position reported in the experimental data is observed in the simulations in color coding. Six out of twenty-six specimen cases detect the fracture type and fracture position in the simulation for the morphed configuration. Ten out of twenty-six cases predicted the fracture type and location reported from the experiments in the positioned configuration. For the morphed configuration, five out of twenty-six cases, the answer of the kinetic evaluation was contradictory to the evaluation of the contour plots. For the positioned configuration, four cases showed conflicting responses.

Discussion

In this study, we investigated the necessary level of individualization of a lumbar spine model in high-dynamic load situations to make a realistic recommendation for potential

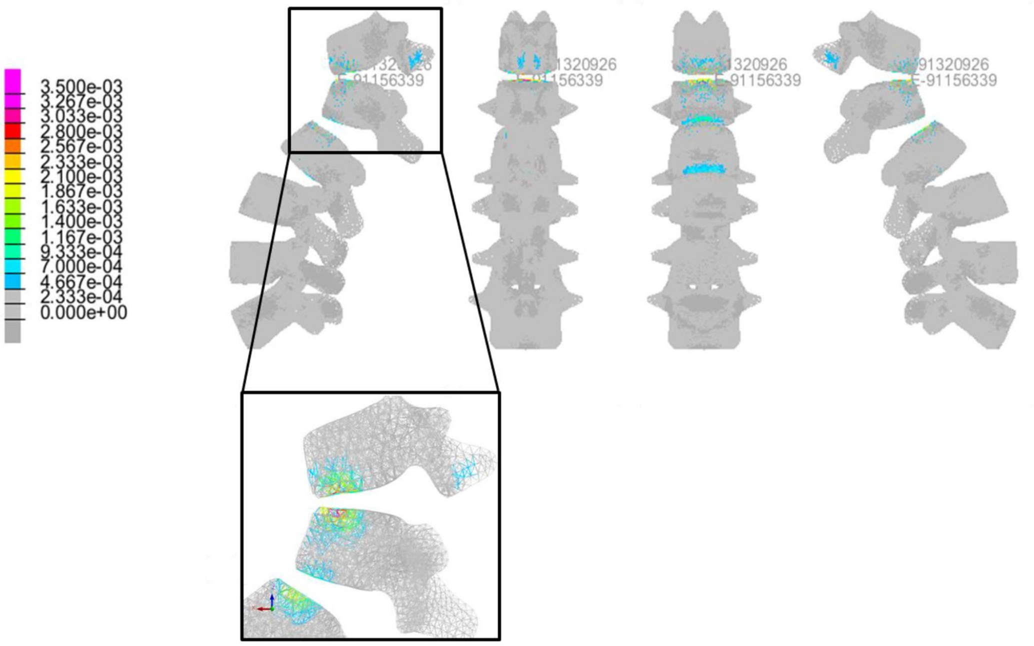

Fig. 6 Finite element model stress field maps (right, rear, front and left side view) of the maximum pressure (negative one third of first invariant) in GPa of the spongiosa of the vertebrae at the moment of peak force exemplarily on one specimen with a wedge fracture at L1. The final step of the filtering is shown and shows how the distribution of pressure is allocated

Table 1 Rating of studied kinetic & kinematic simulation responses vs. experimental response per specimen on a meta level for each configuration. Injury outcomes are color coded (green: injury type and location could be predicted, red: injury type or location were not detected in the contour plots)

Specimens	Kinetic & kinematic rating		
	Morphed	**Positioned**	**Baseline**
1	Fair/good	Good/fair	Bad/bad
3	Good/fair	Fair/bad	Good/bad
4	Good/good	Good/good	Bad/bad
5	Fair/good	Good/fair	Bad/bad
6	Good/fair	Good/fair	Bad/bad
7	Fair/good	Good/good	Bad/bad
8	Good/good	Good/fair	Fair/bad
9	Fair/bad	Fair/bad	Bad/bad
10	Fair/fair	Fair/fair	Bad/bad
11	Bad/bad	Bad/bad	Bad/bad
12	Good/fair	Fair/good	Bad/bad
13	Fair/good	Good/good	Bad/good
14	Fair/good	Fair/good	Bad/fair
15	Fair/bad	Fair/fair	Bad/bad
16	Fair/bad	Good/good	Bad/bad
17	Bad/Bad	Bad/Bad	Fair/fair
18	Fair/fair	Fair/good	Bad/bad
19	Fair/fair	Good/good	Bad/bad
20	Fair/bad	Good/bad	Bad/bad
21	Fair/bad	Good/bad	Bad/bad
22	Fair/fair	Good/fair	Fair/good
23	Fair/bad	Fair/bad	Fair/na
24	Fair/fair	Good/fair	Fair/fair
25	Fair/fair	Fair/bad	Fair/bad
26	Good/bad	Good/bad	Bad/bad
27	Fair/fair	Bad/bad	Bad/bad

Good	Kinematic/kinetic simulation response has same trend & similar magnitude
Fair	Kinematic/kinetic simulation response has same trend
Bad	Neither trend nor magnitude is met

(red)	Fracture type & location cannot be detected
(green)	Fracture type & location can be detected

application in full-scale load cases. Therefore, three different model types with distinct levels of individualization have been selected, and the effects on the kinematic, kinetic, and fracture prediction capabilities have been analyzed.

Model generation

The experimental test setup was abstracted in the simulation to prevent uncertainties from being introduced into the system by too many modeled parameters. Consequently, the measured accelerations for each specimen were applied to the bottom of the test setup. A point mass on top of the setup and a plate was used to simulate the boundary conditions. However, details influencing the results may have been overlooked by doing so. Also, further integration of experiments and simulation would help to objectify the future modeling of experiments [32, 33].

The base for all levels of individualization within this study is the lumbar spine of THUMS v4.1 developed by Toyota Motor Corporation and Toyota Central R&D Labs. In THUMS v4.1, the musculoskeletal system and the internal organs are modeled in detail based on CT scanning data; the material properties of each tissue are defined to reproduce the PMHS response as given in the literature [34]. However, to apply THUMS v4.1 lumbar spine to a detailed study, the material properties of the intervertebral discs and capsular ligaments were updated according to literature data.

The generic THUMS v4.1 lumbar spine with adapted material was selected as the baseline configuration. The lumbar spine model was globally rotated and integrated into the setup afterward. No individualization adaptions were incorporated into the model for the baseline configuration. This generic configuration aimed to understand how implementing the model into an experimental setup for HBM validation purposes without the exact knowledge of the setup could affect the results. As there were no changes to the intervertebral angles, the lumbar spines' curvature only matches the corresponding X-rays in some instances purely by coincidence.

The exact change of intervertebral angles was used for the next level of individualization, named the positioned configuration. Nevertheless, investigation with angles directly measured from the test data might come to different conclusions. During vertebrae positioning using ANSA, spatial difficulties with the spinal processes of adjacent vertebrae occurred. These were expected as the THUMS v4.1 lumbar spine is based on one individual's lumbar spine; with the positioning, we try to adapt the position to the anthropometry of another specimen.

Nevertheless, the needed adjustments in the x- and z-direction to avoid intersections were minor compared to the applied angles. Finally, the information used for the individualization was only in one plane, i.e., the sagittal plane. Thus, this study did not use information on the position in the frontal plane. As the lumbar spine might not be perfectly symmetrical to the sagittal plane, this second level of information could give further insight into lumbar spine fracture biomechanics. However, compared to the spinal segmental angles measured in the sagittal plane, angles in the frontal plane are smaller in subjects without medical conditions. For the most detailed level of individualization, named morphing, in addition to changing the intervertebral angles, the sagittal heights of the vertebral bodies and intervertebral discs have been measured in the pre-test sagittal X-rays and integrated into the modified THUMS v4.1 model.

This partial individualization does not involve parameters from other planes for several reasons:

1. Lack of imaging data with sufficient quality to determine parameters.
2. Adaption of the THUMS lumbar spine would require a method to complete the parametrization of the model.
3. This study aimed to investigate the lowest needed level of individual parametrization.

Studies investigating the sensitivity of lumbar spine loading to anatomical parameters showed that variations of the vertebral body height, disc height, transverse process width, and the curvature of the lumbar spine are most influential [9, 11]. Therefore, the authors decided to reduce the individualization to a minimum level. The morphing and positioning were performed using ANSA. In cases where the adaptions were too big, ligaments were recreated and re-meshed.

Following previous studies [12], averaged material properties were used for the simulations even though interpersonal variance in material properties might significantly influence simulative responses. Also, visco- and poroelastic behavior of the vertebrae is neglected; this might be important when loading is applied with higher velocities. Finally, articular cartilage was not modeled, possibly influencing the facet joint biomechanics. However, it is deemed that the influence on the relative results between the different initial postures will still be valid in the presence of cartilage.

Specimens with excessive disc height loss, bridging osteophytes, or inconsistent alignment were not included in the study [20], however degeneration can have a major influence on the kinematics and kinetics, and thus, affect the fracture behavior of lumbar vertebrae in physiological loading conditions [35]. Therefore, future studies should use the example Natarajan [36–38] et al. to investigate how degeneration affects highly dynamic loading conditions.

The muscle structures on the specimens for the physical experiments were removed [39], so no muscle activation was considered in the simulation models. However, it has been shown that muscle activation has an influence on occupant kinematics and thus on the probability of injury in a crash [40]. Therefore, the influence of autochthonous back muscles on fracture risk in the lumbar spine should be further investigated in future studies.

Validation

The models were validated using kinetic and kinematic responses from simulation locations corresponding to the experiment's measurement locations. Failure criteria were not used for validation. Qualitatively, the configuration with the highest degree of individualization showed the closest agreement with the experiments, followed closely by the positioned configuration. At the same time, the baseline configuration performed worst.

The cosine value calculated to quantify the deviation of the simulation response from the experimental data supports this observation (Figs. 3 and 5). Even though the cosine value is an uncommon way to measure the similarity between an experimental and a simulation response, it is frequently used to measure the similarity in text analysis [31], and it satisfies the need to measure the similarity between experiment and simulation quantitively. Commonly used rating metrics are CORA and EEARTH (ISO/TR 16250:2013). However, the parameter customizations possible within these metrics are inherently subjective and have the potential to produce non-trivial scores, which can, in turn, influence the conclusions drawn from a study [41].

The gross biomechanical behavior of the model, as described by the load-time curves (e.g., Fig. 2) and the intervertebral kinematics (e.g., Fig. 4), was not in good agreement with the experimentally determined data for the baseline configuration. The explanation might be that the model's initial position for the baseline configuration was only globally adjusted to the initial position of the specimen in the experiment; previous validation efforts with THUMS v4.1 [42] or THUMS v5 [43] found similar results.

In comparison, the positioned configuration, i.e., the gross biomechanical behavior of the model, as described by the load-time curves (e.g., Fig. 2) and the intervertebral kinematics (e.g., Fig. 4), was in good agreement with the experimentally determined data. This observation is supported by the respective cosine values (Figs. 3 and 5), indicating that the initial position has an influence not only on kinematics but also on kinetics.

At the highest level of individualization, the gross biomechanical behavior of the model, as described by the load-time curves (e.g., Fig. 2) and the intervertebral kinematics (e.g., Fig. 4), was in slightly better agreement compared to positioned data. In this configuration, the vertebral bodies' angular position and the vertebral bodies' height were individualized; the latter, including the wedge angle, i.e., the relation of the anterior height of the vertebral bodies in relation to their posterior height. As described in Section Model Generation, previous studies found an influence of vertebra body height on lumbar spine kinematics. However, these studies only investigated physiological loading conditions, i.e., non-crash-related dynamic loading. Current studies on the Global Human Body Model Consortium (GHBMC) lumbar spine under dynamic loading conditions [44] indicate that the vertebral height might not influence the response of the lumbar spine that much.

Regarding the correlation of between experimental and simulative responses, the third configuration performed better than the second configuration. However, this study aimed to propose a strategy for considering as many details on different spinal anthropometries as possible. The adaption of the heights, combined with the positioning, dramatically increases the number of possible spine models. A viable alternative could be further investigating the relationship between the relative wedging of vertebral bodies and the spinal position [45]. That could allow vertebral wedging and position to be clustered, thus reducing the complexity of the spinal models. Besides, the model setup in configuration 3 is more time-consuming and can lead to model deficiencies, e.g., intersections need to be re-mesh, which would hinder the model's use in the automotive development processes.

Fracture prediction capabilities

Fracture prediction capabilities were evaluated based on previously developed, completely individualized lumbar spine models [23]. The morphed configuration possesses the best fracture prediction properties. The positioned configuration performed slightly worse. Due to the baseline configuration's poor performance in the validation, it was excluded from further evaluation of the fracture prediction capabilities.

The fracture prediction capabilities are rated in Table 1. First, the kinetic and kinematic response agreement to the experiment is classified as either 'good,' 'fair,' or 'bad.' The pressure distribution explains whether a fracture could be predicted and whether the fracture location is met. If the simulative kinematic response does not align with the experimental response, the fracture location cannot be predicted. That indicates a relationship between the kinematics and the location and type of fracture. As the initial posture influences the kinematics, the initial posture directly influences the spinal injury mechanism. Three models show larger pressure areas than others; the reason might be the vertebral body size, which was not adapted in this configuration, and differences in material properties in the experiment due to sex.

In comparison, the morphed configuration shows a slightly better fracture prediction capability. As an interpersonal variation of the vertebral disc height influences spinal stiffness [12] and disc height was adapted in this configuration, this might be another factor affecting the quality of the fracture prediction. This influence of vertebral disc thickness variation might indicate that the wedging angle influencing the lumbar lordosis has an effect on the spinal response. This hypothesis aligns with previous findings on geometrical personalized finite-element models of lumbar spines [46]. Thus, it is not only the vertebral disc size but also the wedging angle that affects the spinal response [12, 47].

Validation and fracture prediction capabilities draw a similar picture: the morphed configuration performs slightly better than the positioned configuration. However, besides the above arguments regarding fracture prediction capabilities, the positioned models could also predict fractures and the fracture locations. The positioned configuration also slightly overpredicted fractures. If the component load case is abstracted and considered in the full-scale application, it would be preferable to evaluate conservatively using the positioned configuration instead of having a high effort to build a morphed model. Hence, there is support that the positioned configuration is sufficient, for evaluating the performance of safety system for different anthropometries.

However, the study was designed as a pure component load case of the lumbar spine under dynamic compression-flexion. The simulation matrix consisted of two individualization parameters. Future studies could investigate whether completely subject-specific modeling of the lumbar spine improves the kinematic and kinetic responses and injury prediction capabilities. Furthermore, more levels of individualization, including other parameters, could be examined. Moreover, an investigation of how different degrees of customization affect full-scale load cases and a study of the performance under other loading conditions are needed. Finally, the assessment of the fracture prediction capabilities was inherently subjective. Thought should also be given to establish an objective evaluation standard for contour plots.

Conclusions

The main objective of this study was to find the coarsest level of individualization needed to simulate vertebral body fractures to ease full-scale analysis. Therefore, a bottom-up approach was chosen, and three different lumbar spine individualizations were evaluated under dynamic loading. The kinematic and kinetic simulation response was compared to the experimental response for each of the twenty-six specimens, and the fracture prediction capabilities were rated compared to the injuries observed in the experiment. In conclusion, the models with the highest degree of individualization, i.e., morphing, performed best, followed by the positioned configuration. As the morphing of the vertebra and intervertebral discs heights is very elaborate, it might be challenging to routinely integrate it into full-body models. Focusing on the positioning of vertebral bodies, if full-body models are analyzed for injury reconstruction or prediction, may therefore be a suitable approach.

Supplementary Information The online version contains supplementary material available at https://doi.org/10.1007/s00414-024-03225-z.

Acknowledgements Funding/competing interest: This research was supported in part by Naval Air Warfare Center, Aircraft Division; grant number N00421-10-C-0049 and United States Veterans Affairs Medical Research.

Authors' contribution statement: Conceptualization: Laura Kathrin Rieger, Steffen Pelschus, Brian Stemper, Methodology: Laura Kathrin Rieger, Steffen Peldschus, Brian Stemper, Formal analysis and investigation: Laura Kathrin Rieger, Writing - original draft preparation: Laura Kathrin Rieger, Writing - review and editing: Steffen Peldschus, Mirko Junge, Rachel Cutlan, Brian Stemper, Funding acquisition: not applicable, Resources: not applicable; Supervision: Brian Stemper, Steffen Peldschus.

Data availability The study protocol was approved by the Subcommittee on Human Studies at the Clement J. Zablocki Veterans Affairs Medical Center in Milwaukee, WI, USA.

Declarations

Ethics approval All lumbar spine specimens for this study were obtained from donors through the Wisconsin Donor Network.

Clinical trial number Not applicable.

Informed consent Consent to participate/consent to publish: Consent for spine donation was obtained from the next of kin.

Conflict of interest The authors do not have any conflict of interest to disclose.

References

1. Leucht P, Fischer K, Muhr G et al (2009) Epidemiology of traumatic spine fractures. Injury 40(2):166–172. https://doi.org/10.1016/j.injury.2008.06.040
2. Pintar FA, Yoganandan N, Maiman DJ et al (2012) Thoracolumbar spine fractures in frontal impact crashes. Ann Adv Automot Med (56): 277–283
3. Wang MC, Pintar FA, Yoganandan N et al (2009) The continued burden of spine fractures after motor vehicle crashes. J Neurosurg Spine 10:86–92. https://doi.org/10.3171/SPI.2008.10.08279
4. Rao RD, Berry CA, Yoganandan N et al (2014) Occupant and crash characteristics in thoracic and lumbar spine injuries

resulting from motor vehicle collisions. Spine J 14(10):2355–2365. https://doi.org/10.1016/j.spinee.2014.01.038
5. Jorlöv S, Bohman K, Larsson A (2017) Seating positions and activities in highly automated cars – a qualitative study of future automated driving scenarios. In: Proceedings of the IRCOBI Conference, pp 13–22
6. Östling M, Jeppsson H, Lubbe N (2019) Predicting crash configurations in passenger car to passenger car crashes to guide the development of future passenger car safety. In: Proceedings of the IRCOBI Conference, pp 626–643
7. Richardson R, Donlon J-P, Jayathirtha M et al (2020) Kinematic and injury response of reclined PMHS in frontal impacts. Stapp Car Crash J 64:83–153. https://doi.org/10.4271/2020-22-0004
8. Kaufman RP, Ching RP, Willis MM et al (2013) Burst fractures of the lumbar spine in frontal crashes. Accid Anal Prev 59:153–163. https://doi.org/10.1016/j.aap.2013.05.023
9. Niemeyer F, Wilke H-J, Schmidt H (2012) Geometry strongly influences the response of numerical models of the lumbar spine–a probabilistic finite element analysis. J Biomech 45(8):1414–1423. https://doi.org/10.1016/j.jbiomech.2012.02.021
10. Thacker BH, Wu Y-T, Nicolella DP et al (1997) Probabilistic injury analysis of the cervical spine. American Institute of Aeronautics and Astronautics, Inc., pp 2093–2103. https://doi.org/10.2514/6.1997-1135
11. Putzer M, Ehrlich I, Rasmussen J et al (2016) Sensitivity of lumbar spine loading to anatomical parameters. J Biomech 49(6):953–958. https://doi.org/10.1016/j.jbiomech.2015.11.003
12. Meijer GJM, Homminga J, Veldhuizen AG et al (2011) Influence of interpersonal geometrical variation on spinal motion segment stiffness: implications for patient-specific modeling. Spine 36(14):929–935. https://doi.org/10.1097/BRS.0b013e3181fd7f7f
13. Izumiyama T, Nishida N, Iwanaga H et al (2018) The analysis of an individual difference in human skeletal alignment in seated posture and occupant behavior using HBMs. In: Proceedings of the IRCOBI Conference, pp 549–560
14. Izumiyama T, Nishida N, Yamagata H et al (2022) Analysis of individual variabilities for lumbar and pelvic alignment in highly reclined seating postures and occupant kinematics in a collision. In: Proceedings of the IRCOBI Conference, pp 941–955
15. Sato F, Miyazaki Y, Morikawa S et al (2021) The effect of seat back inclination on spinal alignment in automotive seating postures. Front Bioeng Biotechnol 9:1–17. https://doi.org/10.3389/fbioe.2021.684043
16. Zhang K, Cao L, Fanta A et al (2017) An automated method to morph finite element whole-body human models with a wide range of stature and body shape for both men and women. J Biomech 60:253–260. https://doi.org/10.1016/j.jbiomech.2017.06.015
17. Beillas P, Berthet F (2017) An investigation of human body model morphing for the assessment of abdomen responses to impact against a population of test subjects. Traffic Inj Prev 18(Suppl 1):142–147. https://doi.org/10.1080/15389588.2017.1307971
18. Shi X, Cao L, Reed MP et al (2014) A statistical human rib cage geometry model accounting for variations by age, sex, stature and body mass index. J Biomech 47(10):2277–2285. https://doi.org/10.1016/j.jbiomech.2014.04.045
19. O'Cain CM, Gepner BD, Spratley EM et al (2019) Pipeline for specimen specific bone-ligament-cartilage finite element models. Proceedings of Ohio State University Injury Biomechanics Symposium: 1–6
20. Stemper BD, Chirvi S, Doan N et al (2018) Biomechanical tolerance of whole lumbar spines in straightened posture subjected to axial acceleration. J Orthop Res 36(6):1747–1756. https://doi.org/10.1002/jor.23826
21. Mattucci SFE, Moulton JA, Chandrashekar N et al (2012) Strain rate dependent properties of younger human cervical spine ligaments. J Mech Behav Biomed Mater 10:216–226. https://doi.org/10.1016/j.jmbbm.2013.04.005
22. Newell N, Carpanen D, Grigoriadis G et al (2019) Material properties of human lumbar intervertebral discs across strain rates. Spine J 19(12):2013–2024. https://doi.org/10.1016/j.spinee.2019.07.012
23. Rieger LK, Shah AS, Schick S et al (2024) Subject-specific geometry of FE lumbar spine models for the replication of fracture locations using dynamic drop tests. Ann Biomed Eng. https://doi.org/10.1007/s10439-023-03402-y
24. Peldschus S, Wagner A, Muehlbauer J et al (2021) Standardised validation procedure for qualifying the HBM to be used for assessing effectiveness of pilot protection principles
25. Armijo-Olivo S, Jara X, Castillo N et al (2006) A comparison of the head and cervical posture between the self-balanced position and the Frankfurt method. J Oral Rehabil 33(3):194–201. https://doi.org/10.1111/j.1365-2842.2005.01554.x
26. Harrison DE, Harrison DD, Cailliet R et al (2000) Cobb Method or Harrison posterior tangent method. Spine 25(16):2072–2078
27. Berthonnaud E, Dimnet J, Roussouly P et al (2005) Analysis of the sagittal balance of the spine and pelvis using shape and orientation parameters. J Spinal Disord Tech 18(1):40–47. https://doi.org/10.1097/01.bsd.0000117542.88865.77
28. Mac-Thiong J-M, Labelle H, Berthonnaud E et al (2007) Sagittal spinopelvic balance in normal children and adolescents. Eur Spine J 16(2):227–234. https://doi.org/10.1007/s00586-005-0013-8
29. Park S-M, Song K-S, Park S-H et al (2015) Does whole-spine lateral radiograph with clavicle positioning reflect the correct cervical sagittal alignment? Eur Spine J 24(1):57–62. https://doi.org/10.1007/s00586-014-3525-2
30. Rocabado M (1983) Biomechanical relationship of the cranial, cervical, and hyoid regions. J Craniomandib Pract 1(3):61–66. https://doi.org/10.1080/07345410.1983.11677834
31. Han J, Kamber M, Pei J (2012) // 2011) Getting to Know Your Data. In: Han J, Kamber M, Pei J (eds) Data Mining. Concepts and techniques, 3. ed. Elsevier; Elsevier Science, Burlington, pp 39–82
32. Anderson AE, Ellis BJ, Weiss JA (2007) Verification, validation and sensitivity studies in computational biomechanics. Comput Methods Biomech Biomed Engin 10(3):171–184. https://doi.org/10.1080/10255840601160484
33. Fuchs T (2018) Objektivierung der Modellbildung von verletzungsmechanischen Experimenten für die Validierung von Finite-Elemente Menschmodellen. Dissertation, Ludwig-Maximilians University Munich
34. Iwamoto M, Kisanuki Y, Watanabe I et al (2002) Development of a finite element model of the Total Human Model for Safety (THUMS) and application to injury reconstruction. In: Proceedings of International Technical Conference on the Enhanced Safety of Vehicles (ESV)
35. Chosa E, Goto K, Totoribe K et al (2004) Analysis of the effect of lumbar spine fusion on the superior adjacent intervertebral disk in the presence of disk degeneration, using the three-dimensional finite element method. J Spin Disord Tech 17(2):134–139. https://doi.org/10.1097/00024720-200404000-00010
36. Natarajan RN, Williams JR, Andersson GBJ (2004) Recent advances in analytical modeling of lumbar disc degeneration. Spine 29(23):2733–2741. https://doi.org/10.1097/01.brs.0000146471.59052.e6
37. Natarajan RN, Williams JR, Andersson GBJ (2006) Modeling changes in intervertebral disc mechanics with degeneration. J Bone Joint Surg Am 88 Suppl 236–40. https://doi.org/10.2106/JBJS.F.00002
38. Ruberté LM, Natarajan RN, Andersson GBJ (2009) Influence of single-level lumbar degenerative disc disease on the behavior of

the adjacent segments–a finite element model study. J Biomech 42(3):341–348. https://doi.org/10.1016/j.jbiomech.2008.11.024
39. Stemper BD, Storvik SG, Yoganandan N et al (2011) A new PMHS model for lumbar spine injuries during vertical acceleration. J Biomech Eng 133(8). https://doi.org/10.1115/1.4004655
40. González-García M, Weber J, Peldschus S (2021) Potential effect of pre-activated muscles under a far-side lateral impact. Traffic Inj Prev 22(Suppl 1):148–152. https://doi.org/10.1080/15389588.2021.1982597
41. Albert DL (2020) Variations in user implementation of the CORA Rating Metric. Stapp Car Crash J 64:1–30. https://doi.org/10.4271/2020-22-0001
42. Rieger LK, Draper D, Shah AS et al (2022) Subject-specific Lumbar Spine Finite Element Model Creation and Validation using Dynamic Compression. In: Proceedings of the IRCOBI Conference, pp 886–887
43. Draper D, Shah AS, Peldschus S et al (2020) Initial validation of a human body model lumbar spine using dynamic compression. In: Proceedings of the IRCOBI Conference, pp 213–214
44. Tushak SK, Paul Donlon J, Gepner BD et al (2022) Failure tolerance of the human lumbar spine in dynamic combined compression and flexion loading. J Biomech 135. https://doi.org/10.1016/j.jbiomech.2022.111051
45. Whitcome KK, Shapiro LJ, Lieberman DE (2007) Fetal load and the evolution of lumbar lordosis in bipedal hominins. Nature 450(7172):1075–1078. https://doi.org/10.1038/nature06342
46. Naserkhaki S, Jaremko JL, El-Rich M (2016) Effects of inter-individual lumbar spine geometry variation on load-sharing: geometrically personalized finite element study. J Biomech 49(13):2909–2917. https://doi.org/10.1016/j.jbiomech.2016.06.032
47. Natarajan RN, Andersson GBJ (1999) The influence of lumbar disc height and cross-sectional area on the mechanical response of the disc to physiologic loading. Spine 24(18):1873–1881

8 Application in Generic Environment

In Paper I, an evaluation methodology was developed to identify lumbar spine injury risks. Paper II investigated to what extent the lumbar spine of the HBM needs to be individualized to detect injuries. This chapter combines the evaluation methodology from Paper I with the necessary degree of individualization from Paper II and evaluates the HBM response in a full-scale load case in a generic environment. Therefore, a previously generated magnetic resonance imaging (MRI) dataset of one volunteer in three different reclined seating angles was analyzed and compared to Total HUman Model for Safety (THUMS) v4.1 individualized according to findings from Paper II. The response of those setups was evaluated regarding lumbar vertebrae fracture risks with considerations from Paper I applied afterwards.

8.1 Materials

The available data, which form the basis for the subsequent study, is described in the following section. In the following section Upright MRI, the imaging modalities, and configurations for the image acquisition with upright open magnetic resonance imaging (named *upright MRI* in the following) are described.

Upright MRI

To clarify spinal injury mechanisms, it seems essential to gain knowledge about the initial whole spinal alignments in reclined positions. The entire alignment of the spine was evaluated using medical imaging in both supine (Parenteau et al., 2014) and standing positions (Hardacker et al., 1997; Janssen et al., 2009; Ames et al., 2013; M. S. Park et al., 2013). It is of particular importance for traffic safety research that the spinal alignment is described in representative postures for vehicle occupants (Chabert et al., 1998; Klinich et al., 2004; 2012; Reed and Jones, 2017; Sato et al., 2017; Izumiyama et al., 2018; Sato et al., 2019; Izumiyama et al., 2022).

Chabert et al. (1998) investigated the entire alignment of the spine of a male cadaver in a standard vehicle seat. The alignment of the cervical spine in a vehicle seat with a 19 deg backrest angle was the subject of the volunteer studies by Klinich et al. (2004, 2012) and also Reed and Jones (2017). The volunteer studies by Sato et al. (2017, 2019) each examined representative spinal alignments in vehicle seats with seatback angles of 20 deg and 25 deg from C2 to the sacrum and the relationship between the cervical, thoracic and lumbar spinal alignments. Recently, Izumiyama et al. (2018, 2022) analyzed the spinal alignment in vehicle seating postures with a recline angle of 24 deg (2018) and 45 deg in a subsequent study in 2022. However, these studies only covered a single automotive seating posture or small variations to a base single posture.

Besides, these studies focused on angular measurements of single spinal segments. Consequently, the impact of differing seat back inclinations on the initial whole spinal alignment of automotive occupants remains to be determined.

For the radiation-free determination of the spinal curvature and the orientation of vertebral bodies in volunteers in alternative seating positions by means of a reclined seat back (seat back angle > 25deg), two methods are currently used: non-invasive skin-surface methods and MRI methods. A skin-surface method, the *Spinal Mouse* introduced by Mannion et al. (2004), was used by Unger and Hintze (2019) on 25 volunteers to provide a database of different spinal curvatures among different seating positions. However, studies showed that even if the *Spinal Mouse* data is reliable, in comparison with standard radiography limited information on the positions of the vertebrae can be obtained (Ripani et al., 2008; Hanesch et al., 2021). Draper et al. (2019) investigated the spinal alignment of one volunteer via scanning the superficial skin layer by a *Faro Arm*. The authors posit that the manner in which the spine is positioned remains uncertain due to the limitation of the technique in enabling external marker measurement. According to them, using this superficial scanning technique only is not sufficient to determine an unambiguous spinal position and combined their measurements with an upright MRI.

Thus, the spinal curvature in different seating configurations and the impact of the inclination of the seat back on spinal alignment was assessed by comparing automotive seating postures in 20 deg, 40 deg, and 60 deg seat back angles via three-dimensional (3D) computer aided design (CAD) objects representing the bony structure of the pelvis and vertebral bodies, which were created based on MRI scans of a volunteer. After approval of the Ethics Committee[1], the Biomechanics and Accident Research Group at the Institute of Legal Medicine of Ludwig-Maximilians-Universität Munich (LMU) was commissioned by Volkswagen to perform the acquisition of the radiation-free images.

Subject

A 50th percentile asymptomatic male (height 177 cm, weight 76 kg, age 39 yrs.) with no previous medical history in the spine or pelvis was recruited as volunteer. There is a signed consent form for the examination as well as for the data analysis.

Posture Definition

The selected seating configurations defined in preliminary studies included a driving position with 20 deg, a comfort position with 40 deg and a rest position with 60 deg backrest inclination. Via a seat wedge, a seat surface inclination of 20 deg to the horizontal is maintained for all three configurations (Figure 8.1). The volunteer's feet could be placed on a footrest during the recordings.

1 The investigation was additionally reviewed and approved by Volkswagen's internal ethics committee.

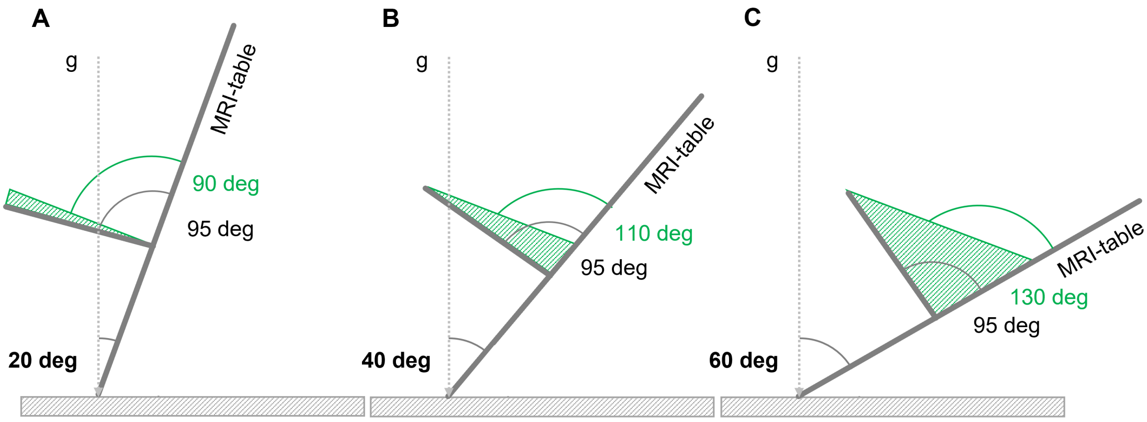

Figure 8.1: Schematic of MRI acquisition setup for the **A** driving, **B** working and **C** resting position in sagittal view relative to gravity (g) after rotation of the back rest and reduction/enlargement of the seat opening angle through a seat wedge.

Image Acquisition

A total of four separate images were taken for each sitting position for the pelvis, lumbar spine, thoracic spine, and cervical spine. Additionally, the spatial orientation of the head, humerus, and femur were documented during the scanning process. MRI datasets were acquired radiation-free using a 0.6 T *upright MRI* machine (Fonar Upright MRI, Fonar Inc., Melville, NY). For the sagittal slice images, T1 weighting with 1.5 mm slice thickness, 512 x 512 pixel matrix size and 40 x 40 mm^2 field-of-view was chosen (3D gradient echo). After quality control, the two-dimensional (2D) slice images were co-registered via image processing software and processed into 3D CAD objects (Figure 8.2).

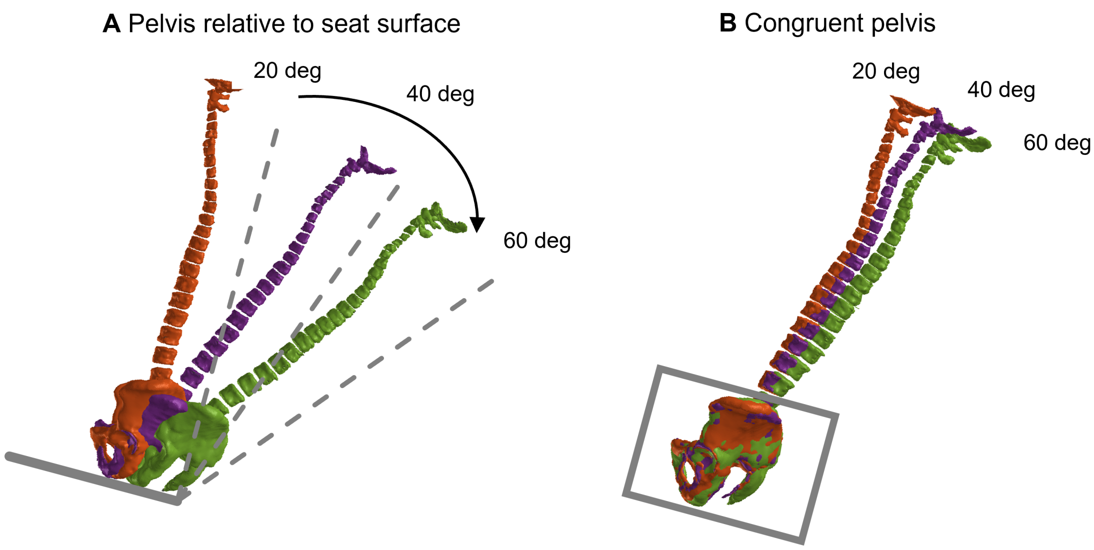

Figure 8.2: Spatial position of the 3D objects of three seating positions **A** relative to the seat surface **B** with a congruent pelvis.

8.2 Methods

The methodological approach, the models used and their modifications, to achieve the objective of this study are described in the following section. In subsection 8.2.1, the use of the 3D segmented MRI data from section 8.1 for positioning the THUMS v4.1 is described. The generic seat setup used to investigate the differences in spinal kinematics and spinal force response is presented in subsection 8.2.2. In subsection 8.2.3, the comparison of the lumbar spine postures of the MRI data is described. At the end of this section, in subsection 8.2.4 the integration of the positioned models in the sled test setup and the selection of the relevant evaluation parameters are presented.

8.2.1 Creation of FE-HBMs

The segmented MRI data has been used to position the standard THUMS v4.1 model, which is supplied in one occupant position. Therefore, the MRI data has been positioned in the global coordinate system and the pelvic angle (PA) measured from anterior superior iliac spine (ASIS) to Pubic Tubercle relative to the global coordinate system has been determined. The THUMS v4.1 model was rotated to match the THUMS pelvis to the measured PA. Via translatoric displacements the MRI data was shifted in z-direction to match the bottom edge of the THUMS v4.1 pelvis and in x- and y-direction, so that the middle of the S1 plateaus are matching (Figure 8.3).

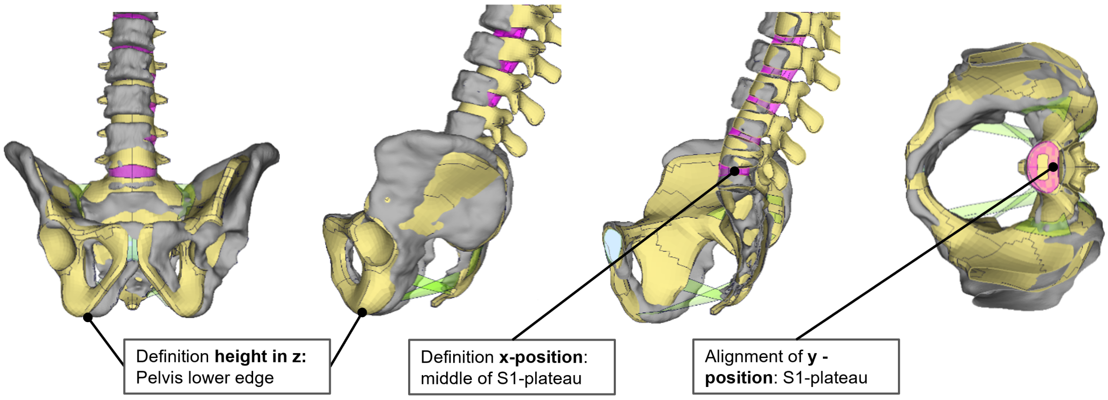

Figure 8.3: Alignment of the MRI data to THUMS v4.1

After the alignment of the MRI data to the THUMS pelvis, a spline through the center of gravity (COG) of the intervertebral discs (IVDs) was generated in sagittal position. This spline was used to determine the displacements needed to position the THUMS v4.1 vertebral bodies. In the cervical area care was taken to keep a horizontal position of the head. A simulation process was used to position the THUMS v4.1 (Figure 8.4). At last, the extremities were correctly positioned.

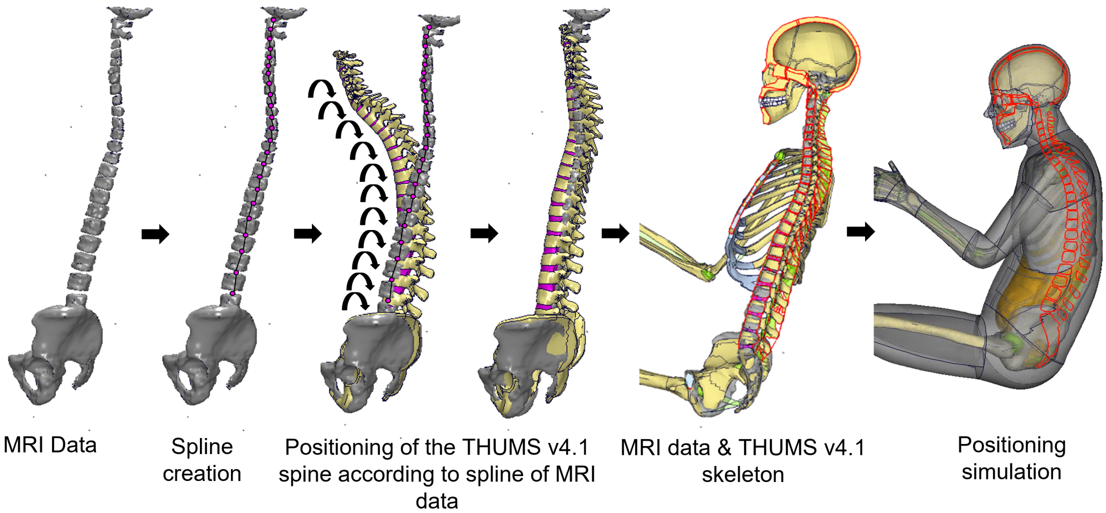

Figure 8.4: Process of using the MRI data for positioning of the THUMS v4.1 spine.

8.2.2 Generic Seat Setup

The full-scale simulations were conducted in a sled test configuration with a semi-rigid seat. This seat setup was initially developed and used by Uriot et al. (2015) to assess the submarining behavior of post mortem human surrogates (PMHS) in an upright seating position. This seat was also utilized by Richardson et al. (2019); the authors wanted to establish biofidelity targets and determine the biomechanical response of PMHS in reclined seating positions. In addition to the aforementioned test series, the semi-rigid seat was also used in a further series of experiments by the University of Michigan Transportation Research Institute and Medical College Wisconsin (MCW).

A FE model of the physical generic environment used in reclined PMHS tests (Richardson et al., 2019) was developed by Mroz et al. (2020) in LS-DYNA. The LS-DYNA model has been translated to PamCrash and validated against the setups in LS-DYNA in the scope of the OSCCAR project.

The model consists of two adjustable plates: the seat and submarining pans. The seat pan angle and the other submarining pan angle were adapted to the surface geometry of the respective position. The respective angles are summarized in Table 8.1. The seat setup was equipped with a three-point belt system with dual lap-belt as well as shoulder belt pretensioner and a force limited shoulder-belt. For a more comprehensive understanding of the system, it is recommended to refer to Mroz et al., 2020.

Table 8.1: Mechanical design and specifications of the semi-rigid seat as used in this study.

Feature	**Parameter name**	**Parameter setting**	**Value**
Seat pan length			280 mm
Springs seat pan side (SS)	SeatP_fs	51128	128 N/mm (2x)
Springs seat pan center (CS)	SeatP_fc	52379	379 N/mm (2x)
Engagement center spring			8 deg / 28 mm
Springs anti-sub ramp	SeatP_f	52132	132 N/mm (2x)
Stop anti-sub ramp		Not included	
Load cells			3x
Anti-rebound function		Off*	
Seat pan initial angle	SeatP_ry	0.5	15.5 deg
Anti-sub pan initial angle:	SubP_ry		
20 deg		-17	15.5 deg
40 deg		-1.8	30.7 deg
60 deg		-17	15.5 deg
Anti-sub pan vertical position	SubP_z		0.0
Seat pan initial gap	SeatP_ig	28	28 mm

**Deactivated spring 241426 (seat pan) as well as springs 241456 and 241457 (sub pan)*

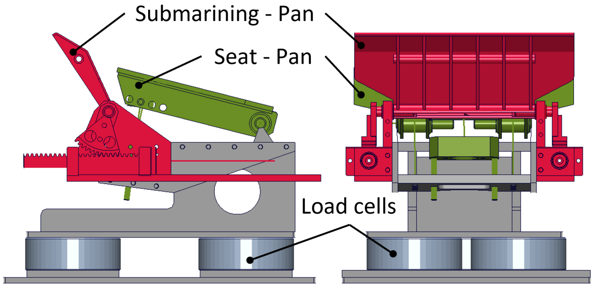

Figure 8.5: Model of the semi-rigid seat (front seat configuration).

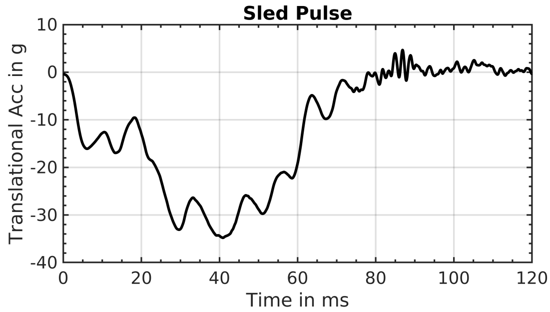

Figure 8.6: Full-frontal, single 30-g (51 km/h ΔV) pulse.

8.2.3 Variabilities of the Spinal Alignment in Different Recline Positions

For the investigation of the differences in alignment of the vertebral bodies, local coordinate systems have been defined for 20 deg, 40 deg, and 60 deg seat back angles in the 3D CAD data as described in chapter 5 for T12 to L5. Figure 8.7 shows the center point of T12 to L5 and the anterior endpoint of the local x-axis for the three different seatback recline angles.

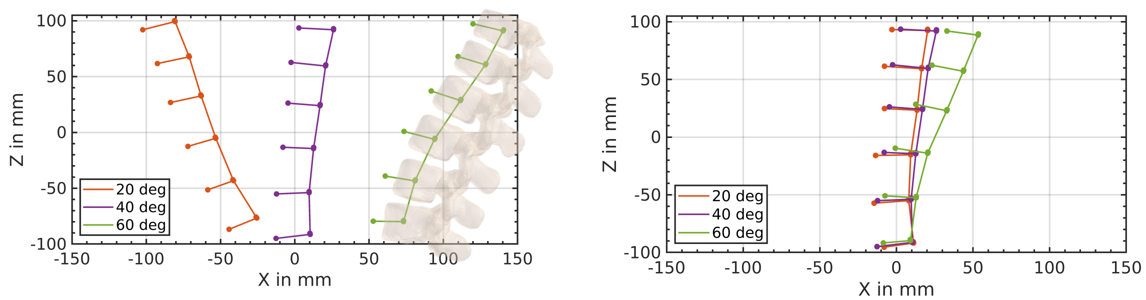

(a) Pelvis relative to seat surface

(b) Congruent pelvis

Figure 8.7: Spinal alignment with 20 deg, 40 deg, and 60 deg seat back angles with (**a**) pelvis relative to seat surface, and (**b**) congruent pelvis.

Figure 8.8 summarizes the most important contrasts between the studied postures. The pelvic angle is defined here as the angle between the connection of ASIS and posterior superior iliac spine (PSIS) and the global coordinate system in the sagittal plane. The intervertebral angles are measured from the local x-axis of one vertebra to the local x-axis of the adjacent vertebra. The lumbar lordosis is determined from the caudal aspect of L5 to the cranial aspect of T12 in the same coordinate system. Besides the pelvic angle was measured in the respective MRI coordinate system (as shown in Figure 8.8).

Figure 8.8: Intervertebral angles in the lumbar area, lumbar lordosis (LL), and pelvic angle (PA) for three different seat recline angles.

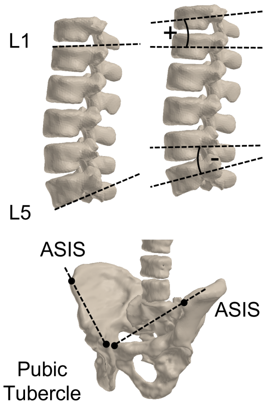

Level	20 deg	40 deg	60 deg	Δ 40 deg	Δ 60 deg
T12 - L1	3.55	4.02	4.74	0.47	0.72
L1 - L2	-0.40	-2.55	1.23	-2.15	3.78
L2 - L3	-8.15	-2.68	-4.25	5.47	-1.57
L3 - L4	-8.05	-6.34	-7.09	1.70	0.75
L4 - L5	-3.61	-6.00	-10.69	-2.40	-4.69
Lumbar Lordosis (LL)	-20.54	-24.64	-25.30	-4.10	-0.96
Pelvic Angle (PA)					
left	102.95	101.97	131.37	0.98	29.40
right	101.59	100.52	122.03	1.07	21.51

8.2.4 Investigation of the Global Behavior of the Positioned Spines Using the Generic Seat Test Setup

Material properties of IVDs as well as material properties of capsular ligaments were adapted as previously described in Paper I and Paper II. Afterwards all positioned models have been seated with gravity and belted (Figure 8.9). These occupant models were then all subjected to a full-frontal, single 30-g (51 km/h ΔV) pulse (Figure 8.6). The crash pulse corresponded to the pulse used in several previous PMHS tests (Uriot et al., 2015; Richardson et al., 2020a).

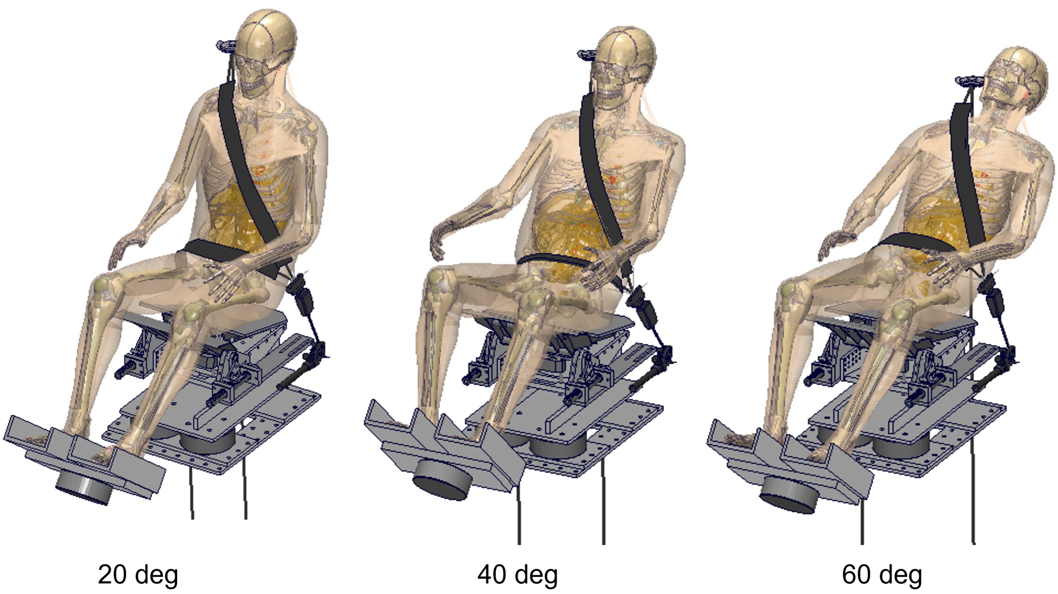

Figure 8.9: Positioned and belted FE simulation models in generic seat environment for 20 deg, 40 deg, and 60 deg recline angle.

8.3 Results

All HBM simulations were launched with a target termination time of 120 ms, and all models achieved a normal termination.

8.3.1 Analysis of Occupant Kinematics

The global kinematics of all three postures at four different states can be seen in Figure 8.10. The first state is the initial state at time 0 ms, the second state is the state at the time of highest acceleration (40 ms), the third state is the state where the highest pressure occurs, and the last state is at 100 ms at the start of the rebound phase. No submarining was observed in any case. In accordance with the majority of PMHS tests, the HBMs pelvis was well restrained via the lap belt, that allowed the occupant's upper body to lean forward into the shoulder belt. In the driving position (20 deg), both the pelvis is effectively constrained via the lap belt and the torso is equally well restrained via the shoulder belt. In contrast, in the reclined positions the torso is mainly restraint via the lap belt and the shoulder belt intervenes much later. Overall, in the driving position there is a folding of the upper body towards the lower body, what leads to greater forward displacement compared to the reclined position, which tends to roll in.

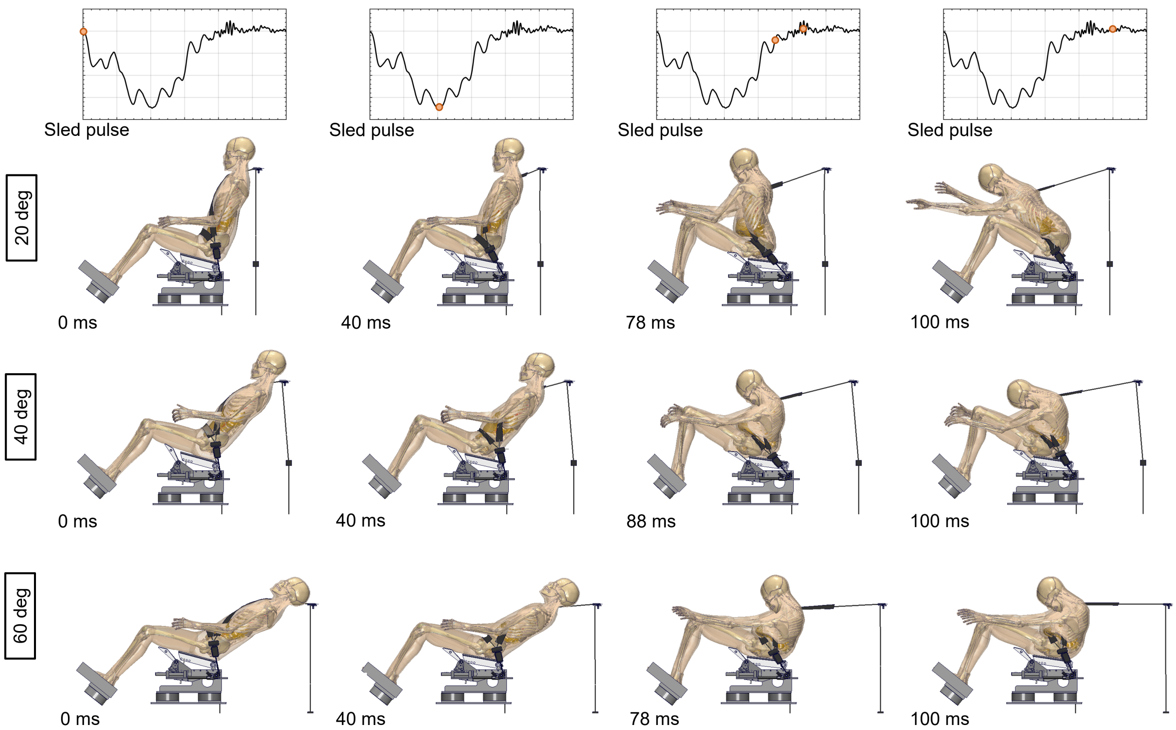

Figure 8.10: Kinematic results of the upright (20 deg) and the two reclined positions (40 deg and 60 deg).

8.3.2 Lumbar Kinematics

For the seating position of 20 deg, as shown in Figure 8.11, the kinematics of the lumbar spine is an extension between T12 and L1, L1 and L2 as well as L2 and L3, followed by a flexion across all lumbar spine levels. The 40 deg posture kinematics track a similar trajectory but stay in flexion only across the lumbar levels. The kinematic characteristics of the 60 deg posture exhibit notable divergence from those observed in the other two postures: T12 to L1 are characterized by a flexion, where all other levels show initial extension, followed by flexion.

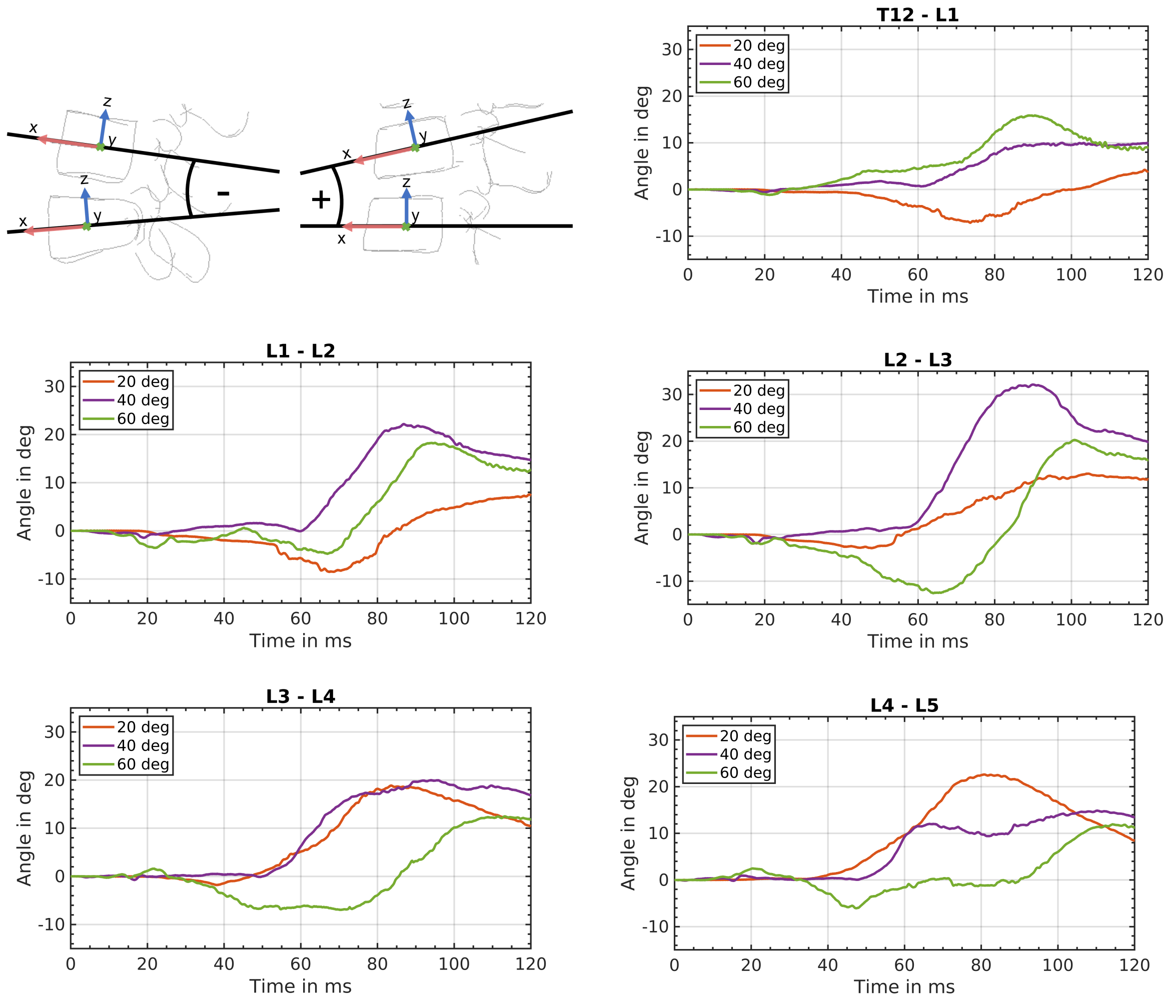

Figure 8.11: Angular kinematic results of the THUMS v4.1 upright (20 deg) and two reclined positions (40 deg and 60 deg) as measured at the lumbar spine. Positive angles denote flexion; negative angles denote extension.

The lumbar spine's pressure distribution for each posture was evaluated as proposed in Paper I (Figure 8.12). Pressure was higher on anterior aspects of lumbar spine vertebrae for all postures. The area of pressure concentration is increasing with increasing recline angle. The location of highest pressure is more caudal (towards L5) in the 20 deg posture and relocates more cranial (towards T12) with higher recline angles.

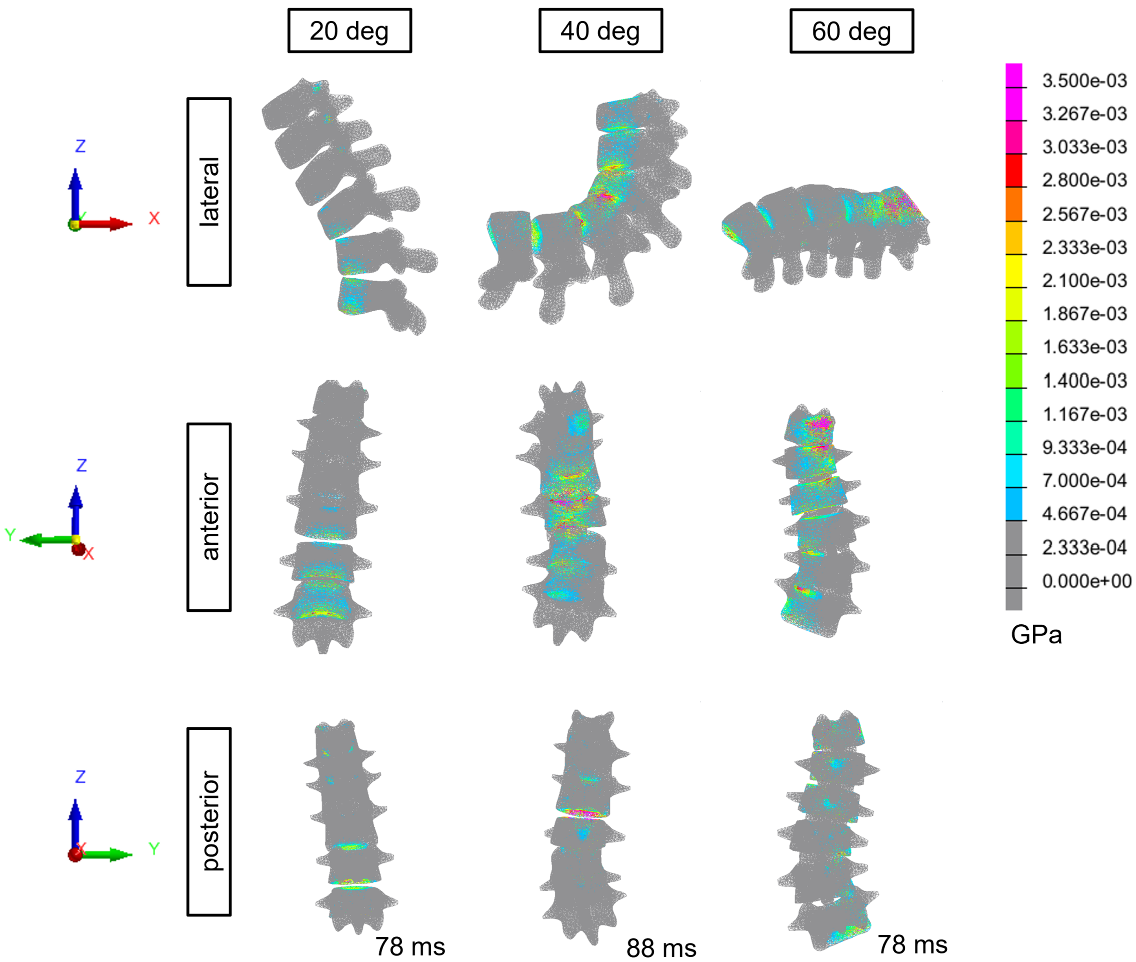

Figure 8.12: The stress field maps depict the maximum pressure in GPa of the spongiosa of the lumbar vertebrae at the instant of maximum peak force for each model.

8.4 Discussion

The objective of this application study was to test the findings of Paper I and Paper II in a full-scale load case and a generic seat setup, which is commonly used not only in simulation load cases but also for the acquisition of experimental test data with PMHS. In this section, the peculiarities and limitations, which are inherent to the used materials, are highlighted. In the aftermath, the HBM kinematics as well as the injury detection methodology and their significance for applications in actual automotive environments are discussed.

8.4.1 Materials

MRI data

The MRI data used for the positioning of the HBMs was, at the time the study was conducted, a unique data set in terms of information content (three different recline postures) and accuracy (MRI data), commissioned by Volkswagen to investigate the positioning of human models. Nevertheless, the acquired MRI data in this study represent only one individual. Even after elaborate pre-selection of the individual, representativeness for an entire population is not guaranteed. The curvature of the individual's spine is not very pronounced, especially in the thoracic region, which results from the individual anatomical characteristics of the volunteer and represents a not infrequently occurring normal variant.

Taking a closer look at the lumbar level (Figure 8.8) it becomes obvious that for the upright posture all levels from L1 to L5 are in extension fitting a Gauss distribution - meaning being more pronounced in the center of the lumbar column. While for the 40 deg recline position still all levels being in extension, the higher lordosis angles are shifted in the direction of the caudal end of the lumbar column. Whereas in the 60 deg recline position lordosis starts at the L2-L3 level and is ascending towards the caudal end. The highest lordosis angle is at L4-L5 level in the 60 deg recline posture. The lumbar lordosis (LL) of the volunteer's spine is -20.54 deg in upright position, -24.64 deg in 40 deg recline position and -25.3 deg in 60 deg recline position. In other words, while the LL is increasing with increasing recline angle, the local lordosis is shifting from cranial to caudal lumbar level.

With regard to the population and the lumbar spine region, it seems that the spinal curvature of the selected volunteer is well within what was reported in the literature. Izumiyama et al. (2018) report a LL of -0.90 $\pm$ 9.21 deg for males in automotive seating positions with a seat recline angle of 24 deg in an X-ray study. In a subsequent study Izumiyama et al. (2022) reported on average LLs of -5.8 deg for 24 deg seat recline angles, -11.3 deg for 35 deg seat recline angles and -17.7 deg for seat recline angles of 45 deg. The study found that a change in posture from 24 deg to 45 deg resulted in not only a pelvic rotation posteriorly, but also a lumbar lordosis in all subjects. In this study pelvic rearward rotation and increase of LL was found. In contrast to the studies by Izumiyama et al. (2018, 2022) the initial LL was higher and the change of LL with increasing seat recline was slightly smaller. This might be reasoned through a lumbar support which is common for automotive seat systems and lacking in a stiff MRI table.

Sato et al. (2021) analyzed LL of males in standard automotive seating positions in an upright MRI study. They found a LL of -20.74 $\pm$ 11.2 deg for 20 deg seat recline angles and -24.36 $\pm$ 3.3 deg for 25 deg seat recline angles. They claim that sitting on a rigid laboratory seat and leaning the entire back against a flat backrest could straighten the lumbar spine. This influence of the MRI table which does not correspond to an automotive seat might also hold true in this study. To provide a more accurate representation of real-world scenarios, future studies should consider the potential variations in the designs of commercially available car seats. In addition, the longer examination time of MRI scans compared to CT or X-ray scans may have an impact on postural stability. Other influences on postural stability can be the driving duration as well as the type of route (Ghaffari et al., 2019). These influencing variables should be considered in future studies on the alignment of the spine in automotive seating postures.

8.4.2 Methods

FE-HBMs

In this study, a simulation-based positioning approach was used to position an HBM (THUMS v4.1) to anthropometric CAD data of one subject in three different sitting positions. As described in subsection 8.2.1, a self-defined pre-simulation routine was used. As shown by Schießler et al. (2020) the choice of the positioning method has an influence on the exact position of the vertebral bodies (vertebra angles varied by up to 5 deg in their study), nevertheless comparable postures could be achieved when the same targets are used. However, Schießler et al. (2020) reported that the overall kinematics seem to be not influenced by the use of different positioning methodologies. A major difficulty every methodology is facing right now is that the HBM anthropometry is unlikely to correlate exactly with another given human anthropometry. Geometric differences between the individual and a FE model in the pelvis or vertebral body region can lead to deviations in positioning or difficulties in adaptation.

Semi-Rigid Seat Setup

The simulations were conducted with a semi-rigid seat. Its stiffness and geometry is representative of a real automotive seat and has been used in previous sled test studies (Uriot et al., 2015; Trosseille et al., 2018; Richardson et al., 2020a). In contrast to the rigid seat featured in other sled test studies (Trosseille et al., 2012), the adaptability of the seat pan offers a boundary condition that more closely resembles an actual vehicle environment and is therefore more realistic (Shaw et al., 2009; Uriot et al., 2015). The semi-rigid seat is adjustable, simplified in its complexity, which makes it advantageous in experimental environments compared to commercial vehicle seats:

Both the spring stiffness and spring configuration of the seat pan and anti-submarining pan can be adapted to a wide range of vehicle seats. As the focus of this study was the evaluation of the difference of occupant kinematics in different postures in isolation, the reduction of seat complexity is advantageous as it eliminates the need for extensive seat validation and possible parameter variation. Another advantage is that by migrating to a (bi-)linear elastic model (e.g. springs), the seat ensures a well-specified and controlled input for the experiment's mathematical or computational simulation and has therefore also been validated in simulation tests (Mroz et al., 2020).

8.4.3 Kinematic Comparison

The deformation mode of the lumbar spine in all postures is predominantly flexion-bending rather than compression, as shown in the global kinematics (Figure 8.10). This subsection presents a comparative analysis of lumbar spine kinematics across the three distinct postural categories: upright and two reclined postures.

Upright Position - 20 deg

The kinematics of the lumbar spine for the 20 deg seating position (Figure 8.11) can be classified as extension between T12 and L1, L1 and L2 as well as L2 and L3, which is followed by flexion throughout all lumbar levels. The lumbar spine levels T12 to L3 start their initial extension right at the beginning of the simulation, whereas the lumbar spine levels L3 to L5 start their initial flexion shortly after 40 ms coincidencing with the time of the highest acceleration pulse. For T12 and L1, and L1 and L2, the peak in angular extension occurs at 70 ms, switching into flexion at 100 ms (T12 to L1) 85 ms for L1 to L2 respectively. The L2-L3 IVD goes into slight extension for a period of 60 ms, after which a gradual transition into flexion occurs. This continues until a plateau is reached at an angle of 13 deg. The largest angular flexion displacement (22 deg) is observed at 80 ms between L4 and L5 at the caudal end of the lumbar column. The observation of the local lumbar kinematics confirms the impression of the global view: the forward displacement is caused by a main flexion in the caudal region of the lumbar spine.

Reclined Position - 40 deg

A comparative analysis of the kinematics for 40 deg position, as shown in Figure 8.10, reveals a markedly distinct response when contrasted with the upright kinematics. In comparison, less forward displacement of the torso occurs; instead, flexion movement occurs throughout the entire spine. Initially, restraint is provided only by the lap belt, and only subsequently the shoulder belt also engages. With regard to the lumbar spine kinematics support the observation on the full-scale level. Flexion without initial extension occurs across all lumbar levels. The 40 deg position has a higher peak of 32 deg at the L2-L3 level as compared to the upright posture with 22 deg at the L4-L5 level. It occurs 10 ms later than that of the upright posture.

Reclined Position - 60 deg

The 60 deg reclined position tracks a similar kinematic response as the 40 deg recline posture of a smaller forward displacement of the torso through flexion of the whole spine (Figure 8.10). Looking at Figure 8.11, it can be seen that the 60 deg recline posture is characterized through pure flexion at the T12-L1 level as it holds true for the 40 deg posture but with slightly larger angular displacement. All other lumbar levels differ from the kinematics in the 40 deg recline posture. They show an initial extension accompanied by a flexion in all lumbar levels. The sharpest peak of the initial L2-L3 extension is at 64 ms with -14 deg. In addition, an initial extension deformation of the L3-L4 disc can also be observed in the 60 deg reclined posture, which was not evident in the other postures.

Looking at the initial position, the 20 deg posture, the lumbar levels, which are in pronounced extension (L2-L5), go into flexion over the course of the simulation. The lumbar kinematics in the 40 deg recline posture show a similar behavior. The 60 deg lumbar kinematics show a contrary behavior. This might be reasoned through inaccuracies stemming from the positioning process. Another plausible reason could be that the applied force and moment angles play a crucial role with a higher seatback recline angle. The leverage arm with respect to the COG of the pelvis acting on the lumbar vertebral bodies increases with increasing recline angle, it might hold true that this forces the T12-L1 angle going into initial flexion while all other lumbar levels going into initial extension as consequences of inertia. The subsequent flexion which is highest for L1-L2 and descending in caudal direction would be a logical consequence of this.

8.4.4 Fracture Detection

The lumbar spine was analyzed regarding the possible occurrence of fracture as described in Paper I (Figure 8.12). For the 20 deg posture the highest pressure occurs in the anterior part at the L4-L5 level coincidencing with the highest angular flexion displacement. The lumbar spine in the 40 deg position shows the highest pressure distribution in the center (L2-L3) of the lumbar column also in the anterior region of the vertebral bodies and also where the highest angular displacement occurs. Compared to an upright position, a higher area of peak stresses occurs predominantly at the top and bottom end plate of L3. In the 60 deg recline posture the highest pressure concentration occurs at the cranial end of the lumbar column but also in the right anterior part of the vertebral body. In contrast to the other postures, the highest angular displacement (20 deg at L2-L3) and the maximum pressure do not coincidence for the 60 deg recline posture. This might indicate that the angular displacement itself is not appropriate to be used as a fracture indication parameter. For all three postures, however, maximum disc angles of 15 deg or more are achieved for this particular load case. In contrast, Adams and Hutton (1986) observed a flexion limit of 14.8 deg for their quasi-static experiments. It therefore remains in question whether the higher strain rates used in this simulation study can be expected to cause not only possible fractures but also comparable damage to the supraspinous and interspinous ligament as reported by Adams and Hutton (1986).

In the 40 deg recline posture the highest pressure occurs at 88 ms, whereas for the other two postures highest pressure occurs 10 ms earlier. Mechanically, the shift in the location of the highest load is plausible: the further back the occupant is reclined, the further the torso moves. This could be an indication, that the fracture location is dependent on the pulse, the distance the torso is pushed forward and the weight of the torso. Overall, it can be concluded that with a higher recline angle, the area sustaining high pressure values increases and, thus, the probability of a fracture is higher. What is also apparent in Figure 8.12 is that at the time of maximum pressure, the three different lumbar spine positions are curved differently. In the 20 deg spine posture there is a minor tilt to the left with an inflection point at the caudal end, whereas the reclined lumbar spine models seem to have an S-shape in the frontal plane with growing buckling with increasing recline angle. This might result from the non-symmetric belt system, which can support the upright seating in a sufficient way.

9 Outlook & Conclusion

The aim of this thesis was to establish a strategy for handling anthropometrical differences in the lumbar spine when assessing spinal injuries within virtual vehicle development using human body models (HBMs). Regarding the objectives formulated in section 4.3, the following observations can be concluded:

- ***To design a method to identify the position and orientation of a vertebra.***

A previously proposed method by Draper et al. (2020) was extended as well as successfully applied to THUMS v4.1 and three-dimensional (3D) medical imaging data. Moreover, local coordinate systems were successfully integrated to finite element (FE) lumbar spine models.

- ***To investigate if subject-specific whole lumbar spine models could match failure patterns and injury mechanisms.***

In Paper I it was investigated, if subject-specific whole lumbar spine models could coincide failure patterns and injury mechanisms based upon reference experiments from Stemper et al. (2018). Therefore, lumbar spine geometries were generated from experimental computer tomography (CT) data and assigned material properties from THUMS v4.1. As all the subject-specific models with standard material properties were too stiff with regard to the angular displacement profiles applied, the material properties of the annulus fibrosus and the capsular ligaments were adapted according to values reported in Mattucci and Cronin (2015) and Newell et al. (2019). Overall, our models were found to correspond considerably well with the experimental data and that with at a pressure distribution cut off value of 3.5 MPa the models were able to predict the existing failure patterns.

However, the studies performed so far to investigate bending and shear of intervertebral discs (IVDs) are not sufficient for the validation of HBMs. Further validation should be performed on IVDs in flexion and extension to observe how the IVD distorts and transfers bending forces. Shear, bending, and axial loading should be investigated independently. In addition, combined bending compression tests, required to determine failure modes and injury criteria, could be developed to validate HBMs for high force, moment, and strain values. As the IVD is not defined as single homogenous material in the HBM - an isolated material characterization of annulus fibrosus and nucleus pulposus would help the definition of material properties in HBMs.

The same holds true for facet joints. There is evidence, showing the importance of facet joints in lumbar spine unit (LSU) loading (Stemper et al., 2015a). In the subject-specific models, facet joints were modelled using the connection via capsular ligaments only as it is realized in THUMS v4.1. Other current models use geometry and friction (Mengoni, 2021). Therefore, studying other modelling methods, which could probably better capture the physiology of facet joints and the influence of individual geometries of facet joints, might be beneficial.

This study concentrated on bony fractures of the lumbar spine. Future studies should investigate the failure patterns of other injuries of the spine with Abbreviated Injury Scale (AIS)3+ coding. Furthermore, to prevent long-term implications, future studies should focus on spinal injuries with Functional Capacity Index (FCI)4- coding. In addition, the investigation of failure patterns and injury mechanisms would enable a more in-depth failure model validation in HBMs.

In this study, the failure of a vertebral body was determined at the time of the maximum load of one element. To exclude load spikes, the area with maximum total load and, thus, the most probable fracture region, was then assessed by manual filtering. Future studies could consider a fracture prediction algorithm that evaluates a well-defined number of adjacent elements over the entire loading period and generates an overall maximum to eliminate manual filtering bias.

- ***To propose a methodology on an approach to deal with different anthropometry in vehicle development.***

In Paper I four subject-specific specimen models were generated. As the process of individualization is very time-consuming, Paper II investigated the required level of individualization under the same boundary conditions. The aim was to better understand which geometrical aspects lead to major changes in response and whether there is a systematic relationship between anthropometric parameters and internal loading and, thus, injury outcome. The sagittal spinal position influenced through vertebral body height and initial vertebral position were found to be the most important factors to still being able to predict failure patterns. Nevertheless, vertebral body height only showed minor improvement, and it was recommended to focus on the vertebral body position in full-scale applications.

Therefore, the lumbar spine position of a volunteer was analyzed in an upright seating position and two recline angles in an upright magnetic resonance imaging (MRI). THUMS v4.1 was positioned according to the position determined in the MRI; the semi-rigid seat setup as performed by Richardson et al. (2020a) was used as simulation basis. It was found that the reclining was initiated primarily by the pelvis, for 20 to 40 deg. From 40 deg to 60 deg the postural change resulted in pelvic rearward rotation plus lumbar lordosis for the volunteer. The global kinematics of the HBM in reclined positions deviated from the kinematics seen in the upright position. This deviation holds true also for the local lumbar kinematics. The evaluation of the pressure in the trabecular part of the vertebrae confirmed the initial expectations. Also, the results were coherent with other studies: with higher recline angle the probability of vertebral fracture increased and the predicted fracture pattern and location changed from caudal to more cranial in the lumbar spine.

As for this simulation no directly comparable experimental data exists, the Richardson et al. (2020a) setup was used to validate the fracture prediction capabilities of the developed method in full-scale. The simulation setup has been described in subsection 8.2.2. The THUMS v4.1 with adapted material properties for annulus fibrosus and capsular ligament was positioned to averaged landmarks using an executable script in the PIPER software (C. Klein et al., 2021) to account for the findings from Paper II. Figure 9.1 shows the global kinematics at four different states. No submarining was observed for the HBM.

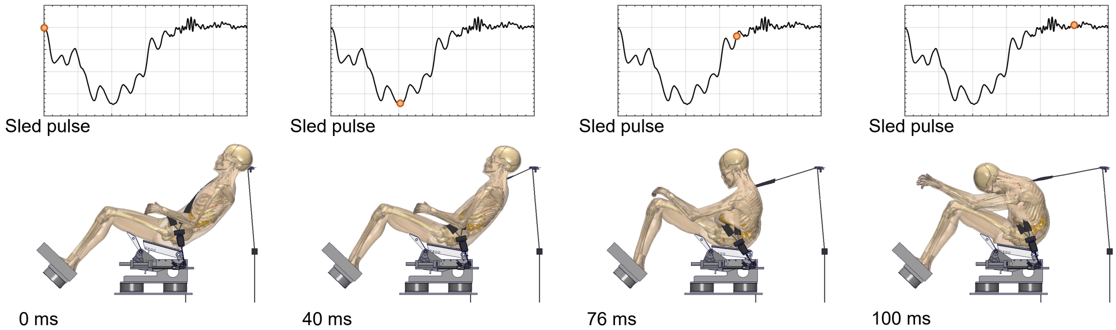

Figure 9.1: Global kinematic results for the reclined position (45 deg).

The fracture prediction methodology as developed in Paper I was applied to the HBM (Figure 9.2). According to this a wedge-type fracture in the upper lumbar spine (between L2 and L3) is probable. In the experiment three out of five post mortem human surrogates (PMHS) sustained lumbar fractures also in the upper lumbar spine (at L1) (Richardson et al., 2020a). As described in Paper II, the initial spinal position plays a major role in identification of fracture mechanism and location. For the positioning only target landmarks from T11, L1 and L3 for the lumbar spine region were available and averaged landmark positions were used. Therefore, it was not possible to reach the exact same position with the HBM. In this way, the positioning process adds another level of uncertainty (C. Klein et al., 2021). However, Richardson et al. (2020a) also mention that the L1 fracture could also have resulted from artificial stiffening and weakening of the bone by the measurement hardware.

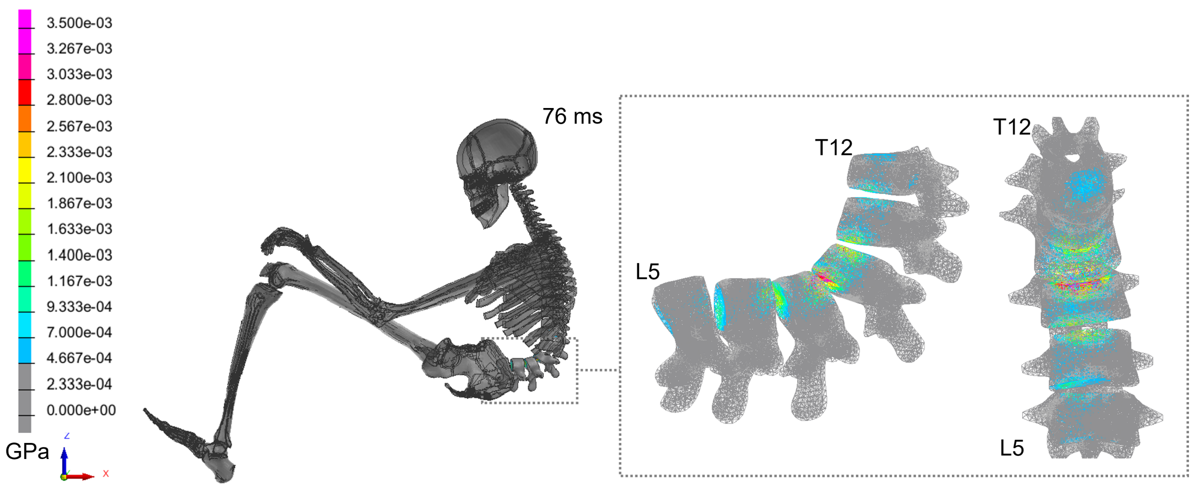

Figure 9.2: The stress field maps depict the maximum pressure in GPa of the spongiosa of the lumbar vertebrae in whole body sled tests at the instant of maximum peak force.

This again emphasizes the need to better dovetail experiments and simulation in order to objectify modelling of injury mechanics experiments in the future (Fuchs, 2018). Due to this and the insight that geometry has a major predictive influence, further studies focusing on the geometries of the lumbar spine in real populations are of great interest; this is a current area of investigation (Booth et al., 2022; Izumiyama et al., 2022). Moreover, it has been shown that muscle activation can affect occupant kinematics and, consequently, on the probability of injury in a crash (González-García et al., 2021). It is thus recommended that further studies be performed to investigate the potential influence of autochthonous back muscles on fracture risk in the lumbar spine.

The experimental results indicated that the lap belt constituted the primary restraint mechanism, resulting in the occurrence of pelvic fractures in certain specimens (Richardson et al., 2020b). With lower hip belt forces submarining may occur. As in a submarining event, there is the probability of internal organ injury, with subsequent haemorrhage and associated rib fractures, the aim is to prevent submarining at all costs. Compared to pelvic fractures, it is difficult to grade submarining on the AIS scale due to the multi-time nature of submarining, but it can be assumed that submarining is more severe. However, the outcome of the AIS is always contingent on the specific circumstances and variables of each individual case.

If a Volkswagen restraint system with conceptually different restraint mechanisms were to be investigated, different physiological loading would occur than in the test series of Richardson et al. (2020a). Similarly, not only are restraint systems different and seating positions modular, but the extent of postural and physiological variation within a population can be large (see also subsection 4.1.4). Further research is needed to quantify population-specific differences to ensure that countermeasures guarantee the same level of safety for all occupants. Evaluating the influence of different anthropometrical spinal postures in a Volkswagen restraint system - airbag, belt, and seat - is beyond the scope of this thesis but would give interesting insights for safety engineers. Nevertheless, full-scale experiments like those from Richardson et al. (2020a) are indispensable for the design of future component level tests (Tushak et al., 2022) for the validation of HBMs in reclined seating positions. Furthermore, the fracture prediction methodology was developed for THUMS v4.1 only. In order to achieve general validity, results using other HBMs and different FE solvers need to be compared. In addition, the spinal kinematics are influenced by various factors, including the musculature of the spine, internal organ pressure, and contact with surrounding structures. Elucidating the aforementioned influences through PMHS experiments is a challenging endeavor. Furthermore, any comparative evaluations conducted using HBM simulation studies currently lack a robust validation basis.

Bibliography

Abraczinskas, Alicia, Christine Beltran, Ardyn Olszko, Jamie L. Baisden, Narayan Yoganandan, Frank A. Pintar, Andrea Dargie, Kimberly Vasquez, and Valeta Chancey (2018). „Injuries and injury risk curves from historical non-human primate whole-body, +Gz acceleration tests“. In: *Proceedings of the IRCOBI Conference*, pp. 739–751. URL: https://www.ircobi.org/wordpress/downloads/irc18/pdf-files/108.pdf.

Abu-Leil, Saher, Yizhar Floman, Yigal Bronstein, and Youssef M. Masharawi (2016). A morphometric analysis of all lumbar intervertebral discs and vertebral bodies in degenerative spondylolisthesis. In: *European Spine Journal* 25.8, pp. 2535–2545. DOI: 10.1007/s00586-016-4673-3.

Acaroglu, Emre R., James C. Iatridis, Lori A. Setton, Robert J. Foster, Van C. Mow, Mark Weidenbaum, E. R. Acaroglu, J. C. Iatridis, L. A. Setton, R. J. Foster, V. C. Mow, and M. Weidenbaum (1995). Degeneration and aging affect the tensile behavior of human lumbar anulus fibrosus. In: *Spine* 20.24, pp. 2690–2701. DOI: 10.1097/00007632-199512150-00010.

ADAC (2023). *Autonomes Fahren: So fahren wir in Zukunft*. URL: https://www.adac.de/rund-ums-fahrzeug/ausstattung-technik-zubehoer/autonomes-fahren/technik-vernetzung/aktuelle-technik/ (visited on 04/30/2023).

Adams, Michael A. and Patricia Dolan (2011). Biomechanics of vertebral compression fractures and clinical application. In: *Archives of Orthopaedic and Trauma Surgery* 131.12, pp. 1703–1710. ISSN: 0936-8051. DOI: 10.1007/s00402-011-1355-9.

Adams, Michael A. and William C. Hutton (1985). The effect of posture on the lumbar spine. In: *The Journal of Bone and Joint Surgery. British volume* 67.4, pp. 625–629. ISSN: 0301-620X. DOI: 10.1302/0301-620X.67B4.4030863.

Adams, Michael A. and William C. Hutton (1986). Has the lumbar spine a margin of safety in forward bending? In: *Clinical Biomechanics* 1, pp. 3–6. ISSN: 0268-0033. DOI: 10.1016/0268-0033(86)90028-8.

Adomeit, Dieter and Alfred Heger (1975). Motion sequence criteria and design proposals for restraint devices in order to avoid unfavorable biomechanic conditions and submarining. In: *SAE Transactions*, pp. 3150–3159. ISSN: 0096736X, 25771531. DOI: 10.4271/751146.

American Heritage (2023). URL: https://www.ahdictionary.com/word/search.html?q=posture (visited on 05/24/2023).

Ames, Christopher P., Benjamin Blondel, Justin K. Scheer, Frank J. Schwab, Jean-Charles Le Huec, Eric M. Massicotte, Alpesh A. Patel, Vincent C. Traynelis, Han Jo Kim, Christopher I. Shaffrey, Justin S. Smith, and Virginie LaFage (2013). Cervical radiographical alignment: Comprehensive assessment techniques and potential importance in cervical myelopathy. In: *Spine* 38.22 Suppl 1, pp. 149–160. DOI: 10.1097/BRS.0b013e3182a7f449.

Anderhuber, Friedrich, Franz Pera, and Johannes Streicher, eds. (2012). *Waldeyer - Anatomie des Menschen: Lehrbuch und Atlas in einem Band*. Berlin, Boston: De Gruyter. ISBN: 9783110228632. DOI: 10.1515/9783110228632.

Anderson, Paul A., Frederick P. Rivara, Roland V. Maier, and Christiana Drake (1991). The epidemiology of seatbelt-associated injuries. In: *The Journal of Trauma* 31.1, pp. 60–67. ISSN: 0022-5282. DOI: 10.1097/00005373-199101000-00012.

Andersson, Gunnar B. J., R. W. Murphy, Roland Örtengren, and Alf Nachemson (1979). The influence of backrest inclination and lumbar support on lumbar lordosis. In: *Spine* 4.1, pp. 52–58. DOI: 10.1097/00007632-197901000-00009.

Anesthesia Key (2016). *The analysis of movement*. URL: https://aneskey.com/the-analysis-of-movement/ (visited on 06/14/2023).

AO Spine (2023). *AO spine classification systems*. URL: https://www.aofoundation.org/spine/clinical-library-and-tools/aospine-classification-systems (visited on 05/23/2023).

Armijo-Olivo, Susan, X. Jara, Norbert Castillo, L. Alfonso, A. Schilling, E. Valenzuela, R. Frugone, and D. Magee (2006). A comparison of the head and cervical posture between the self-balanced position and the Frankfurt method. In: *Journal of Oral Rehabilitation* 33.3, pp. 194–201. ISSN: 0305-182X. DOI: 10.1111/j.1365-2842.2005.01554.x.

Arregui-Dalmases, Carlos, Joseph H. Ash, Eduardo Del Pozo, Jason R. Kerrigan, and Jeff R. Crandall (2010). Characterization of the transverse and spinous vertebral processes: fracture forces under quasi-static and dynamic loading. In: *Biomedical Sciences Instrumentation* 46, pp. 154–159.

ASME, ed. (2020). *Standard for verification and validation in computational solid mechanics: An international standard*. New York, NY: American Society of Mechanical Engineers (ASME). ISBN: 9780791873168.

Automotive World (2020). *Autonomous vehicle testing: in pursuit of perfection*. URL: https://www.automotiveworld.com/articles/autonomous-vehicle-testing-in-pursuit-of-perfection/ (visited on 05/29/2023).

Barthelat, Francois (2015). Architectured materials in engineering and biology: Fabrication, structure, mechanics and performance. In: *International Materials Reviews* 60.8, pp. 413–430. DOI: 10.1179/1743280415Y.0000000008.

Baudrit, Pascal, Jérôme Uriot, Olivier Richard, and Matthieu Debray (2022). Investigation of potential injury patterns and occupant kinematics in frontal impact with PMHS in reclined postures. In: *Stapp Car Crash Journal* 66, pp. 1–30. DOI: 10.4271/2022-22-0001.

Bayliss, Michael T. and Brian Johnstone (1992). *The lumbar spine and back pain*. 4th ed. Biochemistry of the intervertebral disc. Edinburgh, UK: Churchill Livingstone.

Begeman, Paul C., Albert I. King, Priya Prasad, A. I. King, and P. Prasad (1973). Spinal loads resulting from -Gx accleration. In: *SAE Technical Paper*. DOI: 10.4271/730977.

Beillas, Philippe and Fabien Berthet (2017). An investigation of human body model morphing for the assessment of abdomen responses to impact against a population of test subjects. In: *Traffic Injury Prevention* 18.Suppl 1, pp. 142–147. DOI: 10.1080/15389588.2017.1307971.

Belwadi, Aditya and King H. Yang (2008). „Response of the cadaveric lumbar spine to flexion with and without anterior shear displacement“. In: *Proceedings of the IRCOBI Conference*, pp. 397–410. URL: https://www.ircobi.org/wordpress/downloads/irc0111/2008/Session7/7_4.pdf.

Berthonnaud, Eric, Joannès Dimnet, Pierre Roussouly, and Hubert Labelle (2005). Analysis of the sagittal balance of the spine and pelvis using shape and orientation parameters. In: *Journal of Spinal Disorders & Techniques* 18.1, pp. 40–47. DOI: 10.1097/01.bsd.0000117542.88865.77.

Besnault, Benoit, François Lavaste, Hervé Guillemot, Stéphane Robin, and Jean-Yves Le Coz (1998). A parametric finite element model of the human pelvis. In: *SAE Transactions* 107, pp. 2680–2694. ISSN: 0096736X, 25771531. DOI: 10.4271/983147.

Bohlin, Nils I. (1964). „Safety belt device for vehicles“. US3147995A.

Bonaretti, Serena, Christof Seiler, Christelle Boichon, Mauricio Reyes, and Philippe Büchler (2014). Image-based vs. mesh-based statistical appearance models of the human femur: Implications for finite element simulations. In: *Medical Engineering & Physics* 36.12, pp. 1626–1635. DOI: 10.1016/j.medengphy.2014.09.006.

Booth, Gabrielle R., Carolyn W. Roberts, Sarah Romani, Olivia Mergler, Honglin Zhang, Bengt Pipkorn, Gunter P. Siegmund, Peter A. Cripton, and Jason L. Forman (2022). Methodology to measure seat belt fit in relation to skeletal geometry using an upright open MRI. In: *Traffic Injury Prevention* 23.Suppl 1, pp. 199–201. DOI: 10.1080/15389588.2022.2124805.

Boyle, Kyle J., Matthew P. Reed, Lauren W. Zaseck, and Jingwen Hu (2019). „A human modelling study on occupant kinematics in highly reclined seats during frontal crashes“. In: *Proceedings of the IRCOBI Conference*, pp. 282–292. URL: https://www.ircobi.org/wordpress/downloads/irc19/pdf-files/43.pdf.

Brinckmann, Paul, M. Biggemann, and D. Hilweg (1989). Prediction of the compressive strength of human lumbar vertebrae. In: *Clinical Biomechanics* 14.6, pp. 606–610. ISSN: 0268-0033. DOI: 10.1016/0268-0033(89)90071-5.

Bryan, Rebecca, P. Surya Mohan, Andrew Hopkins, Francis Galloway, Mark Taylor, and Prasanth B. Nair (2010). Statistical modelling of the whole human femur incorporating geometric and material properties. In: *Medical Engineering & Physics* 32.1, pp. 57–65. DOI: 10.1016/j.medengphy.2009.10.008.

Buchholz, Kami (2015). *Futurist Kurzweil discusses acceleration of intelligent technology.* Ed. by SAE Mobilus. URL: https://www.sae.org/news/2015/04/futurist-kurzweil-discusses-acceleration-of-intelligent-technology (visited on 04/30/2023).

Bucki, Marek, Claudio Lobos, and Yohan Payan (2010). A fast and robust patient specific finite element mesh registration technique: Application to 60 clinical cases. In: *Medical Image Analysis* 14.3, pp. 303–317. DOI: 10.1016/j.media.2010.02.003.

Cappozzo, Aurelio (1984). Compressive loads in the lumbar vertebral column during normal level walking. In: *Journal of Orthopaedic Research* 1.3, pp. 292–301. DOI: 10.1002/jor.1100010309.

Chabert, Laurent, S. Ghannouchi, C. Cavallero, and J. Bonnoit (1998). „Geometrical characterisation of a seated occupant“. In: *Proceedings of International Technical Conference on the Enhanced Safety of Vehicles (ESV)*, pp. 2073–2079. URL: https://www-esv.nhtsa.dot.gov/Proceedings/16/98s9p19.pdf.

Chance, George Q. (1948). Note on a type of flexion fracture of the spine. In: *The British journal of radiology* 21.249. ISSN: 0007-1285. DOI: 10.1259/0007-1285-21-249-452.

Chandler, Richard F. (1985). Data for the development of criteria for general aviation seat and restraint system performance. In: *SAE Transactions* 850851. ISSN: 0096736X, 25771531. DOI: 10.4271/850851.

Chhabra, Aditya, Sachiv Paruchuri, Kshitij Mishra, Dhruv Kaushik, Anoop Chawla, Sudipto Mukherjee, and Rajesh Malhotra (2017). „Spline-based repositioning for the vertebral column of the GHBMC human body finite element model“. In: *Proceedings of the IRCOBI Conference*, pp. 533–534. URL: https://www.ircobi.org/wordpress/downloads/irc17/pdf-files/66.pdf.

Cobb, John R. (1948). Outlines for the study of scoliosis. In: *The Journal of Bone and Joint Surgery. American volume* 5, pp. 261–275. ISSN: 0021-9355.

Couteau, Béatrice, Yohan Payan, and Stéphane Lavallée (2000). The mesh-matching algorithm: An automatic 3D mesh generator for finite element structures. In: *Journal of Biomechanics* 33.8, pp. 1005–1009. DOI: 10.1016/S0021-9290(00)00055-5.

Dai, Li-Yang, Wei-Fang Yao, Yi-Min Cui, and Qing Zhou (2004). Thoracolumbar fractures in patients with multiple injuries: Diagnosis and treatment-a review of 147 cases. In: *The Journal of Trauma* 56.2, pp. 348–355. ISSN: 0022-5282. DOI: 10.1097/01.ta.0000035089.51187.43.

Davies, W. E., John H. Morris, and V. Hill (1980). An analysis of conservative (non-surgical) management of thoracolumbar fractures and fracture-dislocations with neural damage. In: *The Journal of Bone and Joint Surgery. American volume* 62.8, pp. 1324–1328. ISSN: 0021-9355.

De Carvalho, Diana E. and Jack P. Callaghan (2012). Influence of automobile seat lumbar support prominence on spine and pelvic postures: A radiological investigation. In: *Applied Ergonomics* 43.5, pp. 876–882. DOI: 10.1016/j.apergo.2011.12.007.

Denis, Francis (1983). The three column spine and its significance in the classification of acute thoracolumbar spinal injuries. In: *Spine* 8.8, pp. 817–831. DOI: 10.1097/00007632-198311000-00003.

DeStefano, Leonard A. (1972). *Dynamic response index minimization for personnel escape systems*. Philadelphia, PA. URL: https://apps.dtic.mil/sti/pdfs/AD0750318.pdf (visited on 05/20/2024).

DeWeese, Richard L., David M. Moorcroft, and Joseph A. Pellettiere (2015). „Civil aviation crash injury protection“. In: *Accidental injury*. Ed. by Narayan Yoganandan, Alan M. Nahum, and John W. Melvin. New York, NY: Springer. ISBN: 9781493917327. DOI: 10.1007/978-1-4939-1732-7{\textunderscore}28.

Dissanaike, Sharmila, Robert P. Kaufman, Christopher D. Mack, Charles Mock, and Eileen M. Bulger (2008). The effect of reclined seats on mortality in motor vehicle collisions. In: *Journal of Trauma and Acute Care Surgery* 64.3, pp. 614–619. ISSN: 2163-0755. DOI: 10.1097/TA.0b013e318164d071.

Draper, Dustin (2022). „Validation of human body model lumbar spine performance for use in new seating positions“. Dissertation. Munich: Ludwig-Maximilians University Munich. DOI: 10.5282/edoc.30043.

Draper, Dustin, Andreas Huf, Philipp Wernicke, and Steffen Peldschus (2019). „The influence of reclined seating positions on lumbar spine kinematics and loading in frontal impact scenarios“. In: *Proceedings of International Technical Conference on the Enhanced Safety of Vehicles (ESV)*. URL: https://www-esv.nhtsa.dot.gov/Proceedings/26/26ESV-000062.pdf.

Draper, Dustin, Nicolas Newell, Spyros D. Masouros, and Steffen Peldschus (2021). Multiscale Validation of Multiple Human Body Model Functional Spinal Units. In: *Journal of Biomechanical Engineering* 143.4, pp. 1–8. DOI: 10.1115/1.4049332.

Draper, Dustin, Alok S. Shah, Steffen Peldschus, and Brian D. Stemper (2020). „Initial validation of a human body model lumbar spine using dynamic compression“. In: *Proceedings of the IRCOBI Conference*, pp. 213–214. URL: https://www.ircobi.org/wordpress/downloads/irc20/pdf-files/28.pdf.

Dreischarf, Marcel, Antonius Rohlmann, Friedmar Graichen, Georg Bergmann, and Hendrik Schmidt (2016). In vivo loads on a vertebral body replacement during different lifting techniques. In: *Journal of Biomechanics* 49.6, pp. 890–895. DOI: 10.1016/j.jbiomech.2015.09.034.

Duma, Stefan M., Andrew R. Kemper, David M. McNeely, P. Gunnar Brolinson, and Fumio Matsuoka (2006). Biomechanical response of the lumbar spine in dynamic compression. In: *Biomedical Sciences Instrumentation* 42, pp. 476–481.

Dvorak, Jiri, D. Froehlich, L. Penning, H. Baumgartner, and Manohar M. Panjabi (1988). Functional radiographic diagnosis of the cervical spine: flexion/extension. In: *Spine* 13.7, pp. 748–755. DOI: 10.1097/00007632-198807000-00007.

DYNAmore GmbH (2023). *What are the differences between implicit and explicit?* URL: https://www.dynasupport.com/faq/general/what-are-the-differences-between-implicit-and-explicit (visited on 06/04/2023).

Eggers, Andre and Steffen Peldschus (2022). *What is needed to ensure process integrity in HBM-based virtual testing procedures.* Wiesbaden, Germany. URL: https://www.carhs.de/en/conference_proceedings/product/humo-2022-replay.html.

Elvik, Rune, Alena Høye, Truls Vaa, and Michael Sørensen (2009). *The handbook of road safety measures.* 2nd ed. Bingley, UK: Emerald Group Publishing Limited. ISBN: 978-1-84855-250-0. DOI: 10.1108/9781848552517.

Eskandarian, Azim, ed. (2012). *Handbook of intelligent vehicles.* 2nd. London: Springer. ISBN: 9780857290847. DOI: 10.1007/978-0-85729-085-4.

Ferguson, Ron L. and Ben L. Allen (1984). A mechanistic classification of thoracolumbar spine fractures. In: *Clinical Orthopaedics and Related Research* 189, pp. 77–88. ISSN: 0009-921X.

Forman, Jason L., Adrian Caudillo-Huerta, Justin McMahon, Matthew B. Panzer, William Marshall, Derek Winter, Matthew Seavers, Matthew Dyer, and Paul Lemmen (2021). *Modifications to the THOR-50M for improved usability in reclined postures – update and preliminary findings.* Ed. by RCCADS. URL: `https://www.trcpg.com/media/tnbfmktx/forman_modifications-to-the-thor-50m-for-improved-usability-in-reclined-postures.pdf` (visited on 05/20/2024).

Forman, Jason L., Richard W. Kent, Krystoffer Mroz, Bengt Pipkorn, Ola Bostrom, and Maria Segui-Gomez (2012). Predicting rib fracture risk with whole-body finite element models: development and preliminary evaluation of a probabilistic analytical framework. In: *Annals of Advances in Automotive Medicine* 56, pp. 109–124. ISSN: 1943-2461.

Forman, Jason L., Shubham Kulkarni, Daniel Perez–Rapela, Sayak Mukherjee, Matthew B. Panzer, and Jason J. Hallman (2022). „A method for thoracic injury risk function development for human body models“. In: *Proceedings of the IRCOBI Conference*, pp. 719–746. URL: `https://www.ircobi.org/wordpress/downloads/irc22/pdf-files/2297.pdf`.

Forman, Jason L., Gerald S. Poplin, Greg Shaw, Timothy L. McMurry, Kristin Schmidt, Joseph H. Ash, and Cecilia Sunnevang (2019). Automobile injury trends in the contemporary fleet: Belted occupants in frontal collisions. In: *Traffic Injury Prevention* 20.6, pp. 607–612. DOI: `10.1080/15389588.2019.1630825`.

Fuchs, Therese (2018). „Objektivierung der Modellbildung von verletzungsmechanischen Experimenten für die Validierung von Finite-Elemente Menschmodellen“. Dissertation. Munich: Ludwig-Maximilians University Munich. DOI: `10.5282/edoc.22460`.

Fuchs, Therese and Steffen Peldschus (2016). *Towards a more standardized application of human body models.* Heidelberg.

Funk, James R., Jason R. Kerrigan, and Jeff R. Crandall (2004). Dynamic bending tolerance and elastic-plastic material properties of the human femur. In: *Annual proceedings. Association for the Advancement of Automotive Medicine* 48, pp. 215–233.

Gallagher, Daniel J. and Stephen D. Heinrich (1990). Pediatric chance fracture. In: *Journal of Orthopaedic Trauma* 4.2, pp. 183–187. ISSN: 0890-5339. DOI: `10.1097/00005131-199004020-00015`.

Gepner, Bronislaw D., Dustin Draper, Krystoffer Mroz, Martin Östling, Bengt Pipkorn, Jason L. Forman, and Jason R. Kerrigan (2019). „Comparison of human body models in frontal crashes with reclined seatback“. In: *Proceedings of the IRCOBI Conference*, pp. 293–307. URL: `https://www.ircobi.org/wordpress/downloads/irc19/pdf-files/44.pdf`.

Germanetti, F., F. Cappellino, D. Fiumarella, G. Belingardi, and Alessandro Scattina (2020). „Handling of human body models for crash simulation in the pre and post processing phases“. In: *Proceedings of International Symposium: Human Modeling and Simulation in Automotive Engineering.* Ed. by CARHS.

Ghaffari, Ghazaleh, Karin Brolin, Dan Braase, Bengt Pipkorn, Bo Svanberg, Lotta Jakobsson, and Johan Davidsson (2019). Passenger muscle responses in lane change and lane change with braking maneuvers using two belt configurations: Standard and reversible pre-pretensioner. In: *Traffic Injury Prevention* 20, pp. 12–14. DOI: 10.1080/15389588.2019.1634265.

Glassbrenner, Donna (2013). An analysis of recent improvements to vehicle safety. In: *Annals of Emergency Medicine* 61.2, p. 222. ISSN: 01960644. DOI: 10.1016/j.annemergmed.2012.12.009.

González-García, María, Jens Weber, and Steffen Peldschus (2021). Potential effect of pre-activated muscles under a far-side lateral impact. In: *Traffic Injury Prevention* 22.Suppl 1, pp. 148–152. DOI: 10.1080/15389588.2021.1982597.

Goodworth, Adam D. and Jeremiah Canada (2021). Self-reported non-nominal sitting in passengers is influenced by age and height. In: *Stapp Car Crash Journal* 65, pp. 29–48. DOI: 10.4271/2021-22-0003.

Grassi, Lorenzo, Najah Hraiech, Enrico Schileo, Mauro Ansaloni, Michel Rochette, and Marco Viceconti (2011). Evaluation of the generality and accuracy of a new mesh morphing procedure for the human femur. In: *Medical Engineering & Physics* 33.1, pp. 112–120. DOI: 10.1016/j.medengphy.2010.09.014.

Grosland, Nicole M., Ritesh Bafna, and Vincent A. Magnotta (2009). Automated hexahedral meshing of anatomic structures using deformable registration. In: *Computer Methods in Biomechanics and Biomedical Engineering* 12.1, pp. 35–43. DOI: 10.1080/10255840903065134.

Hanesch, D., Julia Muehlbauer, D. Rasp, Sylvia Schick, and Steffen Peldschus (2021). Comparison of two radiation-free methods for determining spinal curvature and orientation in different positions. In: *European Spine Journal* 30.11, pp. 3328–3414. DOI: 10.1007/s00586-021-07017-6.

Hardacker, James W., Robert F. Shuford, Peter N. Capicotto, and Philip W. Pryor (1997). Radiographic standing cervical segmental alignment in adult volunteers without neck symptoms. In: *Spine* 22.13, pp. 1472–1480. DOI: 10.1097/00007632-199707010-00009.

Hardy, Warren N. (2002). „Instrumentation in experimental design“. In: *Accidental Injury*. Ed. by Alan M. Nahum and John W. Melvin. New York, NY: Springer.

Harrison, Deed E., Donald D. Harrison, Rene Cailliet, Stephane J. Troyanovich, Tadeusz J. Janik, and Burt Holland (2000). Cobb method or Harrison posterior tangent method: which to choose for lateral cervical radiographic analysis. In: *Spine* 25.16, pp. 2072–2078. DOI: 10.1097/00007632-200008150-00011.

Hazrati Marangalou, Javad, Keita Ito, Matteo Cataldi, Fulvia Taddei, and Bert van Rietbergen (2013). A novel approach to estimate trabecular bone anisotropy using a database approach. In: *Journal of Biomechanics* 46.14, pp. 2356–2362. DOI: 10.1016/j.jbiomech.2013.07.042.

Hodgson, V. R., E. S. Gurdjian, L. M. Thomas, Bin Yang, Kwong-Ming Tse, Ning Chen, Long-Bin Tan, Qing-Qian Zheng, Hui-Min Yang, Min Hu, Gang Pan, and Heow-Pueh Lee (1967). Development of a model for the study of head injury during impact tests. In: *Stapp Car Crash Journal* SAE 670923. DOI: 10.1155/2014/408278.

Holdsworth, F. W. (1963). Fractures, dislocations, and fracture-dislocations of the spine. In: *The Journal of Bone and Joint Surgery. British volume* 45.1, pp. 6–20. ISSN: 0301-620X. DOI: 10.1302/0301-620X.45B1.6.

Hou, Yang and Wen Yuan (2012). Influences of disc degeneration and bone mineral density on the structural properties of lumbar end plates. In: *The Spine Journal* 12.3, pp. 249–256. DOI: 10.1016/j.spinee.2012.01.021.

Howland, Willard J., Joseph L. Curry, and Carroll B. Buffington (1965). Fulcrum fractures of the lumbar spine. Transverse fracture induced by an improperly placed seat belt. In: *Japan Automobile Manufactures Association* 193, pp. 240–241. ISSN: 0098-7484. DOI: 10.1001/jama.1965.03090030062025.

Hu, Jingwen, Jonathan D. Rupp, and Matthew P. Reed (2012). Focusing on vulnerable populations in crashes: Recent advances in finite element human models for injury biomechanics research. In: *Journal of the Automotive Safety and Energy* 3, pp. 295–307. DOI: 10.7302/4007.

Huang, Yi, Albert I. King, John M. Cavanaugh, and Yue Huang (1994). Finite element modeling of gross motion of human cadavers in side impact. In: *Stapp Car Crash Journal* SAE 942207. DOI: 10.4271/942207.

Hutton, William C. and Michael A. Adams (1982). Can the lumbar spine be crushed in heavy lifting? In: *Spine* 7, pp. 586–590. DOI: 10.1097/00007632-198211000-00012.

Iatridis, James C., Mark Weidenbaum, Lori A. Setton, and Van C. Mow (1996). Is the nucleus pulposus a solid or a fluid? Mechanical behaviors of the nucleus pulposus of the human intervertebral disc. In: *Spine* 21.10, pp. 1174–1184. DOI: 10.1097/00007632-199605150-00009.

Isaksson-Hellman, I. and Hans Norin (2005). How thirty years of focused safety development has influenced injury outcome in volvo cars. In: *Annual proceedings. Association for the Advancement of Automotive Medicine* 49, pp. 63–77.

ISO/TR 9790 (1999). *Road vehicles — Anthropomorphic side impact dummy - Lateral impact response requirements to assess the biofidelity of the dummy.* URL: https://www.iso.org/standard/29828.html (visited on 04/14/2024).

Iwamoto, Masami, Yoshikatsu Kisanuki, Isao Watanabe, Katsuya Furusu, and Kazuo Miki (2002). „Development of a finite element model of the Total Human Model for Safety (THUMS) and application to injury reconstruction“. In: *Proceedings of the IRCOBI Conference*. Munich, Germany. URL: https://www.ircobi.org/wordpress/downloads/irc0111/2002/Session1/1.2.pdf.

Izumiyama, Tomohiro, Norihiro Nishida, Hideyuki Iwanaga, Xian Chen, Junji Ohgi, Koji Mori, Takafumi Hayashi, Itsuo Sakuramoto, Ryusuke Asahi, Shigeru Sugimoto, and Masaki Ueno (2018). „The analysis of an individual difference in human skeletal alignment in seated posture and occupant behavior using HBMs“. In: *Proceedings of the IRCOBI Conference*, pp. 549–560. URL: https://www.ircobi.org/wordpress/downloads/irc18/pdf-files/84.pdf.

Izumiyama, Tomohiro, Norihiro Nishida, Hirkoi Yamagata, Ryusuke Asahi, Xian Chen, Junji Ohgi, Shigeru Sugimoto, and Masanobu Fukushima (2022). „Analysis of individual variabilities for lumbar and pelvic alignment in highly reclined seating postures and occupant kinematics in a collision". In: *Proceedings of the IRCOBI Conference*, pp. 941–955. URL: https://www.ircobi.org/wordpress/downloads/irc22/pdf-files/22113.pdf.

Jani, Dhaval, Anoop Chawla, Sudipto Mukherjee, Rahul Goyal, Nataraju Vusirikala, and Suresh Jayaraman (2012). Repositioning the knee joint in human body FE models using a graphics-based technique. In: *Traffic Injury Prevention* 13.6, pp. 640–649. DOI: 10.1080/15389588.2012.664669.

Janssen, Michiel M. A., Xavier Drevelle, Ludovic Humbert, Wafa Skalli, and René M. Castelein (2009). Differences in male and female spino-pelvic alignment in asymptomatic young adults: a three-dimensional analysis using upright low-dose digital biplanar X-rays. In: *Spine* 34.23, pp. 826–832. DOI: 10.1097/BRS.0b013e3181a9fd85.

Ji, Peijun, Yi Huang, and Qing Zhou (2017). Mechanisms of using knee bolster to control kinematical motion of occupant in reclined posture for lowering injury risk. In: *International Journal of Crashworthiness* 22, pp. 415–424. ISSN: 1358-8265. DOI: 10.1080/13588265.2016.1275430.

Jolivet, Erwan, Yoann Lafon, Philippe Petit, and Philippe Beillas (2015). Comparison of kriging and moving least square methods to change the geometry of human body models. In: *Stapp Car Crash Journal* 59, pp. 337–357. DOI: 10.4271/2015-22-0013.

Jorlöv, Sofia, Katarina Bohman, and Annika Larsson (2017). „Seating positions and activities in highly automated cars – a qualitative study of future automated driving scenarios". In: *Proceedings of the IRCOBI Conference*, pp. 13–22. URL: https://www.ircobi.org/wordpress/downloads/irc17/pdf-files/11.pdf.

Kahane, Chuck (2015). *Lives saved by vehicle safety technologies and associated federal motor vehicle safety standards, 1960 to 2012: Passenger Cars and LTVs: With Reviews of 26 FMVSS and the Effectiveness Of Their Associated Safety Technologies in Reducing Fatalities, Injuries, and Crashes*. Ed. by NHTSANational Highway Traffic Safety Administration. URL: https://www.nhtsa.gov/sites/nhtsa.gov/files/2015sae-kindelberger-livessaved.pdf (visited on 05/20/2024).

Kallieris, Dimitrios, Rainer Mattern, G. Schmidt, and D. Warth (1984). „Kinematic and spinal column injuries in active and passive passenger protection. Results of simulated frontal collisions". In: *Proceedings of the IRCOBI Conference*. Vol. 12, pp. 279–295. URL: https://www.ircobi.org/wordpress/downloads/irc1984/pdf_files/1984_22.pdf.

Kallieris, Dimitrios, Dietmar Otte, Rainer Mattern, and Peter Wiedmann (1995). Comparison of sled tests with real traffic accidents. In: *Stapp Car Crash Journal*. DOI: 10.4271/952707.

Katsuhara, Tadasuke, Yoshiki Takahira, Shigeki Hayashi, Yuichi Kitagawa, and Tsuyoshi Yasuki (2017). Analysis of driver kinematics and lower thoracic spine injury in World Endurance Championship Race Cars during frontal impacts. In: *SAE International Journal of Transportation Safety* 5.1, pp. 120–132. ISSN: 2327-5634. DOI: 10.4271/2017-01-1432.

Kaufer, H. and J. T. Hayes (1966). Lumbar fracture-dislocation. A study of twenty-one cases. In: *The Journal of Bone and Joint Surgery. American volume* 48.4, pp. 712–730. ISSN: 0021-9355.

Kaufman, Robert P., Randal P. Ching, Margaret M. Willis, Christopher D. Mack, Joel A. Gross, and Eileen M. Bulger (2013). Burst fractures of the lumbar spine in frontal crashes. In: *Accident Analysis and Prevention* 59, pp. 153–163. DOI: 10.1016/j.aap.2013.05.023.

Kazarian, Lean and George A. Graves (1977). Compressive strength characteristics of the human vertebral centrum. In: *Spine* 2.1.

Kemper, Andrew R., Craig McNally, and Stefan M. Duma (2007). The influence of strain rate on the compressive stiffness properties of human lumbar intervertebral discs. In: *Biomedical Sciences Instrumentation* 43, pp. 176–181. DOI: 10.1111/os.12847.

Kent, Richard W., Joseph Cormier, Timothy L. McMurry, B. Johan Ivarsson, James R. Funk, Thomas Hartka, and Mark Sochor (2023). Spinal injury rates and specific causation in motor vehicle collisions. In: *Accident Analysis and Prevention* 186. DOI: 10.1016/j.aap.2023.107047.

Keyes, Donald C. and Edward L. Compere (1932). The normal and pathological physiology of the nucleus pulposus of the intervertebral disc: An anatomical, clinical, and experimental study. In: *The Journal of Bone and Joint Surgery. American volume* 14.4, pp. 897–938. ISSN: 0021-9355.

Kifune, Masao, Manohar M. Panjabi, Marcus Arand, and Weiguo Liu (1995). Fracture pattern and instability of thoracolumbar injuries. In: *European Spine Journal* 4.2, pp. 98–103. DOI: 10.1007/BF00278920.

King, Albert I. (2002). „Injury to the thoracolumbar spine and pelvis“. In: *Accidental Injury*. Ed. by Alan M. Nahum and John W. Melvin. New York, NY: Springer.

King, Albert I. (2018). *The biomechanics of impact injury: Biomechanical response, mechanisms of injury, human tolerance and simulation*. Cham: Springer International Publishing. ISBN: 9783319497921. DOI: 10.1007/978-3-319-49792-1.

Klein, Christoph, María González-García, Jens Weber, Freerk Bosma, Richard Lancashire, Dominik Breitfuss, Stefan Kirschbichler, and Werner Leitgeb (2021). „A methdik for reproducible landmark-based positioning of multibody and finite-element human models“. In: *Proceedings of the IRCOBI Conference*, pp. 477–489. URL: https://www.ircobi.org/wordpress/downloads/irc21/pdf-files/2153.pdf.

Klein, Katelyn F., Jingwen Hu, Matthew P. Reed, Carrie N. Hoff, and Jonathan D. Rupp (2015). Development and validation of statistical models of femur geometry for use with parametric finite element models. In: *Annals of Biomedical Engineering* 43, pp. 2503–2514. DOI: 10.1007/s10439-015-1307-6.

Klinich, Kathleen D., Sheila M. Ebert, and Matthew P. Reed (2012). Quantifying cervical-spine curvature using Bézier splines. In: *Journal of Biomechanical Engineering* 134.11, p. 114503. DOI: 10.1115/1.4007749.

Klinich, Kathleen D., Sheila M. Ebert, Chris A. van Ee, Carol A. C. Flannagan, Monica Prasad, Matthew P. Reed, and Lawrence W. Schneider (2004). Cervical spine geometry in the automotive seated posture: variations with age, stature, and gender. In: *Stapp Car Crash Journal* 48, pp. 301–330. DOI: 10.4271/2004-22-0014.

Langrana, N. A., R. D. Harten, D. C. Lin, M. F. Reiter, and C. K. Lee (2002). Acute thoracolumbar burst fractures: A new view of loading mechanisms. In: *Spine* 27.5, pp. 498–508. DOI: 10.1097/00007632-200203010-00010.

Larson, Sanford J., Dennis J. Maiman, and Rolando F. DelMaestro (1999). *Surgery of the lumbar spine*. 1st ed. Vol. 28. Thieme Medical Publishers Inc. ISBN: 978-1604068924.

Li, Zhigang, Jingwen Hu, and Jinhuan Zhang (2012). „Comparison of different radial basis functions in developing subject-specific infant head finite element models for injury biomechanics study“. In: *Proceedings of Summer Bioengineering Conference*. Vol. 44809, pp. 49–50. DOI: 10.1115/SBC2012-80162.

Lob, Alfons (1954). *Die Wirbelsäulenverletzungen und ihre Ausheilung: Experimentelle, pathologisch-klinische Untersuchungen*. Vol. 64. Thieme.

Louis, L. D. (1977). Fractures instables du rachis. In: *Revue de Chirurgie Orthopédique et Traumatologique* 63, pp. 415–418.

Lubbe, Nils, Hanna Jeppsson, Arian Ranjbar, Jonas Fredriksson, Jonas Bärgman, and Martin Östling (2018). „Predicted road traffic fatalities in Germany: the potential and limitations of vehicle safety technologies from passive safety to highly automated driving“. In: *Proceedings of the IRCOBI Conference*, pp. 17–52. URL: https://www.ircobi.org/wordpress/downloads/irc18/pdf-files/11.pdf.

Mac-Thiong, Jean-Marc, Hubert Labelle, Eric Berthonnaud, Randal R. Betz, and Pierre Roussouly (2007). Sagittal spinopelvic balance in normal children and adolescents. In: *European Spine Journal* 16.2, pp. 227–234. DOI: 10.1007/s00586-005-0013-8.

Magerl, F., M. Aebi, Stanley D. Gertzbein, J. Harms, and S. Nazarian (1994). A comprehensive classification of thoracic and lumbar injuries. In: *European Spine Journal* 3, pp. 184–201. DOI: 10.1007/BF02221591.

Mannion, Anne F., Katrin Knecht, Gordana Balaban, Jiri Dvorak, and Dieter Grob (2004). A new skin-surface device for measuring the curvature and global and segmental ranges of motion of the spine: Reliability of measurements and comparison with data reviewed from the literature. In: *European Spine Journal* 13.2, pp. 122–136. DOI: 10.1007/s00586-003-0618-8.

Marini, Giacomo, Harald Studer, Gerd Huber, Klaus Püschel, and Stephen J. Ferguson (2016). Geometrical aspects of patient-specific modelling of the intervertebral disc: Collagen fibre orientation and residual stress distribution. In: *Biomechanics and Modeling in Mechanobiology* 15.3, pp. 543–560. DOI: 10.1007/s10237-015-0709-6.

Masharawi, Youssef M. (2012). Lumbar shape characterization of the neural arch and vertebral body in spondylolysis: A comparative skeletal study. In: *Clinical Anatomy* 25.2, pp. 224–230. DOI: 10.1002/ca.21203.

Masharawi, Youssef M., Bruce Rothschild, Gali Dar, Smadar Peleg, Dror Robinson, Ella Been, and Israel Hershkovitz (2004). Facet orientation in the thoracolumbar spine: Three-dimensional anatomic and biomechanical analysis. In: *Spine* 29.16, pp. 1755–1763. DOI: 10.1097/01.brs.0000134575.04084.ef.

Masharawi, Youssef M., Bruce Rothschild, Khalil Salame, Gali Dar, Smadar Peleg, and Israel Hershkovitz (2005). Facet tropism and interfacet shape in the thoracolumbar vertebrae. In: *Spine* 30.13, pp. 281–292. DOI: 10.1097/01.brs.0000164098.00201.8d.

Masharawi, Youssef M. and Khalil Salame (2011). Shape variation of the neural arch in the thoracic and lumbar spine: characterization and relationship with the vertebral body shape. In: *Clinical Anatomy* 24.7, pp. 858–867. DOI: 10.1002/ca.21175.

Masharawi, Youssef M., Khalil Salame, Yigal Mirovsky, Smadar Peleg, Gali Dar, Nili Steinberg, and Israel Hershkovitz (2008). Vertebral body shape variation in the thoracic and lumbar spine: characterization of its asymmetry and wedging. In: *Clinical Anatomy* 21.1, pp. 46–54. DOI: 10.1002/ca.20532.

Masharawi, Youssef M., Nili Steinberg, and Khalil Salame (2007). Lumbar facet orientation in spondylosis: A skeletal study. In: *Spine* 6, pp. 176–180. DOI: 10.1097/01.brs.0000257565.41856.0f.

Mattucci, Stephen F. E. and Duane S. Cronin (2015). A method to characterize average cervical spine ligament response based on raw data sets for implementation into injury biomechanics models. In: *Journal of the Mechanical Behavior of Biomedical Materials* 41, pp. 251–260. DOI: 10.1016/j.jmbbm.2014.09.023.

McGill, Stuart M., M. T. Sharratt, and J. P. Seguin (1995). Loads on spinal tissues during simultaneous lifting and ventilatory challenge. In: *Ergonomics* 38.9, pp. 1772–1792. DOI: 10.1080/00140139508925226.

McHenry, R. R. (1963). Analysis of the dynamics of automobile passenger-restraint systems. In: *Annual proceedings. Association for the Advancement of Automotive Medicine* 7, pp. 207–249.

McMurry, Timothy L., Gerald S. Poplin, Greg Shaw, and Matthew B. Panzer (2018). Crash safety concerns for out-of-position occupant postures: A look toward safety in highly automated vehicles. In: *Traffic Injury Prevention* 19.6, pp. 582–587. DOI: 10.1080/15389588.2018.1458306.

McNally, D. S. and Michael A. Adams (1992). Internal intervertebral disc mechanics as revealed by stress profilometry. In: *Spine* 17.1, pp. 66–73. DOI: 10.1097/00007632-199201000-00011.

Mengoni, Marlène (2021). Biomechanical modelling of the facet joints: a review of methods and validation processes in finite element analysis. In: *Biomechanics and Modeling in Mechanobiology* 20.2, pp. 389–401. DOI: 10.1007/s10237-020-01403-7.

Mertz, Harold J. (2002). „Injury risk assessments based on dummy responses“. In: *Accidental Injury*. Ed. by Alan M. Nahum and John W. Melvin. New York, NY: Springer.

Mertz, Harold J., Annette L. Irwin, John W. Melvin, R. L. Stanaker, and Micheal S. Beebe (1989). Size, weight and biomechanical impact response requirements for adult size small female and large male dummies. In: *SAE Technical Paper*, pp. 133–144. DOI: 10.4271/890756.

Motavelli, J. (2015). Automakers rethink seats for self-driving cars. In: *The New York Times* Sect. B, p. 4.

Mroz, Krystoffer, Martin Östling, Rachel Richardson, Jason R. Kerrigan, Jason L. Forman, Bronislaw D. Gepner, Nils Lubbe, and Bengt Pipkorn (2020). „Effect of seat and seat belt characteristics on the lumbar spine and pelvis loading of the SAFER Human Body Model in reclined postures“. In: *Proceedings of the IRCOBI Conference*, pp. 470–486. URL: https://www.ircobi.org/wordpress/downloads/irc20/pdf-files/58.pdf.

Müller, Christian W., Dietmar Otte, Sebastian Decker, Timo Stübig, Martin Panzica, Christian Krettek, and Stephan Brand (2014). Vertebral fractures in motor vehicle accidents - a medical and technical analysis of 33,015 injured front-seat occupants. In: *Accident Analysis and Prevention* 66, pp. 15–19. DOI: 10.1016/j.aap.2014.01.003.

Nachemson, Alf (1960). Lumbar intradiscal pressure: Experimental studies on post-mortem material. In: *Acta Orthopaedica Scandinavica* Suppl 43, pp. 1–104. ISSN: 0001-6470. DOI: 10.3109/ort.1960.31.suppl-43.01.

Nachemson, Alf (1963). The influence of spinal movements on the lumbar intradiscal pressure and on the tensile stresses in the annulus fibrosus. In: *Acta Orthopaedica Scandinavica* 33.1-4, pp. 183–207. ISSN: 0001-6470. DOI: 10.3109/17453676308999846.

Nachemson, Alf (1970). Intravital dynamic pressure measurements in lumbar discs: A study of common movements, maneuvers and exercises. In: *Scandinavian Journal of Rehabilitation Medicine* 1, pp. 1–40.

Nérot, Agathe, Julie Choisne, Célia Amabile, Christophe Travert, Hélène Pillet, Xuguang Wang, and Wafa Skalli (2015). A 3D reconstruction method of the body envelope from biplanar X-rays: Evaluation of its accuracy and reliability. In: *Journal of Biomechanics* 48.16, pp. 4322–4326. DOI: 10.1016/j.jbiomech.2015.10.044.

Netter, Frank H. (2017). *Atlas of human anatomy*. 7th. Netter Basic Science Ser. Philadelphia, PA: Elsevier. ISBN: 9780323393225. URL: https://ebookcentral.proquest.com/lib/gbv/detail.action?docID=5553751.

Newell, Nicolas, Diagarajen Carpanen, Alexandros Christou, Grigorios Grigoriadis, J. Paige Little, and Spyros D. Masouros (2017a). „Strain rate dependence of internal pressure and external bulge in human intervertebral discs during axial compression“. In: *Proceedings of the IRCOBI Conference*, pp. 670–671. URL: https://www.ircobi.org/wordpress/downloads/irc17/pdf-files/87.pdf.

Newell, Nicolas, Diagarajen Carpanen, Grigorios Grigoriadis, J. Paige Little, and Spyros D. Masouros (2019). Material properties of human lumbar intervertebral discs across strain rates. In: *The Spine Journal* 19.12, pp. 2013–2024. DOI: 10.1016/j.spinee.2019.07.012.

Newell, Nicolas, J. Paige Little, Alexandros Christou, Michael A. Adams, C. J. Adam, and Spyros D. Masouros (2017b). Biomechanics of the human intervertebral disc: A review of testing techniques and results. In: *Journal of the Mechanical Behavior of Biomedical Materials* 69, pp. 420–434. DOI: 10.1016/j.jmbbm.2017.01.037.

NHTSA (2017). *Automated driving systems 2.0: A vision for safety*. Ed. by National Highway Traffic Safety Administration. URL: https://www.nhtsa.gov/sites/

nhtsa.gov/files/documents/13069a-ads2.0_090617_v9a_tag.pdf (visited on 06/04/2023).

NHTSA (2022). *Traffic safety facts annual report tables*. Ed. by National Highway Traffic Safety Administration. URL: https://cdan.dot.gov/tsftables/tsfar.htm# (visited on 06/04/2023).

NHTSA (2023). *NHTSA's crash test dummies*. Ed. by National Highway Traffic Safety Administration. URL: https://www.nhtsa.gov/nhtsas-crash-test-dummies (visited on 06/04/2023).

Nicoll, E. A. (1949). Fractures of the dorso-lumbar spine. In: *The Journal of Bone and Joint Surgery. British volume* 31.3, pp. 376–394. ISSN: 0301-620X. DOI: 10.1302/0301-620X.31B3.376.

Niemeyer, Frank, Hans-Joachim Wilke, and Hendrik Schmidt (2012). Geometry strongly influences the response of numerical models of the lumbar spine–a probabilistic finite element analysis. In: *Journal of Biomechanics* 45.8, pp. 1414–1423. DOI: 10.1016/j.jbiomech.2012.02.021.

NTSB (1988). *Performance of lap/shoulder belts in 167 motor vehicle crashes*. Ed. by National Transportation Safety Board (NTSB). URL: https://www.ntsb.gov/safety/safety-studies/Documents/SS8803.pdf (visited on 05/20/2024).

O'Cain, C. M., Bronislaw D. Gepner, E. Meade Spratley, Jason R. Kerrigan, and Richard W. Kent (2019). *Pipeline for specimen specific bone-ligament-cartilage finite element models*. URL: https://ibrc.osu.edu/wp-content/uploads/2019/05/2019-IBS-Manuscript_OCain.pdf.

O'Neill, Brian (2009). Preventing passenger vehicle occupant injuries by vehicle design - A historical perspective from IIHS. In: *Traffic Injury Prevention* 10.2, pp. 113–126. DOI: 10.1080/15389580802486225.

O'Reilly, Meaghan Anne and Cari Marisa Whyne (2008). Comparison of computed tomography based parametric and patient-specific finite element models of the healthy and metastatic spine using a mesh-morphing algorithm. In: *Spine* 33.17, pp. 1876–1881. DOI: 10.1097/BRS.0b013e31817d9ce5..

Oberkampf, William L., Timothy G. Trucano, and Charles Hirsch (2004). Verification, validation, and predictive capability in computational engineering and physics. In: *Applied Mechanics Reviews* 57.5, pp. 345–384. ISSN: 0003-6900. DOI: 10.1115/1.1767847.

Ochia, Ruth S., Allan F. Tencer, and Randal P. Ching (2003). Effect of loading rate on endplate and vertebral body strength in human lumbar vertebrae. In: *Journal of Biomechanics* 36.12, pp. 1875–1881. DOI: 10.1016/s0021-9290(03)00211-2.

Ortiz-Paparoni, Maria, Joost Op 't Eynde, Jason Kait, Brian Bigler, Jay Shridharani, Allison Schmidt, Courtney Cox, Concetta Morino, Frank A. Pintar, Narayan Yoganandan, Jason Moore, Jiang Yue Zhang, and Cameron R. Bass (2021). The human lumbar spine during high-rate under seat loading: A combined metric injury criteria. In: *Annals of Biomedical Engineering* 49.11, pp. 3018–3030. DOI: 10.1007/s10439-021-02823-x.

OSCCAR (2020). *Future occupant safety for crashes in cars*. URL: https://www.osccarproject.eu/ (visited on 07/01/2023).

Östling, Martin, Hanna Jeppsson, and Nils Lubbe (2019). „Predicting crash configurations in passenger car to passenger car crashes to guide the development of future passenger car safety“. In: *Proceedings of the IRCOBI Conference*, pp. 626–643. URL: https://www.ircobi.org/wordpress/downloads/irc19/pdf-files/92.pdf.

Östling, Martin, Cecilia Sunnevang, C. Svensson, and H. O. Kock (2017). „Potential future seating positions and the impact on injury risks in a Learning Intelligent Vehicle (LIV)“. In: *Proceedings of Fahrzeugsicherheit 2017*. Ed. by Verein Deutscher Ingenieure.

Osvalder, A-L, P. Neumann, P. Lövsund, and A. Nordwall (1990). Ultimate strength of the lumbar spine in flexion - an in vitro study. In: *Journal of Biomechanics* 23.5, pp. 453–460. DOI: 10.1016/0021-9290(90)90301-i.

Osvalder, A-L, P. Neumann, P. Lövsund, and A. Nordwall (1993). A method for studying the biomechanical load response of the (in vitro) lumbar spine under dynamic flexion-shear loads. In: *Journal of Biomechanics* 26.10, pp. 1227–1236. DOI: 10.1016/0021-9290(93)90070-u.

Panjabi, Manohar M., Masao Kifune, Weiguo Liu, Marcus Arand, Anita Vasavada, and Thomas R. Oxland (1998). Graded thoracolumbar spinal injuries: development of multidirectional instability. In: *European Spine Journal* 7.4, pp. 332–339. DOI: 10.1007/s005860050084.

Panjabi, Manohar M., Masao Kifune, Liu Wen, Marcus Arand, Thomas R. Oxland, Ruey-Mo Lin, Woo-Suk Steve Yoon, and Anita Vasavada (1995). Dynamic canal enchroachment during thorcolumbar burst fractures. In: *Journal of Spinal Disorders* 8.1, pp. 39–48.

Parenteau, Chantal S., Peng Zhang, Sven Holcombe, and Stewart Wang (2014). Characterization of vertebral angle and torso depth by gender and age groups with a focus on occupant safety. In: *Traffic Injury Prevention* 15.1, pp. 66–72. DOI: 10.1080/15389588.2013.829217.

Park, Gwansik, Jason L. Forman, Taewung Kim, Matthew B. Panzer, and Jeff R. Crandall (2018). Injury risk functions based on population-based finite element model responses: Application to femurs under dynamic three-point bending. In: *Traffic Injury Prevention* 19.Suppl 1, pp. 59–64. DOI: 10.1080/15389588.2017.1398402.

Park, Moon Soo, Seong-Hwan Moon, Hwan-Mo Lee, Seok Woo Kim, Tae-Hwan Kim, Seung Yeop Lee, and K. Daniel Riew (2013). The effect of age on cervical sagittal alignment: Normative data on 100 asymptomatic subjects. In: *Spine* 38.8, pp. 458–463. DOI: 10.1097/BRS.0b013e31828802c2.

Park, Sang-Min, Kwang-Sup Song, Seung-Hwan Park, Hyun Kang, and K. Daniel Riew (2015). Does whole-spine lateral radiograph with clavicle positioning reflect the correct cervical sagittal alignment? In: *European Spine Journal* 24.1, pp. 57–62. DOI: 10.1007/s00586-014-3525-2.

Patrick, L. M. and Robert S. Levine (1975). Injury to unembalmed belted cadavers in simulated collisions. In: *SAE Technical Paper* 751144. DOI: 10.4271/751144.

Perey, Olof (1957). Fracture of the vertebral end-plate in the lumbar spine; an experimental biochemical investigation. In: *Acta Orthopaedica Scandinavica* Suppl 25, pp. 1–101. ISSN: 0001-6470. DOI: 10.3109/ort.1957.28.suppl-25.01.

Pettersson, Ingrid and I. C. MariAnne Karlsson (2015). Setting the stage for autonomous cars: A pilot study of future autonomous driving experiences. In: *IET Intelligent Transport Systems* 9.7, pp. 694–701. ISSN: 1751-9578. DOI: 10.1049/iet-its.2014.0168.

Pintar, Frank A., Joseph F. Cusick, Narayan Yoganandan, John Reinartz, and Mahadevappa Mahesh (1992a). The biomechanics of lumbar facetectomy under compression-flexion. In: *Spine* 17.7, pp. 804–810. DOI: 10.1097/00007632-199207000-00013.

Pintar, Frank A., Narayan Yoganandan, Dennis J. Maiman, Mark Scarboro, Rodney W. Rudd, and W. Rodney (2012). Thoracolumbar spine fractures in frontal impact crashes. In: *Annals of Advances in Automotive Medicine* 56, pp. 277–283. ISSN: 1943-2461.

Pintar, Frank A., Narayan Yoganandan, Thomas J. Myers, Ali Elhagediab, and Anthony Sances (1992b). Biomechanical properties of human lumbar spine ligaments. In: *Journal of Biomechanics* 25.11, pp. 1351–1356. DOI: 10.1016/0021-9290(92)90290-H.

Pintar, Frank A., Narayan Yoganandan, and Liming Voo (1998). Effect of age and loading rate on human cervical spine injury threshold. In: *Spine* 23.18, pp. 1957–1962. DOI: 10.1097/00007632-199809150-00007.

Pipkorn, Bengt, Karl-Johan Larsson, Daniel Perez–Rapela, Craig Markusic, Bryant Withcomb, Murthy Ayyagari, and Cecilia Sunnevang (2018). „Occupant protection in far-side impacts“. In: *Proceedings of the IRCOBI Conference*, pp. 77–105. URL: https://www.ircobi.org/wordpress/downloads/irc18/pdf-files/16.pdf.

Pischinger, Stefan and Ulrich Seiffert (2021). *Vieweg Handbuch Kraftfahrzeugtechnik*. 9th. Wiesbaden: Springer Fachmedien. ISBN: 9783658255572. DOI: 10.1007/978-3-658-25557-2.

Pooni, J. S., D. W. Hukins, P. F. Harris, R. C. Hilton, and K. E. Davies (1986). Comparison of the structure of human intervertebral discs in the cervical, thoracic and lumbar regions of the spine. In: *Surgical and Radiologic Anatomy* 8.3, pp. 175–182. DOI: 10.1007/BF02427846.

Prot, M., T. J. Cloete, D. Saletti, and Sébastien Laporte (2016). The behavior of cancellous bone from quasi-static to dynamic strain rates with emphasis on the intermediate regime. In: *Journal of Biomechanics* 49.7, pp. 1050–1057. DOI: 10.1016/j.jbiomech.2016.02.021.

Putz, Reinhard (1985). „Wirbelsäule, Columna vertebralis.“ In: *Makroskopische und mikroskopische Anatomie des Menschen*. Ed. by Jochen Staubesand, Ernst-Günter Afting, Alfred Benninghoff, Kurt Fleischhauer, Kurt Goerttler, Gerhard Aumüller, Bodo Christ, Wolf-Georg Forssmann, Diedrich von Keyserlingk, Benno Kummer, Erne Maier, Günther Osche, R. Presley, Reinhard Putz, Berton Rahn, Ursus-Nikolaus Riede, Dieter Sasse, Hans G. Schwarzacher, Renate Unsöld, and Christian

Vogel. Makroskopische und mikroskopische Anatomie des Menschen. München: Urban & Schwarzenberg. ISBN: 3541002441.

Raney, E. M. and J. T. Bennett (1992). Pediatric Chance fracture. In: *Spine* 17.12, pp. 1522–1524. DOI: 10.1097/00007632-199212000-00017.

Rao, Raj D., Chirag A. Berry, Narayan Yoganandan, and Arnav Agarwal (2014). Occupant and crash characteristics in thoracic and lumbar spine injuries resulting from motor vehicle collisions. In: *The Spine Journal* 14.10, pp. 2355–2365. DOI: 10.1016/j.spinee.2014.01.038.

Rawska, Katarzyna, Bronislaw D. Gepner, Shubham Kulkarni, Kalle Chastain, Junjun Zhu, Rachel Richardson, Daniel Perez–Rapela, Jason L. Forman, and Jason R. Kerrigan (2019). Submarining sensitivity across varied anthropometry in an autonomous driving system environment. In: *Traffic Injury Prevention* 20.Suppl 2, pp. 123–127. DOI: 10.1080/15389588.2019.1655734.

Reed, Matthew P., Sheila M. Ebert, and Jason J. Hallman (2013). Effects of driver characteristics on seat belt fit. In: *Stapp Car Crash Journal* 57, pp. 43–57. DOI: 10.4271/2013-22-0002.

Reed, Matthew P. and Monika L. H. Jones (2017). *A parametric model of cervical spine geometry and posture.* Ed. by University of Michigan, Ann Arbor, Transportation Research Institute. URL: https://deepblue.lib.umich.edu/handle/2027.42/137652 (visited on 05/20/2024).

Richard, Olivier, Jérôme Uriot, Xavier Trosseille, and M. Sokolowski (2015). „Occupant restraint optimisation in frontal crash to mitigate the risk of submarining in out-of-position situation“. In: *Proceedings of the IRCOBI Conference*, pp. 84–100. URL: https://www.ircobi.org/wordpress/downloads/irc15/pdf_files/19.pdf.

Richardson, Rachel, John-Paul Donlon, Kalle Chastain, Greg Shaw, Jason L. Forman, Sara Sochor, Mohan Jayathirtha, Kevin Kopp, Brian Overby, Bronislaw D. Gepner, and Jason R. Kerrigan (2019). „Test methodology for evaluating the reclined seating environment with human surrogates“. In: *Proceedings of International Technical Conference on the Enhanced Safety of Vehicles (ESV).* URL: https://www-esv.nhtsa.dot.gov/Proceedings/26/26ESV-000243.pdf.

Richardson, Rachel, John-Paul Donlon, Bronislaw Gepner, Jason Forman, Jason Hallman, and Jason Kerrigan (2023). The Effects of Recline Angle and Restraint Geometry on Lap Belt-Pelvis Interaction for Above-Normal BMI Motor Vehicle Occupants. In: *Annals of Biomedical Engineering* 10. DOI: 10.1007/s10439-023-03302-1.

Richardson, Rachel, John-Paul Donlon, Mohan Jayathirtha, Jason L. Forman, Greg Shaw, Bronislaw D. Gepner, Jason R. Kerrigan, Martin Östling, Krystoffer Mroz, Bengt Pipkorn, and Bronislaw Gepner (2020a). Kinematic and injury response of reclined PMHS in frontal impacts. In: *Stapp Car Crash Journal* 64, pp. 83–153. DOI: 10.4271/2020-22-0004.

Richardson, Rachel, Mohan Jayathirtha, Kalle Chastain, John-Paul Donlon, Jason L. Forman, Bronislaw D. Gepner, Martin Östling, Krystoffer Mroz, Greg Shaw, Bengt Pipkorn, and Jason R. Kerrigan (2020b). Thoracolumbar spine kinematics and injuries in frontal impacts with reclined occupants. In: *Traffic Injury Prevention* 21.Suppl 1, pp. 66–71. DOI: 10.1080/15389588.2020.1837365.

Richardson, Rachel, Mohan Jayathirtha, John-Paul Donlon, Jason L. Forman, Bronislaw D. Gepner, Martin Östling, Krystoffer Mroz, Bengt Pipkorn, and Jason R. Kerrigan (2020c). „Pelvis kinematics and injuries of reclined occupants in frontal impacts“. In: *Proceedings of the IRCOBI Conference*, pp. 499–515. URL: https://www.ircobi.org/wordpress/downloads/irc20/pdf-files/60.pdf.

Rickenbacher, J., A. M. Landoldt, Karl Theiler, Heinrich Scheier, J. Siegfried, and Franz Josef Wagenhäuser (2004). *Rücken*. Sonderausgabe der 1982 erschienenen 1. Auflage. Berlin: Springer. ISBN: 3540405666.

Ridella, Stephen A. and Daniel P. Parent (2011). „Modifications to improve the durability, usability and biofidelity of the THOR-NT dummy“. In: *Proceedings of International Technical Conference on the Enhanced Safety of Vehicles (ESV)*. URL: http://www-esv.nhtsa.dot.gov/Proceedings/22/isv7/main.htm.

Ripani, M., A. Di Cesare, A. Giombini, L. Agnello, F. Fagnani, and F. Pigozzi (2008). Spinal curvature: Comparison of frontal measurements with the spinal mouse and radiographic assessments. In: *The Journal of Sports Medicine and Physical Fitness* 48.4, pp. 488–494.

Roaf, Robert (1960). A study of the mechanics of spinal injuries. In: *The Journal of Bone and Joint Surgery. British volume*, pp. 810–823. ISSN: 0301-620X. DOI: 10.1302/0301-620X.42B4.810.

Rocabado, Mariano (1983). Biomechanical relationship of the cranial, cervical, and hyoid regions. In: *The Journal of Cranio-Mandibular Practice* 1.3, pp. 61–66. ISSN: 0734-5410. DOI: 10.1080/07345410.1983.11677834.

Rouhana, Stephen W., Paul G. Bedewi, Sundeep V. Kankanala, Priya Prasad, Joseph J. Zwolinski, Alex G. Meduvsky, Jonathan D. Rupp, Thomas A. Jeffreys, and Lawrence W. Schneider (2003). Biomechanics of 4-point seat belt systems in frontal impacts. In: *Stapp Car Crash Journal* 47, pp. 367–399. DOI: 10.4271/2003-22-0017.

Roussouly, Pierre, Sohrab Gollogoly, and Eric Berthonnaud (2005). Classification of the normal variation in the sagittal alignment of the human lumbar spine and pelvis in the standing position. In: *Spine* 30.3, pp. 345–353. DOI: 10.1097/01.brs.0000152379.54463.65.

Rupp, Jonathan D., Carl S. Miller, Matthew P. Reed, Nathaniel H. Madura, Kathleen D. Klinich, and Lawrence W. Schneider (2008). Characterization of knee-thigh-hip response in frontal impacts using biomechanical testing and computational simulations. In: *Stapp Car Crash Journal* 52, pp. 421–474. DOI: 10.4271/2008-22-0017.

SAE (2018). *Taxonomy and definitions for terms related to driving automation systems for on-road motor vehicles*. Ed. by SAE International. URL: https://www.sae.org/standards/content/j3016_202104/ (visited on 05/20/2024).

Salo, Zoryana, Maarten Beek, David Wright, and Cari Marisa Whyne (2015). Computed tomography landmark-based semi-automated mesh morphing and mapping techniques: Generation of patient specific models of the human pelvis without segmentation. In: *Journal of Biomechanics* 48.6, pp. 1125–1132. DOI: 10.1016/j.jbiomech.2015.01.013.

Sato, Fusako, Yusuke Miyazaki, Shigehiro Morikawa, Antonio Ferreiro Perez, Sylvia Schick, Karin Brolin, Mats Y. Svensson, and Mats Svensson (2021). The effect of seat back inclination on spinal alignment in automotive seating postures. In: *Frontiers in Bioengineering and Biotechnology* 9, pp. 1–17. ISSN: 2296-4185. DOI: 10.3389/fbioe.2021.684043.

Sato, Fusako, Yusuke Miyazaki, Shigehiro Morikawa, Antonio Ferreiro Perez, Sylvia Schick, Kunio Yamazaki, Karin Brolin, and Mats Y. Svensson (2019). Relationship between cervical, thoracic, and lumbar spinal alignments in automotive seated posture. In: *Journal of Biomechanical Engineering* 141.12. DOI: 10.1115/1.4045111.

Sato, Fusako, Mamiko Odani, Yusuke Miyazaki, Kunio Yamazaki, Jonas Östh, and Mats Y. Svensson (2017). Effects of whole spine alignment patterns on neck responses in rear end impact. In: *Traffic Injury Prevention* 18.2, pp. 199–206. DOI: 10.1080/15389588.2016.1227072.

Schaefer, Luise C., Mirko Junge, Illés Vörös, Kaan Koçaslan, and Uwe Becker (2021). Odds ratios for reclined seating positions in real-world crashes. In: *Accident Analysis and Prevention* 161. DOI: 10.1016/j.aap.2021.106357.

Schießler, M., J. Ott, and Andre Eggers (2020). „Positioning methods and their influence on the Human Body Models posture, kinematics and injury prediction“. In: *Proceedings of International Symposium: Human Modeling and Simulation in Automotive Engineering*. Ed. by CARHS.

Schoell, Samantha L., Ashley A. Weaver, Jillian E. Urban, Derek A. Jones, Joel D. Stitzel, Eunjoo Hwang, Matthew P. Reed, Jonathan D. Rupp, and Jingwen Hu (2015). Development and validation of an older occupant finite element model of a mid-sized male for investigation of age-related injury risk. In: *Stapp Car Crash Journal* 59, pp. 359–383. DOI: 10.4271/2015-22-0014.

Schöneburg, Rodolfo, K. H. Baumann, and Rainer Justen (2003). „PRE-SAFE-The next step in the enhancement of vehicle safety“. In: *Proceedings of International Technical Conference on the Enhanced Safety of Vehicles (ESV)*. Vol. 2003.

Shaikh, Junaid, Hasnain Thathia, and Nils Lubbe (2020). „Lumbar spine injuries in motor vehicle crashes“. In: *Proceedings of the IRCOBI Conference*, pp. 37–43. URL: https://www.ircobi.org/wordpress/downloads/irc20-asia/pdf-files/2019a.pdf.

Shaw, Greg, David J. Lessley, Joseph H. Ash, Salvador M. Acosta, Sara B. Heltzel, Patrick Riley, Taewung Kim, and Jeff R. Crandall (2018). Pelvic restraint cushion sled test evaluation of pelvic forward motion. In: *Traffic Injury Prevention* 19.3, pp. 250–255. DOI: 10.1080/15389588.2017.1326106.

Shaw, Greg, Dan Parent, Sergey Purtsezov, David J. Lessley, Jeff R. Crandall, Richard W. Kent, Hervé Guillemot, Stephen A. Ridella, Erik G. Takhounts, Peter G. Martin, David Lessley, Jeff Crandall, Richard Kent, Herve Guillemot, Erik Takhounts, and Peter Martin (2009). Impact response of restrained PMHS in frontal sled tests: skeletal deformation patterns under seat belt loading. In: *Stapp Car Crash Journal* 53, pp. 1–48. DOI: 10.4271/2009-22-0001.

Shi, Xiangnan, Libo Cao, Matthew P. Reed, Jonathan D. Rupp, Carrie N. Hoff, and Jingwen Hu (2014). A statistical human rib cage geometry model accounting for variations by age, sex, stature and body mass index. In: *Journal of Biomechanics* 47.10, pp. 2277–2285. DOI: 10.1016/j.jbiomech.2014.04.045.

Shim, Vickie B., Justin W. Fernandez, Prasad B. Gamage, Camille Regnery, David W. Smith, Bruce S. Gardiner, David G. Lloyd, and Thor F. Besier (2014). Subject-specific finite element analysis to characterize the influence of geometry and material properties in Achilles tendon rupture. In: *Journal of Biomechanics* 47.15, pp. 3598–3604. DOI: 10.1016/j.jbiomech.2014.10.001.

Shin, Jeesoo, John-Paul Donlon, Rachel Richardson, Bronislaw D. Gepner, Jason L. Forman, Martin Östling, and Jason R. Kerrigan (2022). „Biofidelity evaluation of the Hybrid-III 50th male and the THOR-50M in reclined frontal impact sled tests“. In: *Proceedings of the IRCOBI Conference.* URL: https://www.ircobi.org/wordpress/downloads/irc22/pdf-files/2248.pdf.

Somasundaram, Karthik, John R. Humm, Narayan Yoganandan, Hans Hauschild, Klaus Driesslein, and Frank A. Pintar (2022). Obese occupant response in reclined and upright seated postures in frontal impacts. In: *Stapp Car Crash Journal* 66, pp. 31–68. DOI: 10.4271/2022-22-0002.

Staubesand, Jochen, Ernst-Günter Afting, Alfred Benninghoff, Kurt Fleischhauer, Kurt Goerttler, Gerhard Aumüller, Bodo Christ, Wolf-Georg Forssmann, Diedrich von Keyserlingk, Benno Kummer, Erne Maier, Günther Osche, R. Presley, Reinhard Putz, Berton Rahn, Ursus-Nikolaus Riede, Dieter Sasse, Hans G. Schwarzacher, Renate Unsöld, and Christian Vogel, eds. (1985). *Makroskopische und mikroskopische Anatomie des Menschen.* 14th. Makroskopische und mikroskopische Anatomie des Menschen. München: Urban & Schwarzenberg. ISBN: 3541002441.

Stech, Ernest L. and Peter R. Payne (1969). *Dynamic models of the human body.* URL: https://ntrs.nasa.gov/api/citations/19710012123/downloads/19710012123.pdf (visited on 05/20/2024).

Steckler, R. M., J. A. Epstein, and B. S. Epstein (1969). Seat belt trauma to the lumbar spine. In: *Japan Automobile Manufactures Association* 207.4, pp. 758–759. ISSN: 0098-7484. DOI: 10.1001/jama.1969.03150170084028.

Stemper, Brian D., Jamie L. Baisden, Narayan Yoganandan, Frank A. Pintar, John DeRosia, Phillip Whitley, Glenn R. Paskoff, and Barry S. Shender (2012). „Effect of loading rate on injury patterns during high rate vertical acceleration“. In: *Proceedings of the IRCOBI Conference*, pp. 217–224. URL: https://www.ircobi.org/wordpress/downloads/irc12/pdf_files/29.pdf.

Stemper, Brian D., Derek Board, Narayan Yoganandan, and Christopher E. Wolfla (2010). Biomechanical properties of human thoracic spine disc segments. In: *Journal of Craniovertebral Junction and Spine* 1.1, pp. 18–22. DOI: 10.4103/0974-8237.65477.

Stemper, Brian D., Sajal Chirvi, Ninh Doan, Jamie L. Baisden, Dennis J. Maiman, William H. Curry, Narayan Yoganandan, Frank A. Pintar, Glenn R. Paskoff, and Barry S. Shender (2018). Biomechanical tolerance of whole lumbar spines in straightened posture subjected to axial acceleration. In: *Journal of Orthopaedic Research* 36.6, pp. 1747–1756. DOI: 10.1002/jor.23826.

Stemper, Brian D., Frank A. Pintar, and Jamie L. Baisden (2015a). „Lumbar spine injury biomechanics“. In: *Accidental injury.* Ed. by Narayan Yoganandan, Alan M. Nahum, and John W. Melvin. New York, NY: Springer. ISBN: 9781493917327.

Stemper, Brian D., Steven G. Storvik, Narayan Yoganandan, Jamie L. Baisden, Ronald J. Fijalkowski, Frank A. Pintar, Barry S. Shender, and Glenn R. Paskoff (2011a). A new PMHS model for lumbar spine injuries during vertical acceleration. In: *Journal of Biomechanical Engineering* 133.8. DOI: 10.1115/1.4004655.

Stemper, Brian D., Narayan Yoganandan, Jamie L. Baisden, Sagar Umale, Alok S. Shah, Barry S. Shender, and Glenn R. Paskoff (2015b). Rate-dependent fracture characteristics of lumbar vertebral bodies. In: *Journal of the Mechanical Behavior of Biomedical Materials* 41, pp. 271–279. DOI: 10.1016/j.jmbbm.2014.07.035.

Stemper, Brian D., Narayan Yoganandan, Glenn R. Paskoff, Ronald J. Fijalkowski, Steven G. Storvik, Jamie L. Baisden, Frank A. Pintar, and Barry S. Shender (2011b). Thoracolumbar spine trauma in military environments. In: *Minerva Ortop Traumatol* 62, pp. 1–16.

Stemper, Brian D., Narayan Yoganandan, and Frank A. Pintar (2017). „The thoracolumbar spine: Cadaveric testing under vertical loading“. In: *Military injury biomechanics.* Ed. by Melanie Franklyn and Peter Vee Sin Lee. Boca Raton, FL: CRC Press, Taylor & Francis Group, pp. 309–328. ISBN: 9781498742825.

Stokes, Ian A. F. (1994). Three-dimensional terminology of spinal deformity: A report presented to the Scoliosis Research Society by The Scoliosis Research Society Working Group on 3-D terminology of spinal deformity. In: *Spine* 19.2, pp. 236–248.

Sun, J. S., Kim K. Lee, and H. P. Lee (2000). Comparison of implicit and explicit finite element methods for dynamic problems. In: *Journal of Materials Processing Technology* 105, pp. 110–118. ISSN: 0924-0136. DOI: 10.1016/S0924-0136(00)00580-X.

Tang, Liang, Jiajia Zheng, and Jingwen Hu (2020). A numerical investigation of factors affecting lumbar spine injuries in frontal crashes. In: *Accident Analysis and Prevention* 136. DOI: 10.1016/j.aap.2019.105400.

Teshima, Tara Lynn, Vaibhav Patel, James G. Mainprize, Glenn Edwards, and M. Antonyshyn (2015). A three-dimensional statistical average skull: Application of biometric morphing in generating missing anatomy. In: *Journal of Craniofacial Surgery* 26.5, pp. 1634–1638. DOI: 10.1097/SCS.0000000000001869.

Thorbole, Chandrashekhar K. (2016). „Dangers of seatback recline in a moving vehicle: How seatback recline increases the injury severity and shifts injury pattern“. In: *Proceedings of International Mechanical Engineering Congress & Exposition.* Ed. by ASME. Vol. 3. ISBN: 978-0-7918-5738-0. DOI: 10.1115/IMECE2015-51809.

Thyagarajan, Ravi, Jaisankar Ramalingam, and Kumar B. Kulkarni (2014). „Comparing the use of dynamic response index (DRI) and lumbar load as relevant spinal injury metrics“. In: *ARL Workshop on Numerical Analysis of Human and*

Surrogate Response to Accelerative Loading, pp. 7–9. URL: https://apps.dtic.mil/sti/tr/pdf/ADA591409.pdf.

Toyota Motor Corporation (2011). *Documentation Total Human Model for Safety (THUMS): THUMS_AM50_V4_Document_20111003*. URL: https://www.toyota.co.jp/thums/about/.

Tran, Nam T., Nathan A. Watson, Allan F. Tencer, Randal P. Ching, and Paul A. Anderson (1995). Mechanism of the burst fracture in the thoracolumbar spine. The effect of loading rate. In: *Spine* 20.18, pp. 1984–1988. DOI: 10.1097/00007632-199509150-00004.

Trosseille, Xavier, Carole Luet, Pascal Drazétic, Pascal Potier, and Guy Vallancien (2012). Kinematics and dynamics of the pelvis in the process of submarining using PMHS sled tests. In: *Stapp Car Crash Journal* 56, pp. 411–442. DOI: 10.4271/2012-22-0011.

Trosseille, Xavier, Philippe Petit, Jérôme Uriot, Pascal Potier, Pascal Baudrit, Olivier Richard, Sabine Compigne, Mitsutoshi Masuda, and Richard Douard (2018). Reference PMHS sled tests to assess submarining of the small female. In: *Stapp Car Crash Journal* 62, pp. 93–118. DOI: 10.4271/2018-22-0003.

Tushak, Sophia K., Bronislaw D. Gepner, Jason L. Forman, Jason J. Hallman, Bengt Pipkorn, and Jason R. Kerrigan (2023). Human lumbar spine injury risk in dynamic combined compression and flexion loading. In: *Annals of Biomedical Engineering* 51.6, pp. 1216–1225. DOI: 10.1007/s10439-022-03126-5.

Tushak, Sophia K., Bronislaw D. Gepner, Bengt Pipkorn, and Jason R. Kerrigan (2022). „Evaluation of the GHBMC Lumbar Spine in Sub-injurious and Injurious Loading". In: *Proceedings of the IRCOBI Conference*, pp. 866–883. URL: https://www.ircobi.org/wordpress/downloads/irc22/pdf-files/22102.pdf.

Unger, Martin and Daniel Hintze (2019). „Entspannte Sitzpositionen im automatisierten Fahrmodus - Gefahr für die Lendenwirbelsäule bei einem Crash?" In: *Proceedings of Fahrzeugsicherheit 2019*. Ed. by Verein Deutscher Ingenieure.

Unselt, T., Rodolfo Schöneburg, and J. Bakker (2013). „Insassen-und Partnerschutz unter den Rahmenbedingungen der Einführung autonomer Fahrzeugsysteme". In: *Proceedings of Fahrzeugsicherheit 2013*. Ed. by Verein Deutscher Ingenieure.

Uriot, Jérôme, Pascal Potier, Pascal Baudrit, Xavier Trosseille, Philippe Petit, Olivier Richard, Sabine Compigne, Mitsutoshi Masuda, and Richard Douard (2015). Reference PMHS sled tests to assess submarining. In: *Stapp Car Crash Journal* 59, pp. 203–223. DOI: 10.4271/2015-22-0008.

van Gowdy, Richard L. DeWeese, Micheal S. Beebe, Barry Wade, John Duncan, Randy Kelly, and James L. Blaker (1999). A lumbar spine modification to the Hybrid III ATD for aircraft seat tests. In: *SAE Transactions* 108, pp. 367–379. ISSN: 0096736X, 25771531. DOI: 10.4271/1999-01-1609.

van Ratingen, Michiel, Aled Williams, Anders Lie, Andre Seeck, Pierre Castaing, Reinhard Kolke, Guido Adriaenssens, and Andrew Miller (2016). The European new car assessment programme: A historical review. In: *Chinese Journal of Traumatology* 19.2, pp. 63–69. ISSN: 1008-1275. DOI: 10.1016/j.cjtee.2015.11.016.

Vavalle, Nicholas A., Samantha L. Schoell, Ashley A. Weaver, Joel D. Stitzel, and F. Scott Gayzik (2014). Application of Radial Basis Function methods in the development of a 95th percentile male seated fea model. In: *Stapp Car Crash Journal* 58, pp. 361–384. DOI: 10.4271/2014-22-0013.

VIRTUAL (2023). URL: https://projectvirtual.eu/ (visited on 07/01/2023).

Volkswagen AG (2021). *Tiguan, Tiguan Allspace Digital Manual: e.g. FIN: WVG ZZZ 5NZ NM0 414 90*. URL: https://userguide.volkswagen.de/public/vin/login/de_DE (visited on 07/01/2023).

Wallace, Robert J., Pankaj Pankaj, and A. Hamish R. W. Simpson (2013). The effect of strain rate on the failure stress and toughness of bone of different mineral densities. In: *Journal of Biomechanics* 46.13, pp. 2283–2287. DOI: 10.1016/j.jbiomech.2013.06.010.

Wang, Marjorie C., Frank A. Pintar, Narayan Yoganandan, and Dennis J. Maiman (2009). The continued burden of spine fractures after motor vehicle crashes. In: *Journal of Neurosurgery. Spine* 10, pp. 86–92. DOI: 10.3171/SPI.2008.10.08279.

Westerborn, Anders and Ove Olsson (1951). Mechanics, treatment and prognosis of fractures of the dorso-lumbar spine. In: *Acta Chirurgica Scandinavica* 102.1, pp. 59–83.

Whitcome, Katherine K., Liza J. Shapiro, and Daniel E. Lieberman (2007). Fetal load and the evolution of lumbar lordosis in bipedal hominins. In: *Nature* 450.7172, pp. 1075–1078. DOI: 10.1038/nature06342.

White, Augustus A. and Manohar M. Panjabi, eds. (1990). *Clinical biomechanics of the spine*. 2nd. Philadelphia, PA: J.B. Lippincott. ISBN: 0397507208.

Whitesides, Thomas E. (1977). Traumatic kyphosis of the thoracolumbar spine. In: *Clinical Orthopaedics and Related Research* 128, pp. 78–92. ISSN: 0009-921X.

WHO (2018). *Global status report on road safety 2018*. URL: https://www.who.int/violence_injury_prevention/road_safety_status/2018/en (visited on 03/17/2023).

WHO (2020). *The Top 10 Causes of Death*. Ed. by World Health Organization. URL: https://www.who.int/news-room/fact-sheets/detail/the-top-10-causes-of-death (visited on 06/04/2023).

Wilke, Hans-Joachim, K. Wenger, and Lutz Claes (1998). Testing criteria for spinal implants: recommendations for the standardization of in vitro stability testing of spinal implants. In: *European Spine Journal* 7.2, pp. 148–154. DOI: 10.1007/s005860050045.

Willén, Jan, Sven Lindahl, L. Irstam, B. Aldman, and A. Nordwall (1984). The thoracolumbar crush fracture: An experimental study on instant axial dynamic loading: The resulting fracture type and its stability. In: *Spine* 6, pp. 624–631. DOI: 10.1097/00007632-198409000-00014.

Wittenberg, Ralf H., Stefan Hargus, Reinhard Steffen, Gert Muhr, and U. Bötel (2002). Noncontiguous unstable spine fractures. In: *Spine* 27.3, pp. 254–257. DOI: 10.1097/00007632-200202010-00010.

Yang, King H., ed. (2018a). *Basic finite element method as applied to injury biomechanics*. London United Kingdom: Elsevier/Academic Press. ISBN: 0128098317.

Yang, King H. (2018b). „Material laws and properties“. In: *Basic finite element method as applied to injury biomechanics*. Ed. by King H. Yang. London United Kingdom: Elsevier/Academic Press, pp. 231–256. ISBN: 0128098317.

Yang, King H. (2018c). „Modeling the spine upper and lower extremities for impact scenarios“. In: *Basic finite element method as applied to injury biomechanics*. Ed. by King H. Yang. London United Kingdom: Elsevier/Academic Press, pp. 609–654. ISBN: 0128098317.

Yang, King H., Jingwen Hu, and Nicholas A. White (2006). Development of numerical models for injury biomechanics research: A review of 50 years of publications in the Stapp Car Crash Conference. In: *Stapp Car Crash Journal* 50, pp. 429–490. DOI: 10.4271/2006-22-0017.

Yoganandan, Narayan, Mike W. J. Arun, Brian D. Stemper, Frank A. Pintar, and Dennis J. Maiman (2013). Biomechanics of human thoracolumbar spinal column trauma from vertical impact loading. In: *Annals of Advances in Automotive Medicine* 57, pp. 155–166. ISSN: 1943-2461.

Yoganandan, Narayan, Joseph F. Cusick, Frank A. Pintar, K. Droese, and John Reinartz (1994). Cyclic compression-flexion loading of the human lumbar spine. In: *Spine* 19.7, pp. 784–790. DOI: 10.1097/00007632-199404000-00010.

Yoganandan, Narayan, Nicholas DeVogel, Jason Moore, Frank A. Pintar, Anjishnu Banerjee, and Jiang Yue Zhang (2020). Human lumbar spine responses from vertical loading: Ranking of forces via Brier Score Metrics and Injury Risk Curves. In: *Annals of Biomedical Engineering* 48.1, pp. 79–91. DOI: 10.1007/s10439-019-02363-5.

Yoganandan, Narayan, Sanford J. Larson, Frank A. Pintar, Dennis J. Maiman, John Reinartz, and Anthony Sances (1990). Biomechanics of lumbar pedicle screw/plate fixation in trauma. In: *Neurosurgery* 27.6, pp. 873–881. DOI: 10.1097/00006123-199012000-00003.

Yoganandan, Narayan, Dennis J. Maiman, Frank A. Pintar, Gautam Ray, Joel B. Myklebust, Anthony Sances, and Sanford J. Larson (1988a). Microtrauma in the lumbar spine: A cause of low back pain. In: *Neurosurgery* 23.2, pp. 162–168. DOI: 10.1227/00006123-198808000-00006.

Yoganandan, Narayan, Jason Moore, Mike W. J. Arun, and Frank A. Pintar (2014). Dynamic responses of intact post mortem human surrogates from inferior-to-superior loading at the pelvis. In: *Stapp Car Crash Journal* 58, pp. 123–143. DOI: 10.4271/2014-22-0005.

Yoganandan, Narayan, Frank A. Pintar, Anthony Sances, Dennis J. Maiman, Joel B. Myklebust, Gerald Harris, and Gautam Ray (1988b). Biomechanical investigations of the human thoracolumbar spine. In: *SAE Transactions* 97, pp. 676–684. ISSN: 0096736X, 25771531. DOI: 10.4271/881331.

Zhang, Xiaoyan, Zhen Tang, Michael A. K. Liebschner, Daeseung Kim, Shunyao Shen, Chien-Ming Chang, Peng Yuan, Guangming Zhang, Jaime Gateno, and Xiaobo Zhou (2016). An eFace-template method for efficiently generating patient-specific anatomically-detailed facial soft tissue FE models for craniomaxillofacial surgery simulation. In: *Annals of Biomedical Engineering* 44, pp. 1656–1671. DOI: 10.1007/s10439-015-1480-7.

Zhu, Feng, Binhui Jiang, Jingwen Hu, Yulong Wang, Ming Shen, and King H. Yang (2016). Computational modeling of traffic related thoracic injury of a 10-year-old child using subject-specific modeling technique. In: *Annals of Biomedical Engineering* 44.1, pp. 258–271. DOI: 10.1007/s10439-015-1372-x.

Appendix

A.1 Preliminary Investigations - Intervertebral Discs

Newell et al. (2019) conducted compressive experiments to determine the material properties of human lumbar intervertebral discs (IVDs) at different strain rates using inverse finite element (FE) technique. This technique permits the acquisition of material properties that are dependent on strain rate without the necessity of dissecting individual components or gripping dissected specimens. Using the inverse FE method, a model of an entire system (e.g. the entire IVD) can be developed. In parallel, the material properties of individual components can be optimized to ensure a high level of consistency between the experimental data and the FE results. The underlying human cadaveric experimental study is part of the THUMS User Community 2 (TUC2) validation kit of an FE human body model (HBM) and was used by Draper et al. (2021) for validation of THUMS TUC v3.01, THUMS v5.02, THUMS v4.01, GHMBMC v4-5, and ViVa HBM in LS-DYNA. In this study it is used to validate the behavior of the THUMS v4.1 lumbar IVDs in Visual-Crash PAM (VCP) and to test the modified annulus fibrosus stress-strain curve used in Paper I and Paper II.

A.1.1 Experimental Setup by Newell et al. (2019)

The material response of the composite components was essential to accurately predict the structural response of the IVD. Thus, compressive experiments were conducted on 16 lumbar IVDs at different strain rates to obtain the structural response.

Sample preparation

Four fresh frozen lumbar motion segments were derived from four human cadavers (40±18 years old). Ethical approval was granted by the Tissue Management Committee of the Imperial College Tissue Bank Ethics Committee (ethical approval number: 12/WA/0196). Intactness of the vertebral bodies was checked via computer tomography (CT), disc degeneration level was assessed using magnetic resonance imaging (MRI) imaging and subsequent ranking according to the Pfirrman scale. Each spine was defrosted overnight at room temperature before testing. Soft tissues and posterior elements were removed, whilst anterior and posterior longitudinal ligaments were kept intact. Following preparation, each specimen was wrapped in a paper towel soaked in phosphate-buffered saline (0.15 m/L) to maintain hydration. three-dimensional (3D)-printed wedges above and below each specimen were used to ensure that the midplane of each IVD was perpendicular to the loading axis. The specimens were fixated with polymethylmethacrylate (PMMA) bone cement.

Experimental procedure

The deformation of the embedded specimens was applied using a servo-hydraulic materials testing machine (8872; Instron, Canton, MA, USA). Each IVD was exposed to four compression cycles with a strain rate up to 1s^{-1} to 15 percent strain. Preliminary tests showed that a strain of 15 percent would not compromise the IVDs allowing for multiple tests on each specimen after a 5-minute relaxation period. During the experiments, reaction forces were recorded using the machine integrated load cell. The vertical displacements of the specimens were determined using two Linear Variable Displacement Transducers (LVDTs) attached to the top and the bottom pot. To measure the internal pressure a pressure transducer was inserted into the nucleus of each sample (Figure A.1 left).

A.1.2 Finite Element Simulation

The load case description and validation protocol from the THUMS User Community (TUC) validation repository has been used to reconstruct the reference experiment in Visual-Crash PAM 16.5.4 (VCP, ESI Group, Rungis Cedex, France) with the THUMS v4.1 under license at Volkswagen. The IVDs (L1-L2, L2-L3, and L3-L4) were isolated from the full-scale THUMS v4.1 analogous to the reference experiments in preprocessing software VCP. Soft tissues and posterior elements were excised, leaving the disc and anterior and posterior ligaments intact. Each IVD was positioned in accordance with the physical IVDs position in the experiment, maintaining the center plane of each disc perpendicular to the test direction. To minimize off-axis bending, the specimens are positioned so that the center of the crosshead of the testing machine is at 1/3 of the anterior-posterior distance from the most posterior aspect of the disc as described in the validation protocol. As THUMS v4.1 has deformable bones, the shells of the cortical bone were rigidly attached to the potting material via *Multiple Nodes to one Node Constraints (MTOCOs).* The disc displacements of 12 experiments (L1-L2, L2-L3, and L3-L4) measured via LVDTs served as displacement boundary conditions in the FE model. Four experiments (L4-L5) were excluded from the inputs[1] due to a shorter time scale compared to the other experiments. The output force variables were measured in the simulation at the same location where the force sensors were installed for the experiments, whereby the outputs also being stratified by lumbar level (Figure A.1 right).

1 and also from the corridor calculation used as outputs

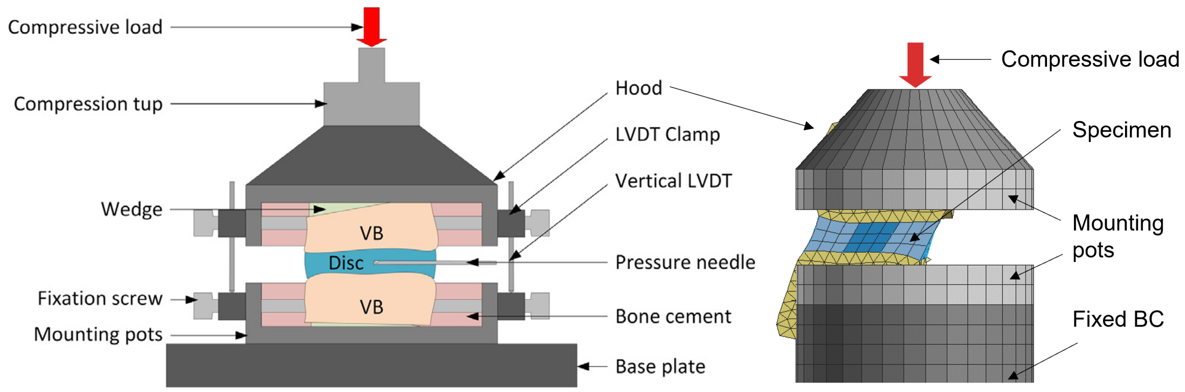

Figure A.1: Schematic representation of the reference test setup (left) and the respective FE model (right). The specimen is attached to the servo-hydraulic materials testing machine via PMMA embedding. Forces, displacements, and internal pressures are measured using a load cell, LVDTs, and a pressure transducer in the experimental setup (modified after Newell et al. (2019)). The displacement boundary condition is applied at the top and the specimen is rigidly attached to the pots in the simulation setup.

A.1.3 Validation Results

Figure A.2 depicts a comparison of the force-displacement response of the experimental and numerical result.

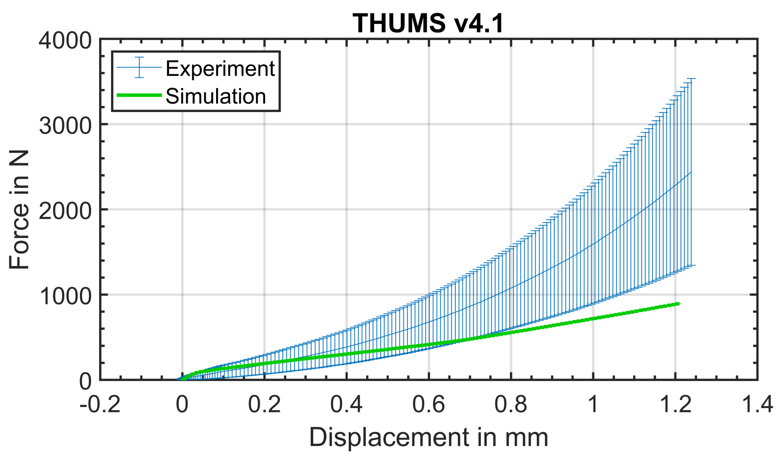

Figure A.2: A comparison of the force-displacement response of the experimental and numerical result. The experimental result is shown with ±1 SD. The cause of the rigid boundary conditions, penetrations of the vertebral body and the lower mounting pot are irrelevant here.

A.2 Preliminary Investigations - Total Lumbar Spine

In the following, the design of a total lumbar spine validation setup is described that was also used by Draper et al. (2020). Subsequently, the results of sensitivity studies are shown, which form the basis for studies presented in Paper I and Paper II.

A.2.1 Drop-Tower Experiment by Stemper et al. (2011b)

To experimentally quantify the axial tolerance of the lumbar spine, the authors (Stemper et al., 2011b) dynamically tested 23 intact human lumbar spines (T12-L5) at sub-failure and failure levels with a drop-tower test setup. The drop-tower had two decoupled platforms, each attached to a monorail via low-friction bearings to ensure compression-flexion loading. The lower and upper platforms were equipped with linear acceleration sensors for measuring vertical accelerations. Forces and moments were measured using a load cell with which the caudal fixation of the specimen was mounted to the lower platform. A laterally oriented cylinder was positioned between the upper sample fixture and the upper platform. To generate a realistic acceleration pulse, a piece of foam was added at the site of impact. A mass of 32 kg was imposed on the upper platform to simulate the static torso mass of a 50th percentile man (Figure A.4).

Sample Preparation

Pre-test CT scans allowed evaluation of each specimen. Specimens with excessive loss of disc height, bridging osteophytes or inconsistent alignment were excluded. To facilitate attachment to the experimental apparatus, the cranial (T12) and caudal (L5) vertebrae were embedded in PMMA. The L2-L3 IVD level was placed horizontally in the global coordinate system to ensure interspecimen comparability without altering the natural lordosis of the individual specimens. After checking the integrity of the specimens, a preflexion moment of 5 Nm was applied to minimize off-center loads. A cable was then placed between the platforms to limit the recoil of the specimens prior to testing and any substantial vertical displacement or impact during the dynamic test.

During deceleration, the upper platform could inertially compress the lumbar spine specimen by reducing the vertical distance from the lower platform. Every specimen was subjected to one or several dynamic tests from specified drop heights until injury was detected. 3D-vertebral kinematics were captured with a Vicon system (Vicon Corp., Oxford Metrics Group, Oxford England) and three spherical targets. One target was placed in the anterior region of the body and one in each transverse process. Throughout the posterior wall of each vertebral body, the origins of the local Cartesian coordinate system were defined at mid-height and mid-width. To recreate the vertebral kinematics, the target movements were taken. For each segment (T12-L1 to L4-L5), sagittal segmental angulation was calculated as the angle of the sagittal plane of a vertebra relative to the adjacent vertebra (Stemper et al., 2011b). Each specimen was x-rayed after each test for fractures or notable changes in spinal alignment or

IVD heights. Palpation of the specimens and assessment of flexion stiffness eliminated endplate or soft tissue injury. X-rays and post-test CT scans were used to assess the type of fracture and the affected level of the spine (Figure A.3).

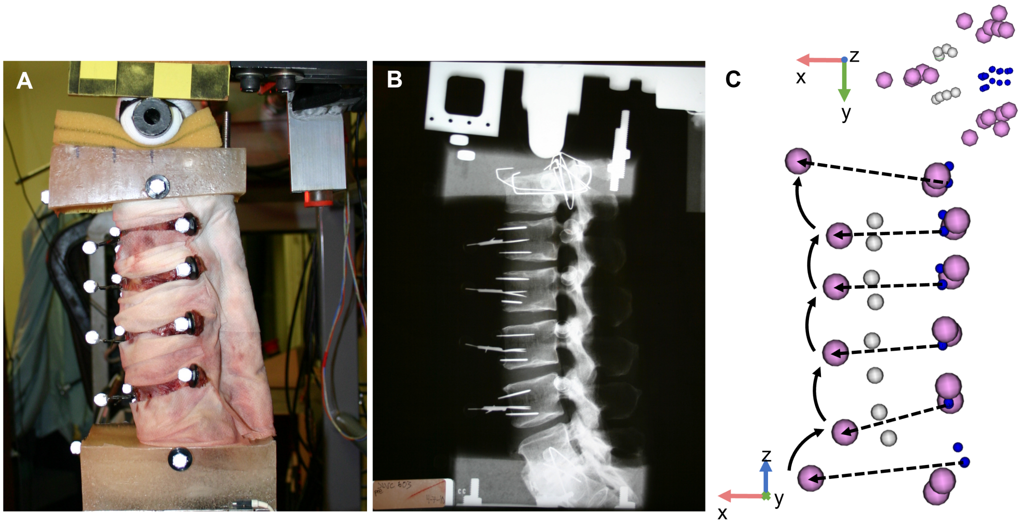

Figure A.3: Configuration of experimental setup. **A** Photography with visible Vicon markers. **B** X-ray and visualization of Vicon markers from the top and lateral side view in Mokka. **C** The local Cartesian coordinate system is shown in blue; the black dashed line resembles the fictional local x-axis from the origin of the coordinate system to the anterior targets. The arrows show the sagittal segmental angulation measured in the experiment.

A.2.2 Finite Element Simulation of the Drop-Tower Experiment

To simulate the experiments from Stemper et al. (2011b) the THUMS v4.1 lumbar vertebral column is prepared according to the specimen preparation described in the reference experiment. The specimen is rigidly fixed to the upper and lower specimen pot using node constraints to simulate PMMA embedding. The cylinder with a non-structural mass of 32 kg at the upper part is positioned according to the experimental description and pre-test X-rays. Between the cylinder and the upper specimen pot, a TIED contact definition is defined. The measurement of section forces in the global coordinate system is enabled via section forces in the upper and lower specimen pot. To ensure accurate force measurement, the accelerations measured in the lower platform in the experiment are applied as boundary conditions below the section force to the lower platform. Translation in the global z-direction and rotation around the global y-axis are guaranteed by the boundary conditions for the cylinder and the lower platform. Similarly to the measurement of forces and moments in the simulation model at the points equivalent to the load cells in the experiments, the intervertebral kinematics are also recorded in the simulation. Therefore, vertebral reference points and local coordinate systems were defined as described in chapter 5.

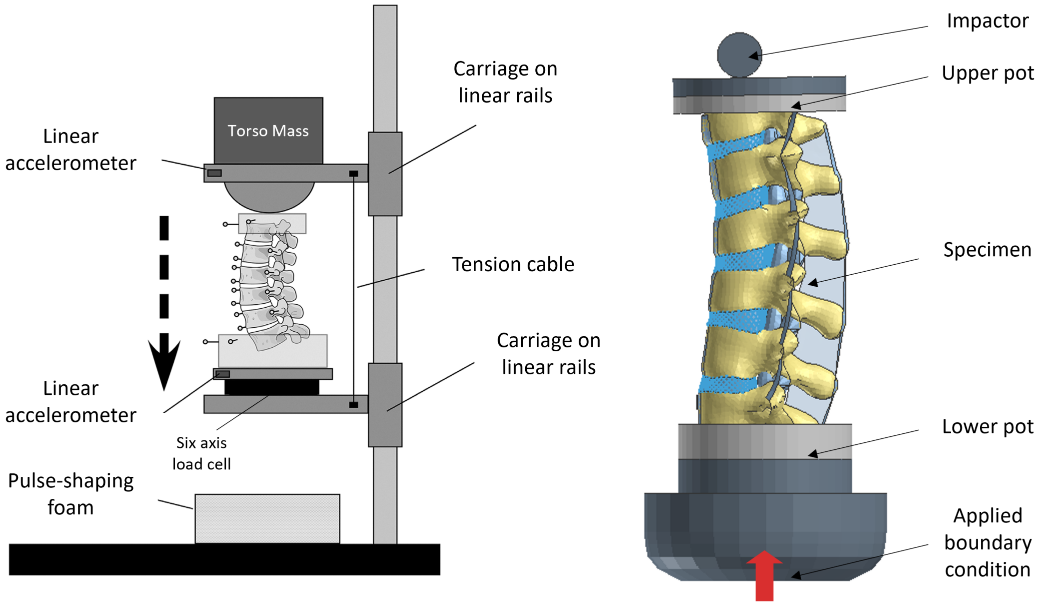

Figure A.4: Schematic representation of the vertical drop-tower setup to simulate high-rate loading of the specimen by Stemper et al. (2011b) (left) and its FE representation (right). The specimen is attached to the experimental apparatus via PMMA embedding. Acceleration, forces, and moments are measured using linear accelerometers and a six-axis load cell at the top and the bottom of the attachment platforms. Both platforms are connected to a vertical 7.6 m long monorail by low friction precision linear steel bearings. A mass of 32 kg was imposed to the upper platform to simulate static torso mass for a 50th percentile male. A more realistic acceleration pulse is provided by a pulse-shaping foam at the drop-tower base (modified after Stemper et al. (2011b)).

Excursion: Evaluation of Intervertebral Kinematics

The coordinates of the newly constructed midpoint of the vertebrae and the endpoint of the new local x-axis were exported using Animator (Animator4 2.4.5, GNS - Gesellschaft für Numerische Simulation mbH, Brunswick, Germany) for the evaluation of the intervertebral kinematics. A Matlab script[2] (Math-Works, Natick, Massachusetts, USA) was used for the calculation of the angle$_{\text{InterVB}}$ using the following mathematical relation:

$$\text{angle}_{\text{InterVB}} = \text{atan2}(\text{norm}(\text{cross}(a, b)), \text{dot}(a, b)) \tag{A.1}$$

where a is the vector from one midpoint to the endpoint of the local x-axis of one vertebra and b is the vector from the midpoint to the endpoint of the local x-axis of the adjacent vertebra. As per definition in the experiment, intervertebral angles in extension are negative and angles in flexion are positive. To account for this definition the vector from one midpoint to the midpoint of the adjacent vertebra, and the vector

2 The code is available at the TUC repository.

from one x-axis endpoint to the next x-axis endpoint have been compared. Flexion is defined as having a higher midpoint to midpoint distance as x-axis endpoint to x-axis endpoint.

Validation of the Evaluation Concept

To validate this evaluation scheme the coordinates of the Vicon markers provided by courtesy of Medical College Wisconsin (MCW) as .cd3-data have been exported using the open-source 3D Motion Kinematic & Kinetic Analyzer Mokka (Mokka 0.6.2, Biomechanical ToolKit (BTK), https://biomechanical-toolkit.github.io/mokka/). The computed angles were then compared to the angles provided by courtesy of MCW.

Figure A.5 exemplarily shows the difference between the endnode-distance and the midnode-distance for each pair of vertebrae over time for one nonfailure load case where both Vicon and kinematics data evaluated by Stemper et al. were available. A positive difference - meaning the endnode-distance is larger than the midnode-distance - is defined as extension in the experiment. For flexion it is the other way round. The area for extension is colored grey and the area for flexion is white in the graph. The different pairs of vertebrae are color coded. T12-L1, L2-L3 and L3-L4 are extended, while L1-L2, and L4-L5 are flexed during the experiment.

The kinematic curves for the experimental output data as normalized angular displacement as well as angular displacements computed by coordinates are presented in Figure A.5. Dotted lines represent experimental results and solid lines computed displacements. Negative angles are defined as extension (positive delta of midnode to midnode and endnode to endnode distance) and positive angels as flexion (see also Figure 8.11). In accordance with the delta of distances shown on the left, T12-L1, L2-L3, and L3-L4 show negative angles here, whereas the angular displacements between L1-L2 and L4-L5 are positive. The curves for the vertebrae pairs T12-L1, L1-L2, L3-L4, and L4-L5 seem remarkably similar, whereas there is a slight offset on the y-axis for L2-L3. The progression of the curve over time seems to be quite similar, too.

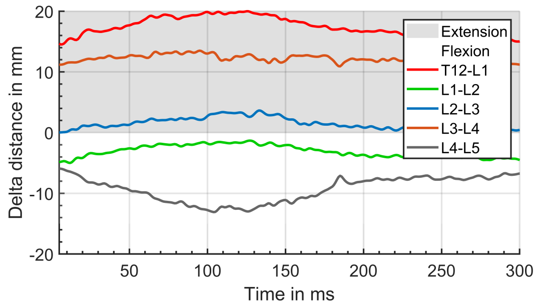

(a) Distances between midnodes of adjacent vertebrae

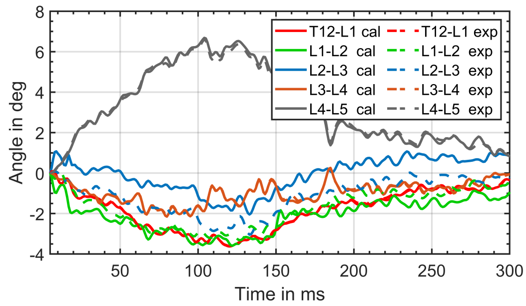

(b) Experimental (exp) and computed (cal) angular displacements

Figure A.5: (a) Delta of the distance between one midnode and the midnode of the adjacent vertebra and the distance of one x-axis endnode and the endnode of the adjacent vertebra. The different pairs of vertebrae are color-coded. A positive delta means extension and a negative delta flexion. (b) Comparison of the results of the experiments as angular displacements as output and the angular displacements exported as nodal coordinates and computed.

A.2.3 Validation of the Total Lumbar Spine in a Subinjurious Load Case

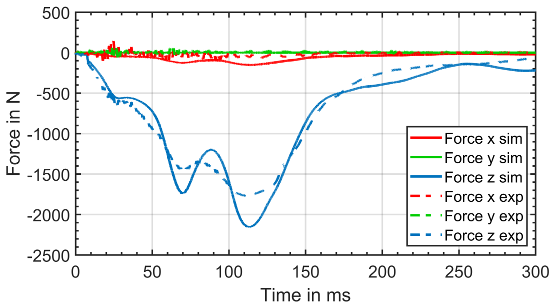

(a) Force-time

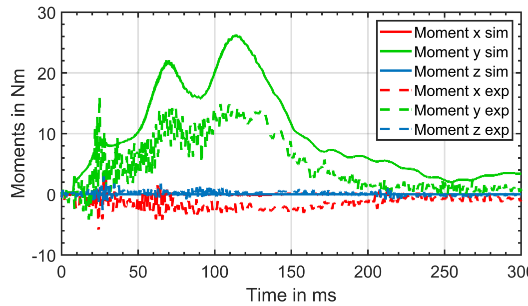

(b) Moment-time

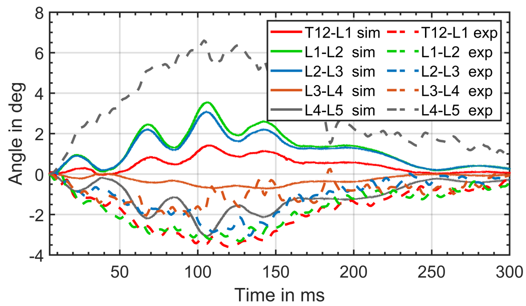

(c) Angular displacement

Figure A.6: A comparison of the (a) force-time, (b) moment-time and (c) angular displacement response of the experimental and numerical results.

A.3 Subject-Specific Model Creation

In this section, the methodology for the reconstruction of the subject-specific lumbar spine models (Paper I) is described. In Figure A.7 the steps to be taken for the development of subject-specific FE models of the lumbar spine are described.

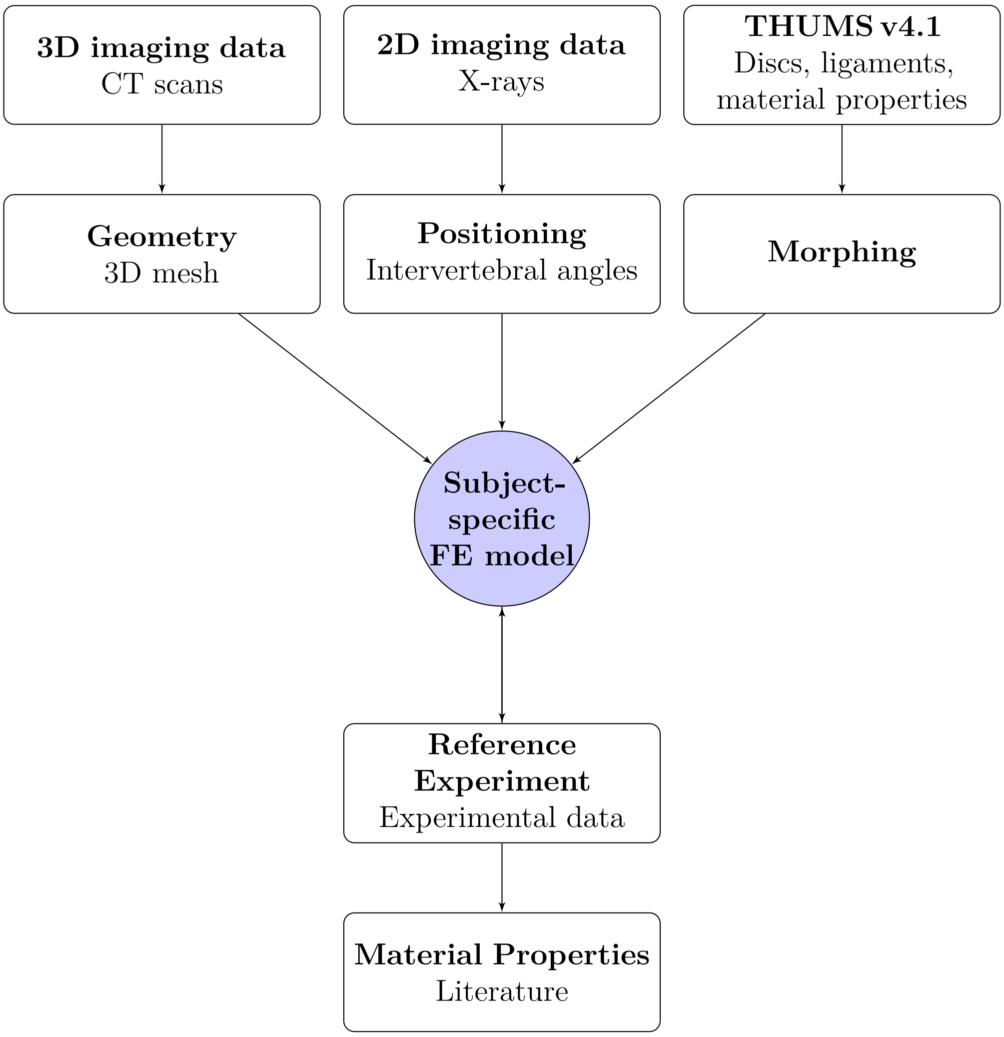

Figure A.7: Overview of the reconstruction of the subject-specific lumbar spine models. The geometry of the vertebral bodies is extracted from CT scans in supine position through segmentation. Positioning in test-position is achieved through measurement of intervertebral angles in X-rays, numerical midplane construction and positioning. Disc and ligamentous structures are extracted from THUMS v4.1 and morphed to fit the subject-specific geometry. Where possible, appropriate material properties from THUMS v4.1 or literature are assigned. Boundary conditions to replicate the drop-tower experiment by Stemper et al. (2018) are applied.

For the reconstruction of four subject-specific FE models of the T12-L5 lumbar spine unit, vertebral body geometry was derived from CT scans provided courtesy of MCW.

Discs and ligamentous structures as well as material properties were initially used from THUMS v4.1. More details on the boundary conditions in the reference experiments can be found in Stemper et al. (2018).

A.3.1 Geometry & Mesh Generation

The feasibility of using the CT data for reconstruction of subject-specific lumbar spine models was assessed using the following criteria:

1. Availability criterion:
   CT data from either pre-test or non-fractured specimens
2. Completeness criterion:
   CT data needs to include all relevant structures of T12 to L5
3. Quality criterion:
   Resolution of CT data (in plane resolution as well as in layered image plane)

Geometry & Material

For the purpose of image segmentation, all feasible CT data were transferred to Mimics (Version 22.0, Materialise, Plymouth, MI, USA). The six lumbar vertebrae of each subject were segmented using a semi-automatic thresholding method. Spikes and holes on the surface of the vertebral geometries were then removed by smoothing. The vertebral geometries were exported in stereo-lithography (.stl) and in initial-graphics-exchange-specification (.iges) format. Figure 5.1 shows the segmentation process. The cortical and trabecular bone were modelled using PamCrash material model as defined according to THUMS v4.1.

Meshing

Meshing was done in ANSA pre-processor software (BETA CAE Systems SA, Epanomi, Thessaloniki, Greece). Cortical bone thicknesses of 1, 1.29, 1.29, 1.39, 1.72, and 1.98 mm from T12 to L5 respectively was modelled using quad meshing with a target element length of 2 mm of the outer surface of the segmented vertebral bodies. In the edges, to avoid stiffening effects through triangular elements, reconstruction, smooth, and reshape options were used. Tetrahedral elements were used to model the remaining volume of each vertebra, which was considered as trabecular bone. Figure A.8 shows an example of the resulting mesh of a segmented L3 vertebra.

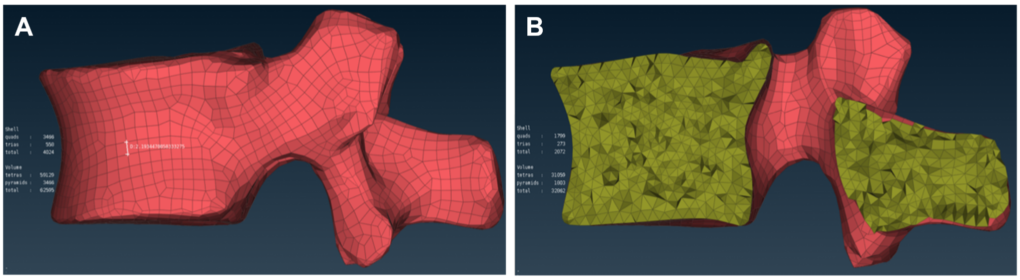

Figure A.8: Example of the resulting mesh of a segmented L3 vertebra. **A** outer surface. **B** cross section showing core structure (green).

The parameters of mesh quality, which were used to check the quality of shells and solids are listed in Table A.1. After meshing each vertebra applying the quality parameters, it was ensured that the model passed the pre-surface and volume meshing tests to confirm that there were no penetrations or close proximities.

Table A.1: Shell and solid mesh quality parameters.

Shell mesh			**Solid mesh**		
Criteria	Calculation	Failed	Criteria	Calculation	Failed
Aspect ratio	PATRAN	10.	Aspect ratio	PATRAN	10.
Skewness	PATRAN	62.	Skewness	PATRAN	65.
Warping	PATRAN	20.	Warping	PATRAN	20.
Jacobian	ANSA	0.3	Jacobian	ANSA	0.3
Min angle quads	IDEAS	20.	Min angle tetras	ABAQUS	20.
Max angle quads	IDEAS	160.	Max angle tetras	ABAQUS	150.
Min angle trias	IDEAS	15.	Min angle pentas	ABAQUS	13.
Max angle trias	IDEAS	120.	Max angle pentas	ABAQUS	160.
			Min angle pentas	ABAQUS	20.
			Max angle pentas	ABAQUS	160.
			Collapse		0.2

A.3.2 Model Positioning

The poses of the individual lumbar vertebrae had to be modified to the upright test position, as the CT scans were acquired in the supine position. Therefore, the intervertebral angles were quantified in midsagittal X-ray images[3] using the image processing software ImageJ (http://rsb.info.nih.gov/ij/; US National Institutes of Health Bethesda, Maryland, USA). In this study, the intervertebral angles T12-L1, L1-L2, L2-L3, L3-L4 and L4-L5 were measured. The intervertebral angle is measured in the midsagittal plane and specified here as the angle between the superior and inferior surfaces in the median plane of the vertebral body. A positive angle indicates

3 The X-rays were provided courtesy of MCW.

flexion or upward inclination relative to the horizontal plane, while a negative angle indicates extension or downward inclination relative to the horizontal plane.

Definition of midplanes

For the adjustment of the vertebrae to the angles measured in the X-rays, midplanes for each vertebral body needed to be defined. Therefore, tangent planes to the endplates of the vertebral bodies needed to be defined in a first step (Figure A.9 A). After that two kinetic bodies were defined using the *Kinetics* functionality of ANSA - one kinetic body being the plane and the other kinetic body being the vertebral bodies endplate (Figure A.9 B). Via force-based simulation the kinetic body plane approaches the vertebral endplate until the minimum distance between both kinetic bodies is reached. The average of the tangent planes forms the midplane of the vertebral body (Figure A.9 C).

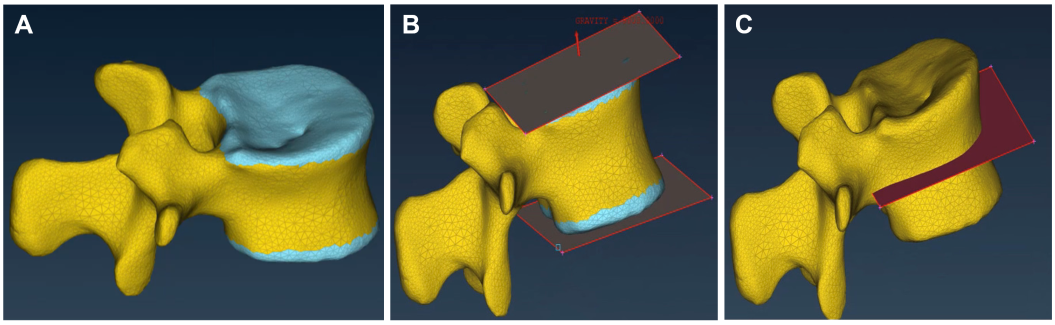

Figure A.9: Definition of midplanes. **A** Identification of endplates. **B** Definition of tangent planes. **C** Midplane.

Reorientation of the vertebral bodies

Finally, for the reorientation of the vertebral bodies, a rotation axis was defined via extension of the midplanes until intersection. The position of the rotation axis is defined as the location of the facet joints (Figure A.10 A). The angles were adjusted by transformation corresponding to the intervertebral angles as measured in midsagittal X-ray images (Figure A.10 B).

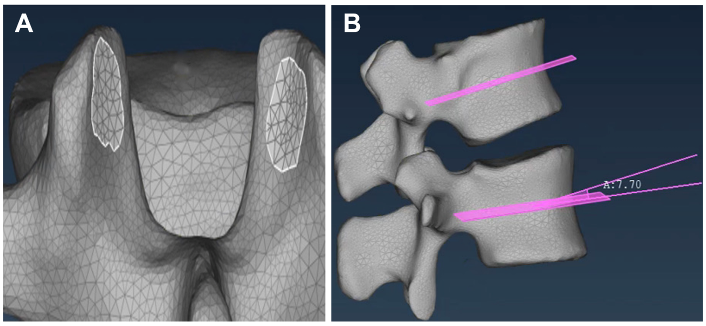

Figure A.10: Reorientation of the vertebrae. **A** Facet joints for rotation axis. **B** Adjustment of angles.

A.3.3 Model Assembly

After the reorientation followed by the shell and solid meshing of the subject-specific vertebrae model, the soft tissues comprising the IVDs, cartilage, and ligaments were modelled. Based on the positioned alignment, the IVDs were inserted between the endplates. The anterior & posterior longitudinal ligament (anterior longitudinal ligament (ALL) & posterior longitudinal ligament (PLL)), ligamentum flavum (LF), intertransverse ligament (ITL) and interspinous ligament (ISL) were also shifted to the endplates, as was the intervertebral disc.

Isolation of IVD & Membranes from THUMS v4.1 and Alignment with Target Vertebral Model

In the first step, the subject-specific vertebral model is globally aligned so that its re-orientation corresponds to the original orientation of the THUMS v4.1 (x-axis from posterior to anterior, z-axis from caudal to cranial). Next IVDs, ligaments, and membranes were isolated from THUMS v4.1. After isolation, the soft tissues of THUMS v4.1 and the target model were aligned with some translational offset and merged with the target subject-specific vertebral model.

Mesh Morphing

Soft tissues were morphed to the target vertebral model using four subordinate definition steps in the *Direct Morphing DFM* toolkit in ANSA.

In the first definition step, curves of the source model were fitted to curves defined on the target model to help position the discs, the ALL, PLL, and ISL. These curves were defined in the *Topo* module using the *Curve Creation* tool in ANSA. Then, source curves were defined on the top and the bottom of the edges of the IVD and the top most and bottom most ends of left and right ALL, PLL and ISL. Target curves were defined on the target bones so that it resembles the periphery of the IVD and at the anterior and posterior target bones and the spinous processes (Figure A.11 A). The

Direct Morphing module with *Edge Fitting* was used to morph the IVBs and ligaments to the subject-specific vertebral bodies.

To make sure that the top and bottom face of the morphed IVDs are better fitted with the geometrical inhomogeneity of the target bones, the *DFM Align* tool is used. First, skin shell elements were created from the top and the bottom face of the hexa meshed IVDs to serve as control entities using the *Shell Mesh* module and *VolShell* option (Figure A.11 B). The *Direct Morphing* module with *DFM Align* was used to morph the IVBs and ligaments to the subject-specific vertebral bodies.

To ensure the effective morphing, the ALL and PLL to the anterior respectively the inferior of the VB, the ALL and PLL were defined as control entities in the *DFM Align* tool in a subordinate step (Figure A.11 C & D).

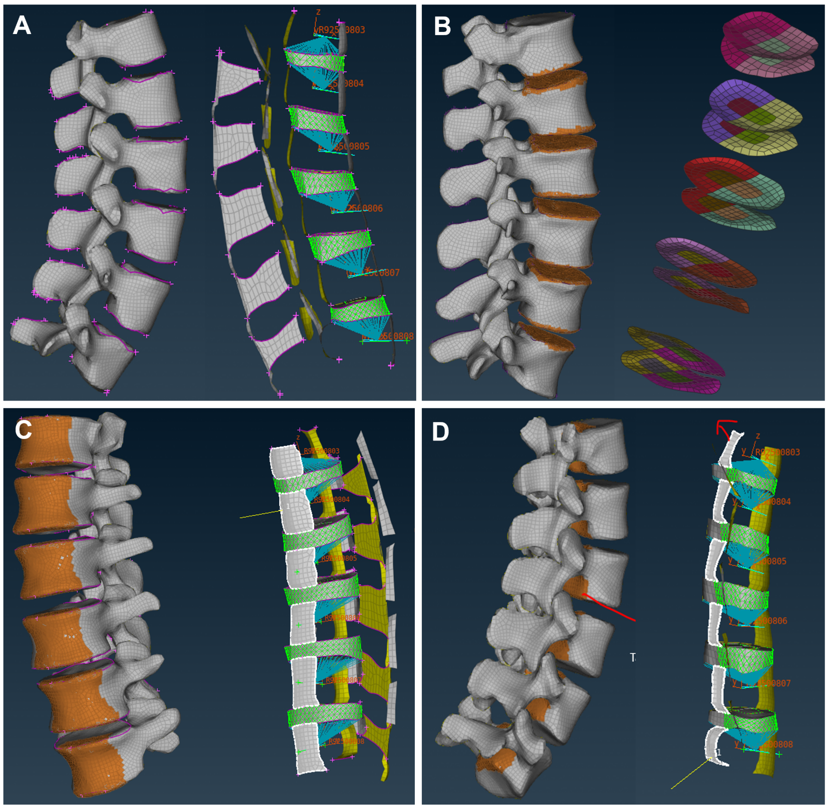

Figure A.11: Mesh morphing process. **A** Definition of curves on source and target model for *Direct Morphing* with *Edge Fitting*. **B** Creation of skin shell elements for *Direct Morphing* with *DFM Align*. **C** & **D** Definition of ALL and PLL as control entities for *Direct Morphing* with *DFM Align*.

Connection of Intervertebral Discs and Ligaments to Target Bones

To connect the IVDs and the ligaments to the subject-specific target bones, the meshes of these entities were projected to the target vertebral structures using the *Shell Mesh Projection* tool in ANSA.

First, the meshes of the ALL, PLL as well as the top and bottom faces of the IVDs were pasted to the target vertebral structures using the *Shell/Facet* option of the *Shell Mesh Projection* tool.

In a second step, the *Edge* option was used to project the insertion points of the ISL onto the posterior aspects of the superior and inferior medial ridges of the spinous processes. Likewise, the superior attachments of the LF are projected to the rim of the vertebral foramen and the inferior insertions to the base of the vertebral foramen, where the concave shape of the lamina transitions into the convex shape of the spinous process. The projection tool is also used for the attachment of the ITL to the transverse process on both sides of the vertebra. After each projection step the model was checked for initial penetrations.

Interspinous Ligament

The ISL in the FE model is defined using shell elements. The insertion points for the ISL are determined via curves that are created along the posterior aspects of the superior and inferior median crests of the spinous process. Shells are created between two curves by using the *Free Curves* tool in the *Shell Mesh Fill* module in ANSA. The created shell mesh was quality checked with the quality criteria defined in subsection A.3.1. To avoid buckling, both planarity and penetration were visually checked. In the case of penetration, the projection procedure described above followed. After formation of the ISL, material was defined according to THUMS v4.1.

Facet Joints

It is not possible to determine the actual position and thickness of the facet joints from the CT scan. Therefore, an approximation based on the facet surface of the vertebra is necessary. In this study, the facet joint is modeled by capsular ligaments only, as it is also realized in THUMS v4.1. To exclude initial penetration, the gap between two facet surfaces is first evaluated and modified. If there is no initial penetration, the gap remains unchanged. Hence, each specimen can have a different gap according to its geometry. The capsular ligaments (CLs) are modeled for each facet joint with one layer of shell elements in the FE model. This is implemented manually with the *Free Shell* tool in the *Shell Mesh* module in ANSA. The nodes on the corresponding facet joint surfaces, which are opposite each other in a ring structure, were set as insertions for the CL. After forming the CL, a penetration check was performed. In the case of penetration, either projection procedure (see above) or manually elimination of the penetrations followed. After formation of the CL, material was defined according to THUMS v4.1. Once the model had been compiled, the reference points and section forces were incorporated into each subject-specific model, as previously described in chapter 5.

A.4 Drop-tower Simulation Setup Sensitivity

To assess the sensitivity of the setup, the parameters listed in Table A.2 were iteratively altered and their influence on the kinematic and kinetic response of the setup was evaluated.

Table A.2: Drop-tower simulation setup sensitivity parameters.

	Parameter	
Setup related	Upper pot	Tilt (y-rotation)
		Embedding height
	Impactor	Weight
		Connection to upper pot
		Position in x
	Alignment of model in setup	Tilt (y-rotation)
		Position in x
	Application of boundary conditions	
Model related	Ligaments	Influence of posterior longitudinal ligament (PLL)
		Influence of interspinous ligament (ISL)
		Influence of supraspinous ligament (SSL)
		Capsular ligament (CL) material
	Intervertebral discs (IVDs)	Annulus fibrosus material
		Fiber material
		Nucleus material
	Vertebral body	Failure

Acknowledgements

Die vorliegende Arbeit entstand in Zusammenarbeit mit dem Fachbereich Fahrzeugsicherheit der Volkswagen AG und wurde im Juli 2024 dem Institut der Rechtsmedizin der Ludwig-Maximilians-Universität München als Dissertation vorgelegt.

Besonderer Dank gebührt meinem Doktorvater Prof. Dr. Steffen Peldschus, der meine Arbeit zu jeder Zeit in hervorragender Art und Weise betreut hat und mich von Beginn an außergewöhnlich konstruktiv unterstützt hat.

Ganz herzlich möchte ich mich auch bei Brain D. Stemper, PhD und seinem Team des Medical College of Wisconsin bedanken, die durch das Bereitstellen ihrer experimentellen Ergebnisse überhaupt erst die Grundlage der vorliegenden Dissertation ermöglicht haben und gemeinsamen Veröffentlichungen offen gegenüberstanden. Insbesondere danke ich außerdem Dr. Mirko Junge für die vielen bereichenden Gespräche, den fachlichen Input zum Thema, die Unterstützung der Promotionsphase und das Korrekturlesen. Danke auch an Prof. Dr. Gerold Schneider von der Technischen Universtität Hamburg, der mir nicht nur eine besondere Unterstützung bei der Verwirklichung meines Auslandsaufenthalts während meines Masterstudiums war, sondern auch zu Beginn meiner Doktorarbeit die richtigen, wichtigen Fragen zum richtigen Zeitpunkt gestellt hat. Ebenso danke ich Prof. Dr. Gunter Woelky für die Unterstützung bei einer sehr richtungsweisenden Entscheidung - ich denke ich habe die Richtige getroffen.

Besonders danken möchte ich ebenfalls den vielen Gesprächspartnern der letzten Jahre, denen ich in der ein oder anderen Weise Anregungen, Denkanstöße, Einsichten, Korrekturleseungen und Unterstützung verdanke: insbesondere Dr. Dustin Draper, Dr. Friedrich von Bülow, Dr. Jan Tschorn und Dr. Johannes Sperber. Weiterhin möchte ich mich beim gesamten Team der Fahrzeugsicherheit der Volkswagen AG bedanken - insbesondere Michael Otto und Till Boing - ihr habt mir die Welt der Crash-Simulation näher gebracht und hattet immer ein offenes Ohr - sowie Christoph Vieler. Auch möchte ich mich beim Team der Biomechanik und Unfallforschung des Institut der Rechtsmedizin der Ludwig-Maximilians-Universität München bedanken, welches meinen Anliegen jederzeit Gehör schenkten. Ich möchte mich außerdem bei allen Studenten bedanken, die mich beim Aufbau der Simulationen unterstützt haben.

Mein größter Dank jedoch gebührt zum einen meinem Partner Dominik Schmidt, der mich bei der Entstehung der Arbeit unentwegt, in jeglicher Weise unterstützt und motiviert hat, sowie meinen Eltern, der ich meinen gesamten Werdegang verdanke.

Wolfsburg im Januar 2025 *Laura Kathrin Rieger*